2-P

SIXTH INTERCENTER AND CONTRACTORS CONFERENCE ON PLASMA PHYSICS

Program and Abstracts

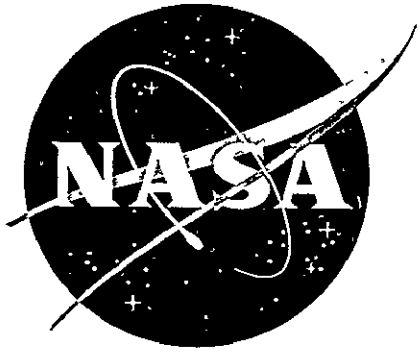

LANGLEY RESEARCH CENTER
DECEMBER 8, 9, 10, 1969

SIXTH NASA INTERCENTER AND CONTRACTORS CONFERENCE
ON PLASMA PHYSICS

Activities Building (Bldg. 1222)
NASA Langley Research Center, Hampton, Va.

December 8 - 10, 1969

AGENDA/TABLE OF CONTENTS

Monday Morning, Dec. 8, 1969

8:30-9:00 a.m.	Registration, Building 1222	
9:00-9:20 a.m.	Welcome	E. M. Cortright, Director, Langley Research Center
	Introduction	K. Thom, NASA Headquarters

9:20 a.m.-12:30 p.m. - Chairman: G. R. Seikel, NASA Lewis Research Center

A. PLASMA ACCELERATION

MPD Arcs

2:30-4:45 p.m. - Chairman: R. V. Hess, NASA Langley Research Center

G. ION AND MOLECULAR GAS LASERS

4:45-5:30 p.m. - Discussion Provocateur: R. G. Jahn, Princeton University

Open discussion on the topic "MHD and Plasma Physics - What Has Been Done, How Do We Stand, and Where Are We Heading?" In order to give as many as possible a chance to have their say, participants are asked to organize their initial statements and keep the time within a few minutes.

5:30-7:30 p.m. - Social Hour and Dinner (At Langley - busses will return to the motel after dinner.)

Wednesday Morning, Dec. 10, 1969

9:00 a.m.-12:30 p.m. - Chairman: G. P. Wood, NASA Langley Research Center

H. PLASMA-FOCUS, θ-PINCH, AND LASER-PRODUCED PLASMAS

12:30-1:30 p.m. - Lunch

Wednesday Afternoon, Dec. 10, 1969

1:30-4:30 p.m. - Chairman: P. W. Huber, NASA Langley Research Center

I. FUNDAMENTAL PLASMA PROBLEMS

PULSED ELECTROMAGNETIC GAS ACCELERATION: ACCELERATION PROCESSES IN QUASI-STEADY ARCS

R. G. Jahn, W. Von Jaskowsky, and K. E. Clark
Department of Aerospace and Mechanical Sciences
Princeton University, Princeton, New Jersey

(NGL 31-001-005)

A series of basic experiments has demonstrated that pulsed plasma accelerators can attain quasi-steady operation in a few tens of microseconds when provided with suitably protracted and synchronized inputs of driving current and mass flow.[1-5] This quasi-steady mode is characterized by stationary, diffuse discharge current patterns, constant terminal voltage, and constant exhaust velocity in a range encouraging propulsion application. Such devices are thus of interest both as pulsed plasma thrusters, and as laboratory simulators of the corresponding steady flow accelerators in power ranges where the latter cannot be conveniently studied in steady operation.

For example, Fig. 1 shows a schematic diagram of a quasi-steady accelerator employing a coaxial electrode configuration like that of the conventional magnetoplasmadynamic arc. Mass flow is provided by a gasdynamic shock tube which can very rapidly produce a high pressure reservoir behind suitable injector orifices. Arc current is derived from an array of capacitors and inductors which, depending on the particular configuration, provide rectangular pulses from 4000 amp x 600 μsec to 140,000 amp x 20 μsec.[6-8] The corresponding range of arc power--100 kW to 100 MW--is commensurate with relatively large arc chamber dimensions, which in turn permits more detailed study of the discharge structure than would be possible in smaller scale facilities.

A considerable variety of diagnostic studies have been performed in this facility and in other related apparatus involving Kerr-cell photography, electric and magnetic probing, velocity field mapping, spectroscopy, laser interferometry, and terminal measurements of current, voltage and mass flow. From these an instructive, yet incomplete, picture of the arc operation begins to emerge. Figure 2 shows a series of Kerr-cell photographs of arc luminosity at a given current for three different mass flows: one matched to the current value in terms of the classical MPD arc criteria, the others representing conditions of mass "starvation" and "overfeed," respectively. The importance of matching the mass flow to the arc current is demonstrated here and in many other experiments,[2] most notably in a tendency for underfed arcs to erode electrode and insulator material.

Figure 3a displays the distribution of current within a 17,500 amp argon arc as determined by magnetic probing. Two particularly significant features are the participation of the entire

cathode surface in the discharge, which should minimize the erosion of that surface, and the rather small protraction of the current pattern downstream of the anode orifice in contrast to the experience with external field MPD accelerators.[9-12] Figure 3b shows contours of floating potential for the same arc operation. Roughly, this pattern consists of four domains of significant potential drop: (a) a 10—20-volt anode fall, (b) a 20-volt cathode fall, (c) a drop roughly equal to the ionization potential across the injected gas jets, and (d) a 100-volt envelope around the cathode. Of these, it is the last which dominates the potential pattern, and probably holds the key to the performance range and efficiency of this type of accelerator.

Time-of-flight velocity measurements made downstream with biased double probes yield values inconsistent with any simple electrostatic acceleration model based on the potential patterns.[13] For the sample case of Fig. 3, centerline ion speeds of the order of 25,000 m/sec are found, which imply ion energies of some 150 eV, and are therefore far above the difference between the anode and downstream plasma potentials, far above the Alfvén critical value,[14] and, in fact, comparable to the full interelectrode potential. Apparently some complex but effective electromagnetic-electrothermal conversion process functions within or just downstream of the cathode potential envelope. Small wedges placed in this flow indicate that it is substantially supersonic, and that the ion temperature is of the order of 10 eV.

While the full import of these various observations is not clear, the prognosis for efficient gas acceleration by this quasi-steady technique seems favorable. Repetitive pulse operation of thrusters of this type should combine the advantages of the high-power arc operation with tolerable mean power requirements and variable thrust capability via duty-cycle adjustment.[15] Systems aspects of this concept, including the major problems of power-conditioning and mass injection are also under basic study in this program, along with the development of suitable techniques for assessing the performance of thrusters of this type.[16]

References

1. Clark, K. E. and Jahn, R. G., "Quasi-steady plasma acceleration," A.I.A.A. Paper 69-267 (1969). Also A.I.A.A. Journal, February 1970.

2. Clark, K. E., "Quasi-steady plasma acceleration," (Ph.D. dissertation), Department of Aerospace and Mechanical Sciences Report No. 859, Princeton University, Princeton, N. J., May 1969.

3. Eckbreth, A. C. and Jahn, R. G., "Current pattern and gas flow stabilization in pulsed plasma accelerators," A.I.A.A. Paper 69-112 (1969). Also A.I.A.A. Journal, January 1970.

4. Eckbreth, A. C., "Current pattern and gas flow stabilization in pulsed plasma accelerators," (Ph.D. dissertation), Department of Aerospace and Mechanical Sciences Report No. 857, Princeton University, Princeton, N. J., December 1968.

5. Eckbreth, A. C., Clark, K. E., and Jahn, R. G., "Current pattern stabilization in pulsed plasma accelerators," A.I.A.A. Journal 6, 11, 2125-2132 (1968).

6. Wilbur, P. J. and Jahn, R. G., "Energy transfer from a pulse network to a propagating current sheet," A.I.A.A. Paper 69-113 (1969). Also A.I.A.A. Journal, January 1970.

7. Wilbur, P. J., "Energy transfer from a pulse network to a propagating current sheet," (Ph.D. dissertation), Department of Aerospace and Mechanical Sciences Report No. 846, Princeton University, Princeton, N. J., September 1968.

8. Black, N. A., "Dynamics of a pinch discharge driven by a high-current pulse-forming network," (Ph.D. dissertation), Department of Aerospace and Mechanical Sciences Report No. 778, Princeton University, Princeton, N. J., May 1966.

9. Schneiderman, A. M. and Patrick, R. M., "Axial current distribution in the exhaust of the magnetic annular arc," A.I.A.A. Journal 5, 2, 249-253 (1967).

10. Cann, G. L., Harder, R. L., Moore, R. A., and Lenn, P. D., "Hall current accelerator," Electro-Optical Systems, EOS Report 5470-Final, (February 1966).

11. Powers, W. E., "Measurements of the current density distribution in the exhaust of an MPD arcjet," A.I.A.A. Journal 5, 545-550 (1967).

12. Fradkin, D. B., Blackstock, A. W., Roehling, D. J., Stratton, T. J., Williams, M., and Liewer, K. W., "Experiments using a 25 kW hollow cathode lithium vapor MPD arc jet," A.I.A.A. Paper 69-241 (1969).

13. Jahn, R. G., Clark, K. E., Oberth, R. C., and Turchi, P. J., "Acceleration patterns in quasi-steady MPD arcs," A.I.A.A. 8th Aerospace Sciences Meeting, New York, January 1970.

14. Alfvén, H., "Collision between a nonionized gas and a magnetized plasma," Reviews of Modern Physics 32, 10, 710-713 (1960).

15. Ducati, A. C. and Jahn, R. G., "Repetitively-pulsed quasi-steady vacuum MPD arc," A.I.A.A. 8th Aerospace Sciences Meeting, New York, January 1970.

16. Jahn, R. G. et al., "Pulsed electromagnetic gas acceleration," Princeton University Aerospace and Mechanical Sciences Report No. 634m, July 1969.

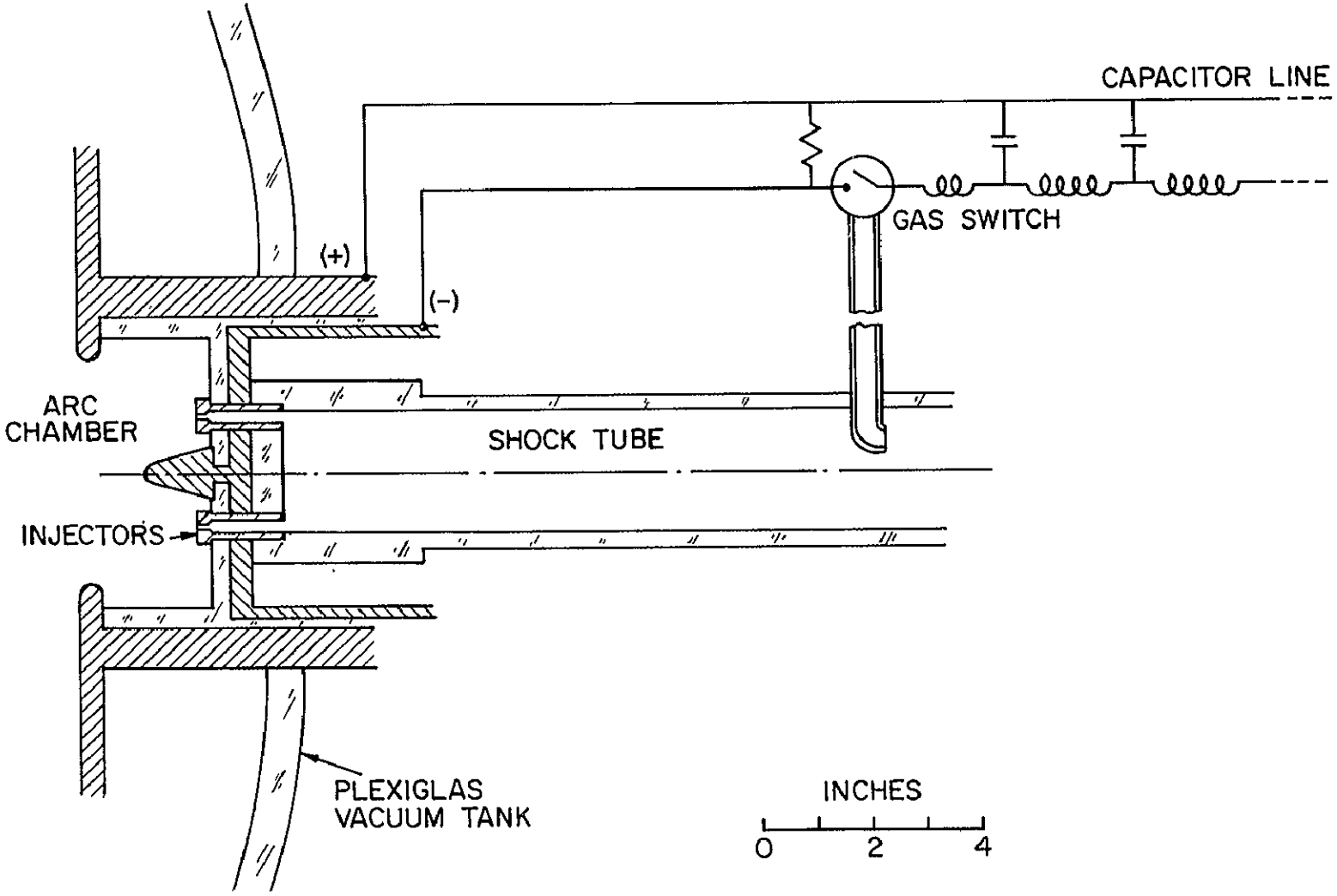
CAPACITOR LINE
GAS SWITCH
(+)
(-)
ARC
CHAMBER
SHOCK TUBE
INJECTORS
PLEXIGLAS
VACUUM TANK
INCHES
0
2
4

FIGURE 1

$\dot{m}$ = 1.2 g/sec

$\dot{m}$ = 5.9 g/sec

$\dot{m}$ = 36.9 g/sec

EXHAUST LUMINOSITY PATTERNS AT 17.5 kA

FIGURE 2

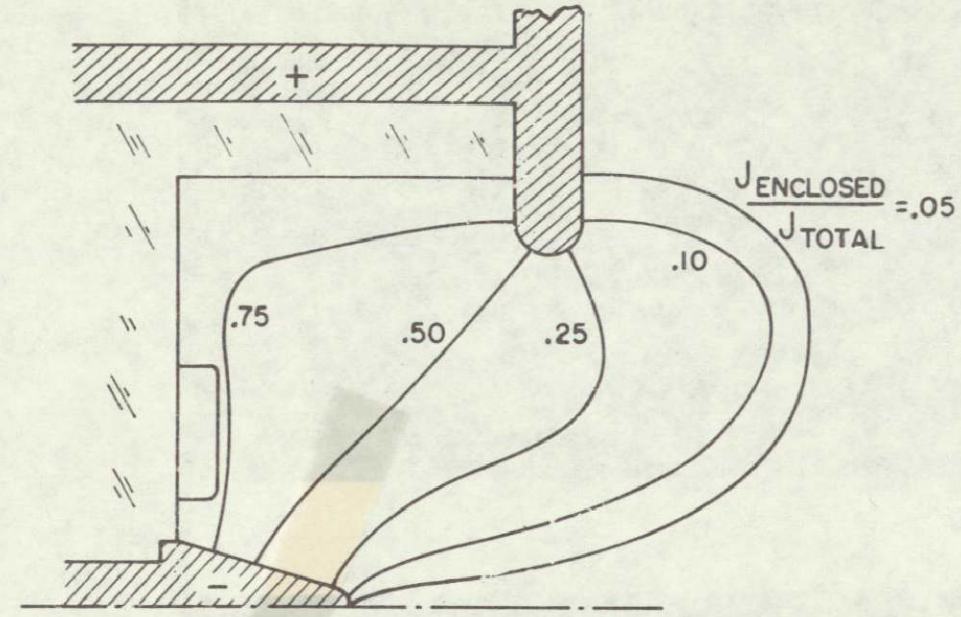

a) CURRENT DISTRIBUTION

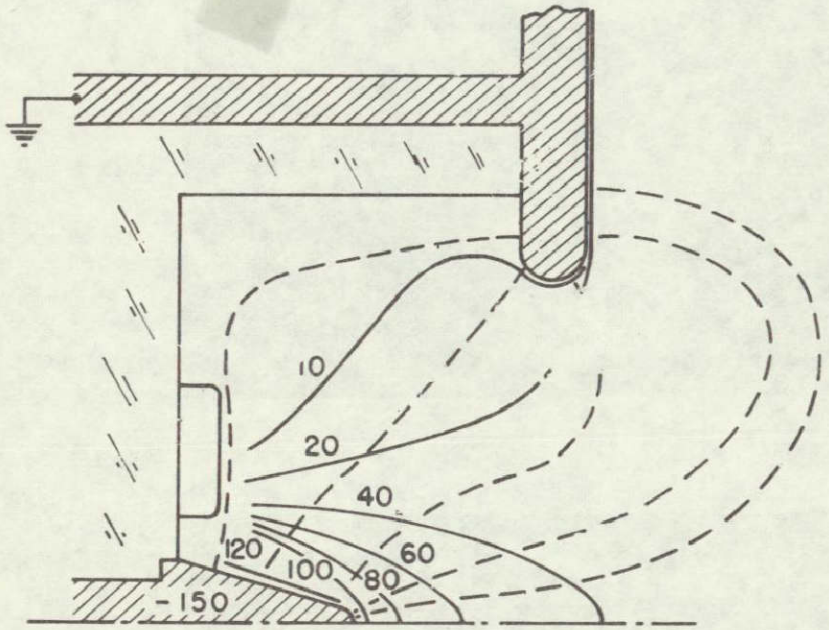

b) EQUIPOTENTIAL CONTOURS

CURRENT AND POTENTIAL PATTERNS IN
QUASI-STEADY MPD ARC
J = 17.5 kA
$\dot{m}$ = 5.9 g/sec

FIGURE 3

DYNAMIC CURRENT-VOLTAGE CHARACTERISTICS OF A PULSED MEGAWATT MPD-ARC

by Charles J. Michels, NASA Lewis Research Center

The investigation of the voltage-current (V-I) characteristics of a pulsed, megawatt, MPD-arc is described for various amplitudes of auxiliary magnetic field (0.5 to 2.0 T). The pulsed arc is powered by a crowbarred capacitor bank and the data is dynamically gathered for a hundred microseconds after the voltage and current traces have stabilized. The tungsten cathode is heated to emitting condition just prior to powering the arc. A puff of argon or nitrogen gas is admitted into the evacuated arc chamber and allowed to distribute prior to powering the arc. From cold flow transient pressure traces, the time to power the arc is determined, as well as the chamber pressure at firing time. The experiments were operated for two different weight flows through the arc annulus, 6.0 g/sec and 1.5 g/sec.

The gross physical processes, such as the V-I characteristics, impedances, and plume characteristics described in this paper, are part of the means of identifying these arcs in relation to the varied forms of arcs in the literature. This paper extends the knowledge to the 0.2-2.5 megawatt level. Spoking instabilities are not noted for these power levels and time durations.

The V-I characteristic obtained for each shot shows a positive-sloped, curvilinear trend. A series of these characteristics, for currents from 2 to 14 kA, shows them to be dynamic characteristics (as defined in Ref. 1) and not connected curves. A static characteristic curve can be estimated from the family of dynamic characteristic curves. As the magnetic field is increased, the dynamic curves, although still curvilinear, tend to be more identifiable as part of a connected curve. For instance, at 20 kG, the dynamic curves are almost part of the estimated linear static characteristic curves. That is, the increased field has made the arc system almost resistor-like and the short duration pulsed operation is sufficient to obtain static V-I characteristics. Positive sloped static characteristics for higher arc current cases are observed as suggested in Ref. 1.

REFERENCES

1 J. D. Cobine, "Gaseous Conductors," Dover Publ., Inc., 1958, p. 344-52.

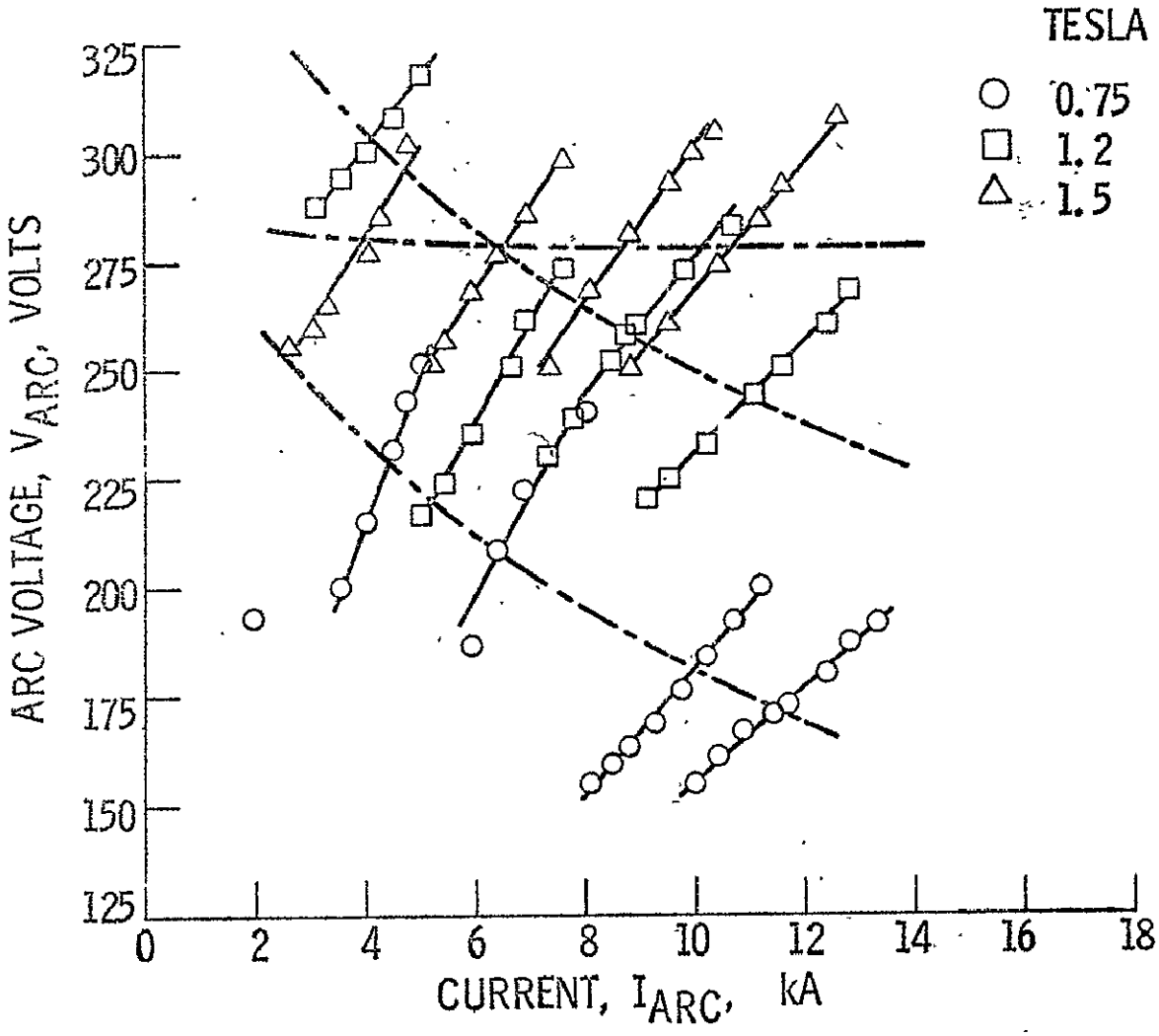

Figure 1. - Dynamic current-voltage characteristics of a hot cathode, nitrogen MPD-arc.

EXPLORATORY ELECTROMAGNETIC THRUSTER RESEARCH

Adriano C. Ducati
Plasmadyne, a division of Geotel, Inc.
Santa Ana, California

(NAS 1-9297)

Recent work[1, 2, 3] has been concerned with obtaining an improved understanding of MPD thruster operation including pulsed (quasi-steady)[4, 5] as well as continuous arc devices. A large fraction of the effort has focussed on evaluating the effect of ambient conditions on the measured performance. It has been demonstrated that ambient gas is entrained in a region of the plume that forms a part of the arc path and can therefore be subject to electromagnetic forces.

Using a large insulating vacuum tank it was found to be possible to detect the flow of charged particles in the plume utilizing a large coil wrapped around the test chamber to introduce changes in the ambient magnetic field strength. The field deflects portions of the plume which carry charged particles (as distinguished from excited particles). The phenomenon was observed in the insulated tank as well as a nonmagnetic metal tank, indicating that large scale current flow paths in the plume do not depend on a return flow path through the tank. Other observations[6] show evidence of a flow of electrons returning in an annular path to the anode with sufficient intensity to cause severe heating of the exterior anode face. These results provide evidence that a significant fraction of the arc current follows a path in the luminous plume outside of the thruster.

To evaluate the rate of entrainment of ambient gas in the excited portion of the plume, tests were made with hydrogen as the working fluid and with an additional flow of hydrogen or some other gas introduced directly into the test chamber. It was found that the arc voltage is strongly dependent on both the ambient pressure and the type of ambient gas used (although a constant arc chamber pressure is maintained, and the propellant gas is not changed). Also, the color of the plume depends on the environmental gas (apparently even at the center of the jet).

These observations suggest that the jet mixes very rapidly with the surrounding gas, and strongly indicate that a large fraction of the arc energy is expended on ambient gas mixed with propellant in the plume. The rapid mixing is confirmed by another study[6] in which detailed surveys were made to determine the flow pattern in the vicinity of a small jet in a vacuum chamber. This work also indicates that more rapid entrainment rates can be expected as pressure is reduced as long as continuum flow conditions predominate. A clear cut evaluation of entrainment effects appears to require very precise measurement of thrust for a range of ambient pressures in the molecular flow regime. For steady operation this is only possible with very small thrusters; and has not yet been accomplished, even though a sizable effort has been expended toward this end. It is concluded that we are not yet able to predict the performance of continuous (steady) MPD thrusters in space from laboratory tests.

On the other hand, quasi-steady MPD thrusters appear to offer a better opportunity for obtaining performance data in ambient conditions approaching those in space. The test chamber can be thoroughly evacuated before triggering a pulse. No interference will be felt until the pulse front reaches the chamber wall and is reflected back to the vicinity of the thruster. Interference free periods hundreds of microseconds long can be obtained in this manner in test chambers of moderate size. During this interval the thrust level can be high enough to produce an impulse that can be readily measured.

Another important reason for investigating performance in the quasi-steady mode is that MPD thrusters show progressively better performance as the power level is increased. Since much higher power levels can be handled in momentary pulses than would be feasible with steady operation, strong interest has developed in determining the performance attainable with quasi-steady MPD thrusters. However, performance has not yet been determined accurately enough to establish the degree of correlation with theoretical models or with steady state performance.

Work has been initiated for determining the performance of quasi-steady arc jets operating at energies as high as 20,000 joules per pulse. These devices typically operate for a large fraction of a millisecond and at power levels measured in megawatts during a pulse. The investigation is concentrating on the use of solid and liquid propellants which are vaporized by the action of the arc. A critical design problem which is being actively studied is the choice of a feed system that will provide propellant at the proper rate to match the power pulse, and avoid wasteful expenditure of propellant. The problem is complex because it involves the power pulse shape and the electrode design as well as the propellant properties and the propellant feed system itself.

Some refined instrumentation is required to accurately determine the performance of quasi-steady thrusters. For precisely measuring small values of thrust, a torsional ballistic pendulum is being developed. The complete pulse generating circuit is mounted on the thrust platform so that the connecting leads can be reduced to instrumentation and control lines and light power leads for recharging the condensers. Other equipment used includes a high speed motion picture camera to record the growth and tail-off of the plume, a spectroscope which is used to obtain data on the material in the plume by repeatedly exposing the same film during successive pulses until an adequate record is obtained, and various probes for determining conditions in the plume.

An effort will be made to establish trade-off factors which will permit a reasonable choice to be made of design variables such as thruster geometry, size, duty cycle, and propellant; and tests will be made at a range of vacuum levels to see if performance is affected by ambient pressure to a measurable degree.

REFERENCES

1. Ducati, A. C., Jahn, R. G., Muehlberger, E. and Treat, R. P., "Exploratory Electromagnetic Thruster Research," Giannini Scientific Corporation Annual Report TR 117-1513, NASA CR 62047 (Feb. 1968).

2. Ducati, A. C., Jahn, R. G., Muehlberger, E. and Treat, R. P., "Exploratory Electromagnetic Thruster Research - Phase II," Plasmadyne Final Report FR-059-1513, NASA CR TR-105204 (June 1969).

3. Ducati, A. C., "Exploratory Electromagnetic Thruster Research - Phase III," Plasmadyne Progress Report PR 809-9297 (Aug. 1969).

4. Eckbreth, A. C., Clark, K. E. and Jahn, R. G., "Current Pattern Stabilization in Pulsed Plasma Accelerators," AIAA J. 6, 2125 - 2132 (Nov. 1968).

5. "Quasi-Steady Plasma Acceleration," Ph.D. Thesis of Kenn E. Clark, Report No. 859, Department of Aerospace and Mechanical Sciences, Princeton University (May 1969).

6. Ducati, A. C., "Losses in Plasma Acceleration," Plasmadyne Final Report FR 109-1743 (Oct. 1969).

DESIGN OF A QUASI-STEADY MPD THRUSTER AND SPECTROSCOPIC VELOCITY MEASUREMENTS

J. M. Hoell, J. Burlock, and O. Jarrett
NASA, Langley Research Center
Hampton, Va.

Performance data obtained for d.c. MPD thrusters during the past few years have indicated an efficiency increase with power. To verify and exploit this trend, the power applied to d.c. arcs has been extended to the limit of conventional electrode capability and, even more important, beyond the capacity of forseeable space-rated power supplies. The short pulse mode of operation (i.e. pulses of 1 to 10 μs duration) which has been studied by a number of laboratories solves the electrode problems and when repetitively pulsed permits use of average powers well below space-rated power supply capabilities. However, this mode of operation has had problems concerning proper matching of the propellant distribution with the short current pulse.

An alternate mode of operation which takes advantage of the increasing efficiency with power associated with the true steady state MPD arc and with repetitive pulsing provides the low average input power condition of the short pulsed mode is a mode of operation, designated as "quasi-steady" (Q.S.)[1]. In this mode a high current pulse and a propellant pulse are applied for periods of time which are long enough to allow important parameters to reach steady state, i.e., ∿ 1 msec. This note will describe research which has been underway at Langley during the past few months to develop a Q.S. MPD thruster and to spectroscopically measure the velocity distribution in a Q.S. thruster.

The MPD arc used during these tests is a hollow cathode device which has been operated at Langley for a number of years. The cathode is a barium impregnated tungsten tube 2 inches long by one-quarter inch O.D. by one-eighth inch I.D. The anode is a copper-tungsten ring with a 1 inch I.D. and 32-1/16 inch O.D. gas-feed holes around the circumferance. A block diagram of the electrical circuit is shown in figure 1. The Q.S. power supply is coupled to the electrodes through an impedance matching transformer designed to work into a load of 0.14 Ω. Operating into a properly matched load this power supply is capable of a square wave output of 1 megawatt for 1 msec with a rise and fall time of approximately 50 μs. Using the circuit shown in figure 1, the arc can be operated with or without a D.C. current and with or without an external B-field before applying a Q.S. current pulse. The time control block consists of several time-delay generators which are used to synchronize the Q.S. current pulse with the spectrograph shutter, the D.C. arc, and the gas pulse.

In developing a Q.S. thruster, the first component considered was the Q.S. power supply. Of equal importance, however, is the gas-feed system and the region of gas injection. Using the present MPD arc, gas can be injected from three different positions: (1) through the hollow cathode, (2) through the anode, and (3) between the electrodes. Tests have been made using the first two methods. A fast-acting gas value capable of producing a gas pulse with a rise time of ∿ 100 μs and a duration of several millisec. was used to introduce the gas into the arc chamber. The rise time of gas pulse for both

cathode and anode injection was approximately 500 μs. The light intensity produced by the 4806.017 Å line of argon was used as a measure of the effectiveness of gas injection from a particular position. It was found that when the propellant was injected through the anode, the light intensity from the 4806.017 Å line increased by approximately a factor of 5 over that for cathode injection. This suggests that for the latter case most of the gas was missing the discharge. A similar test is planned for injection between the electrodes.

It is of some concern in the development of a Q.S. thruster whether or not "quasi-steady" thermionic emission from the cathode exists during the current pulse as this relates to cathode life time, efficiency, and duplication of the steady MPD mode. As a check on the emission from the cathode, experiments were made in which the pulsed current and voltage was measured for first a hot cathode and then a cold cathode. For the hot cathode case the Q.S. pulse was applied $\sim$ 20 millisec. after a d.c. arc of 40 amps used to heat the cathode was extinguished. Figure 2 shows the current and voltage traces for these two conditions as well as for the condition of hot and cold cathode with $B = 620$ g. It can be seen that even for a pulse current of only 2000 A there is no measurable difference between a hot and cold cathode for the same external field; there is, however, considerable difference between the case of $B \neq 0$ and $B = 0$.

A major part of the Q.S. program at Langley consists of spectroscopically measuring the exhaust velocity from a Q.S. thruster. For d.c. operation accurate measurements are relatively straightforward using a spectrograph with a resolution of 0.03 Å or better.[2] For pulsed operation the major obstacle is insufficient light for good exposure for each pulse; consequently, for the pulsed powers that have been used to date, it has been necessary to use from three to six pulsed exposures per plate. The preliminary results that have been obtained have qualitatively demonstrated that just as the region of propellant injection is important (see above) so is the uniformity of gas distribution. For example, figure 3 shows a radial distribution of the axial velocity which exhibits a radial gradient in axial velocity. The assymmetry in the axial velocity corresponds to an assymmetry that has been measured in the pulsed gas distribution. The unfavorable propellant distribution is due to the use of a single valve to inject gas from one side of the anode. To eliminate this nonuniformity in the velocity distribution a more uniform gas injection system is being designed; extensive surveys of velocity distribution will be made for this system.

References

1. Clark, Kenn E.: Quasi-Steady Plasma Acceleration. Princeton University Report 859, May 1969.

2. Kogelschatz, U.: Doppler Shift Measurements of Axial and Rotational Velocities in an MPD Arc. AIAA Paper 69-110 (1969).

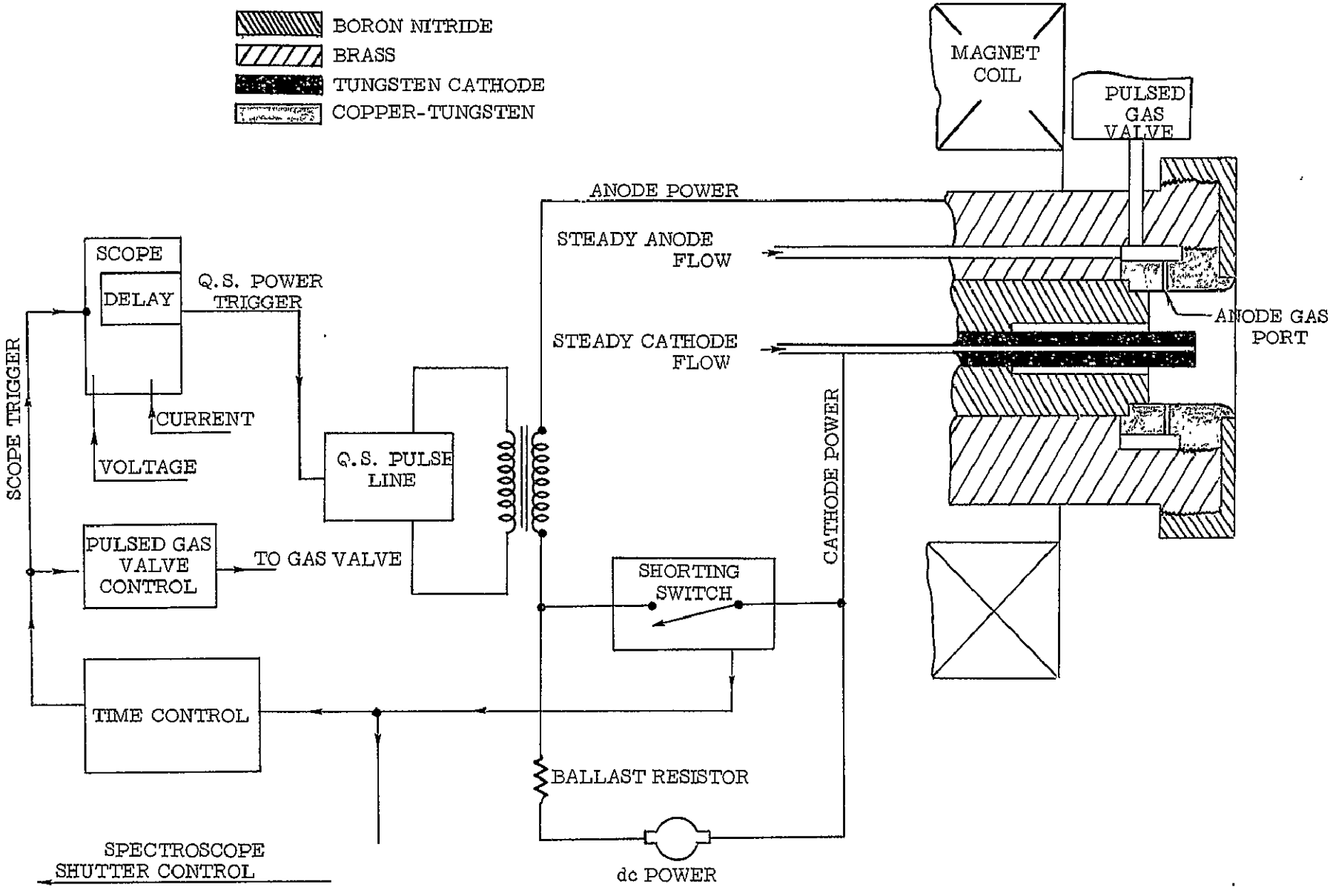

Figure 1. - Schematic of Q. S. thruster system

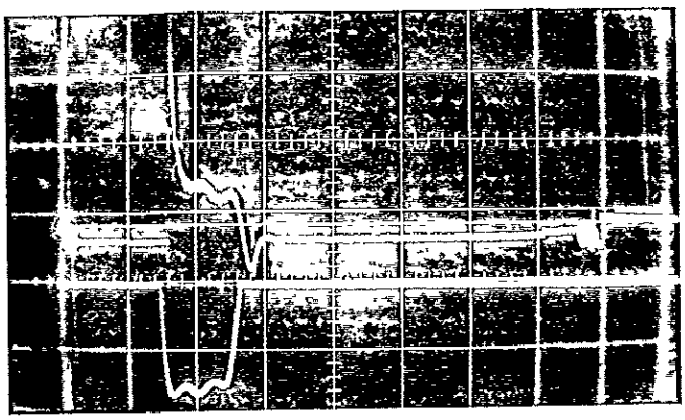

a. Hot cathode, B = 0

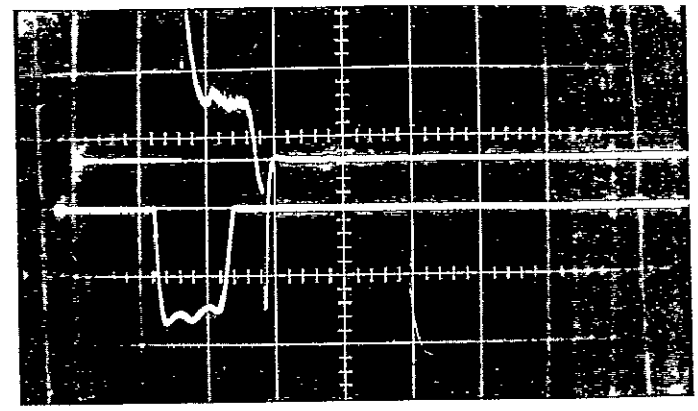

b. Cold cathode, B = 0

Upper trace : 100 V/cm
Lower trace : 2000 A/cm
Time sweep : 1 ms/cm

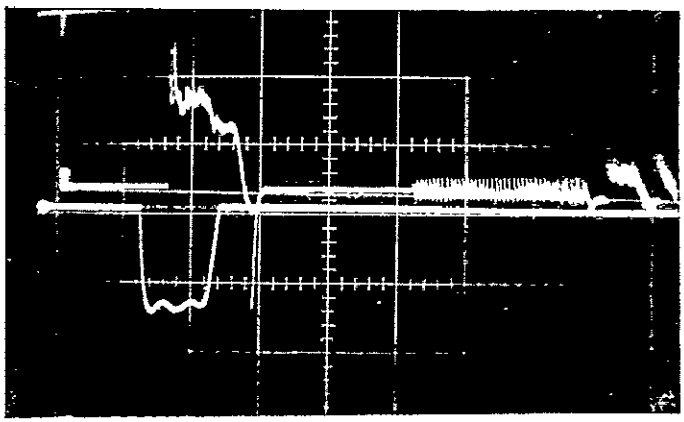

c. Hot cathode, B = 620 g

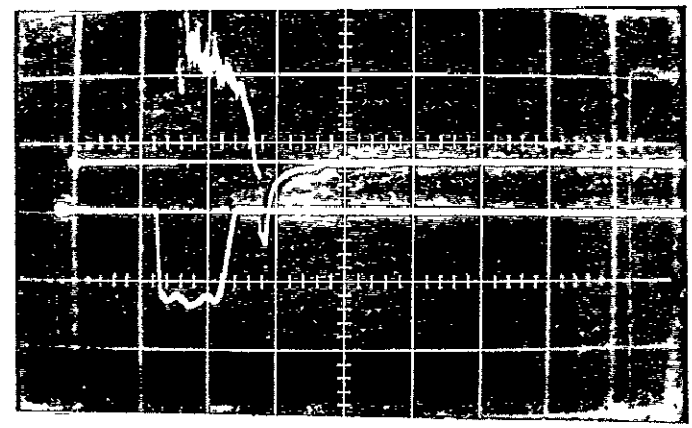

d. Cold cathode, B = 620 g

Figure 2. - Pulsed current and voltage

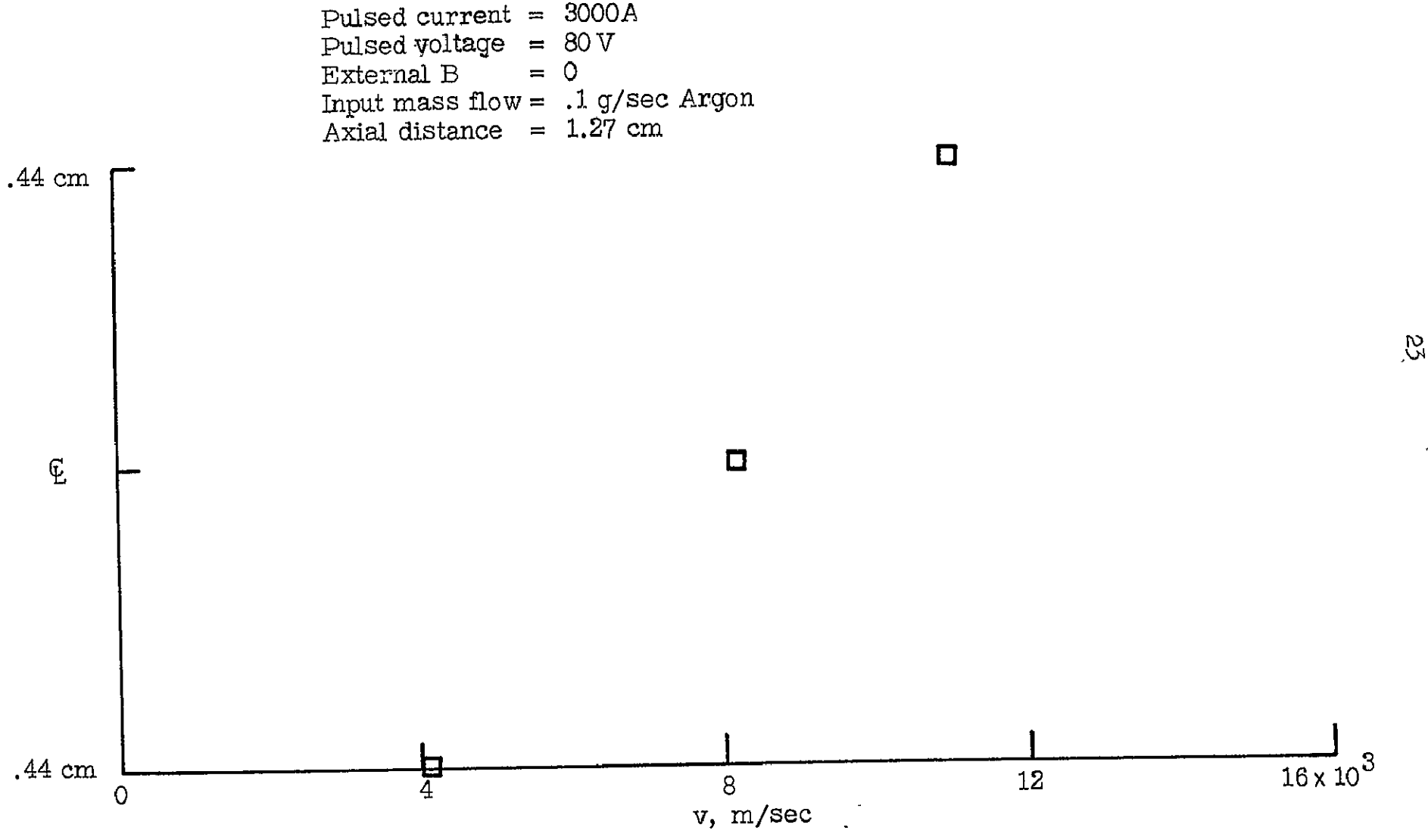

Figure 3. - Radial profile of axial velocity

SPECTROSCOPIC STUDY OF ION-NEUTRAL COUPLING IN PLASMA ACCELERATION*

A. C. Malliaris and D. R. Libby

Applied Technology Division, Avco Corporation,
Wilmington, Massachusetts

The acceleration of a partially ionized gas by electromagnetic means might be quite inefficient, if the coupling between the ions and the neutrals, for momentum transfer, is weak. Poor efficiency may arise from large velocity disparities between ions and neutrals in the same plasma flow. In the work reported here the absence or presence of a sufficiently strong coupling is generally revealed by velocity disparities determined spectroscopically, for several species, both ionic and neutral. Velocities are determined by Doppler shift measurements of selected spectral lines. Such lines are obtained not only from species which occur naturally in the main propellant, but also from any desired additives.

Results regarding two different situations are being obtained, from experiments where two basically similar axisymmetric configurations operate under significantly different conditions. In the first case, a large disparity in ion-neutral velocities is observed, while in the second case, the said disparity disappears. In this second case, the common ion-neutral velocities are in good agreement with the center-of-mass velocity, as determined independently from measurements of motionally induced potentials in the flow, as well as from measurements, of the local momentum and mass fluxes.

A satisfactory interpretation of the results is obtained when the calculated mean free path for momentum exchange is compared with a typical dimension of the electromagnetic acceleration region.

A detailed paper will be presented at the AIAA 8th Aerospace Sciences Meeting, New York, N. Y., January 1970.

*Work supported by NASA/LaRC Contract NAS 1-9298

NEUTRAL DENSITY MEASUREMENTS IN AN NH_3 MPD ARC*

Per Gloersen, General Electric-Space Sciences Lab, King of Prussia, Penna.

The program described in this paper was to determine experimentally the range of applicability of a vacuum ultraviolet absorption spectrometry technique to detecting neutral atom and molecule constituents in the exhaust stream of an MPD arc jet. Specifically, emphasis was on measuring the nitrogen atom densities in an ammonia-fueled MPD arc jet exhaust. To date, no other techniques have been established for measuring this quantity, possibly important for the corroboration of arc jet propulsion efficiency figures obtained from thrust and input mass flow measurements. An analysis is presented for the reduction of transmissivity data in terms of nitrogen atom flow rates. The main purpose of this program was to establish the experimental technique for this new application; more systematic use of this technique to help determine the operating characteristics of the NH_3 MPD arc would be undertaken in subsequent programs.

The light source used in these studies consisted of an air-cooled quartz capillary through which nitrogen flowed. A 250 micron slit was placed at the vacuum chamber end of this tube to permit higher operating pressures in the tube than are maintained in the vacuum test chamber. Excitation is achieved in a tuned cavity driven by a 2.145 KMC, 125 watt oscillator. The background light source produced a 1200 Å nitrogen atom line received in the spectrometer, reflected from a freshly coated mirror, some 15 times brighter than that received directly from the arc in ammonia; thus, meaningful absorption measurements were readily accomplished.

The arc was constructed according to plans supplied by Langley Research Center and is identical with one of the configurations used in a number of experiments. Absorption measurements were made at a downstream position in the arc plume about 52 cm from the external nozzle (see Figure 1). The flow range covered was from 6-18 mg/sec. The arc was operated at 300 amperes and 63-80 volts dc, depending on the flow rate. The magnetic field was maintained at 5000 gauss for all of the runs. Observed transmissivity (I/I_o) of the arc under these conditions is indicated in Figure 2, along with similar data for the cold ammonia flow with the arc power turned off.

Under the conditions of the present experiment, the background emission line is much narrower than the absorption line in the arc plume, principally because of the symmetrical Doppler broadening due to the arc plume spreading. Therefore, the only useful part of the absorption coefficient, $k(\nu)$, is at the line center, which we shall call k_o. Thus, one can immediately write the expression for the integrated absorption as

$$I/I_o = e^{-k_o nL} \qquad (1)$$

Solving for the unknown, $$n = (1/k_o L) \ln (I_o/I) \qquad (2)$$

where, for a Doppler-broadened line,

$$k_o = \pi^{\frac{1}{2}} r_e \, cf\lambda_o/\bar{v}\tan\alpha,$$

and

$$r_e = 2.82 \times 10^{-13} \text{ cm},$$

$$c = 3 \times 10^{10} \text{ cm/sec},$$

$f = 0.35$, $\lambda_o = 1200$ Å, α is the half angle of spreading in the exhaust plume and $\bar{v}$ is the average axial velocity of the absorbing species in the plume. The total rate of flow of the absorbing species is given by

$$\dot{N} = nA\bar{v} = (\pi^{\frac{1}{2}}/16 \, r_e \, cf\lambda_o) \, \bar{v}^2 \, L\tan\alpha \ln (I_o/I) \qquad (3)$$

where the radius of the cross-sectional area A has been taken as L/4. α was taken to be 20^o, as defined by the arc position and baffle aperture. It should be noted, however, that the visual appearance of the arc plume was indicative possibly of a somewhat smaller angle. Based on Kogelschatz's results from his Doppler shift measurements in a similar arc, $\bar{v}$ for the nitrogen atom is taken to be 3×10^5 cm/sec. over the operating range covered here. Two things should be noted in this regard. First, the range of operating conditions in these experiments extended to lower flow rates than those of Kogelschatz; it is assumed that the constancy of the velocity noted by him extends also to the lower flow rates. Second, Kogelschatz's observations involve the luminous nitrogen atoms whereas these experiments involve the ground state atoms. In view of the short radiative lifetime of the atomic states, it is assumed that the excited atoms observed by him resulted from re-excitation in the exhaust plume as a consequence of the extended currents from the arc. It therefore seems reasonable to assume that the excited and ground state atoms are moving with the same average velocity.

Using these data and assumptions, Equation 3 can be evaluated for a number of different operating conditions. The results are shown in Figure 3. It can be seen that maximum fractional amount of ammonia observed in the plume was about 1.5% and that this fraction is almost independent of flow rate. The absolute accuracy of these results is no better than the ± 50% available for the oscillator strength, f, and depends also heavily on the assumed applicability of the value used for $\bar{v}$. Thus, if the velocity of the non-luminous nitrogen atoms were significantly higher than observed by Kogelschatz for the luminous ones, the role of these consituents could be converted from minor to major.

*Work performed under Contract No. NASI-8461

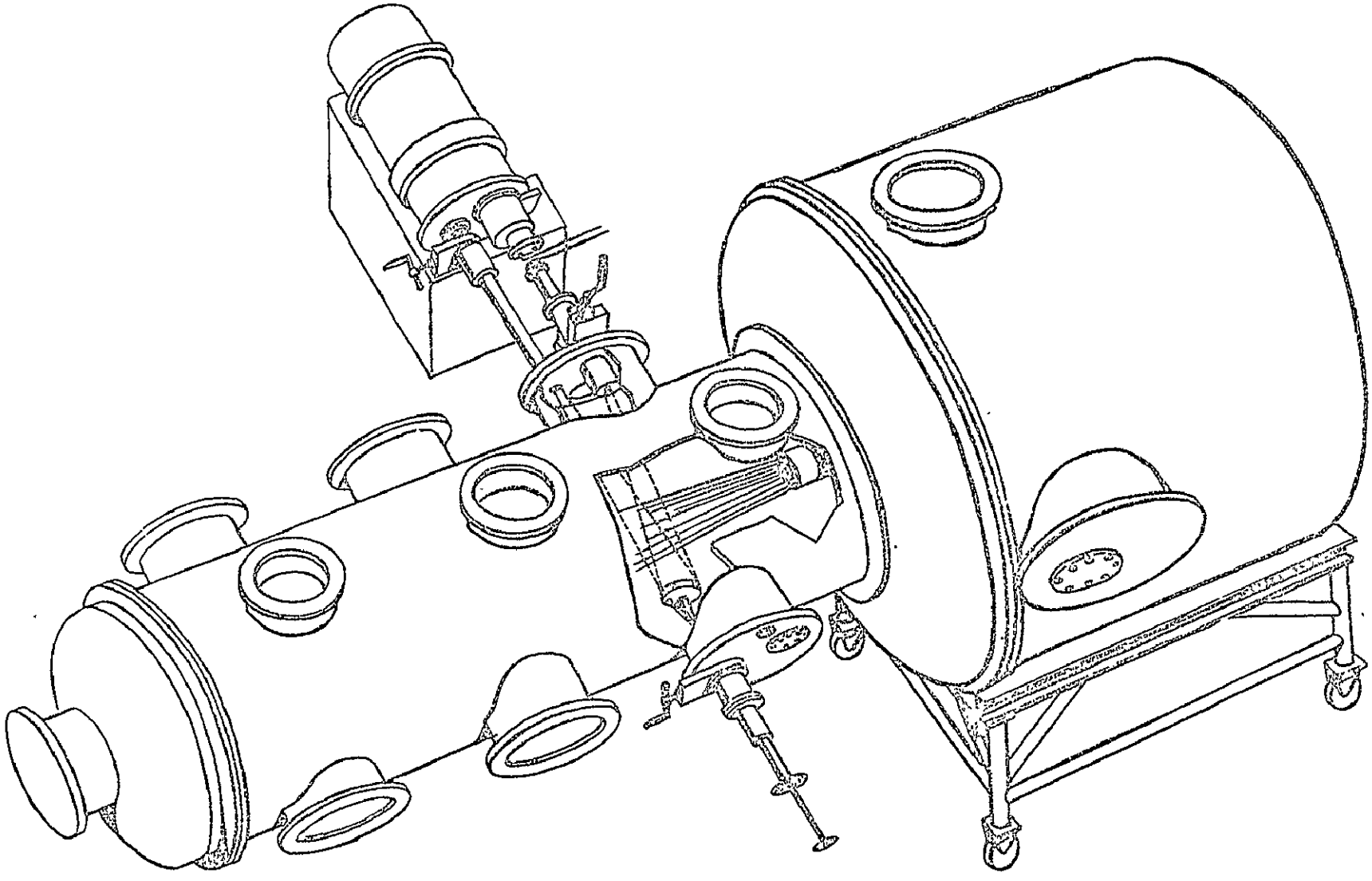

Figure 1. Optical Arrangement for Vacuum Ultraviolet Measurements

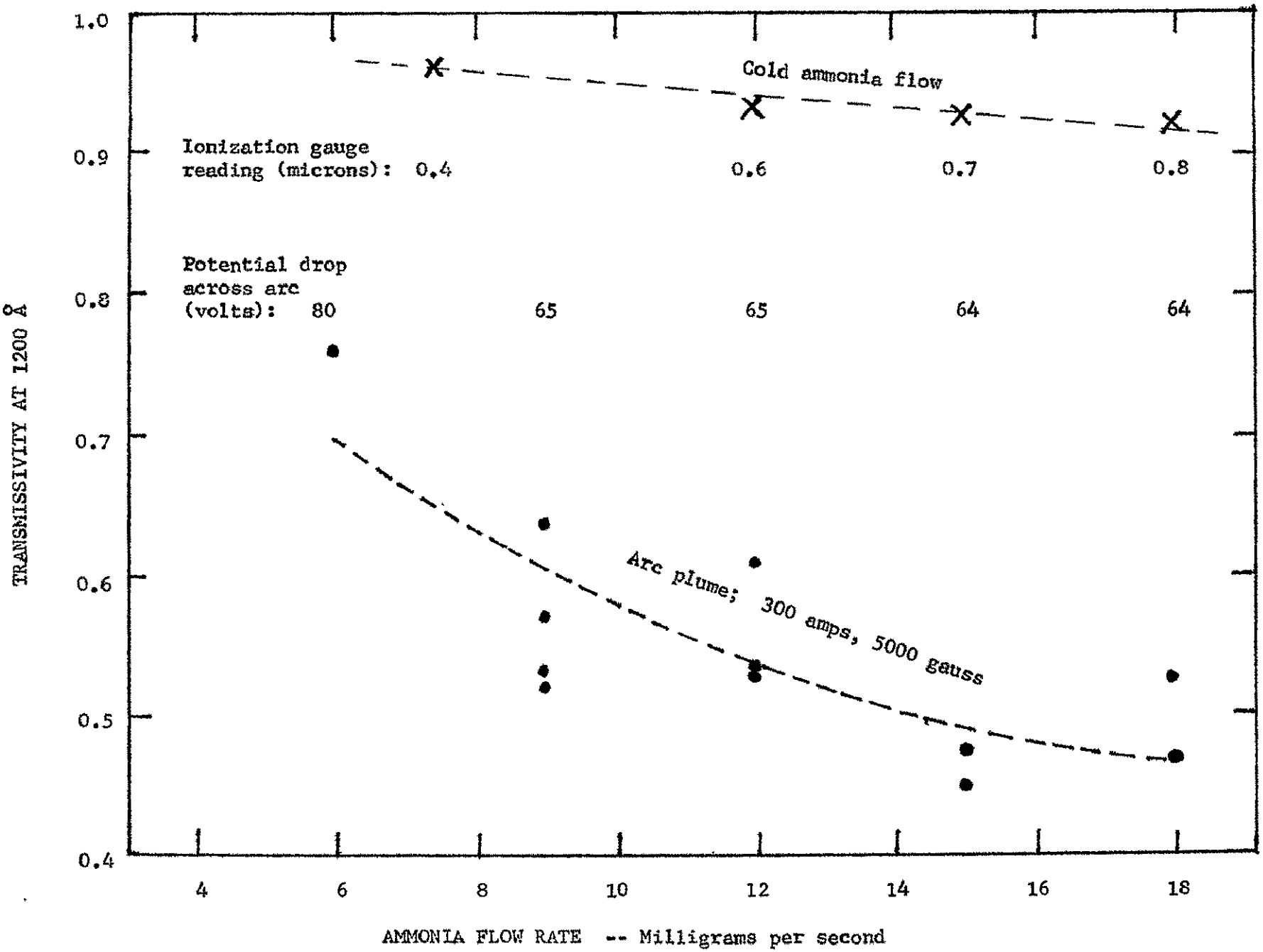
1.0
0.9
0.8
0.7
0.6
0.5
0.4
TRANSMISSIVITY AT 1200 Å
Cold ammonia flow
Ionization gauge reading (microns): 0.4 0.6 0.7 0.8
Potential drop across arc (volts): 80 65 65 64 64
Arc plume; 300 amps, 5000 gauss
4
6
8
10
12
14
16
18
AMMONIA FLOW RATE -- Milligrams per second

Figure 2.

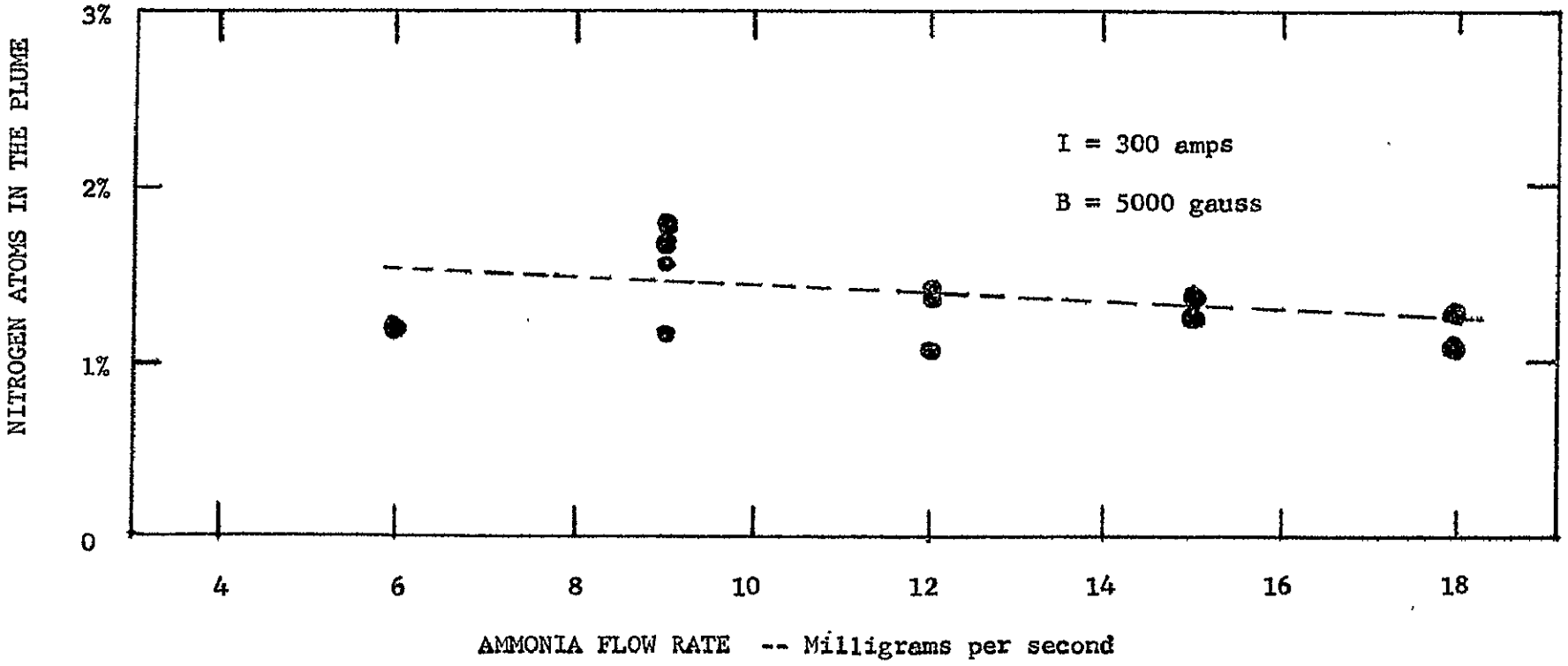

Figure 3. Fraction of ammonia molecules at the inlet appearing as nitrogen atoms in the plume, 52 cm downstream from the nozzle.

SUMMARY OF LEWIS MPD ARC THRUSTER PROGRAMS

by George R. Seikel, NASA Lewis Research Center

This presentation will briefly review the various phases of Lewis' MPD arc thruster program including: (1) low power (100 to 1000 W) radiation cooled thruster; (2) 30 kW radiation cooled NH_3 thruster; (3) spectroscopic exhaust diagnostic measurements; and (4) MPD arc spoke phenomena. The scope of this program has been to investigate the feasibility of building lightweight completely radiation-cooled long-life thrusters and to simultaneously perform diagnostic studies of the plasma processes with the aim of improving thruster performance. A low power thruster has been operated in a hands off life test of 638 hours, except for 11 intentional starts and stops. An automatic current control was used in this test, but with more recent cathode configurations no control appears necessary and no significant erosion has occurred during 100 hr. tests. The propellant yielding the highest performance is xenon but operation with many other propellants has been possible including a combination of H_2 and CO_2. Recently a lightweight thruster was constructed. This thruster has very low power radiation-cooled magnetics and starter circuits. Presently parametric tests of this thruster are in progress.

The present performance of the 30 kW NH_3 radiation cooled thruster is shown in an attached figure. This Lewis data shows both that the efficiency increases with arc power and that at constant power the specific impulse can be varied over a wide range. This thruster was developed and life tested for over 500 hrs. by McDonnell Douglas under contract to Lewis. It represents the first truly radiation cooled high power MPD arc thruster. The thruster is designed with adequate insulation between the anode and the magnet so that a radiation cooled permanent magnetic could be utilized. The anode heat loss (40 to 60% of the total power) is the major inefficiency in this thruster, and the requirement that this heat be radiated by the anode limits its power level to 40 kW. We are looking into the processes which affect the arc voltage particularly the way current attaches to the cathode, in the hope that by learning to control this we can raise the arc voltage to lower the anode losses while maintaining the current distribution that is presently yielding as thrust over 70% of the net power put into the plasma. Why the conversion of the net plasma power into thrust can be so efficient has been shown by our spectroscopic measurements in the exhaust. These show both that the exhaust can be primarily high velocity neutrals and that the acceleration takes place in the magnetic nozzle outside the physical thruster.

At present it is not clear whether the current spoke generally present in these thrusters is detrimental to performance. It does, however, greatly complicate theory and experiments to no clear advantage. Therefore, in addition to analytically and experimentally investigating spoke phenomena we are looking for ways to get rid of it. Preliminary tests with the low-power thruster for example indicate that use of inductors in series with an azimuthally segmented anode will eliminate the current fluctuations on the segments.

SPECIFIC IMPULSE VERSUS ARC EFFICIENCY

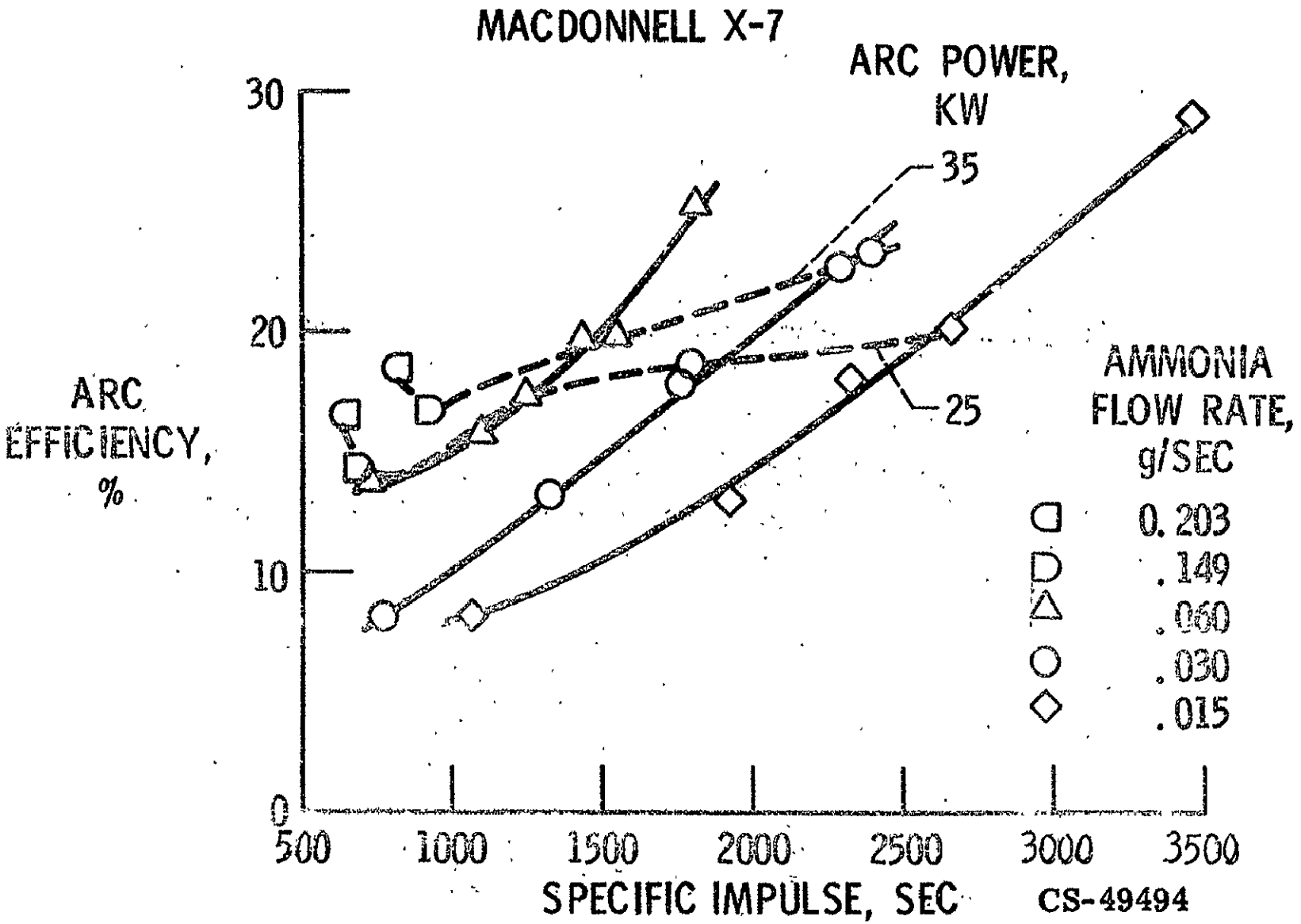

500 HOUR TEST OF A RADIATION COOLED MPD ARC THRUSTER

D. W. ESKER AND J. C. KROUTIL
MCDONNELL RESEARCH LABORATORIES
ST. LOUIS, MISSOURI 63166

The successful development of a MPD arc thruster to flight hardware status requires a demonstration of long term reliability. The work described represents an initial step towards this goal. Specifically, a 500 hour life test of a radiation cooled MPD arc thruster is described. The thruster, (Fig. 1), developed under contract to NASA, consisted of a radiation cooled anode-cathode-insulator assembly connected to a water cooled electromagnet. The design and performance characteristics of this thruster have been reported previously.[1] The test was conducted in a three foot diameter vacuum chamber at a background pressure of approximately 9.0×10^{-3} Torr with a propellant mass flow rate of ammonia of 30 mg/sec. Test instrumentation included arc voltage and current, magnet voltage and current, propellant flow rate, anode surface temperature, magnet heat transfer, and photographic observation of the interelectrode region.

The test was initiated with a propellant flow rate of 30 mg/sec., arc current of 560 amperes, and axial magnetic field at the cathode tip of 0.14 tesla. These conditions produced a specific impulse of 1770 seconds with an efficiency of 17.1 percent. The thruster operated in a high voltage mode condition for the majority of the run with only several hours of low mode operation at the start and end of the test. The arc voltage gradually increased from a value of near 55 volts early in the test to 64 volts after 425 hours. Photographs of the cathode electrode indicated that the voltage increase correlated closely with the formation of a nodule or tit at the tip of the conical cathode. This nodule left the cathode at t= 428 hours with a subsequent decrease in voltage, after which a new module began to form.

The test was voluntarily shut down after 508.5 hours for inspection of the thruster. An additional 45.5 hours was logged before the thruster was disassembled. The increasing voltage characteristic served to increase the thrust so that the performance of the thruster varied over the course of the test, with a specific impulse of 1900 seconds being recorded prior to the shut down for inspection. Erosion of the boron nitride insulator was the greatest at 41% of its original weight. The cathode suffered a 2.9% weight loss and the anode gained a slight amount of weight over its initial value.

The results of this test suggest that the cathode electrode is the most significant component affecting long term operation rather than the anode. The control of voltage mode and the erosion of the cathode and insulator are items for future study.

[1]Esker, D. W., Kroutil, J. C. and Checkley, R. J., "Design and Performance of Radiation Cooled Arc Thrusters", AIAA Paper 69-245, March 1969.

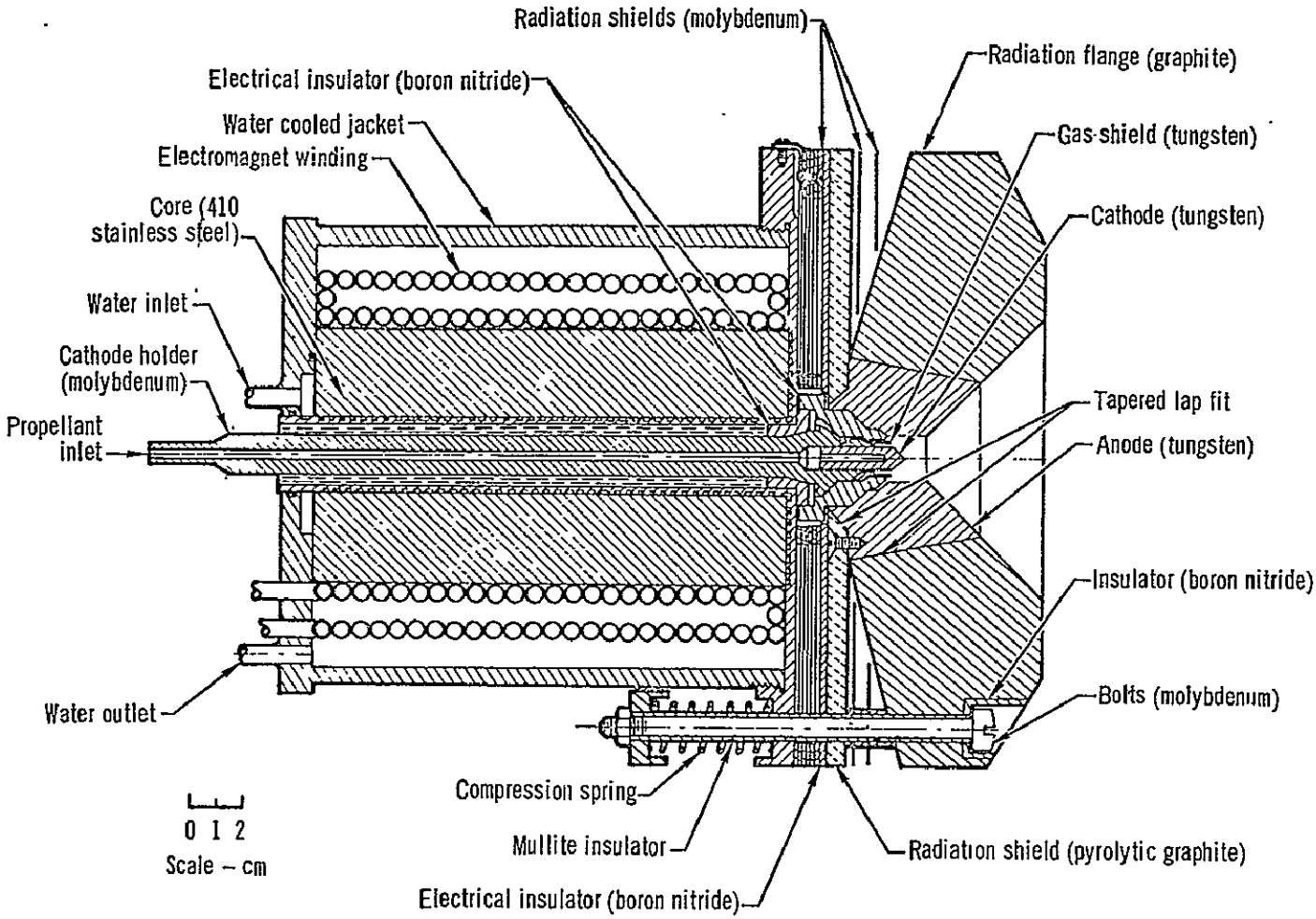

FIGURE 1 MCDONNELL RADIATION COOLED MPD THRUSTER

EXPERIMENTS FOR PLASMA DISTURBANCE IN MPD ARC AND LINEAR HALL ACCELERATOR IN THE PLASMA PHYSICS AND GAS LASER BRANCH

O. Jarrett, F. Allario, B. D. Sidney and R. V. Hess
NASA, Langley Research Center
Hampton, Va.

Onset of a rotating disturbance has been examined in two MPD accelerators, the linear Hall accelerator (LHA) and the MPD arc, as shown in figures 1 and 2. This paper summarizes the results previously obtained[1,2] and presents results of recent experiments.

The geometry of the MPD arc and the LHA is discussed in detail in references 1 and 2. The LHA has an approximately radial magnetic field and an axial electric field while the MPD arc has a coaxial electrode arrangement with a diverging axial magnetic field. The onset of the rotating disturbance in the two devices shows certain similarities despite the difference in power range; the LHA operating typically at a power of 0.1 kw and the MPD arc as high as 30 kw. In figures 3 and 4, the critical magnetic field, B_c, at onset of the instability is shown for the MPD arc as a function of mass flow and for the LHA as a function of pressure. Since pressure in the electrode region increases with mass flow in either device, B_c increases with mass flow in each case. In addition, for a given mass flow, B_c increases with molecular weight.

Through variation of the radial magnetic field distribution near the cathode of the LHA (due to the magnetic field of the cathode heating current) it was determined that the total magnetic field near the cathode determined the onset of the instability in the entire electrode region. Because of the similarity in behavior of the rotating disturbance in the two accelerators, it was of interest to examine the MPD arc to see if the onset of the disturbance also occurred in the region near the cathode.

In order to lower the power range of the MPD arc closer to the LHA, a hollow instead of a solid cathode was used. Stable operation of the MPD arc with a hollow cathode could be maintained from below 1 kw to 25 kw. Furthermore, a second solenoid with an independent power supply was installed downstream from the anode to permit changes of the magnetic field configuration in the electrode region. The tip of the cathode was repositioned 1/4 inch behind the anode so that superposition of the magnetic fields of the two coils permitted a wide variation of magnetic field in the electrode region. By comparing results from five different magnetic field configurations obtained at onset, it was determined that the axial magnetic field in a region close to the center plane of the anode determined the onset of the rotating instability. This result appears to be different from that obtained in the LHA where the magnetic field near the cathode determines the onset. The following considerations suggest, however, a common basis for the phenomena.

Previous studies of the MPD arc indicate a downstream bulging of the current, with formation of a cathode jet which is closer to cathode than anode potential.[3] It is reasonable to expect then that electrons emitted from the cathode follow the axial magnetic field lines for some distance downstream of the cathode, eventually crossing the magnetic field lines where the combination of crossed electric and magnetic field energetically allow it. The observed onset of the instability for the MPD arc near the center plane of the anode could coincide with the region where the mobile electrons begin to cross the magnetic field. This criterion appears to be satisfied also for the LHA where the magnetic field is perpendicular to the electric field everywhere including the immediate vicinity of the cathode in contrast to the MPD arc geometries, therefore, in the LHA emitted electrons are forced to cross the magnetic field within a short distance from the cathode. More sensitive magnetic field shaping and diagnostics are planned to gain a better understanding of the onset of rotating instabilities in an MPD arc.

REFERENCES

1. Allario, F.; Jarrett, O., and Hess, R. V.: Onset of Rotating Disturbance in the Interelectrode Region and Exhaust Jet of an MPD Arc. AIAA Seventh Electric Propulsion Conference, Williamsburg, Va. 1969.

2. Sidney, B. D.; Allario, F., and Hess, R. V.: Onset of Rotating Disturbance in Linear Hall Current Accelerator. AIAA Seventh Electric Propulsion Conference, Williamsburg, Va. 1969.

3. Hoell, J. M., and Brooks, D. R.: Distribution of Plasma Potential for an MPD Thrustor. AIAA Journal, vol. 6, no. 4, 1968, pp. 723-725.

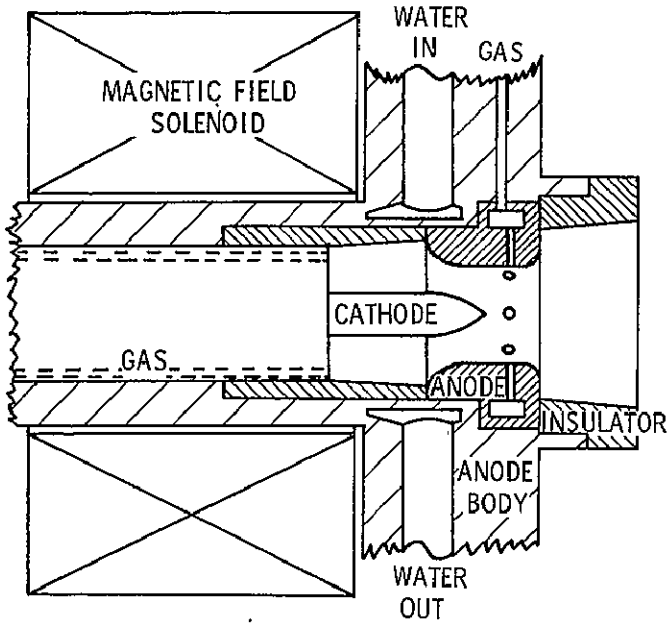

Figure 1.- Schematic of MPD arc.

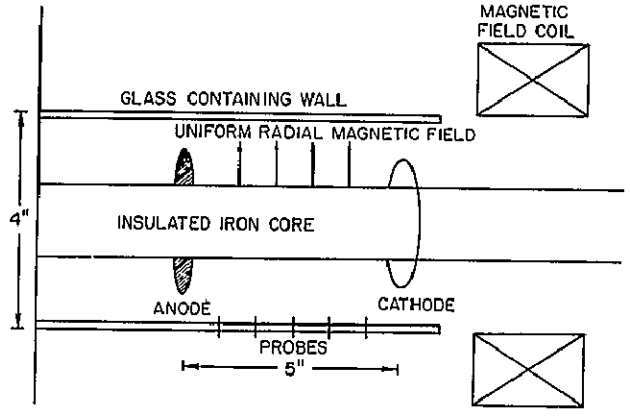

Figure 2.- Schematic of LHA.

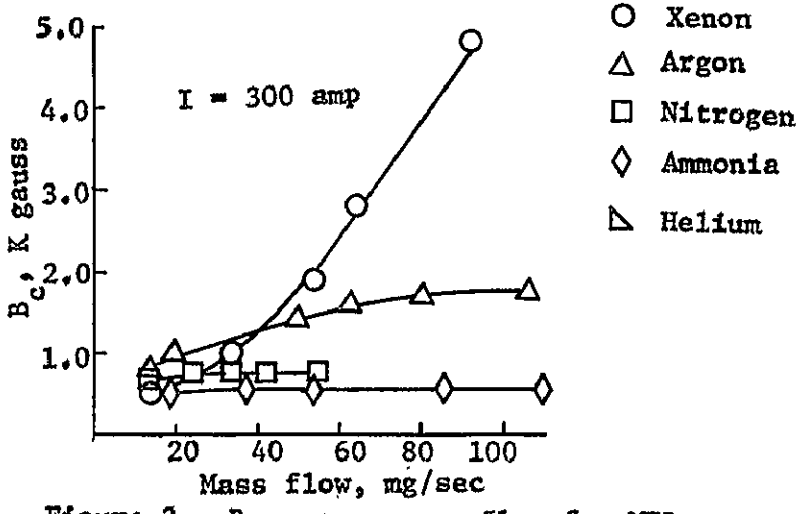

Figure 3.- B_c versus mass flow for MPD arc.

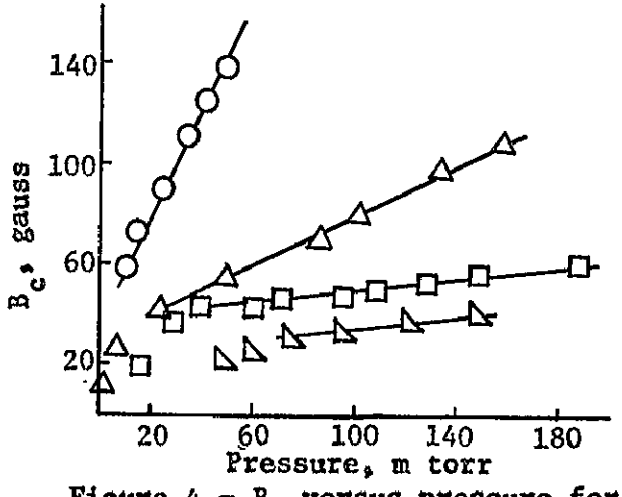

Figure 4.- B_c versus pressure for LHA

ANALYSIS OF PLASMA EXPANSION IN A MAGNETIC NOZZLE

by E. L. Walker, NASA Lewis Research Center

An analysis is made of the expansion of a plasma through an axisymmetric magnetic nozzle produced by Helmholtz coils. The plasma is assumed to be inviscid and to consist of hot electrons and cold ions. The steady state mass, momentum, and energy conservation equations along with Maxwell's equations are solved numerically near the axis of symmetry for the ratio of the ion exhaust energy to the initial electron thermal energy

$$\tau_{max}^{-1} = \left(\tfrac{1}{2} m_i u_\infty^2\right) / \left(\tfrac{3}{2} k T_{e,max}\right)$$

The solutions (see figure) are given by a family of curves which are described by two parameters: (1) the location of the on-axis sonic point $x = z/a$ where a is the coil radius; and (2) a dimensionless magnetic field β which involves an effective electron Hall parameter. The solutions show that the inclusion of electron heat flow gives values of τ_{max}^{-1} which are significantly higher than that for an adiabatic expansion. These results can be used to calculate an upper limit on the efficiency vs. specific impulse of a device such as the small MPD arc.

PLASMA EXPANSION IN A MAGNETIC NOZZLE

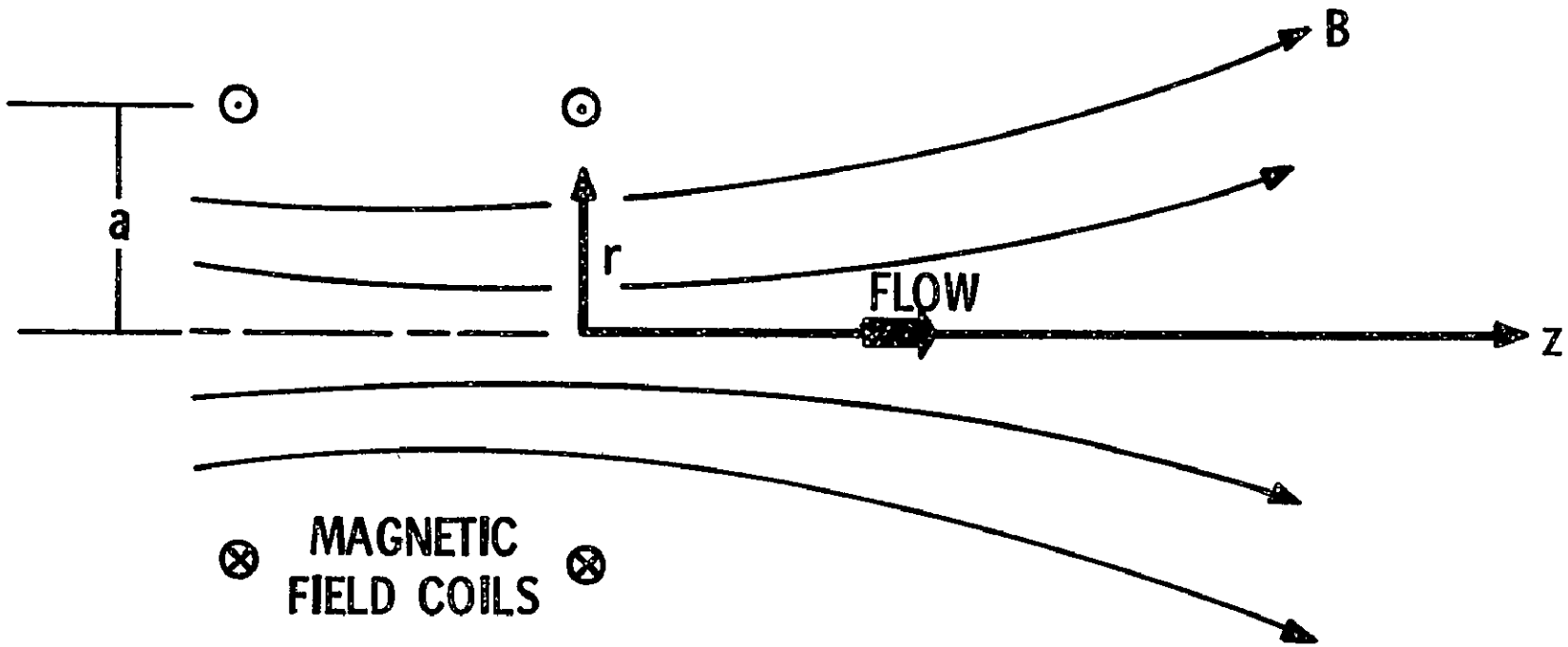

CS-51807

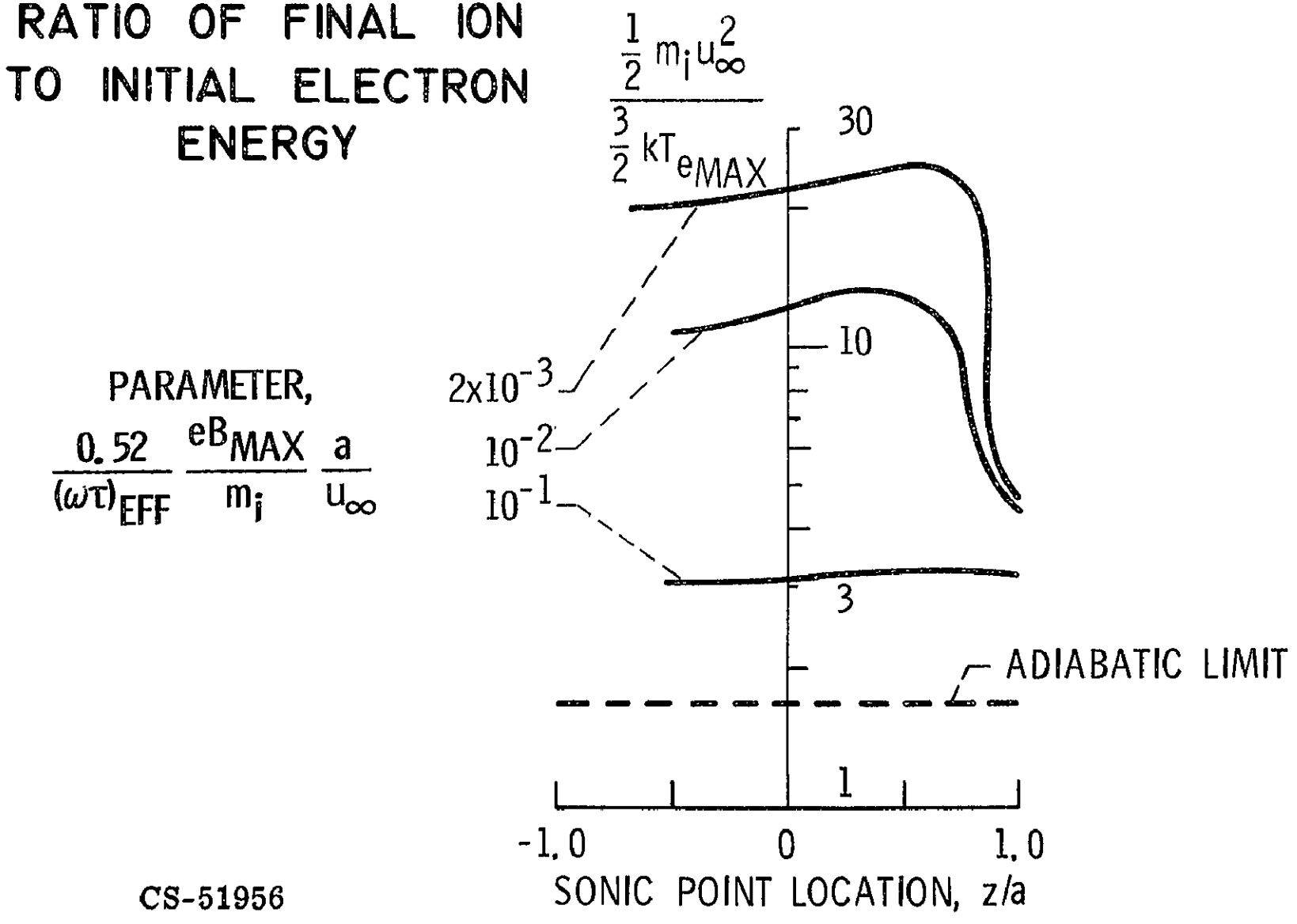
RATIO OF FINAL ION TO INITIAL ELECTRON ENERGY
$\frac{\frac{1}{2} m_i u_\infty^2}{\frac{3}{2} kT_{eMAX}}$
PARAMETER,
$\frac{0.52}{(\omega\tau)_{EFF}} \frac{eB_{MAX}}{m_i} \frac{a}{u_\infty}$
30
10
3
1
$2x10^{-3}$
10^{-2}
10^{-1}
ADIABATIC LIMIT
-1.0
0
1.0
SONIC POINT LOCATION, z/a
CS-51956

PERFORMANCE LIMITS OF ION THRUSTERS AND LOW POWER MPD ARC THRUSTERS

by George R. Seikel, NASA Lewis Research Center

By examining a power balance for these DC discharges an understanding of the plasma processes that limit their performance can be obtained. If only unavoidable discharge losses are considered then the limiting performance is determined. The two major unavoidable losses in a DC discharge are the power carried to the anode by the current and the power consumed in the ionization and competing excitation processes in the plasma volume.

If only the minimum anode power and ionization power losses are considered then the limiting performance of a DC bombardment ion thruster can be evaluated. The limiting efficiency vs. specific impulse is a function of only the plasma discharge energy expended per AMU of beam ion produced (i.e. eV/ion-AMU). If the discharge has a constant electron kinetic temperature, then for a given propellant, discharge voltage, and anode work function, the discharge energy per beam ion AMU is only a function of electron temperature. For any discharge voltage there is an optimum discharge electron temperature. The calculated minimum values of eV/ion indicate that present 36 V Hg ion sources may be approaching a fundamental limit. This analysis also indicates performance gains possible through raising the discharge voltage and the potential performance of thrusters using propellants other than Hg.

In a similar manner a power balance for the low power MPD arc thruster results in predicting the limiting efficiency vs. specific impulse. This analysis makes use of the results of a plasma expansion analysis (to be presented by Walker) and considers the minimum anode and volume ionization losses. The theoretical performance limit so calculated is compared with present NASA-Lewis low power xenon MPD arc thruster data. The discrepancy between the theoretical limit and present performance indicates that substantial performance improvement may be possible. In making these theoretical limit calculations both the magnetic field and sonic point location were optimized. If the sonic point were actually further downstream then the theoretical limit would be lower. This point brings up one of the big questions yet to be answered for such flows. Where does the sonic point occur and why?

EXPERIMENTAL INVESTIGATION OF CURRENT ROTATIONS IN A MPD ARC

ROBERT A. COCHRAN, Research Assistant, and JAMES A. FAY, Professor, Department of Mechanical Engineering, Massachusetts Institute of Technology, Cambridge, Mass.

Recent experimental studies indicate that under certain conditions the current in the inner electrode region of a MPD arc is not uniformly distributed throughout the inner electrode region but is confined to an azimuthally localized region or spoke which rotates in the Amperian direction at steady frequencies on the order of 100 Khz..This study experimentally determines the conditions under which this highly non-uniform current distribution occurs and investigates the variation in the frequency of the conducting region as well as the electrode voltage of the MPD arc operating in both the diffuse and spoke mode. The experiment was conducted in a pulsed quasi-steady MPD arc of 500 μsec duration. The electrode geometry consisted of two concentric copper rings of 1cm axial length having a 1cm radial gap. The inner ring had an outer radius of 2cm. The primary propellant used was argon and the arc behavior was investigated for large variations in m(.056-4.0 gm/sec), I(100-5000 Amp), and B (0.1-2.0 telsa). Additional measurements were also made using xenon, helium, and hydrogen as propellants.

It was found that the single rotating current spoke occurs at intermediate current levels above a certain magnetic field strength. The discharge is very uniform and diffuse at low current levels and at high currents it consists of many small fluctuations each corresponding to a small percent of the total current delivered to the arc. A comparison of the spoke frequency measurements with the actuator disk theory of Fay and Cochran (1) shows that the actuator disk model gives a satisfactory prediction of the behavior of the spoke frequency until a limiting frequency is reached after which the spoke approaches a constant rotational speed which is the same for all gases. The point at which the actuator disk model becomes invalid corresponds to a magnetic Reynolds number based on the spoke speed of order one for all gases investigated. The variation in the electrode voltage was found to obey the correlation of Patrick and Schneiderman (2) when the arc was operated in the diffuse mode at low current levels. In the spoke mode voltages several times this prediction were measured and can be explained in terms of the EMF generated by the rotating spoke.

1. Fay, J.A., and Cochran, R.A., "An Actuator-Disk Model for Azimuthally Nonuniform MPD Arcs," AIAA Journal, Vol. 7, No. 9, Sept. 1969,pp. 1688-1692.
2. Patrick, R.M., and Schneiderman, A.M., "Performance Characteristics of a Magnetic Annular Arc," AIAA Journal, Vol. 5, No. 2, Feb. 1966, pp. 283-290.

JXB ACCELERATOR WORK AT AMES

James R. Jedlicka

NASA Ames Research Center, Moffett Field, California

The present steady-state accelerator, which was installed two years ago, receives plasma from a constricted arc. This combination offers high plasma entering velocity and electrical conductivity without the need for seed. The flow through the accelerator approximates fully developed pipe flow, a consequence of its high temperature, and results in severe circulating currents upon application of a transverse magnetic field. For many combinations of J and B, no net acceleration of the stream occurs.

The most favorable combination of operating conditions has produced a velocity increase of 2½ times that for which J=B=0, or 4 times that before J was applied but with non-zero B. The absolute velocity for these conditions, however, was only 8 km/s, which is not spectacular when compared to the 6.3 km/s available from the constricted arc alone under other conditions.

Possible means to improve performance are discussed.

THE DESIGN OF THE LANGLEY TWENTY MEGAWATT LINEAR PLASMA ACCELERATOR FACILITY

Arlen E. Carter
NASA, Langley Research Center

A linear, crossed-field plasma accelerator facility for high-speed aerodynamic testing and basic research in high-speed magnetohydrodynamics has been designed. Use was made of the experience and results obtained with previous smaller, lower speed accelerators together with a quasi-one-dimensional theoretical analysis. General design philosophy centered around three criteria: (1) make J x B as large as practicable; (2) operate with approximately constant current density; (3) maintain a constant Hall potential gradient. Convergent and divergent channel geometries were considered and rejected because of, among other things, lack of uniform gas properties across the channel cross section and the difficulty of properly matching the device to an existing power supply. The final design has a constant-area channel designed for constant electrode potential difference with the magnetic field tailored to achieve this condition. A compromise in the magnetic field strength at the upstream end of the accelerator to help assure proper operation of the arc heater resulted in a small decrease in the electrode potential difference and an increase in electrode current for the first four or five electrodes. Figures 1 and 2 are computer predictions of velocity and current density based on the modified magnetic field distribution shown in figure 3.

The matching of the accelerator to the existing 10 megawatt power supply is difficult. The power supply has eight separate modules which may be connected in any series-parallel combination. The number of accelerator electrodes greatly exceeds the number of modules available for power. Without individual power supplies for each set of electrodes an extensive resistance network is needed to properly divide the current among the many electrodes since the applied potential distribution along the anode and cathode walls must match the internally generated Hall potential distribution or circulating Hall currents will result, degrading the accelerator performance. A special resistor network was designed to handle the high power dissipation.

Figure 4 is a schematic diagram of the facility. The arc heater is shown at the left and consists of a cathode, constrictor, anode, plenum, and supersonic nozzle. Nozzle exit conditions are a velocity of approximately 3800 m/s, enthalpy of 1.6×10^7 J/kg, mass flow of 18 g/s. The working gas is nitrogen seeded with 2 percent mole fraction of cesium vapor. One 10 megawatt power supply is used to power the arc heater and a second 10 megawatt supply is used for the accelerator which mounts between the poles of a large c-magnet. The accelerator channel is 6.3 cm square and 50 cm long; it contains 36 pairs of individually water-cooled electrodes. The sidewalls are boron nitride plates backed by water-cooled copper, coated with beryllium oxide for electrical insulation. Each water and electrical connection is of a "quick-disconnect" type, greatly facilitating the attachment of the 156 water leads

and 72 electrical leads. The accelerator forms its own environmental chamber eliminating the need for mounting it within a vacuum tank. Immediately downstream of the accelerator is a test section used for flow observation and diagnostics. The flow is exhausted into a five-foot diameter duct which is cooled by spraying water on its outer surface. A four-stage steam ejector provides a vacuum source. The expected accelerator exit conditions are: Velocity of 13,000 m/s, enthalpy of 11.8×10^7 J/kg, Mach number of 7.0, density corresponding to 58 km altitude, stagnation point heating rate of 7.2 kW/cm^2 to a hemispherical body 2.54 cm in diameter.

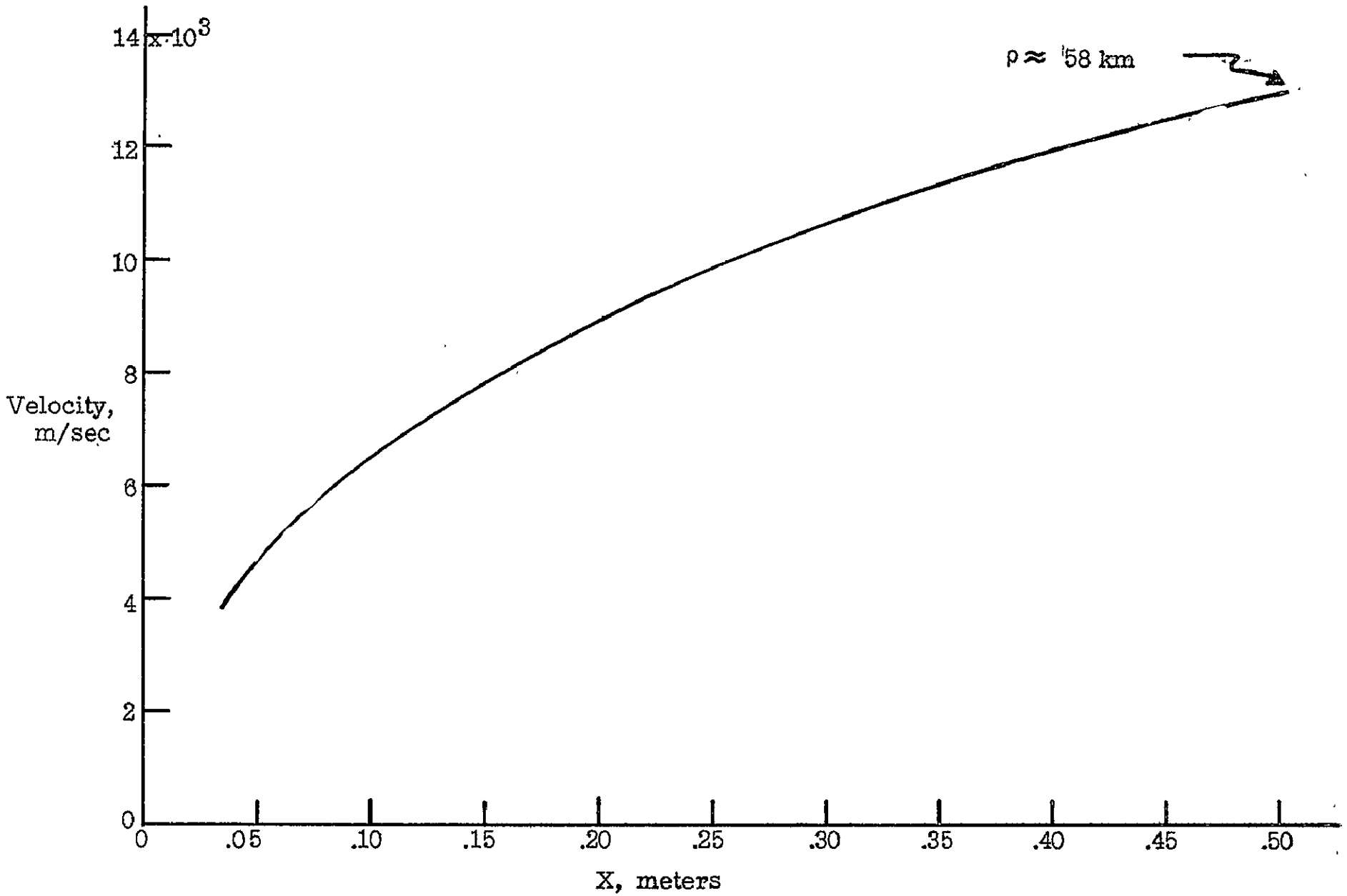
14 x 10^3
12
10
8
6
4
2
0
Velocity, m/sec
p ≈ 58 km
0
.05
.10
.15
.20
.25
.30
.35
.40
.45
.50
X, meters

FIGURE 1.

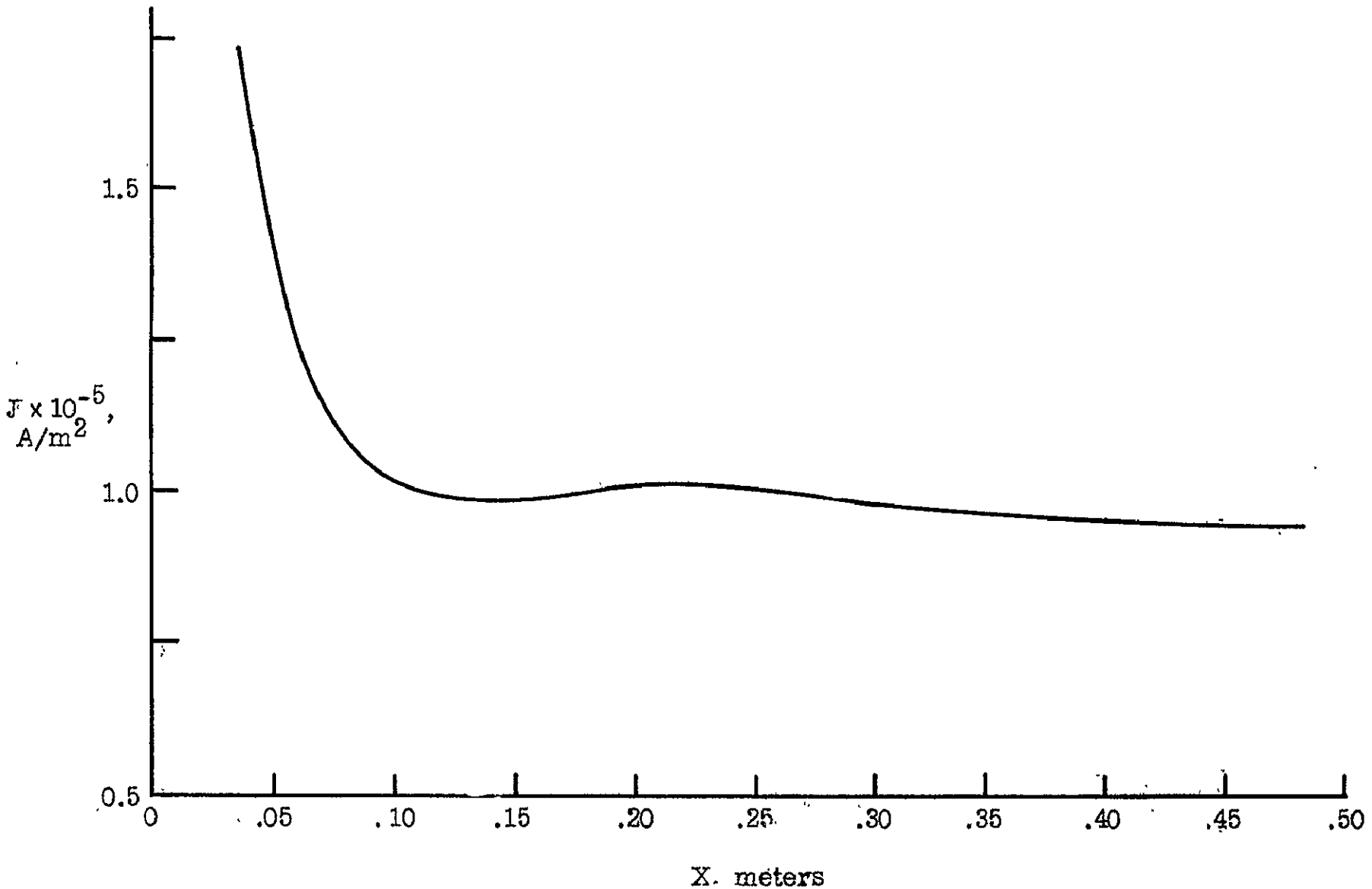

FIGURE 2.

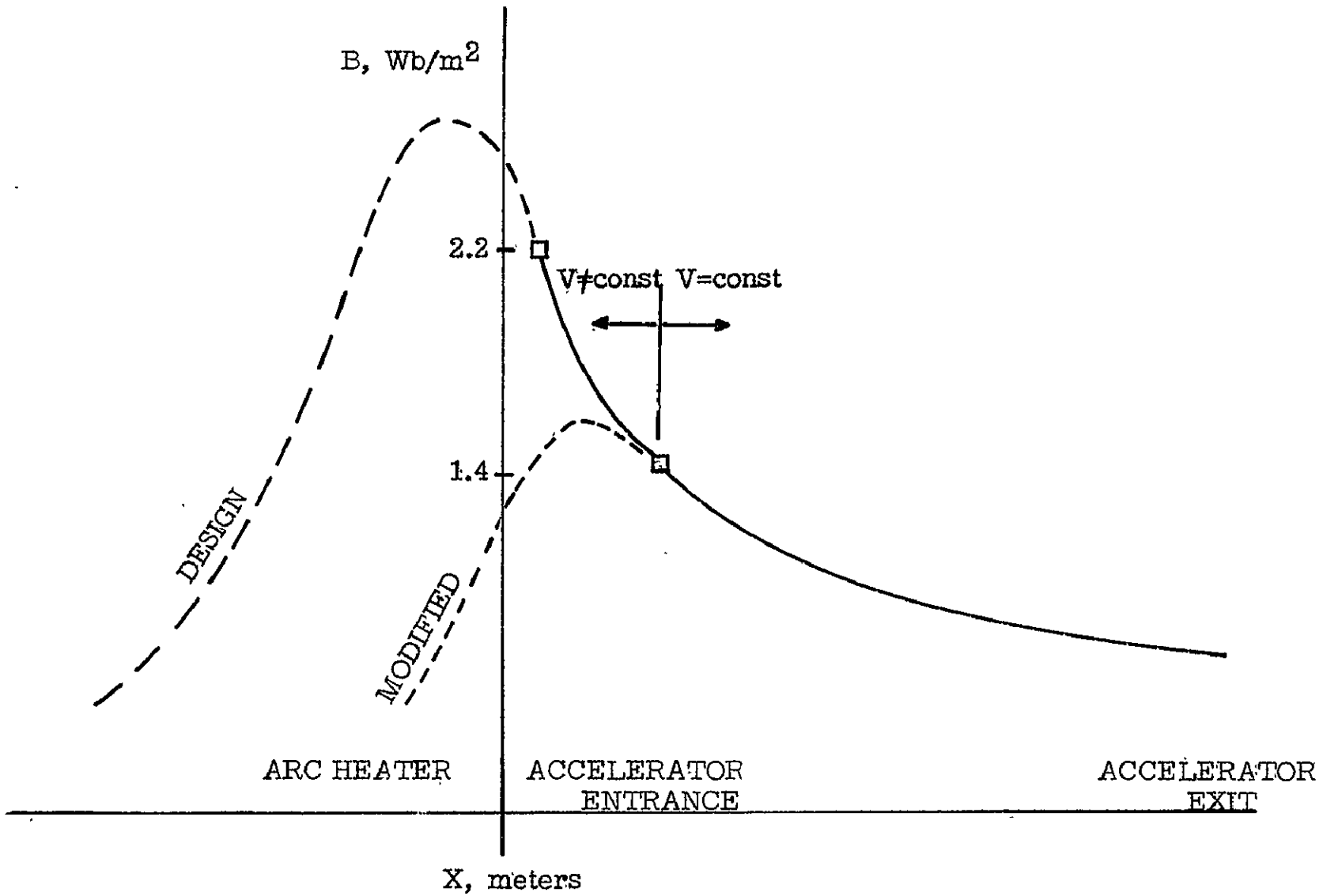
B, Wb/m2
2.2
1.4
V≠const
V=const
DESIGN
MODIFIED
ARC HEATER
ACCELERATOR ENTRANCE
ACCELERATOR EXIT
X, meters

47

20 - MEGAWATT PLASMA ACCELERATOR FACILITY

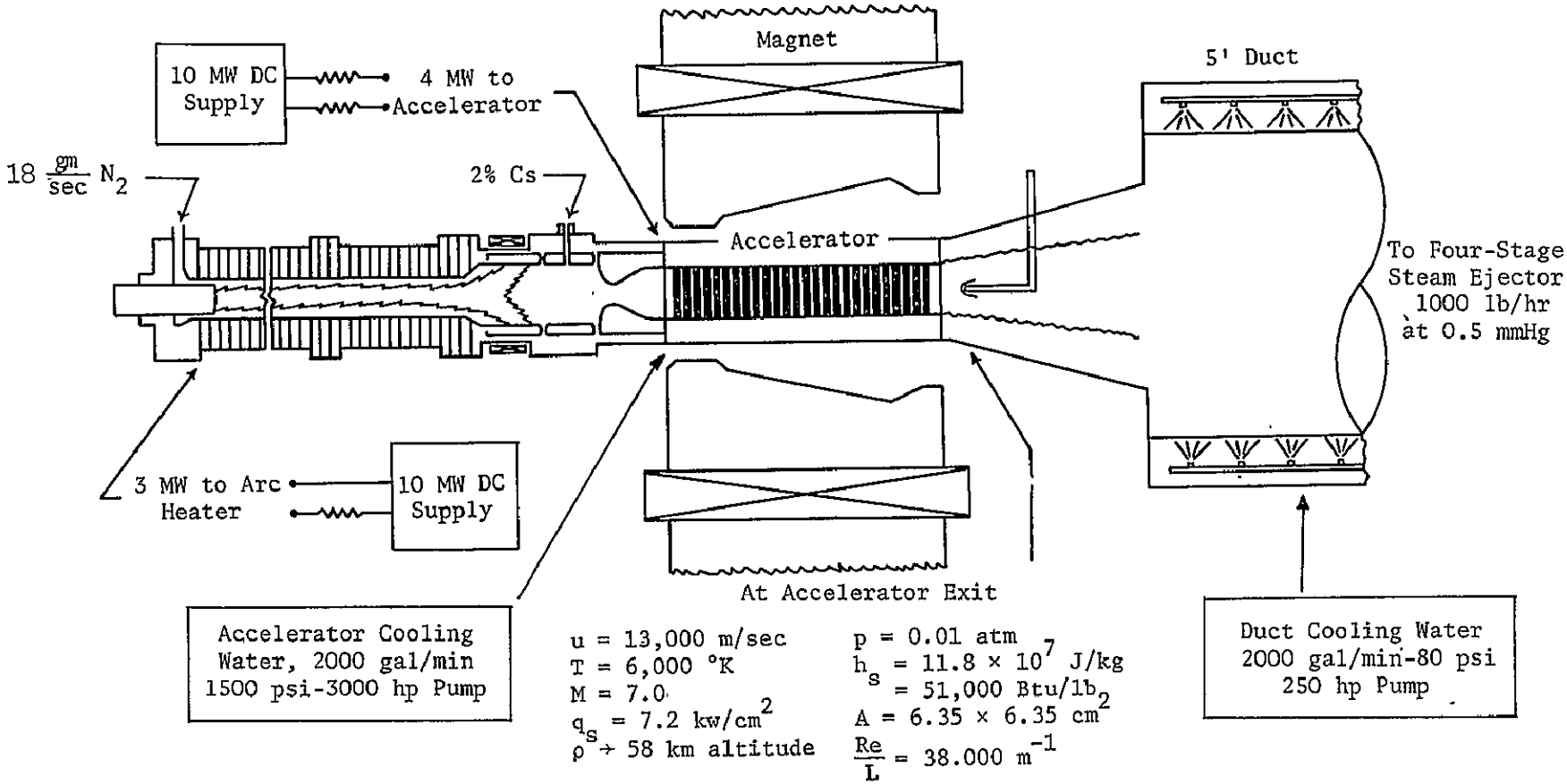

FIGURE 4.

OPERATING CHARACTERISTICS AND INITIAL TESTS OF THE LANGLEY 20 MW LINEAR PLASMA ACCELERATOR

W. R. Weaver
NASA, Langley Research Center
Hampton, Va.

The Langley Research Center's 20 MW Linear Plasma Accelerator Facility has been made operational. The initial problems with the arc heater and the improvements necessary to make it a suitable plasma source are described. The initial accelerator tests consisted of powering a small number of the upstream electrodes, adjusting the resistor network until the Hall currents were eliminated, and then connecting more electrodes and adjusting their resistors until 30 electrode pairs were connected and the desired current through each pair was obtained. The final current distribution, electrode potential difference, and the electrode-wall potential distributions are given. Pitot pressure measured at the accelerator exit was 0.45 atmosphere, which indicated a velocity of 80% of the design velocity of 12,000 meters per second.

ELECTRODE POTENTIAL DISTRIBUTIONS AND POWER SUPPLY CONNECTIONS

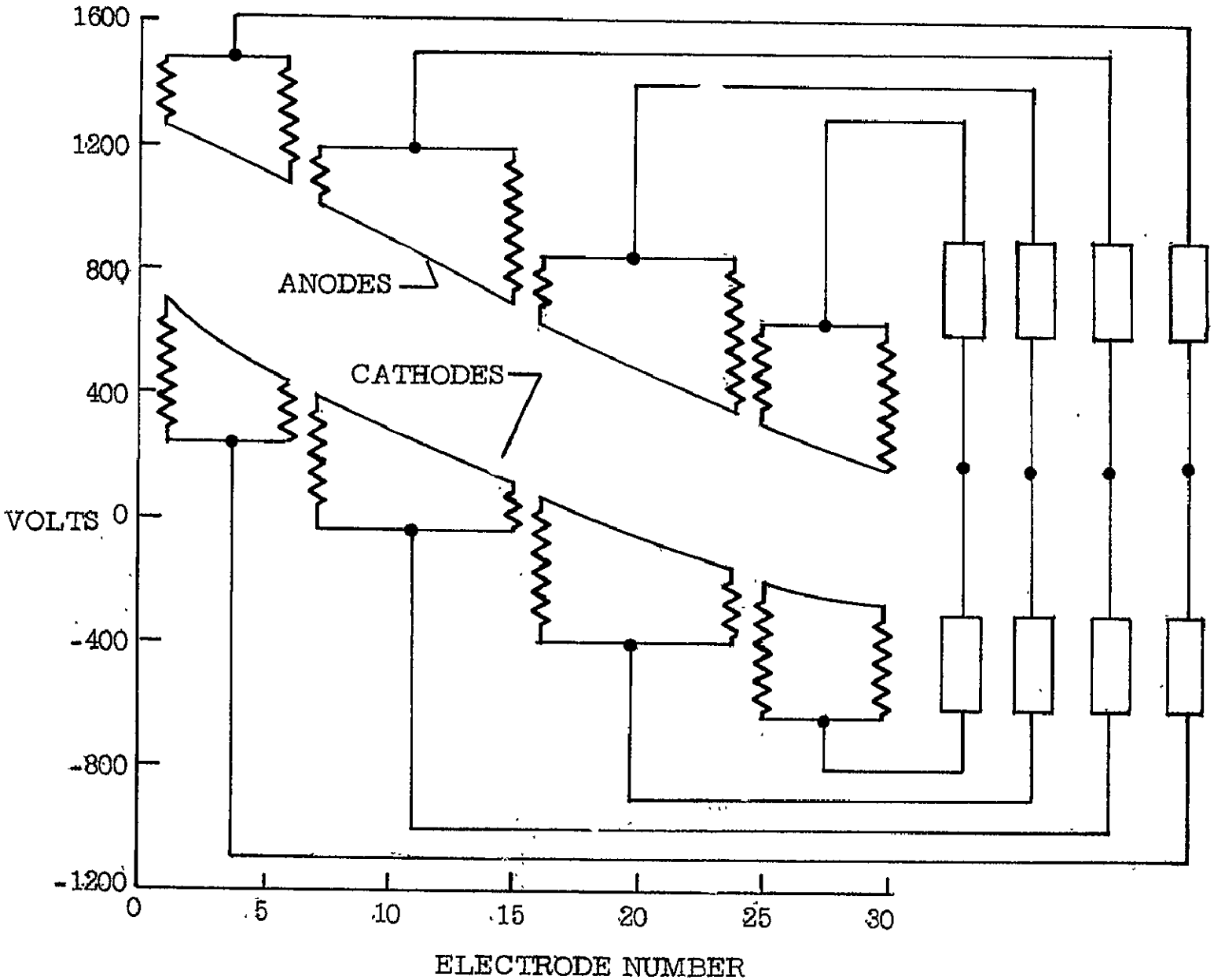

FIGURE 1.

ACCELERATOR CURRENT DISTRIBUTION

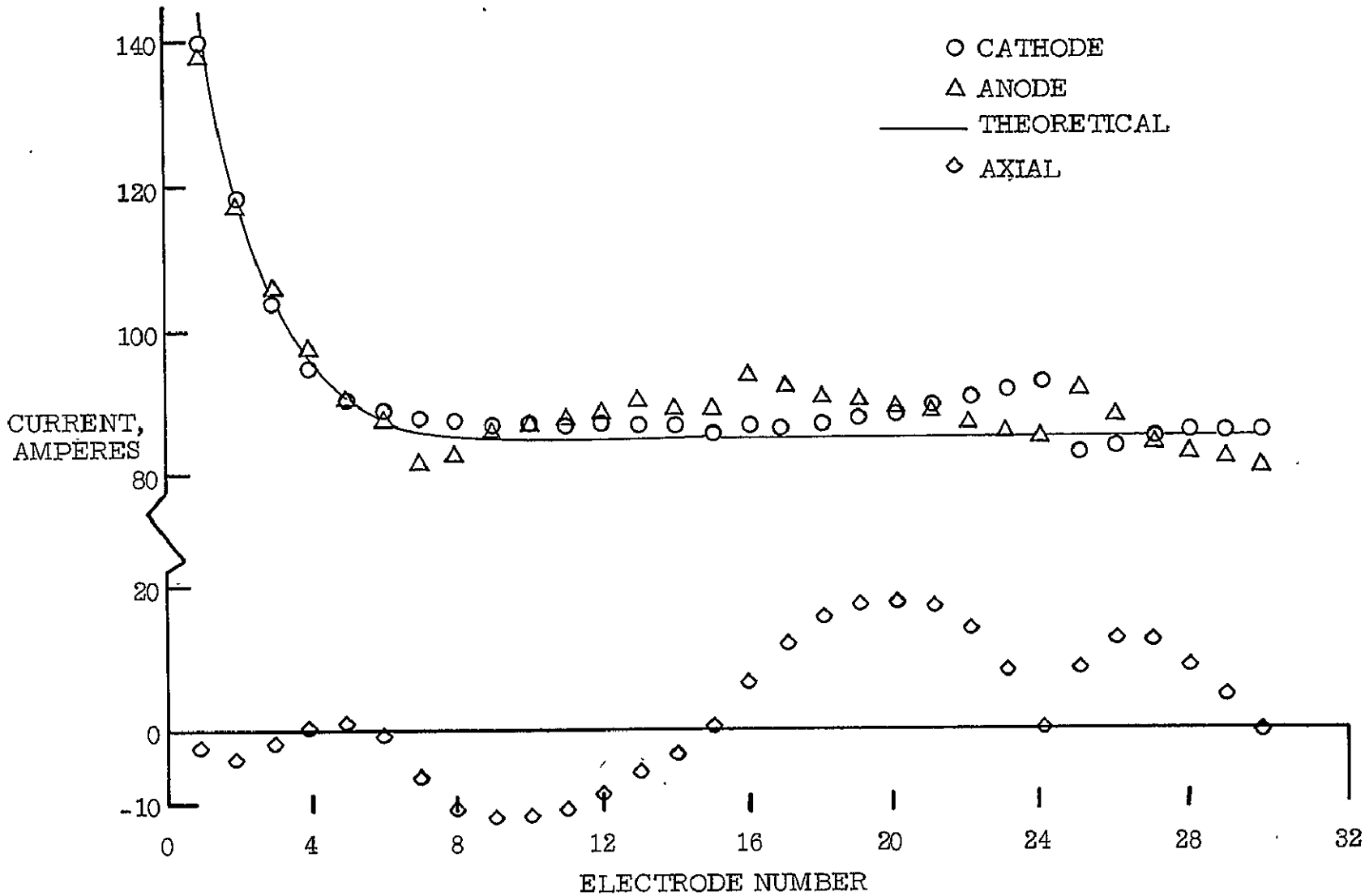

FIGURE 2.

ACCELERATOR ELECTRODE POTENTIAL DIFFERENCE

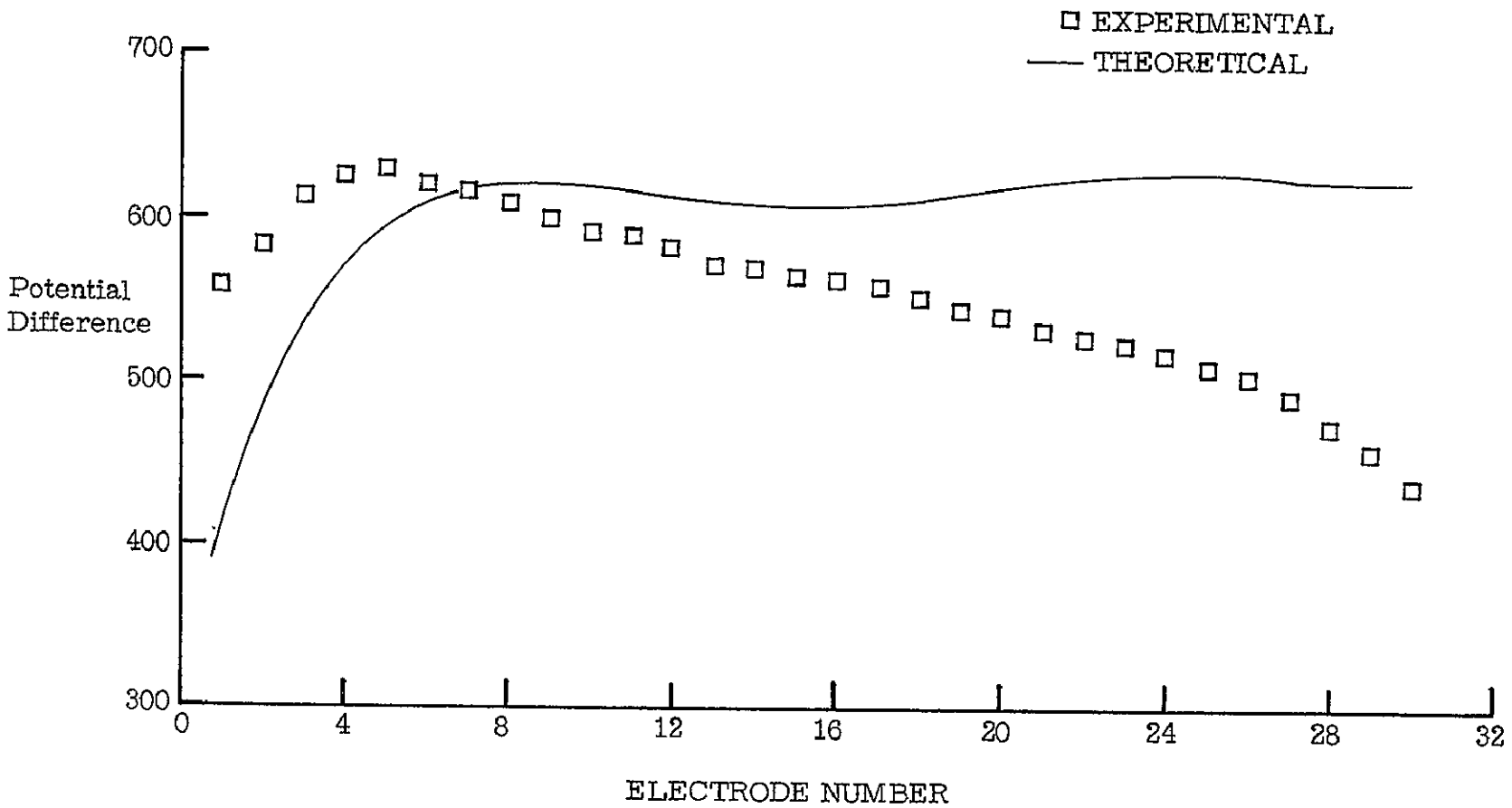

FIGURE 3.

PRESENT STATUS OF THE EXPERIMENTAL MHD POWER GENERATION PROGRAM

by R. J. Sovie and L. D. Nichols
NASA Lewis Research Center

The NASA-Lewis closed loop MHD facility (Fig. 1) has been operated several times at 3200° F in the past year with no facility problems. Consequently, we have been able to concentrate on the plasma and generator problems. In order to increase the plasma conductivity it was necessary to install an impurity purge system and a new cesium injection system. The method of pre-ionization was also changed. The significance of these design changes will be discussed briefly. As far as the generator data is concerned open circuit voltages and short circuit currents have been measured. The effects of internal current leakages on the measured generator performance have been ascertained and will be discussed. It was also found that a coating is formed on the generator electrodes that seriously inhibits the current flow in the external load circuit. Various starting techniques are presently being investigated in order to eliminate this coating and these results will also be presented.

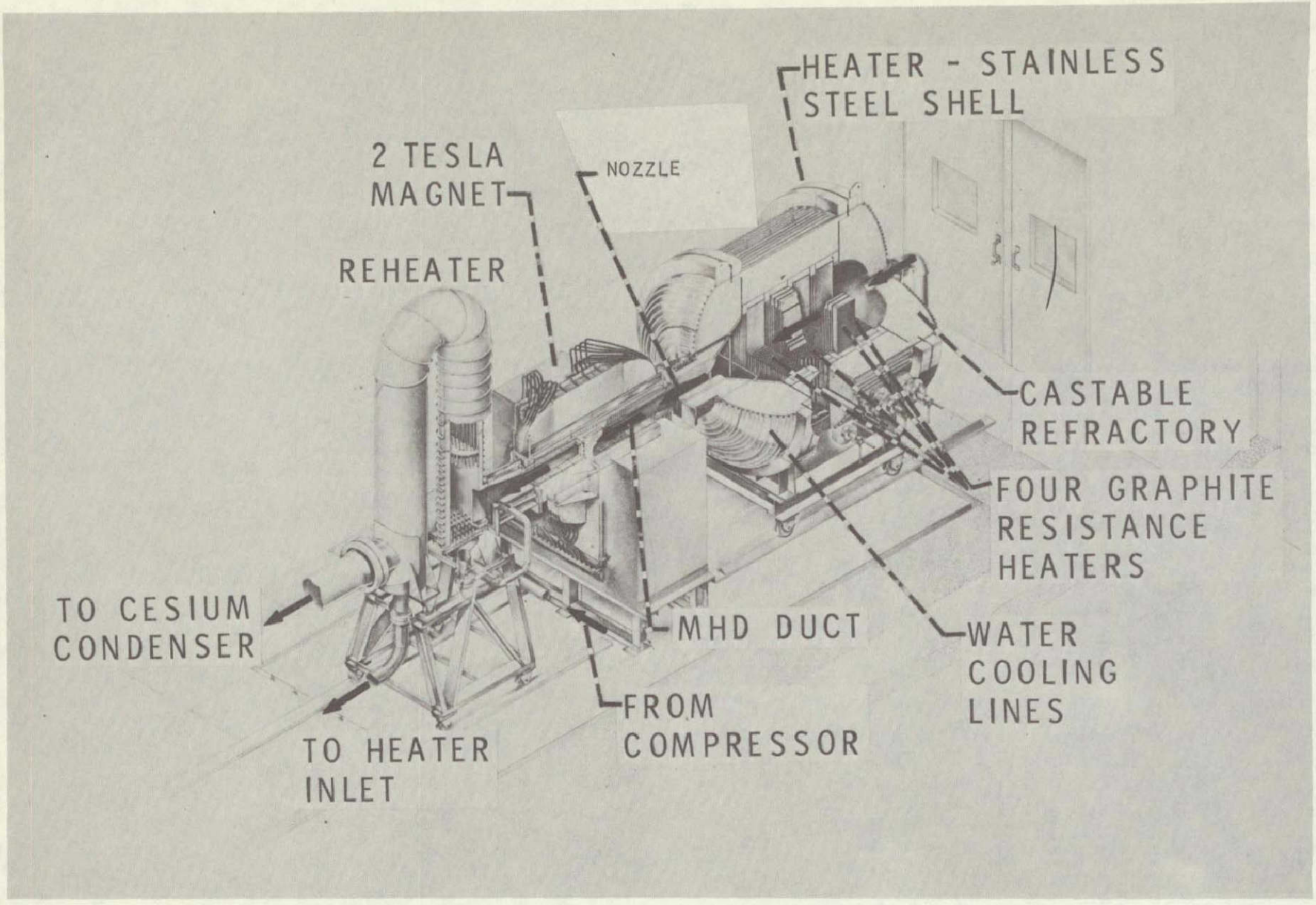

Figure 1 - Bedplate showing heater, nozzle MHD duct, magnet, and reheater. The flow distributor at the heater inlet is not shown.

THE EFFECTS OF ELECTROTHERMAL INSTABILITIES ON SEVERAL NON-EQUILIBRIUM PLASMAS

by Allan R. Bishop, NASA Lewis Research Center

The effects of electrothermal instabilities on several different non-equilibrium plasmas is examined. In argon seeded with cesium the effect of a molecular impurity magnifies the instability losses. A one-tenth percent carbon monoxide impurity combined with the instability reduces the maximum power density to one-eighth of its ideal value. This maximum value occurs at a load parameter of about 0.2.

The effect of the instability on the output power of a specific generator, using neon seeded with cesium, is also examined. With generator shape, Mach number, pressure drop, and magnetic field specified, the output power loss as a function of stagnation temperature is determined. The loss varies from a factor of four at 1800° K down to zero at about 2500° K, where the instability disappears.

The feasibility of using helium seeded with uranium as a working fluid in generators driven by liquid or gas core nuclear reactors is discussed. The use of a helium-uranium mixture appears to be a possibility although the power density is lower than with more conventional working fluids. The optimum mixture ratio is about six parts uranium per thousand parts helium. Even with the electrothermal instability losses included, the non-equilibrium conductivity is higher than the equilibrium conductivity.

"HOT" ELECTRODE SHEATH DROPS IN A MHD GENERATOR

by M. A. Mantenieks, NASA Lewis Research Center

Electrode sheath drops in an arc heated argon, supersonic MHD generator were measured. The Mach 3.5 generator has carbonized 2% Th-W electrodes and is capable of generating currents of up to 34 amps and open circuit voltages of about 20 volts with a magnetic field of .55 Tesla depending on the electrode gap. The other parameters measured in the experiment included gas pressure, gas temperature (measured calorimetrically) and electrode temperature as a function of generated current through the electrode. Because of the highly non-equilibrium state of the plasma (due to the arc heater and frozen flow) zero current sheaths at the anode and cathode are of the order of one volt. The cathode sheath drop increases from this value, as the current increases, to 6.5-10.3 volts depending on the initial cathode temperature and plasma conditions. Once this level is reached the sheath drop becomes relatively independent of the current. The anode voltage decreases with increasing current and becomes negative at higher currents (-4.6 volts at 30 amps).

The cathode temperature was found to first decrease with current and then increase linearly at higher currents. (For example: Temp. drops from 2250° K at I = 0 amps to 2232° K at I = 3.5 amps and increases to 2310° K at I = 22 amps). The anode temperature increases linearly with increasing current. A current balance at the electrodes following the work of Lyubimov[1] and an energy balance at the electrode surface give qualitative agreement with the experimental results except for the high current regime.

REFERENCES

1 G. A. Lyubimov, "Layers of Abrupt Change of Potential on 'Hot' Electrodes," translated from Teplofizika Vysokikh Temperatur, vol. 4, no. 1, pp. 120-132, January-February 1966.

ANALYTICAL AND EXPERIMENTAL STUDIES OF MHD GENERATOR CATHODES EMITTING IN A "SPOT" MODE

by Lester D. Nichols and Maris A. Mantenieks,
NASA Lewis Research Center

The mode of electron emission from an MHD generator cathode can affect the performance of the generator. Under certain conditions the emission of the electrons is confined to a small spot on the cathode. These spots are similar to the spots observed in any thermionic arc (1). There are many theoretical studies of these arc spots - and they have in common the assumption that the spot is formed by ion energy transfer to the cathode. The ions are formed in a region near the cathode as a result of electron collisions with gas atoms. The differences among the previous studies involve their treatment of the ionization region and the number of unknown parameters which must be specified in order to use the model to predict current voltage characteristics. Ecker (2) determines the ion current from the solution which gives the minimum voltage as a function of a "contraction parameter" rather than considering the energy conducted from the spot. Bauer (3) and Lee and Greenwood (4) leave the ion current as a free parameter to be determined experimentally. Adams and Robinson (5) consider a rather complete set of heat transfer mechanisms, but require the specification of the angle between the current stream tube and the normal to the cathode before comparison between their model and experiment can be made. The aim of this study is to present a model which requires no empirical constants. Such a theory is presented by Bade and Yos (6). But they make many assumptions about the nature of the phenomena to develop a simple theory. The present report is an attempt to improve the Bade and Yos theory by using fewer assumptions but retaining simplicity. Bade and Yos assume that the ions and electrons are at the same temperature, all the atoms are ionized, and that the electron current carries no energy from the ionization region into the discharge. We offer a means of calculating electron temperature, ion density, and the energy carried by the electrons from the ionization region to the discharge volume. In all other respects these two models are the same. The results for given gas conditions and electrode work function predict a sheath voltage which decreases with both increasing current for a fixed undisturbed (i.e., far from the spot) cathode temperature, and increasing undisturbed cathode temperature at a fixed current. Experimental data is shown which supports the conclusions predicted by the model.

REFERENCES

1 J. M. Somerville, The Electric Arc, John Wiley & Sons, Inc., 1959, pp. 64-68.

2 G. Ecker, "Die Stabilisierung des Lichtbogens for Anode und Kathode," Zeitschrift fur Physik, vol. 136, 1953, pp. 1-16.

3 A. Bauer, "Untersuchunger uber den Kathodenfall in den Ubergangsbereichen vom Thermobogen zum Feldbogen und vom Bogen zur Glimmentladung," Annelen der Physik, vol. 18, 1956, pp. 387-400.

4 T. H. Lee and A. Greenwood, "Theory for the Cathode Mechanism in Metal Vapor Arcs," Journal of Applied Physics, vol. 32, no. 5, May 1961, pp. 916-923.

5 R. C. Adams and E. Robinson, "Electrode Processes in MHD Generators," Proceedings of IEEE, vol. 56, no. 9, September 1968, pp. 1519-1535.

6 W. L. Bade and J. M. Yos, "Theoretical and Experimental Investigation of Arc Plasma-Generation and Technology, Part II: Applied Research on Electric Phenomena, Vol. 1: A Theoretical and Experimental Study of Thermionic Arc Cathodes," Avco Corporation, ASD-TDR-62-729, September 1963.

USE OF A HIGH-INTENSITY R-F PLASMA RADIANT ENERGY SOURCE FOR RESEARCH ON GASEOUS-CORE NUCLEAR REACTORS*

John S. Kendall, Supervisor Fluid Dynamics
United Aircraft Research Laboratories
East Hartford, Connecticut

ABSTRACT

The nuclear light bulb rocket engine concept is based on the transfer of energy by thermal radiation from gaseous nuclear fuel through an internally cooled transparent wall to seeded hydrogen propellant (Fig. 1). In a reference engine design, the effective radiating temperature of the nuclear fuel is 15,000 R and the hydrogen propellant exit temperature is 12,000 R. For this design, the calculated specific impulse is 1870 sec, the engine thrust is 92,000 lb, and the engine weight is 70,000 lb. The gaseous nuclear fuel is kept away from the transparent wall by a vortex created by the tangential injection of neon near the inside surface of the transparent wall. The neon discharging from the cavity contains gaseous nuclear fuel which is then condensed, centrifugally separated from the neon, and pumped back into the fuel-containment region of the vortex. The neon is also pumped back into the cavity. The closed-cycle fuel system leads to the possibility of providing perfect containment of the gaseous nuclear fuel and fission products.

Experiments were conducted to simulate the thermal environment in a unit cavity of a nuclear light bulb engine. These experiments include development of a high-intensity r-f induction-heated light source, transparent-wall model tests, and propellant heating tests.

The objective of the high-intensity r-f light source research is to develop a non-nuclear source having a radiant energy flux in the range of interest for the full-scale engine (equivalent black-body radiating temperatures between 8000 and 15,000 R). This research was conducted using the UARL 1.2-megw r-f induction heater to deposit energy in argon plasmas (Fig. 2). The configuration used in these experiments consists of two concentric fused silica tubes located within the coils of the induction heater; argon is injected at one end to produce a vortex flow and is exhausted through ports located at the centers of the water-cooled copper end walls. Tests were conducted at pressures between 2 and 16 atm.

For the maximum-power test condition achieved to date, a total of 216 kw was deposited in the discharge (Fig. 3); of this, approximately 156 kw

---

* This research was supported by the joint AEC-NASA Space Nuclear Propulsion Office as part of Contracts NASw-847 and SNPC-70 and is reported in Refs. 1-3.

(75 percent) was radiated outward through the peripheral wall of the test chamber. The corresponding radiant energy flux was 36.8 kw/in.^{2}, which is equivalent to a black-body radiating temperature of 10,200 R. This is well into the range of interest for the engine; hence, the development has progressed to the point where useful experiments related to the thermal environment of the engine are being conducted.

The objective of the transparent-wall model tests is to test models (Fig. 4) adjacent to the high-intensity light source to determine their operating limits. The heat deposition rate expected in the full-scale engine due to thermal radiation from the nuclear fuel at an equivalent black-body radiating temperature of 15,000 R is approximately 1.65 kw/in.^{2} of wall surface area. Tests employing a 0.005-in. wall thickness model resulted in heat deposition rates on the inside surface of the model as high as 2.2 kw/in.^{2} (i.e., greater than that expected for the full-scale engine) with no apparent damage to the fused silica coolant tubes.

The objectives of the propellant heating experiments are (1) to develop methods for injecting solid particle seeds into a simulated propellant stream, (2) to study the effectiveness of buffer layers for preventing wall coating, and (3) to conduct experiments in which a large percentage of the incident radiation from the light source is absorbed in a simulated propellant stream. This work is still in the initial stages. The propellant heating configurations used are generally similar to the geometries of the components expected to be employed in the nuclear light bulb engine. Argon seeded with micron-sized carbon particles (instead of hydrogen seeded with tungsten particles) was used as the simulated propellant. At the low radiant energy source power levels of up to 3 kw that were used in these initial tests, temperature rises up to 223 R were obtained. Further increases in simulated propellant temperature rise will be obtained primarily by means of increased power, improved particle deagglomeration to increase absorption, and more effective buffer layers to reduce the coating of particles on the transparent walls.

REFERENCES

(To be published as NASA Contractor Reports)

1. Roman, W. C., J. F. Klein, and P. G. Vogt: Experimental Investigation to Simulate the Thermal Environment, Transparent Walls, and Propellant Heating in a Nuclear Light Bulb Engine. United Aircraft Research Laboratories Report H-910091-19, prepared under Contract NASw-847, September 1969.
2. Mensing, A. E. and J. F. Jaminet: Experimental Investigations of Heavy-Gas Containment in R-F Heated and Unheated Two-Component Vortexes. UARL Report H-910091-20, September 1969.
3. Latham, T. S., H. E. Bauer, and R. J. Rodgers: Studies of Nuclear Light Bulb Start-Up Conditions and Engine Dynamics. UARL Report H-910375-4, September 1969.

FIG. 1

NUCLEAR LIGHT BULB ENGINE CONCEPT
UNIT CAVITY

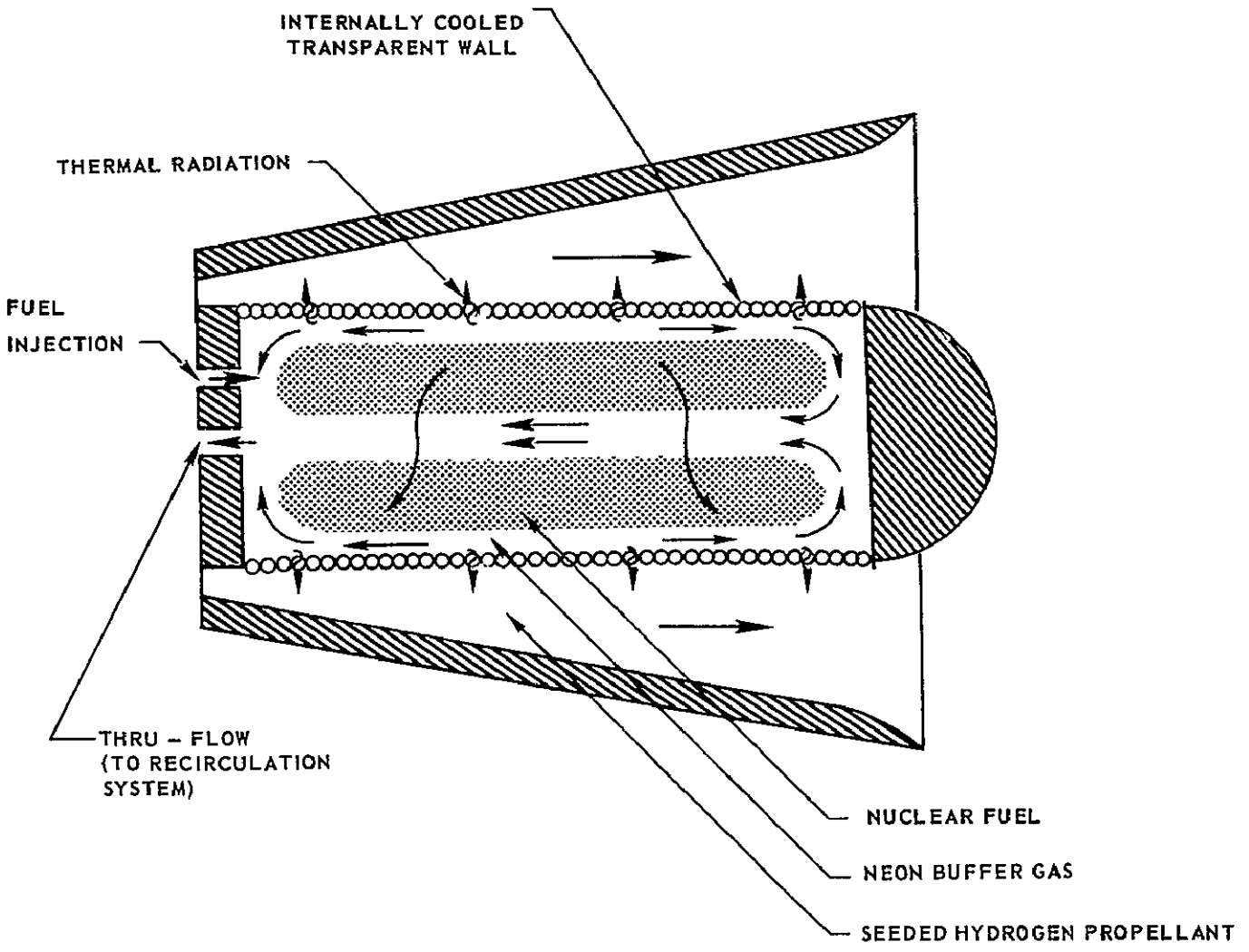

SKETCH OF RADIANT ENERGY SOURCE CONFIGURATION USED IN TESTS

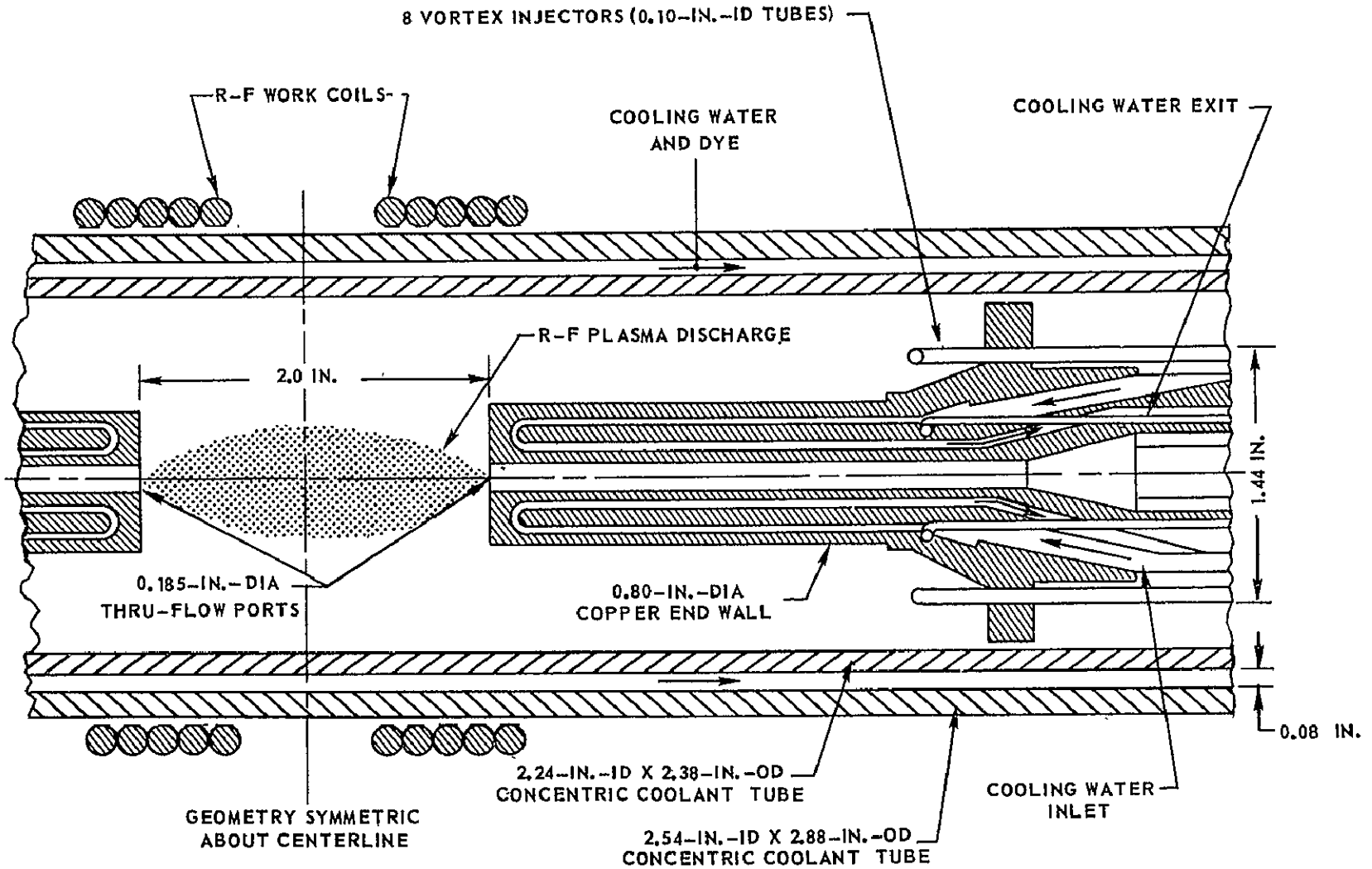

FIG. 2

FIG. 3

VARIATION OF RADIANT ENERGY FLUX WITH TOTAL R-F DISCHARGE POWER

1.2-MEGW R-F INDUCTION HEATER
RANGE OF CHAMBER PRESSURE, P_D = 2 TO 16 ATM
RANGE OF ARGON WEIGHT FLOW, W_A = 0.010 TO 0.041 LB/SEC

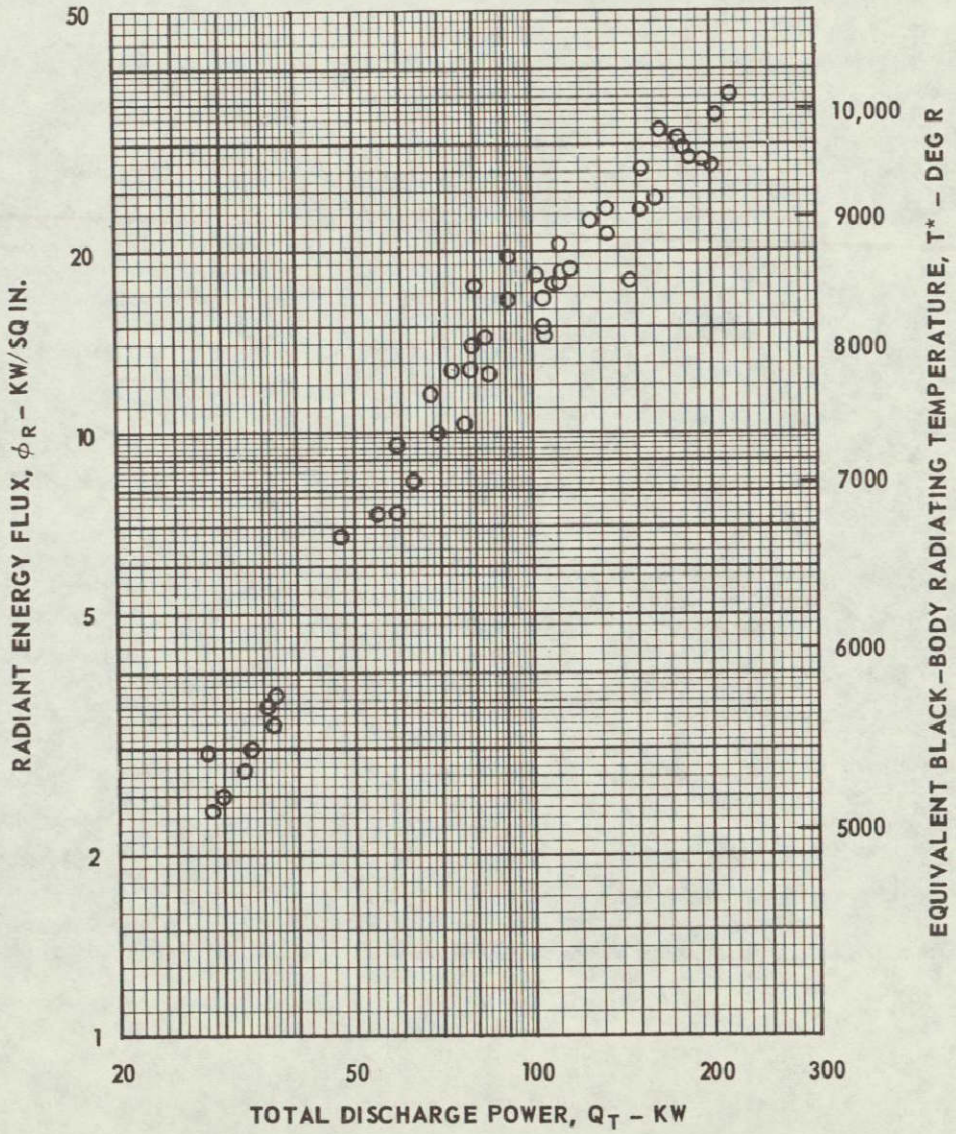

FIG. 4

PHOTOGRAPHS OF TRANSPARENT-WALL AXIAL COOLANT-TUBE MODEL

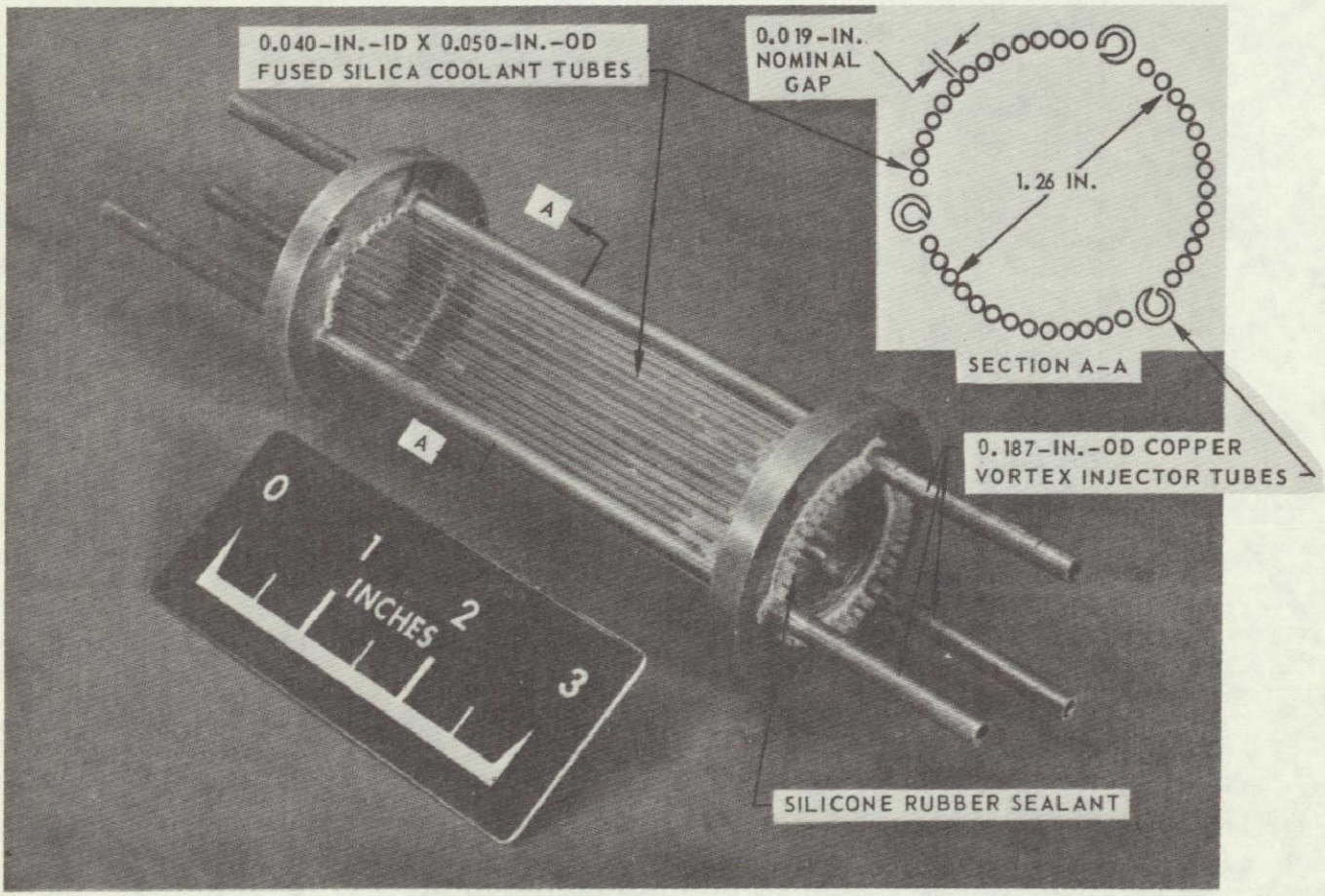

URANIUM PLASMA RESEARCH AT THE UNIVERSITY OF FLORIDA

R. T. Schneider, C. D. Kylstra and M. J. Ohanian
University of Florida
Gainesville, Florida

The eventual successful operation of a nuclear energy source utilizing fuel in the plasma state, whether for propulsion or other applications, will require knowledge of the radiation emitted by the uranium plasma as a function of operating pressures, temperatures, wavelengths, and system geometry. Supplementary to this is the composition of the plasma, i.e., the partial pressure distributions of the various uranium ionic species and the electrons, as well as that of any working fluid present. Calculations concerning criticality, radiative heat transfer to the working fluid, and system startup and control all need the above information.

The object of the uranium plasma research program at the University of Florida is to acquire at least some of the radiation emission and composition data needed in addition to some nuclear data (Ref. 1-5). This paper will be concerned with the preliminary experimental results of the measurement of temperature and partial pressure of a uranium plasma. (For other research efforts on radiation and composition of uranium plasmas see Ref. 6 and 7.)

The experimental apparatus is a high pressure chamber capable of 100 atmosphere pressure with water cooling to the thermal shield, tungsten cathode, and tungsten crucible with a uranium insert as the anode, the uranium is vaporized by a D.C. arc.

The measurement method used for the arc temperatures and temperature distributions is the Boltzmann Plot technique and the single-line relative intensity method which can be used when the radial intensity distribution shows an off-axis maximum.

The partial pressure distributions of the individual uranium ionic species can be obtained from a correlation of the temperature distribution from the Boltzmann Plot techniques and the temperature distributions from the single-line relative intensity method. Fig. 1 shows the result of a temperature determination using Boltzmann Plots for singly ionized uranium. Fig. 2 shows the partial pressure distribution for singly ionized uranium (UII).

The thermodynamic characteristics of uranium at high temperatures ($T > 3000^{o}K$) are important for several applications, e.g., accident analysis. Due to temperature limitations little experimental data is available. One important property falling into this category is the vapor pressure. Recent work using the effusion method (Ref. 8 and 9), has been limited to a maximum temperature of approximately $2500^{o}K$. For higher temperatures, the vapor pressure must be extrapolated. The boiling point temperature predicted by extrapolation is in excess of $4000^{o}K$ at one atmosphere. For these conditions, uranium is already a plasma.

Nottingham (Ref. 10) has shown that for an arc, the voltage-current characteristic can be related to the anode boiling temperature. Thus, the boiling temperature can be determined by measuring the voltage-current characteristics.

Figure 3 illustrates a typical set of arc voltage-current characteristics. Figure 4 shows the uranium boiling temperatures determined in this experiment. There is good agreement between the experimentally determined boiling temperatures and the boiling points predicted by extrapolation from low temperature vapor pressure measurements. The determined boiling temperature is 3,837°K for 1.0 atmosphere.

Future plans for the research effort are the determination of the emission coefficient of a uranium plasma for a wide range of temperatures and pressures, the study of a fissioning plasma and the study of the interaction of fission products with a noble gas plasma.

REFERENCES

1. Schneider, R. T., Kylstra, C. D., Randol, A. G., III, and Ohanian, M. J., "Radiation from a Uranium Plasma," presented at the 15th Annual Meeting of the American Nuclear Society, June 1969.

2. Randol, A. G., III, "A Determination of High Pressure, High Temperature Uranium Plasma Properties," Ph.D. Dissertation, University of Florida, August, 1969.

3. Schneider, R. T., Randol, A. G., III, Kylstra, C. D., and Ohanian, M. J., "Measurement of the Emission Coefficient of a Uranium Plasma," to be presented at the 15th Winter Meeting of the American Nuclear Society, December, 1969.

4. Schneider, R. T., Randol, A. G., III, and Shipman, G. R., "Measurement of the Temperature and Partial Pressure of a Uranium Plasma," presented at the 20th Annual Mid-American Symposium on Spectroscopy, Chicago, Illinois, May, 1969, and to be published in Applied Spectroscopy, March-April, 1970.

5. Campbell, H., Schneider, R. T., and Kylstra, C. D., "Properties of a Uranium Plasma," to be presented at the Plasma Dynamics session of the AIAA 1970 Aerospace Sciences Meeting, New York, 1970.

6. "Investigation of the Spectral Emission Characteristics of Argon-Tungsten and Argon-Uranium Plasmas," United Aircraft Reports No. G910092-10 and G910092-11 (1968).

7. Parks, D. E., Lane, G., Stewart, J. C., and Peyton, S., "Optical Constants of Uranium Plasma," Gulf General Atomic Report No. GA-8244 (1968).

8. Storms, E. K., Thermodynamics, Vol. I, IAEA, Vienna, 1966.

9. Pattoret, A., Drowart, J., Smoes, S., Thermodynamics of Nuclear Materials, IAEA, Vienna, 1968.

10. Nottingham, W. B., AIEE, Transactions, 42, 302 1923.

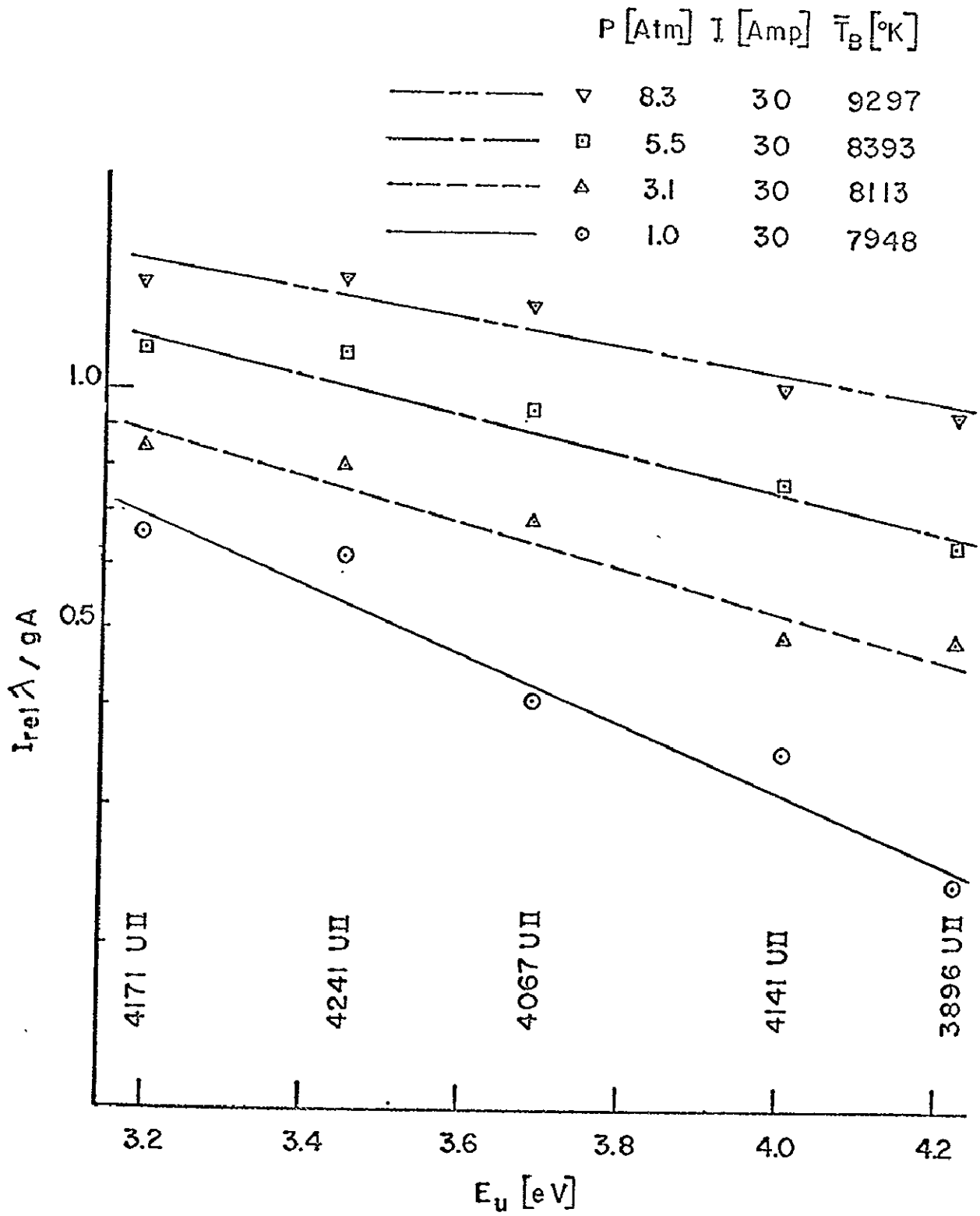

FIG. 1 IONIC BOLTZMANN PLOT USING CHORDAL INTENSITIES OF UII LINES

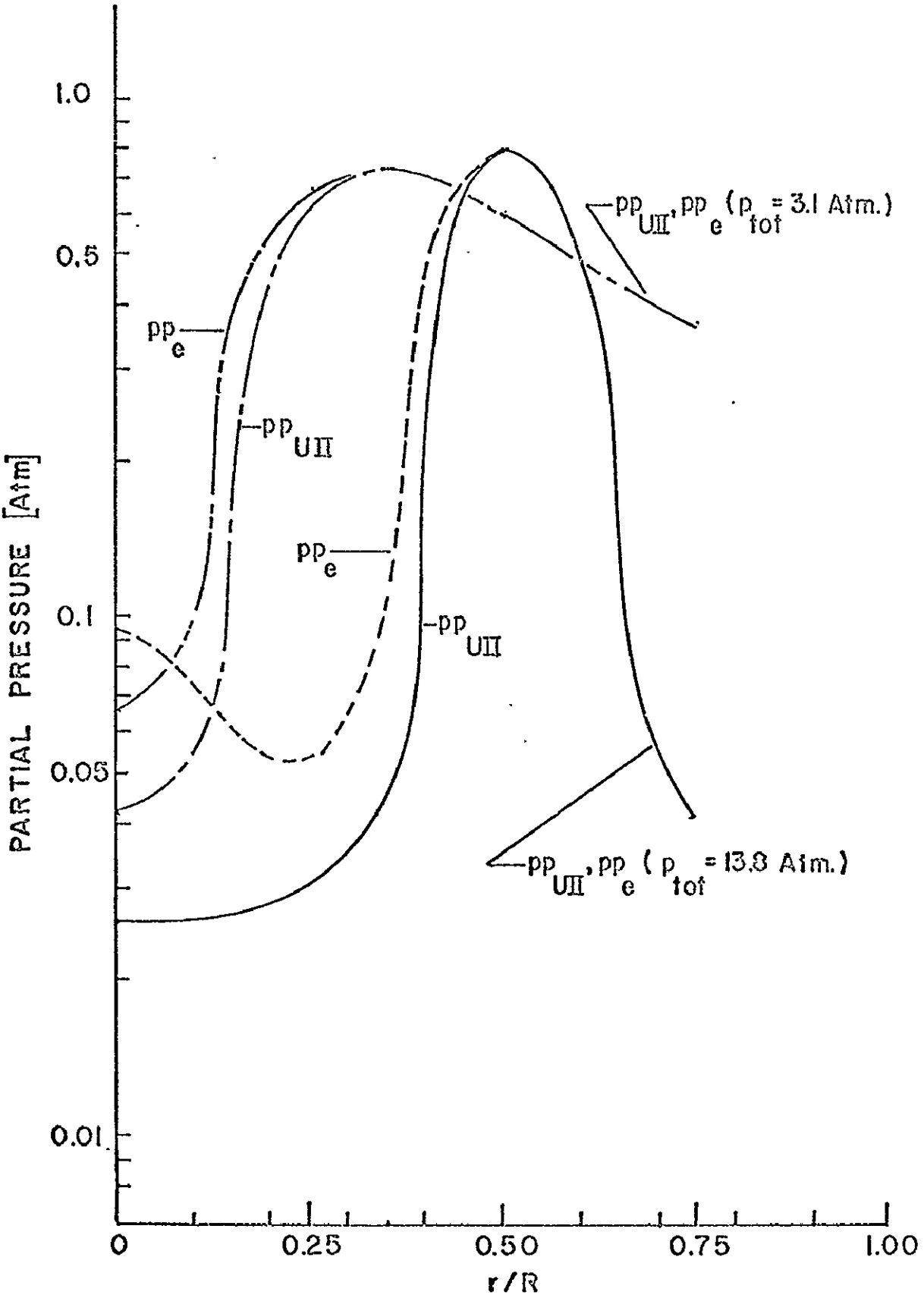

FIG. 2 URANIUM II AND ELECTRON PARTIAL PRESSURE PROFILES.

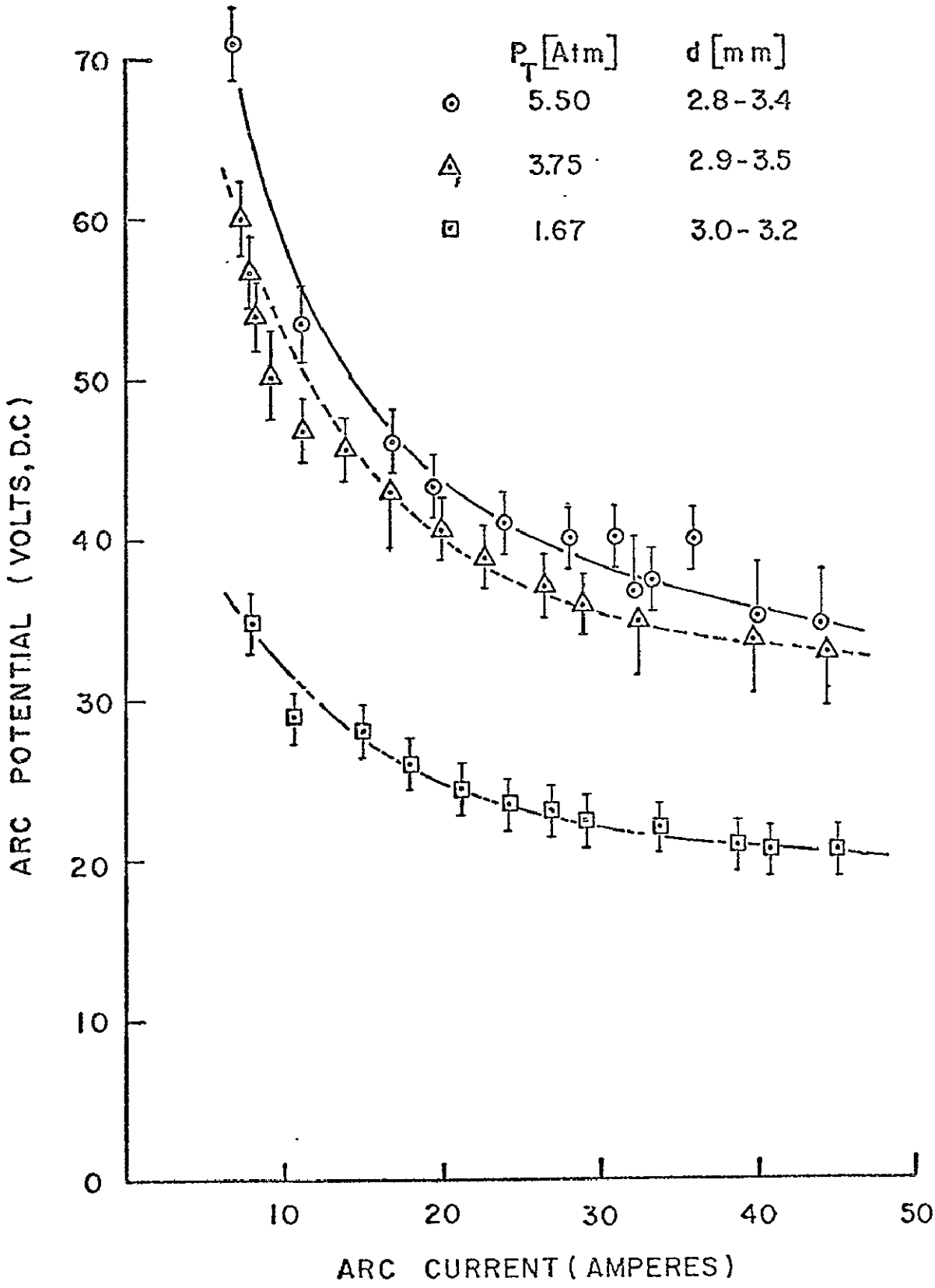

FIG. 3 HIGH PRESSURE URANIUM ARC VOLTAGE-CURRENT CHARACTERISTICS

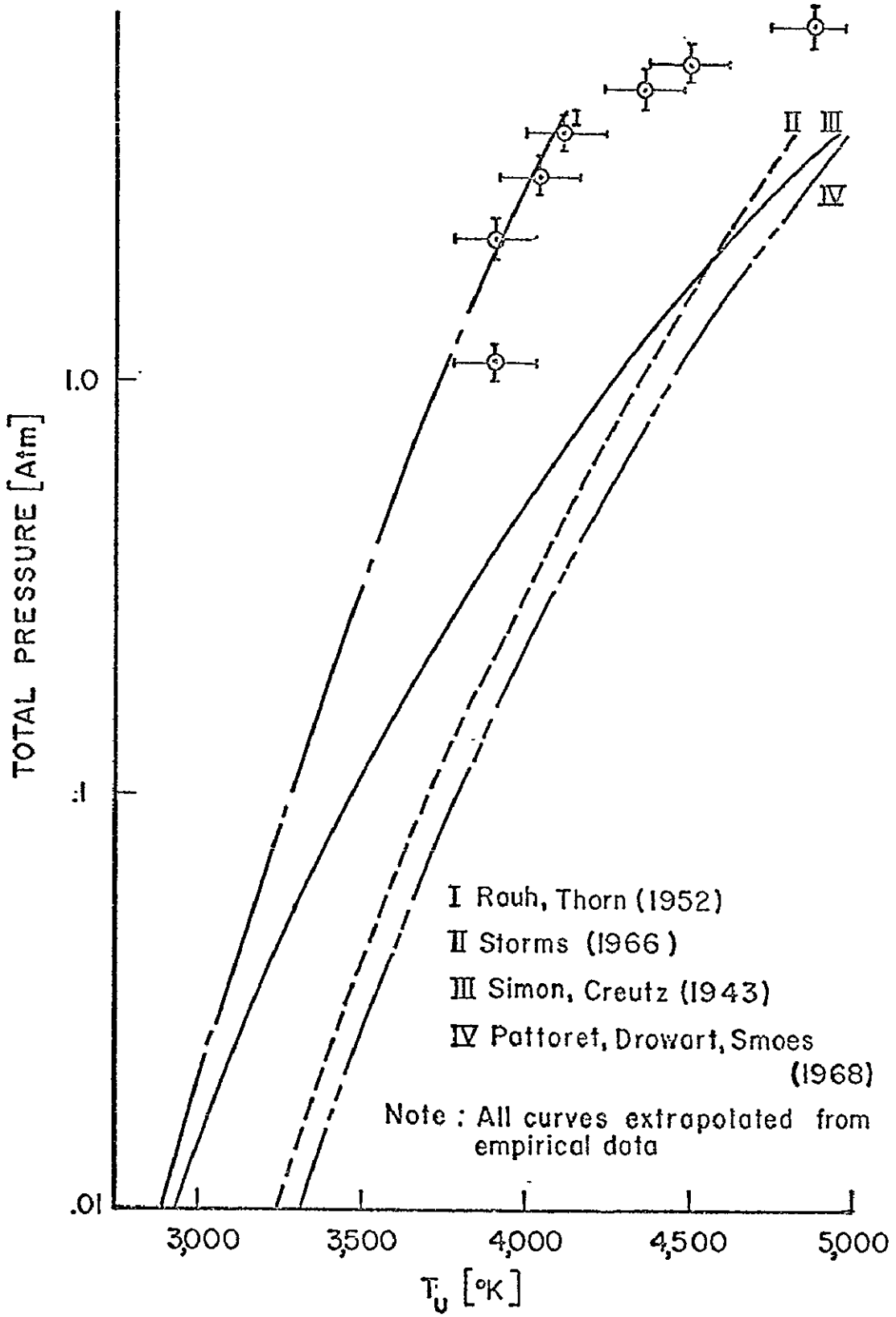

FIG. 4 TOTAL PRESSURE VERSUS ANODE BOILING TEMPERATURE

COMBINED THEORETICAL AND EXPERIMENTAL RESULTS OF HEAT TRANSFER TO AN ANODE*

P. F. Massier[+] and T. K. Bose[#]

Jet Propulsion Laboratory
Pasadena, California

ABSTRACT

The purpose of this investigation is to evaluate the heat transfer to an anode in the presence of a transverse gas flow. The work was initiated because the heat transfer to some of the elements of plasma propulsion devices, especially to the anode, can be significantly higher than that encountered in chemical propulsion thrust chambers. Furthermore, impingement of electrons on the anode can produce an amount of heating greatly exceeding that caused by convection from the bulk motion of the plasma. Experimental heat transfer results are analyzed in conjunction with a theoretical prediction method for ionized gas flows over a segmented flat surface with an electric field applied to the upstream segment, which is the anode (Fig. 1). Under the influence of the transverse gas flow, the arc attaches near the downstream end of the anode, and the discharge is deflected from a vertical plasma column into an elongated U-shape by the motion of the argon gas giving a boundary layer type appearance over the anode and the segments downstream of the anode. Tests have been conducted in an argon atmosphere at a nominal pressure of 50 mm Hg and a current of approximately 40 amps over a gas velocity range of about 55 to 260 ft/sec. Each of the electrode segments are individually cooled and the heat transfer rate is determined from the coolant flow rate and the rise in the coolant temperature. In the absence of plasma free-stream temperature measurements, which are planned, the temperature is deduced from heat loads to the three segments downstream of the anode. By matching the heat load distribution of the downstream segments with the theoretical predictions by considering convection and diffusion only, it has been established that the origin of the thermal boundary layer for all tests occurred at a distance of about 0.8 of the segment length (0.20 in.) from the leading edge of the anode. It is also deduced, with the help of Fig. 2, that the free stream temperature associated with the heat transfer for one that was around 13,000°R, and was almost constant along the flow direction. From the experimental heat load to the anode, the theoretical heat load to the anode due to convection and diffusion is subtracted to obtain the contribution of the electric current, which was 0.247 Btu/sec or 87 percent of the total heat load. This was then used in conjunction with the theoretical prediction as shown in Fig. 2 to estimate the combined anode fall potential and work function which was found to be 4.9 volts. This value seems quite reasonable compared with measurements of other investigations.

---

*This work represents the results of one phase of research carried out in the Propulsion Research and Advanced Concepts Section of the Jet Propulsion Laboratory, California Institute of Technology, under Contract NAS7-100, sponsored by the National Aeronautics and Space Administration.

[+]Group Supervisor

[#]NASA-NRC Resident Research Associate

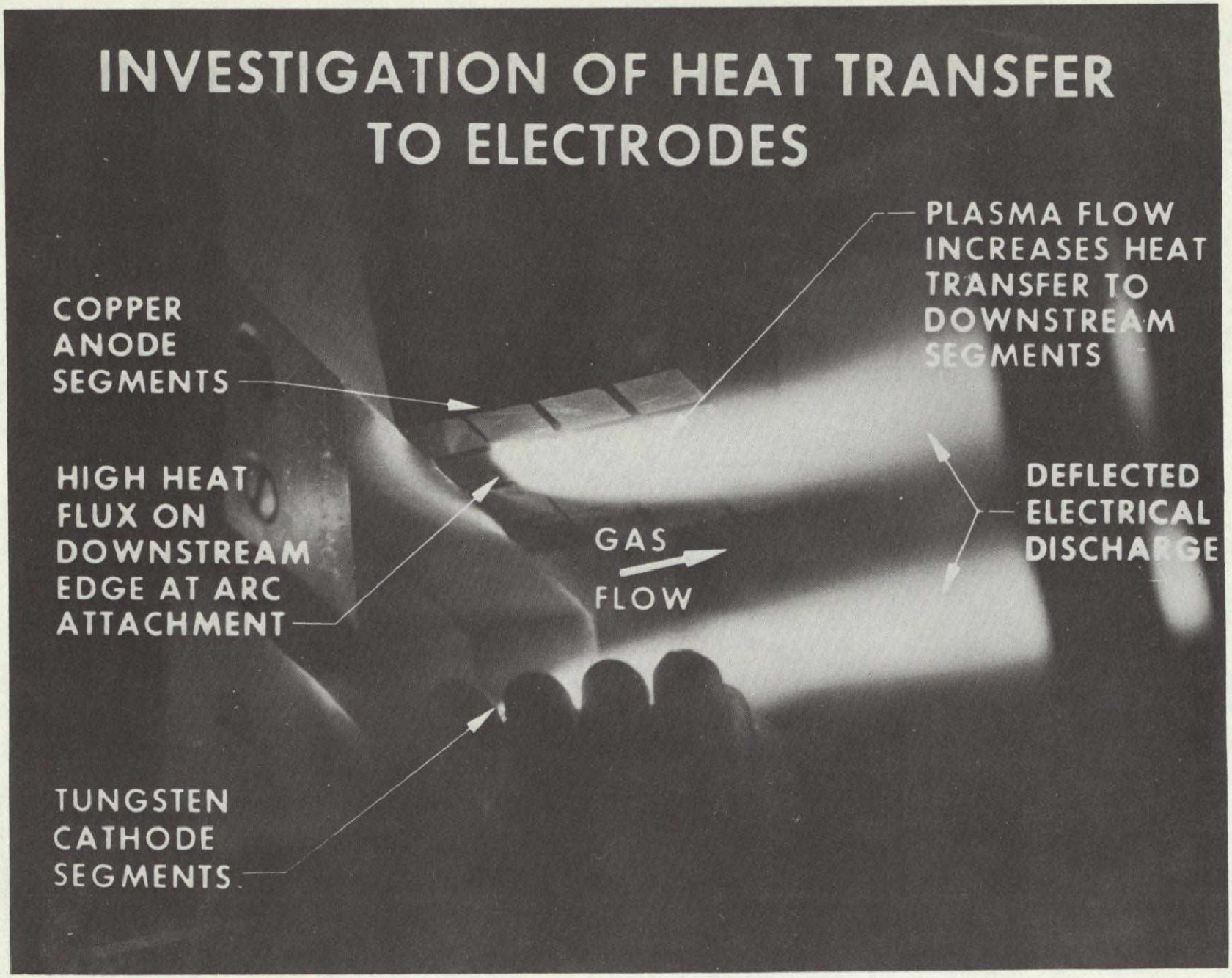
INVESTIGATION OF HEAT TRANSFER TO ELECTRODES
PLASMA FLOW INCREASES HEAT TRANSFER TO DOWNSTREAM SEGMENTS
COPPER ANODE SEGMENTS
HIGH HEAT FLUX ON DOWNSTREAM EDGE AT ARC ATTACHMENT
GAS FLOW
DEFLECTED ELECTRICAL DISCHARGE
TUNGSTEN CATHODE SEGMENTS

FIGURE 1

ANODE HEAT TRANSFER

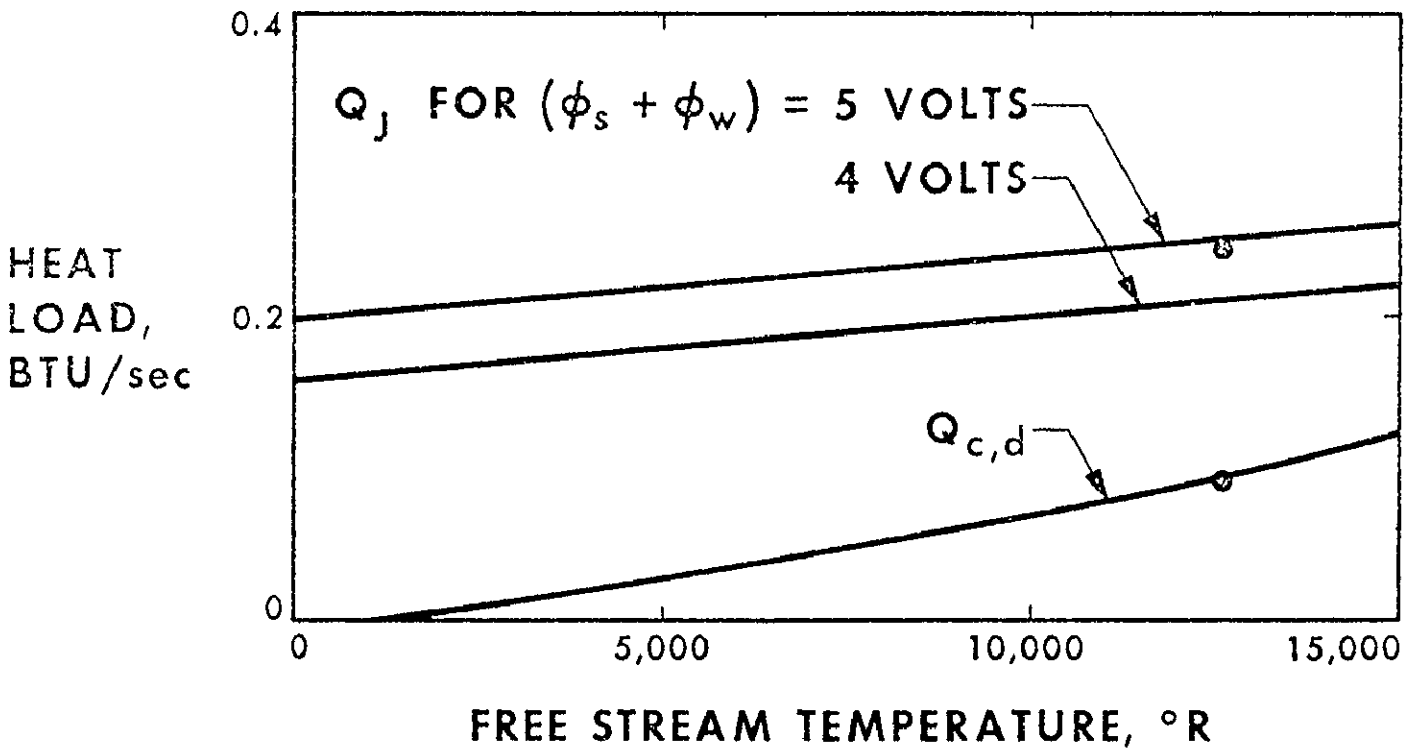

PROPULSION DIVISION
RESEARCH AND ADVANCED CONCEPTS SECTION

FIGURE 2

A STUDY OF THE EFFECT OF ION INTERACTIONS IN PLASMA ACCELERATORS

Sol Aisenberg and K. W. Chang
Space Sciences, Incorporated
Waltham, Massachusetts

As part of the study of plasma boundary interactions in magnetically accelerated plasmas, it was established that as much as 15 percent of the plasma driving force was transferred by the positive ions to the cathode. This ion current drag at the cathode contributes to the cathode damage as well as to the reduced plasma propulsion efficiency. The study of the translational cathode drag due to the positive ions (and to the neutral gas component as well) indicated that there is a threshold in the tangential drag force as well as a saturation effect. The threshold can be ascribed either to a threshold in the tangential ion velocity, in the ion current partitioning, or in the tangential accommodation coefficient. In studying the effect of ion currents on the cathode it was established that there is a need for an accurate measurement of the ion and plasma velocity. With this velocity measurement as a function of magnetic field and current it is possible to determine if there is, indeed, a threshold in the tangential velocity. At the same time, the measurement of the velocity together with the drag measurement can permit one to deduce the ion current partitioning at the cathode. The determination of the ion current partitioning at the cathode spot will also be of help in the establishment of a model for the electron emission at arc cathodes.

The recent effort, therefore, has been devoted to the determination of the plasma velocity in order to determine the 1) ion current fraction at the cathode spot, 2) any possible threshold in ion tangential velocity, and 3) the existence of a saturation effect in ion velocity.

There are a number of different ways of measuring ion velocity: one is the back EMF method where the terminal voltage is measured as a function of transverse magnetic field for a constant arc current and gap spacing. A second method of determination of plasma velocity is by means of a time-of-flight measurement where the velocity of a moving plasma is measured by means of photo-multipliers, and is an unsatisfactory method of determining plasma velocity since it actually measures the velocity of propagation of the plasma phase rather than the velocity of the individual plasma components. This is shown by the existence of the phenomenon of retrograde motion.

Measurements were made in a circular accelerator channel to compare the velocity deduced from back EMF with the velocity deduced by time-of-flight measurements for the identical J x B accelerator situation. The analysis of Alfven suggests the existence of an ionization limiting velocity. Measurements have shown that the back EMF determination of plasma velocity is much

closer to the values expected from the ionization limiting velocity and that the time-of-flight method gives about two orders of magnitude of lower velocity and is, therefore, unsuited for velocity determination. The ionization limiting velocity as determined by the theory of Alfven is predicted to be a constant independent of magnetic field. Some results are illustrated in Figure 1. The velocity deduced from the back EMF method is essentially a constant since it is related to the slope of terminal voltage with respect to magnetic field and it was observed that the slope is essentially a constant. The time-of-flight method indicates a slight increase of transit velocity as a function of magnetic field. The concept of ionization limiting velocity suggests that this velocity is independent of pressure while measurements of the velocity determined from back EMF and also from time-of-flight show a decrease of velocity with increasing pressure.

As part of this research program a technique has been developed for the direct measurement of plasma ions and atoms by means of a Doppler shift technique. The system is illustrated in Figure 2. Light from the plasma is sampled by means of fiber optics and can be used to measure velocities for both approaching and receding plasmas. The wave length shifts of the radiation is measured very accurately by the means of a Fabry-Perot interferometer. By modulation of the interferometer mirror and by means of a phase sensitive detector it is possible to close the feedback loop in order to operate the system as an optical discriminator where a resonant frequency of the interferometer is locked to the line center. In this way the Doppler shift signal consists of a DC output voltage which is directly proportional to the ion or atom velocity. Preliminary measurements of the Doppler shift velocity indicate that it is comparable with the values determined from the back EMF method as well as with the values approximately expected from the ionization limiting velocity. Doppler shift measurements are being made for different gases and electrodes and as a function of gas pressure, arc current and transverse magnetic field.

The role of positive ions in the cathode spot has also been studied. It is well known that in the arc discharge, as the gas pressure is reduced, the current density at the cathode decreases gradually until at a lower pressure, a transition phase is reached, after which the current density suddenly increases to very high values. This transition is believed to be a change from a thermionic cathode to a field type of cathode. The usual model of field emission, which is based on the electrostatic field of the average ion space charges in the bipolar sheath, is inadequate to explain the observed level of emission current densities. A new model based on a modified field emission process which takes into account the local electric field associated with each individual ion is presented. Preliminary calculations show that this added effect due to the intense local ionic force field can indeed provide an emission current large enough to account for the observed current densities. Experimental verification of this model requires an experimental determination of the positive ion current fraction at the cathode.

Despite recent advances in the area of arc and plasma research, there has been no satisfactory way of measuring the fraction of electron current at the cathode surface. Although this information is vital for the understanding of the emission mechanisms, only very crude estimates are available in the literature. These estimates are usually obtained from energy balance calculations, and they are inaccurate because of the uncertainty in various unknown parameters. The present results of the tangential drag measurements and the Doppler shift determination of velocity will permit evaluation of the ion current fraction at the cathode spot. An additional method for the determination of current partitioning at the cathode is proposed, based on the principle of perpendicular force and momentum balance at the cathode surface. A unique model for various components of electrode forces is presented which is capable of explaining the known behavior of cathode forces at different pressure and current levels. The fraction of electron current at the cathode can be determined from the following equation:

$$f = \frac{I_e}{I} \cong 1 - \frac{F + n_e k T_e A - \Gamma_{evap} \sqrt{2kT_c/\pi m_c}\ A}{(I/e)(1-\sigma)\sqrt{2 m_i e |\phi_{cd}|}}$$

Where I is the measured total arc current, I_e, the electron current at the cathode, σ, the normal momentum accommodation coefficient, e, the electronic charge, m_i, the ionic mass, ϕ_{cd}, the cathode drop, F, the measured resultant force on the cathode, N_e, the electron number density of the arc spot, T_e, the electron temperature of the arc spot, Γ_{evap}, the flux of evaporating cathode material, T_c, the cathode temperature, m_c, the molecular mass of the cathode material, A, the cathode spot area and k, the Boltzmann constant.

Because in the low pressure range of interest the conditions of $F >> \Gamma_{evap} \sqrt{\frac{2kT_c}{\pi m_c}}\ A$ and $F >> n_e k T_e A$ are usually satisfied (as a simple, order of magnitude calculation indicates), the present method is believed to be effective and accurate especially in the low pressure range where the arc is supported by the ion microfield emission process.

CUMMULATIVE LIST
REPORTS, PUBLICATIONS, AND PRESENTATIONS
UNDER THIS PROGRAM

1. S. Aisenberg, P. Hu, V. Rohatgi, and S. Ziering, "A Study of Electrode Effects in Crossed Field Accelerators," Summary Report, Contract NASw-1014, prepared for National Aeronautics and Space Administration (1965).

2. P. N. Hu and S. Ziering, "Kinetic Model for Three Component Plasmas with Ionization,"Physics of Fluids, 9, 1983 (1966).

3. P. N. Hu and S. Ziering, "Collisionless Theory of a Plasma Sheath Near an Electrode," Physics of Fluids, 9, 2168 (1966).

4. S. Aisenberg and V. Rohatgi, "A Study of Arc Constriction Processes," presented at the Seventh Symposium on the Engineering Aspects of Magnetohydrodynamics, March 1966.

5. S. Aisenberg and V. Rohatgi, "Measured Tangential Electrode Forces for an Arc in a Transverse Magnetic Field," Applied Physics Letters, 8, 194 (1966).

6. V. Rohatgi and S. Aisenberg, " Composite Metallic and Dielectric Insulators for High Current Arc Electrodes, " Rev. Sci. Instr., 37, 1603 (1966).

7. P. N. Hu and S. Ziering, "Collisionless Plasma Sheath with Transverse Flow." Presented at the Eighth Annual Meeting of the Plasma Physics Division, American Physical Society, Boston, Mass., Nov. 1966.

8. V. Rohatgi and S. Aisenberg, "Tangential Momentum Transfer to the Electrodes of a Magnetically Accelerated Arc." Presented at the Eighth Annual Meeting of the Plasma Physics Division, American Physical Society, Boston, Mass., Nov. 1966.

9. S. Aisenberg and V. Rohatgi, "A Study of Electron Emission Processes at Arc Cathodes." Presented at the Eighth Annual Meetinf of the Plasma Physics Division, American Physical Society, Boston, Mass., Nov. 1966.

10. S. Aisenberg, "Plasma Propagation Theory of Arc Retrograde Motion." Presented at the Eighth Symposium on the Engineering Aspects of MHD, March 1967.

11. V. Rohatgi and S. Aisenberg, "Ion Drag and Current Partitioning at the Cathode of a Plasma Accelerator." Presented at the AIAA Joint Electric Propulsion and Plasma Dynamics Conference, Colorado (September 1967).

12. P. N. Hu and S. Ziering, "Collisionless Plasma Sheath with Transverse Flow," Physics of Fluids, 11, 451 (1968).

13. P. N. Hu and S. Ziering, "Collision and Ionization Effects in a Plasma Sheath," Journal of Plasma Physics, 2, 110 (1968).

14. S. Aisenberg, P. N. Hu, V. Rohatgi and S. Ziering, "Plasma - Boundary Interactions," NASA Contractor Report, NASA CR-868, Washington, D. C. August, 1967.

15. S. Aisenberg, P. N. Hu, V. Rohatgi, and S. Ziering, "Plasma - Boundary Interactions - II", NASA CR-1072, Washington, D. C. June, 1968.

16. V. Rohatgi and S. Aisenberg, "Ion Drag and Current Partitioning at the Cathode of a Plasma Accelerator." AIAA Journal, 7, 502, 1969.

17. S. Aisenberg and V. Rohatgi, "Plasma Boundary Interactions - III", (Submitted to NASA for approval).

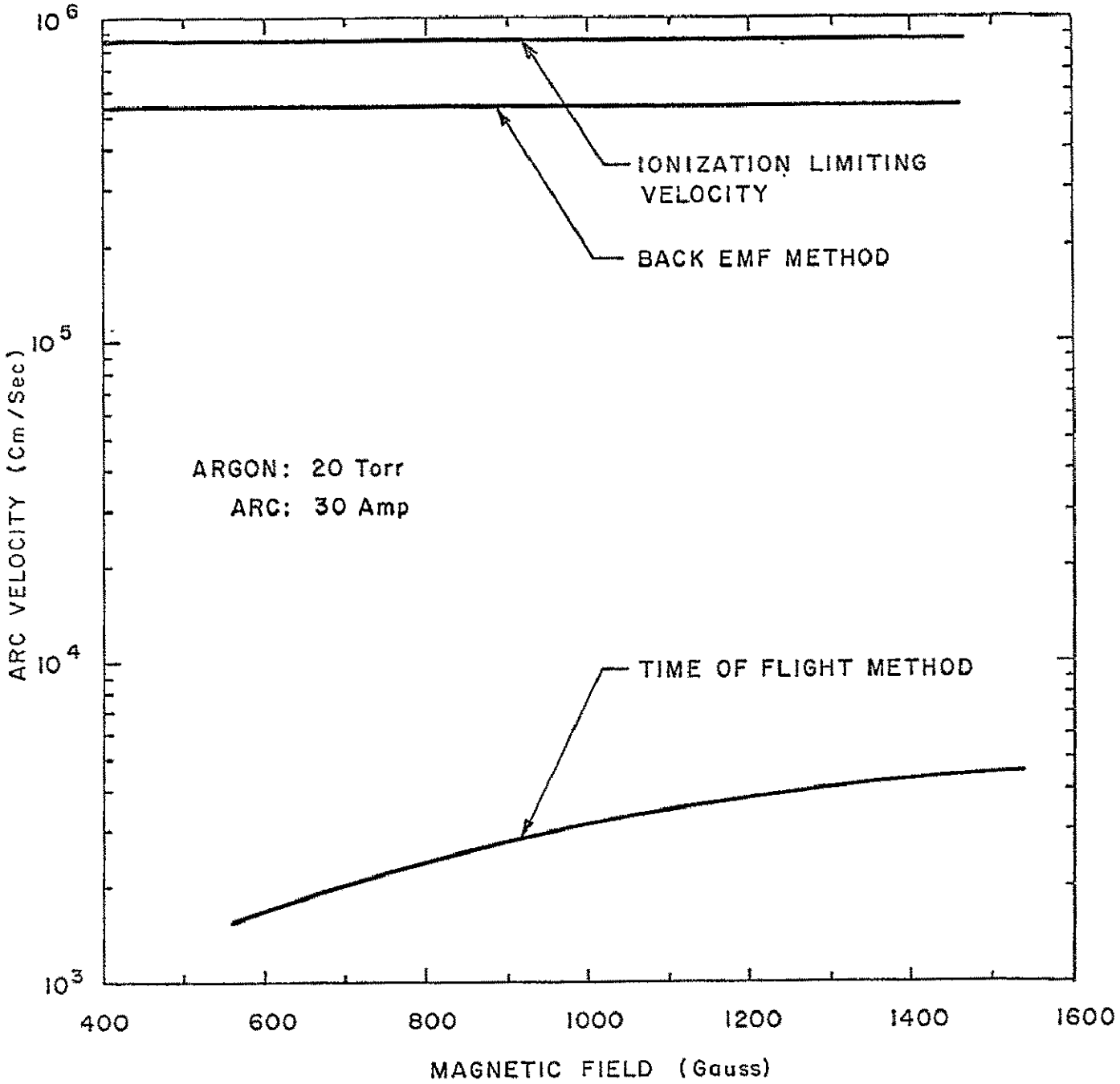

FIGURE 1

COMPARISON OF ARC VELOCITY AS DETERMINED BY VARIOUS METHODS.

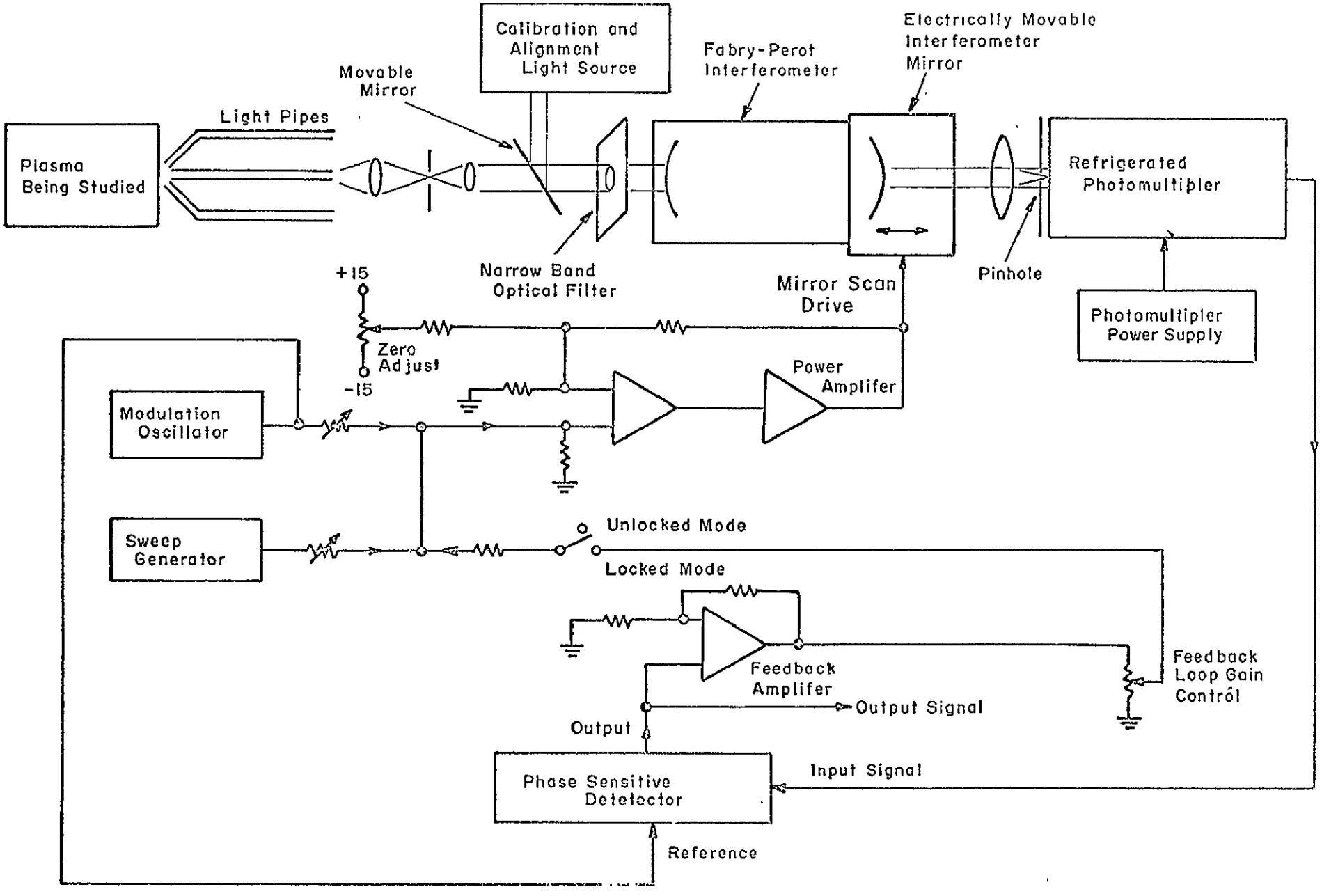

FIGURE 2

ILLUSTRATION OF SYSTEM FOR THE MEASUREMENT OF DOPPLER SHIFT AND LINE SHAPE OF RADIATING IONS AND ATOMS.

MHD BOUNDARY LAYERS WITH NONEQUILIBRIUM IONIZATION AND FINITE RATES

Arthur Sherman[1], Hsuan Yeh[1], and Eli Reshotko[2]

During a previous NASA research contract an analysis was made of the nonequilibrium plasma boundary layer developing over an insulator wall including imbedded electrodes. Such a case was chosen to simulate the boundary layer in an MHD channel with finite electrodes. The primary difficulty in that analysis proved to be the singularity at the initial and trailing edges of the electrode which made the numerical solution tedious. In the earlier analysis we had assumed the flow to be in quasi-equilibrium such that the electron density could be calculated from the Saha Law using the electron temperature. The primary objective of the present analysis is to extend the previous study to the situation where ionization and recombination rates are slow enough to cause significant departures from quasi-equilibrium. In other words, we wish to consider finite rates and study flows which are to some extent frozen.

In the earlier work, the electron temperature was taken into account by considering the partial differential equation governing the conservation of electron energy. In order to provide the wall boundary condition the plasma sheath was considered in a simple manner. For the present investigation it is necessary to include one additional equation governing the electron density, which is the partial differential equation for the conservation of electron species. Including this additional equation means that we are solving four highly nonlinear partial differential equations by the finite difference method we have developed. This has the effect of substantially slowing down an already tedious numerical calculation, since now 4×4 matrices have to be inverted at each calculation point rather than 3×3 as before.

To date, the new system of equations allowing for finite rates have been formulated and their transformation completed. The transformed equations have also been reduced to finite difference format in a much more compact form than had been done before. The hope here is that this new form will permit a reduction in computer time. A computer program has been written to solve these equations in their finite difference form, and calculations are in progress.

[1]Computer and Applied Sciences, Inc.
[2]Case Western Reserve University

STRUCTURE OF A COLLISIONLESS SHEATH IN THE PRESENCE OF A MAGNETIC FIELD*

H. A. Hassan

North Carolina State University, Raleigh, North Carolina 27607

The objective of this Grant is to study the surface-sheath-plasma interactions in devices being considered for plasma acceleration and MHD power generation. In such devices the electron temperature is different from the heavy particle temperature and one needs to consider the structure of the sheath near the electrode to obtain necessary boundary conditions. The description of the plasma in a given device is then obtained by matching the sheath solution and the solution of the conservation equations of the various plasma constituents at the sheath edge.

The appropriate transport properties for a plasma in a magnetic field and the influence of the surface parameters on the sheath structure were studied under this Grant[1-4]. At present, we are in the process of integrating these studies so that we may obtain an understanding of the coupling between surface, sheath and the bulk of the plasma. The work is in the computational stage.

The work carried out in References 2-4 assumes that the sheath thickness is less than the mean free paths and the Larmor radii. When the restriction on the Larmor radii is relaxed, the equations governing the collisionless sheath are the Vlasov equation and the appropriate Maxwell's equations. These equations can be expressed as

$$\vec{\xi}_j \cdot \frac{\partial f_j}{\partial \vec{r}} + \frac{e_j}{m_j} [\vec{E} + \vec{\xi}_j \times \vec{B}] \cdot \frac{\partial f_j}{\partial \vec{\xi}_j} = 0 \qquad (1)$$

$$\vec{B} = \nabla \times \vec{A} \ , \quad \nabla^2 \vec{A} = - \mu_o \vec{J} \qquad (2)$$

$$\vec{E} = - \nabla \phi \ , \quad \nabla^2 \phi = - \rho / \varepsilon_o \qquad (3)$$

with

$$\vec{J} = \Sigma e_j \int \vec{\xi}_j f_j \, d\vec{\xi}_j \ , \ \rho = \Sigma e_j n_j = \Sigma e_j \int f_j \, d\vec{\xi}_j \qquad (4)$$

and $\vec{\xi}_j$, e_j and m_j are the velocity, charge and mass of species j; $\vec{E}$ and $\vec{B}$ are the electric and magnetic fields; ϕ and $\vec{A}$ are the electric and magnetic potentials, and μ_o and ε_o are the permeability and permittivity of free space. For the case of an infinite planar electrode with uniform work function, the electric and magnetic potentials and the distribution functions are functions of the coordinates normal to the electrode. Solution of the Lagrangian subsidiary equations gives the constants of the motion which can be written as

---

* Work Supported, in part, by Grant NGR 34-002-048.

$$\varepsilon_j = \frac{1}{2} m_j \xi_j^2 + e_j \phi \ , \ C_y = \frac{e_j}{m_j} A_y + V_j$$

$$C_z = \frac{e_j}{m_j} A_z + W_j \qquad (5)$$

where U_j, V_j and W_j are the velocity components in the x, y and z directions. If one assumes that particles far from the electrode have no velocity components parallel to the electrode, then the distribution function may be chosen as

$$f_j = a_j \, \delta(W_j) \, \delta[V_j + \frac{e_j}{m_j} (A_y - A_y(\infty))] \, (\frac{m_j}{2\pi k T_j})^{1/2} \exp\left[-\left(\frac{\varepsilon_j - e_j \phi_j}{k T_j}\right)\right] \qquad (6)$$

where subscript ∞ designates conditions at the sheath edge, a_j is constant proportional to the number density, and δ is the Dirac delta function.

Examination of the solution shows that in order for the collected particles, j=1, to reach the electrode, their energy must be greater than ε_m, where

$$\varepsilon_m = \max \left[\frac{1}{2} \frac{e_1^2}{m_1} (A_y - A_y(\infty))^2 + e_1 \phi \right] \qquad (7)$$

The quantity ε_m is obtained as part of the solution of the two coupled nonlinear equations

$$\frac{d^2\phi}{dx^2} = -\frac{\rho}{\varepsilon_o} \ , \ \frac{d^2 A_y}{dx^2} = -\mu_o J_y \qquad (8)$$

It should be noted that, in this case, one needs not invoke the Bohn sheath criterion because the solution is always stable.

The results of the above analysis were employed to study the anode losses in plasma device where the dominant energy transfer to the anode is that due to the electron current. It was shown that the heat flux to the anode is given by

$$q \simeq j \left[\frac{k T_1}{e} + \phi_A + W + \varepsilon \right] \ , \ \varepsilon = \frac{\varepsilon_m - e_1 \phi_\infty}{e} \qquad (9)$$

where ϕ_A is the anode drop, W is the work function and j is the current density. The results of the computation show that ε, which depends on the magnetic field strength, is much less than ϕ_A. Hence, in those devices where the dominant energy transfer to the anode is that due to the electron current, the anode losses are independent of the magnetic field [5,6].

REFERENCES

1. Hassan, H. A., "Drift Velocities and Thermal Flux Vectors in a Seeded Plasma with Magnetic Fields" The Physics of Fluids, Vol. 11, No.1, pp. 106-111, January 1968.
2. Hassan, H. A., "Surface Effects on the Structure of a Collisionless Sheath near an Electrode," The Physics of Fluids, Vol. 11, No. 5, pp. 1085-1096, April 1968.
3. Hassan, H. A., and McDonald, P.W. "Parametric Study of Sheath-Boundary Interactions," The Physics of Fluids, Vol. 11, No. 12, pp. 2273-2275, December 1968.

4. Hassan, H. A., and Smith, N. S. "Influence of Surface Parameters on Anode Losses in Arcjets," AIAA Paper 69-107, January 1969. To appear in the AIAA Journal.
5. Shih, K. T., et. al. "Experimental Anode Heat-Transfer Studies in a Coaxial Arc Configuration," AIAA Journal, Vol. 6, No.8, pp. 1482-1487, August 1968.
6. Shih, K. T., "Anode Current and Heat Flux Distributions in an MPD Engine" AIAA Paper 69-244, March 1969.

Other Publications Generated by This Grant

1. Seals, R. K., Jr. and Hassan, H. A., "Analysis of MPD Arcs with Nonequilibrium Ionization," AIAA J., Vol. 6, No. 12, pp. 2273-2278, 1968.

2. Hassan, H. A., and Thompson, Charles C., "Onset of Instabilities in Coaxial Hall Current Accelerators," AIAA Paper No. 69-230, 1969. To appear in AIAA J.

3. Hassan, H. A., "A Criterion for Electrode Erosion or Entrainment in MPD Arcs," To appear in Energy Conversion.

ANALYSIS OF NOISY LANGMUIR PROBE CHARACTERISTICS

by Roman Krawec, NASA Lewis Research Center

The theory of current collection by a probe immersed in a plasma was developed in 1924 by Langmuir and Mott-Smith for the case of a quiescent plasma. Unfortunately, plasmas of interest in fusion research are seldom, if ever, quiescent.

A static current-voltage characteristic is generally obtained by filtering out any noise, and the resulting curve is then analyzed in the normal manner to obtain electron temperature.

It is not generally realized that the variation in noise amplitude as probe voltage is changed may possibly be used as a means of estimating the electron temperature. In some cases it may even be possible to determine whether the electron temperature, number density, or plasma potential is the time varying quantity. This note will investigate the effect of a sinusoidal variation of the above quantities on peak-to-peak probe noise.

Consider a plane probe and let the electron current to it be given by

$$I = q n A \left(\frac{kT}{2\pi m}\right)^{1/2} \exp\left[-qV/kT\right] \qquad (V \le 0) \qquad (1a)$$

$$I = q n A \left(\frac{kT}{2\pi m}\right)^{1/2} \qquad (V \ge 0) \qquad (1b)$$

where V is the probe voltage measured with respect to plasma potential, and the other quantities have their customary meanings. Let the time variation in electron temperature, density, and plasma potential be of the respective forms:

$$T = T_0\left(1 + T'/T_0 \cos\omega t\right) = T_0\left(1 + \beta_T \cos\omega t\right)$$

$$n = n_0\left(1 + n'/n_0 \cos\omega t\right) = n_0\left(1 + \beta_n \cos\omega t\right)$$

$$V_p = V_{p0}\left(1 + V_p'/V_{p0} \cos\omega t\right) = V_{p0}\left(1 + \beta_V \cos\omega t\right)$$

This allows us to write eqn. (1) in the form

$$I = q n_0 A \sqrt{\frac{kT_0}{2\pi m}}\left(1+\beta_n \cos\omega t\right)\left(1+\beta_T \cos\omega t\right)^{1/2} \exp\left\{-\frac{\varphi + \alpha\beta_V \cos\omega t}{1+\beta_T \cos\omega t}\right\} \qquad (2)$$

where $\varphi = qV/kT$; $\alpha = qV_{p0}/kT$

A dimensionless peak-to-peak noise is now defined as:

$$\eta = \left(I_{max} - I_{min}\right)/I_0$$

where I_{max} and I_{min} are the maximum and minimum values of eqn. (2) respectively, for a given value of probe voltage.

In this note we look at the peak-to-peak noise for the case when only a single parameter is time varying and the perturbation, β, is held constant as probe voltage is varied. Three typical cases are shown in Fig. 1. Both a time varying density or plasma potential have the same effect on the noise in the electron retarding region until probe voltage approaches plasma potential. Noise caused by variation of density remains constant in the electron accelerating region, while that due to variation in plasma potential goes to zero. The slope of the $\ln \eta$ against probe voltage gives the correct value of the electron temperature in both cases. A variation in plasma temperature manifests itself by having a non-linear portion for the electron retarding region, and by taking on a fixed value within the accelerating region.

After the particular time-varying parameter is determined, its amplitude may be found from a measurement of noise amplitude at plasma potential as shown in Fig. 2.

FIG 1. TYPICAL RESULTS WHEN $\beta = .25$

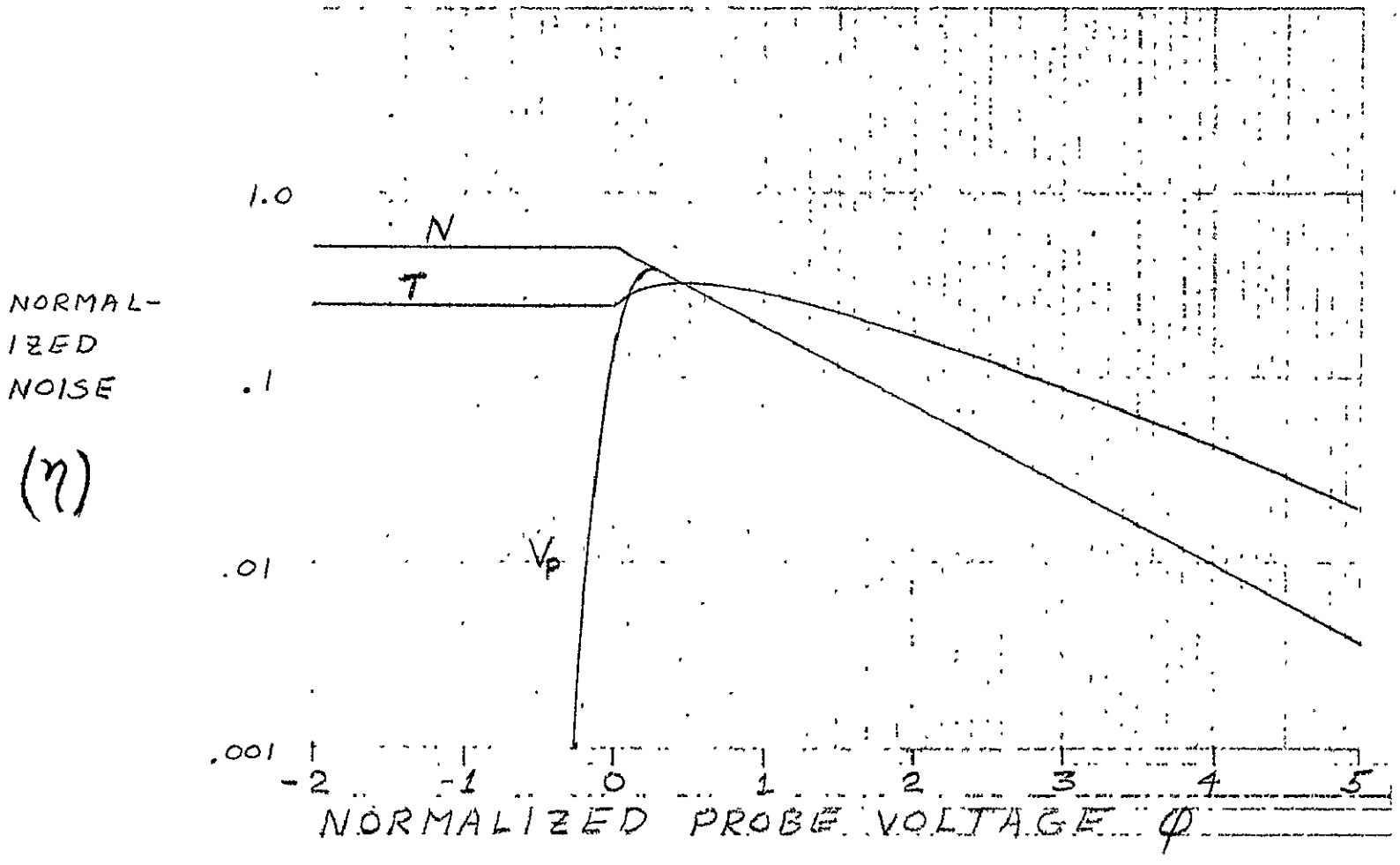

FIG 2
EFFECT OF VARIATION OF N, T, OR V_P
ON PEAK TO PEAK NOISE AMPLITUDE

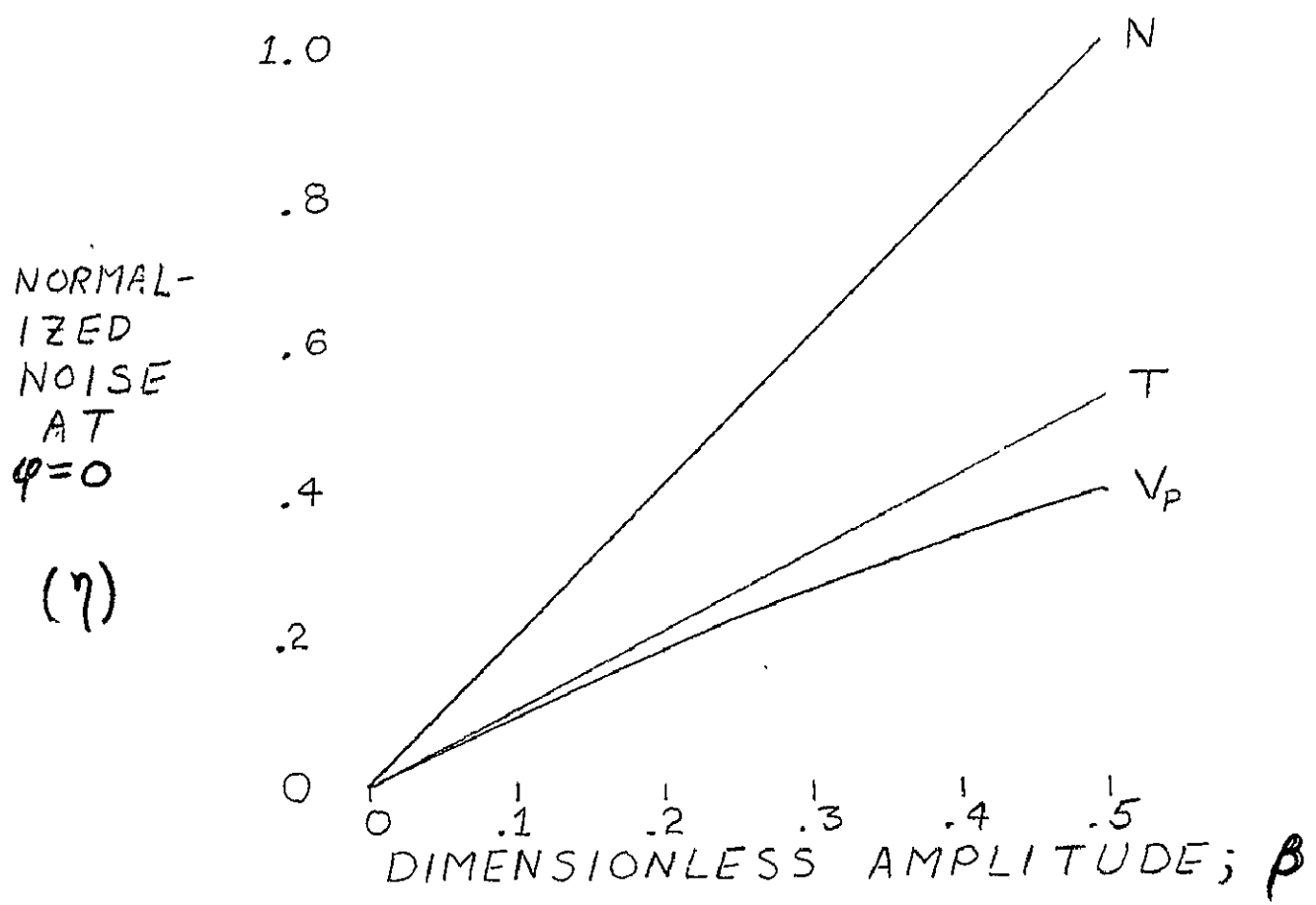

THE EFFECT OF SPACE CHARGE ON THE OPERATION OF ELECTRO-STATIC ENERGY ANALYZERS

by Richard R. Woollett
NASA-Lewis Research Center

When electrostatic energy analyzers are operated in plasmas, space charge inside the analyzer may lead to incorrect ion and electron temperature measurements. These space charge effects may become important when: (a) the plasma density is high; (b) the magnetic field is high; (c) or the spacing between the analyzer grids is large. The potential of the analyzer aperture plate, which is in contact with the plasma, also may affect the ion temperature measurements. This can also be related to space charge effects.

According to theory, space charge effects should become less pronounced as the grid spacing is reduced. To look for this effect, two energy analyzers were tested, each with a different grid spacing as shown on the analyzer schematic in figure 1. The analyzers were immersed in a 2 inch diameter plasma of about 10^{10} cm $^{-3}$ density. A 1,000 gauss field was alined with the analyzer axis. The plasma space potential was about -15v and the probe floating potential about -40v. The analyzer aperture plate was used as a planar Langmuir probe. A cylindrical Langmuir probe was also used to determine the plasma characteristics.

The plasma electron temperature, as determined from both the planar and the cylindrical Langmuir probes, was 8.6 ev. The cylindrical Langmuir probe gave the same electron temperature when its location was varied from 3 to 25 mm ahead of the aperture plate. Changing the potential of the aperture plate did not change the temperature determined by the cylindrical probe in any of its positions.

The electron temperature was also measured with the analyzers. Analyzer #2 measured the same electron temperature as the Langmuir probes. The #1 analyzer gave an electron temperature of 14 ev or roughly 1½ times higher than the Langmuir probes. Since the #2 analyzer had a grid spacing of roughly a third of the #1 probe, we conclude that decreasing the grid spacing improved the accuracy in electron temperature measurement. This trend is consistent with the space charge effects.

Ion temperatures determined by both analyzers are shown on figure 2 as a function of aperture plate voltage. The effect of varying the aperture plate voltage below the space potential is quite dramatic, especially for analyzer #1. For analyzer #1, the measured ion temperature varies by a factor of five over the range of aperture plate voltages shown. This variation is reduced to a factor of two in analyzer #2. Again we see a result that can be shown to be consistent with space charge effects, namely, that reducing the grid spacing reduces the variation in ion temperature measurement.

In all of the tests care was taken to insure cleanliness of all internal surfaces of the analyzers. If these surfaces are contaminated, especially the grids, a large hysteresis effect results. This is probably due to charge accumulation on the dirty surfaces. In this condition the analyzer would be unreliable.

There are two well-known one dimensional space charge models that predict the above mentioned trends. In both models we assume that only one species of charged particles is present. In model A the charged particles have no initial drift velocity, only thermal motion. In model B the particles have an initial uniform drift velocity, but no thermal motion. In both models, the potential variation between two adjacent grids is determined from the Child-Langmuir space charge expressions. Between adjacent grids the charge flow is considered as a current flowing between two plates. The ensuing space charge sets up a potential barrier that can affect the collected currents.

To approximate a one-dimensional energy analyzer the aperture plate would have to be replaced by a screen. And then if the analyzer were operated in a strong magnetic field, the charged particles would be tied tightly to the field lines, yielding a good approximation to a one-dimensional model.

In figure 3, results are presented for model A along with results for a model without space charge. Figure 3 is a plot of current to the gate versus gate voltage. The charged particles had a temperature of 7 ev and no initial drift velocity. A space charge will be set up between the entrance screen and the gate. If an exponential is fit to the model A curve we get a temperature of 40 ev. Therefore, space charge results in a temperature that is almost 6 times greater than the true value. In our experiments analyzer #1 gave electron temperatures that were about 1½ times the Langmuir probe results. Since an aperture produces a pencil beam, the one-dimensional approximation used in figure 3 is probably too severe.

The results for model B are given in figure 4. In this case the plasma had zero temperature. Grid A was set at 60 volts to separate the ions and electrons. The electrons reaching grid A therefore had zero temperature, and a uniform drift velocity equivalent to 60 ev. Consequently at grid A we have electrons flowing toward the gate. The electron density at grid A was assumed to be 10^9 cm^{-3}. The current collected on the gate is presented in figure 4 as a function of gate voltage. If space charge were not present, the full electron current would reach the gate for zero gate voltage as shown for the no-space-charge curve. But since space charge does exist between grid A and the gate, the knee is displaced. If an exponential is fit to this curve a temperature of 38 ev is obtained. The displacement of the knee of the curve is a characteristic observed experimentally.

We have derived expressions for a new one-dimensional model where both thermal and drift velocities are included. This was done for

both a single species and a two species model. The resulting equation requires a solution to an integral non-linear differential equation with two point boundary conditions. A solution was obtained by converting the problem to a single point boundary condition. The single boundary condition was the minimum potential point where the electric field is zero. Figure 5 compares the results with model A for which the drift velocity is zero. We see that the results for the new model are considerably different than those of model A. The difference between the curves is large enough to show that the simplified model does not predict the space potential sufficiently accurate to yield a correct current versus voltage curve for an electrostatic analyzer. Similar results are obtained when a comparison is made with model B.

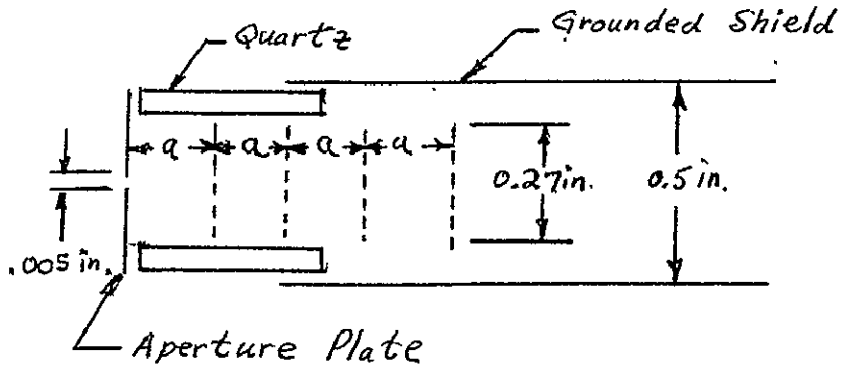

Analyzer	a(in.)
# 1	.15
# 2	.05

Figure 1. Schematic of electrostatic analyzer.

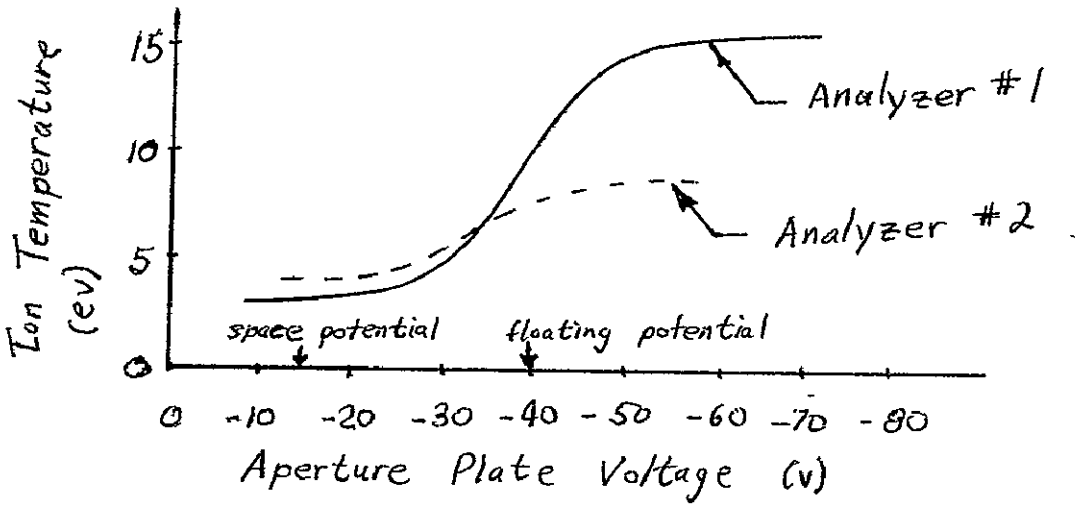

Figure 2. Effect of Aperture Plate Voltage on Measured Ion Temperature.

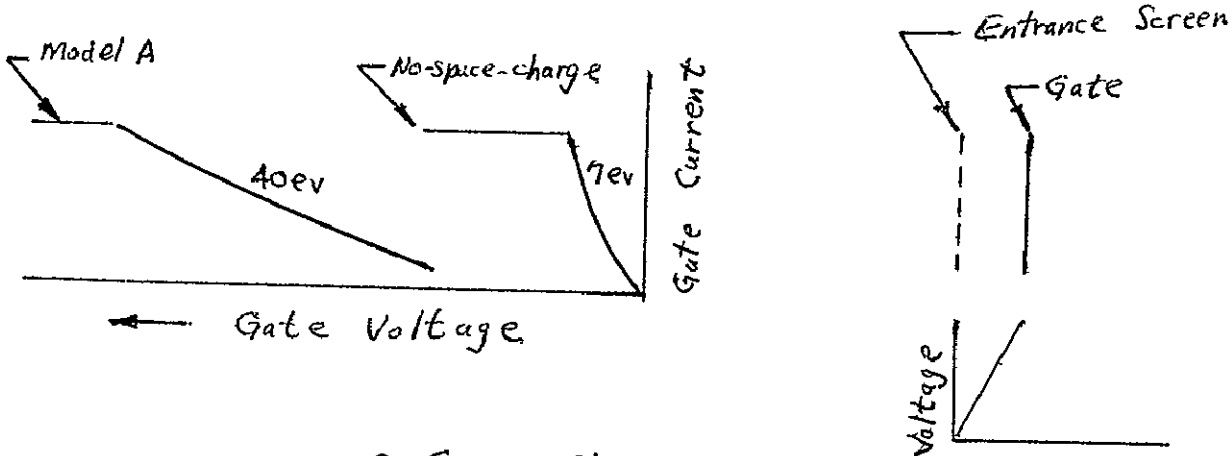

Figure 3. Effects of Space Charge on Current-Voltage Trace (Model A)

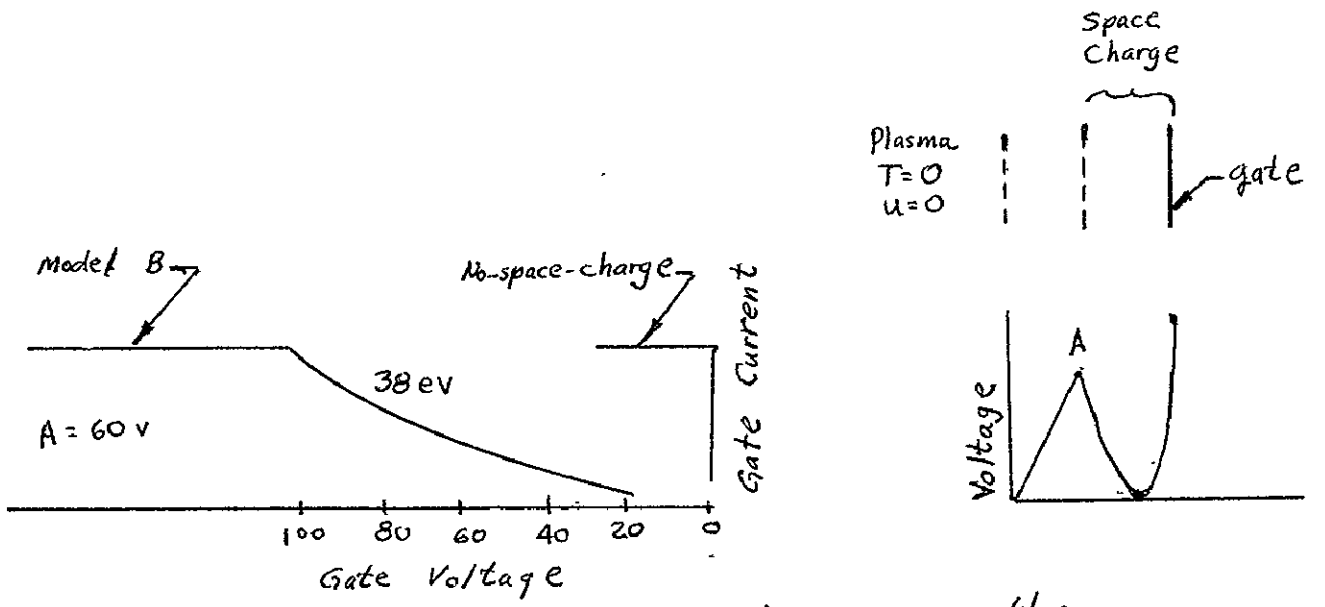

Figure 4. Effects of Space Charge on the Current-Voltage Trace (Model B)

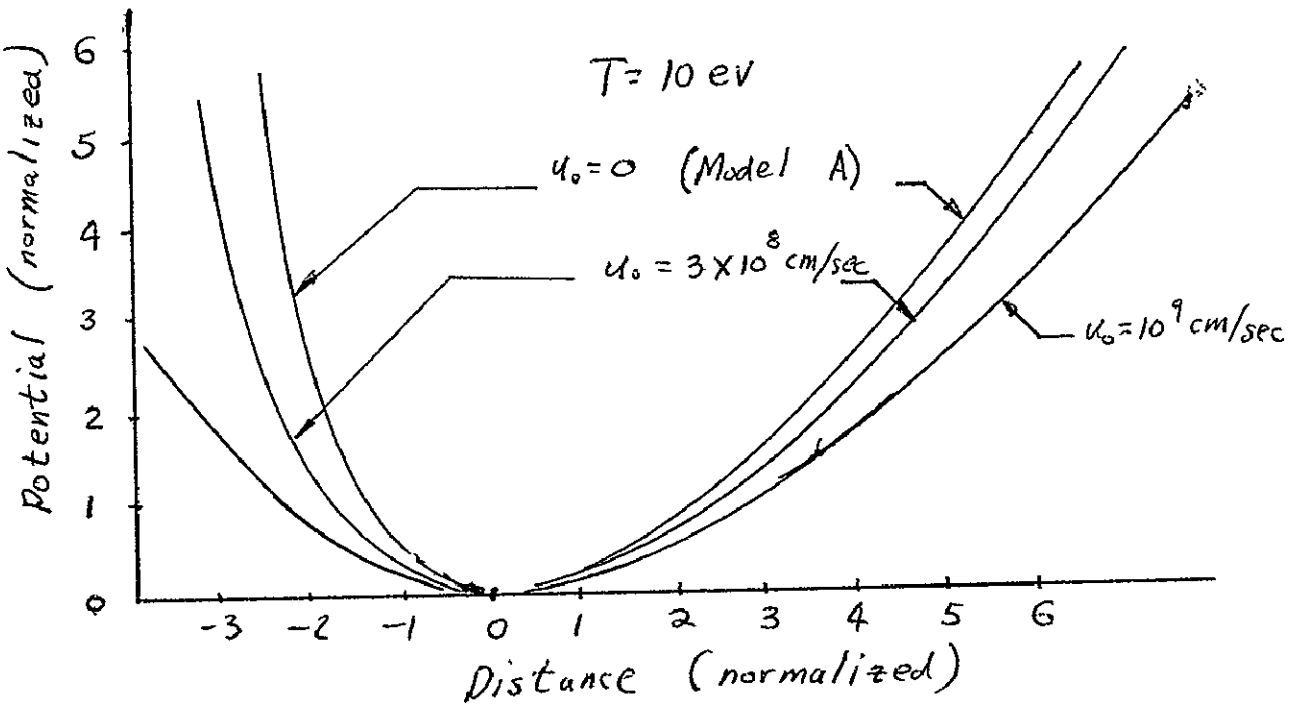

Figure 5. Space Potential Between Parallel Plates

CALCULATIONS OF ION-CYCLOTRON WAVE PROPERTIES IN A HOT PLASMA

by Donald R. Sigman, NASA Lewis Research Center

In the past, a Fourier integral technique was used to calculate electric and magnetic wave fields excited in an infinitely long plasma column by the current of a finite length radiofrequency coil. To solve the Fourier integral using the residue method, it was necessary to find the roots of a complicated function of the axial wave number, $T(k)$. This could be done with little difficulty when the plasma was cold with no damping, so that the roots of $T(k) = 0$ were real.

However, in a hot plasma (or one dominated by collisions) the terms making up $T(k)$ are complex and the roots are likewise complex. In this case it is often difficult to find a numerical technique to locate the roots quickly and easily. To avoid this difficulty with roots, one can use a Fourier series approach. For a finite length system of length 2L, the fields can be written as a Fourier series as follows

$$\underline{E}(r,z,t) = \sum_{n=0}^{\infty} \underline{E}(r,t)_n f(L,z)_n e^{i\omega t}$$

The function $f(L,z)_n$ is either a sine or cosine function of argument $n\pi z/L$ or $n\pi z/2L$ depending on whether the current distribution in the coil is asymmetric or symmetric about $Z = 0$ and on whether open circuit or short circuit boundary conditions are assumed at the ends of the plasma column ($Z = \pm L$). $\underline{E}(r,t)_n$ is the Fourier transform of the electric field evaluated at $k = n\pi/L$ or $k = n\pi/2L$ again depending on the end boundary conditions.

The solutions of the Fourier series and integral techniques become identical when the damping is sufficient to damp the normal modes in a distance short compared to L. But the important point is that roots of $T(k) = 0$ do not have to be found when using the series method.

The series method has been used to calculate fields and power transfer to the plasma for conditions favorable for the generation of ion-cyclotron waves (i.e. $\omega \approx \Omega_{ci}$). The coil used was a Stix coil and the effects of varying ion and electron temperatures were studied. It has been found that whenever ion or electron temperature is increased the efficiency of transferring energy to the plasma waves is reduced. This effect becomes appreciable when the damping length of the natural modes is of the order of, or less than, the coil length. When temperatures are high the electron density for which optimum coupling occurs is higher. In addition, the use of shorter Stix coil wavelengths reduces the coupling, while increased ion temperature anisotropy ($T_{\perp i}/T_{\parallel i}$) improves coupling for a fixed $T_{\parallel i}$. The effect of reduced efficiency with increasing temperature may explain why efficiency goes down with increasing coil current in experiments at the Lewis Research Center.

MODEL FOR THE CALCULATIONS

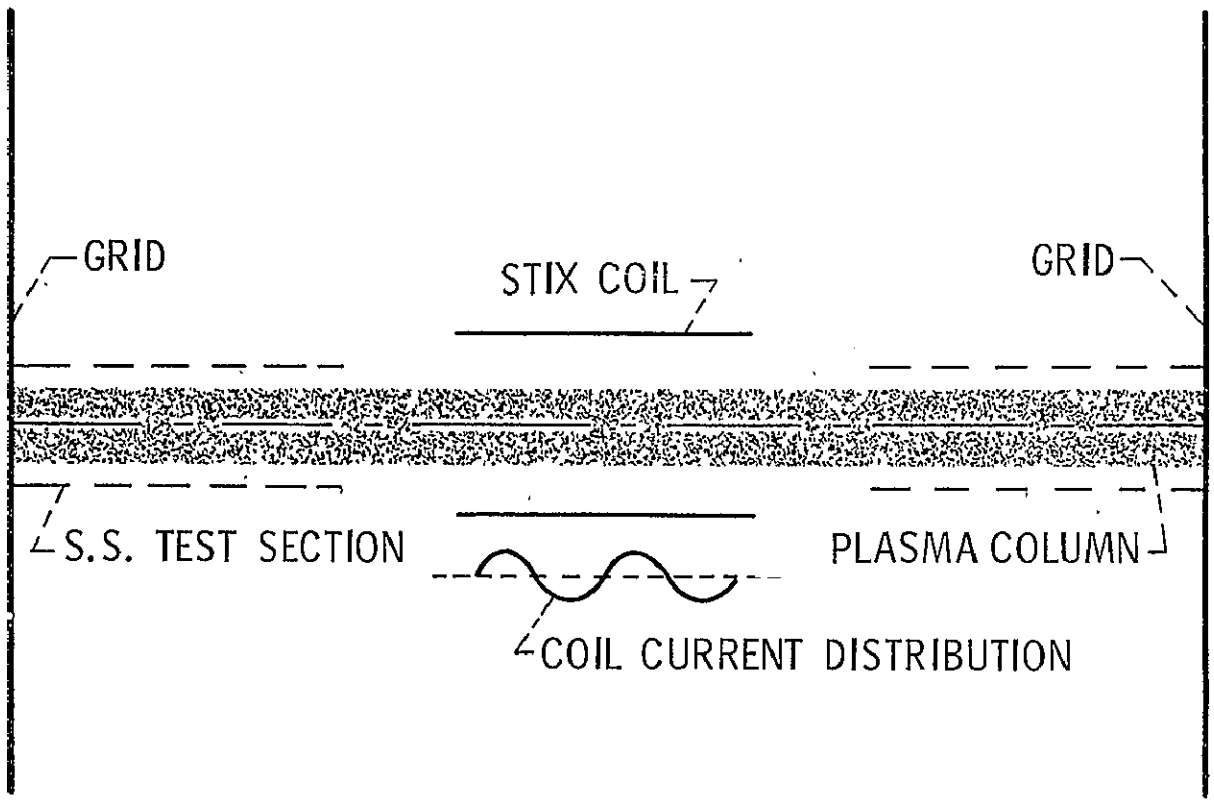

PEAK POWER TRANSFER TO PLASMA VERSUS ELECTRON DENSITY WITH ION-TEMPERATURE AS A PARAMETER

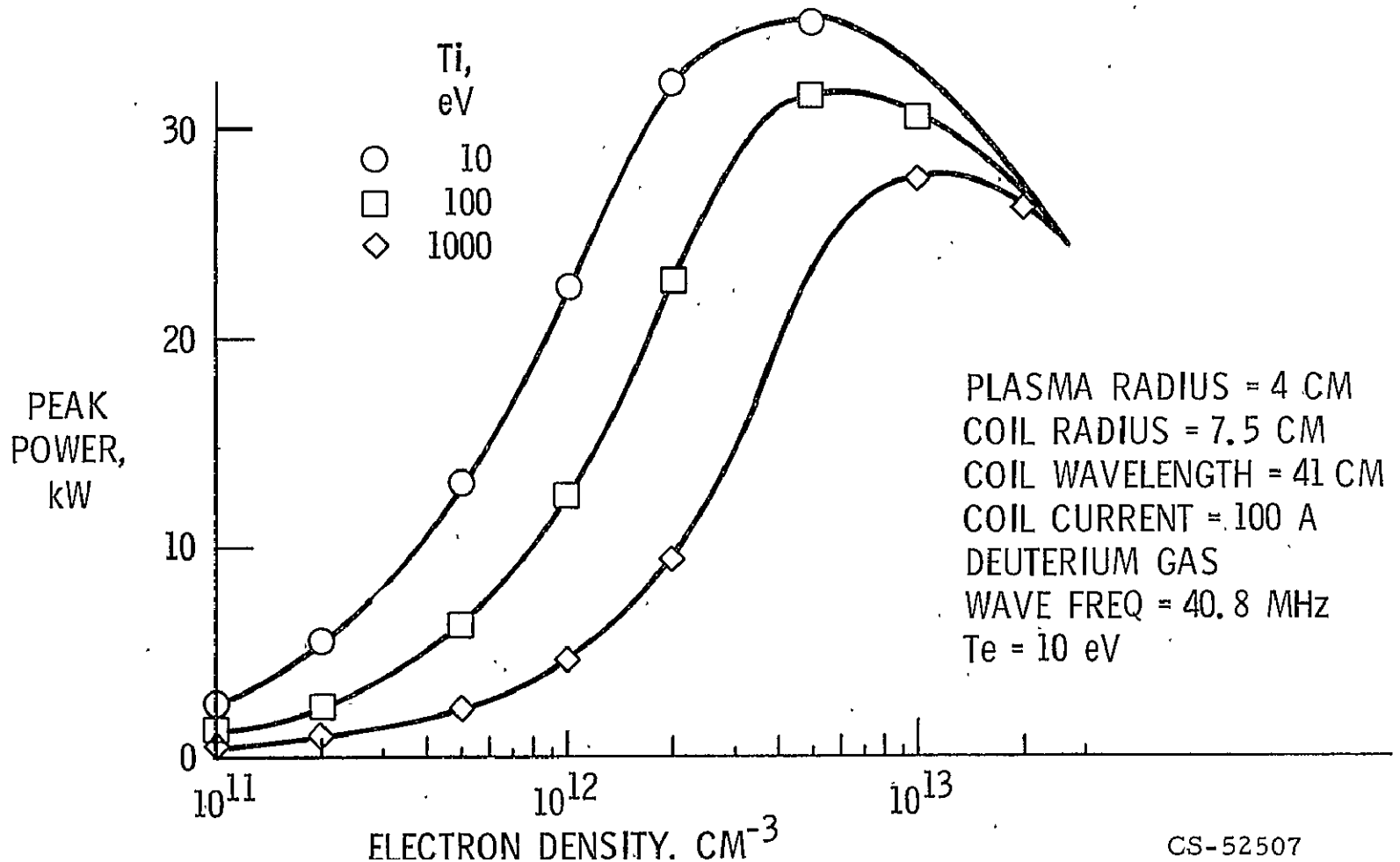

POWER TRANSFER TO PLASMA VERSUS ION–CYCLOTRON FREQUENCY WITH ION TEMPERATURE AS A PARAMETER

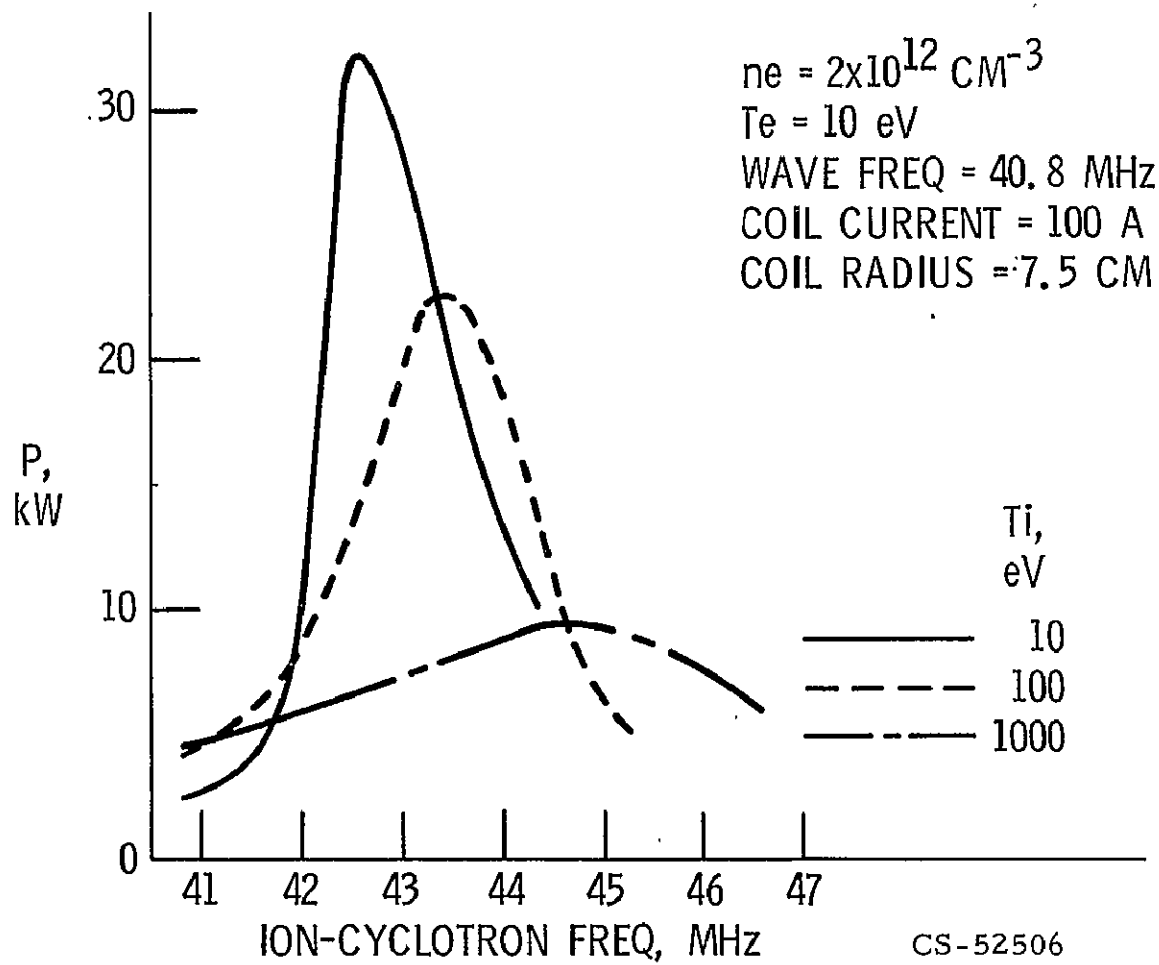

THERMALIZATION OF ION-CYCLOTRON WAVES IN A MAGNETIC BEACH

by Clyde C. Swett, NASA Lewis Research Center

An experimental program is being conducted to study the ion-cyclotron-wave method of producing high ion temperatures in a hydrogen or deuterium plasma. In this method waves are propagated in the plasma along an axial magnetic field into a region of slightly lower magnetic field (called the magnetic-beach region) where the wave energy is converted into thermal energy of the ions. This method is capable of heating ions to the kilo-electron-volt range.

The magnetic-field and vacuum-chamber configuration used is shown in Figure 1. It consists of an rf center-section with two side-arms in a magnetic-mirror geometry. A 45 kW rf transmitter, operated at 6.5 megahertz, supplies a constant current to a Stix coil. This coil is wound so that ion-cyclotron waves propagate out both of its ends. The plasma, although initially started by a hot-cathode discharge, is maintained by the rf alone when metal grids are located at the peaks of the mirrors. There are three ways of operating the magnetic field: flat field, near beach, or far beach. In the beach regions the wave frequency will match the ion-cyclotron frequency and the wave will be thermalized.

In previous experiments the capability of transferring rf power efficiently to the wave has been shown, the wave has been identified by magnetic probing, and the wave has been damped in a beach. The purpose of the recent experiments has been to measure the ion temperature resulting from damping of the wave. Ion temperatures were determined by means of coils located in the near-beach region which measured the diamagnetism of the plasma when the transmitter was unkeyed.

Ion temperature measurements are shown in Figure 2 for an electron density of 2×10^{12} cm^{-3}, deuterium gas, and maximum power. The wave is propagating from left to right. The magnetic field of the near beach is shown in the lower curve and the temperatures measured by 10 diamagnetic coils are shown by the points in the upper curve. The points at which the operating frequency is equal to the ion-cyclotron frequency is shown as $\Omega = 1$. As the wave propagates into the beach it becomes damped and should be completely damped at the position $\Omega = 1$. Because of the local mirrors created by the beach the ions become trapped. The data show that the highest transverse ion temperature ($\sim$500 ev) is at the position of minimum field. The neutron flux measured at the beach was compared with theoretical predictions to verify the temperatures measured.

REFERENCES

1 Clyde C. Swett, "Thermalization of Ion-Cyclotron Waves in a Magnetic Beach," NASA TM X-52717, November 1969.

2 Clyde C. Swett, Henry J. Hettel, and R. Krawec, "Further Experiments on Ion-Cyclotron-Wave Generation in the RF Self-Sustained Mode," NASA TM X-52493, November 1968.

3 Clyde C. Swett, Roman Krawec, and Henry J. Hettel, "Operation of an Ion-Cyclotron-Wave Generation Apparatus in a RF Self-Sustained Mode," NASA TM X-52365, November 1967.

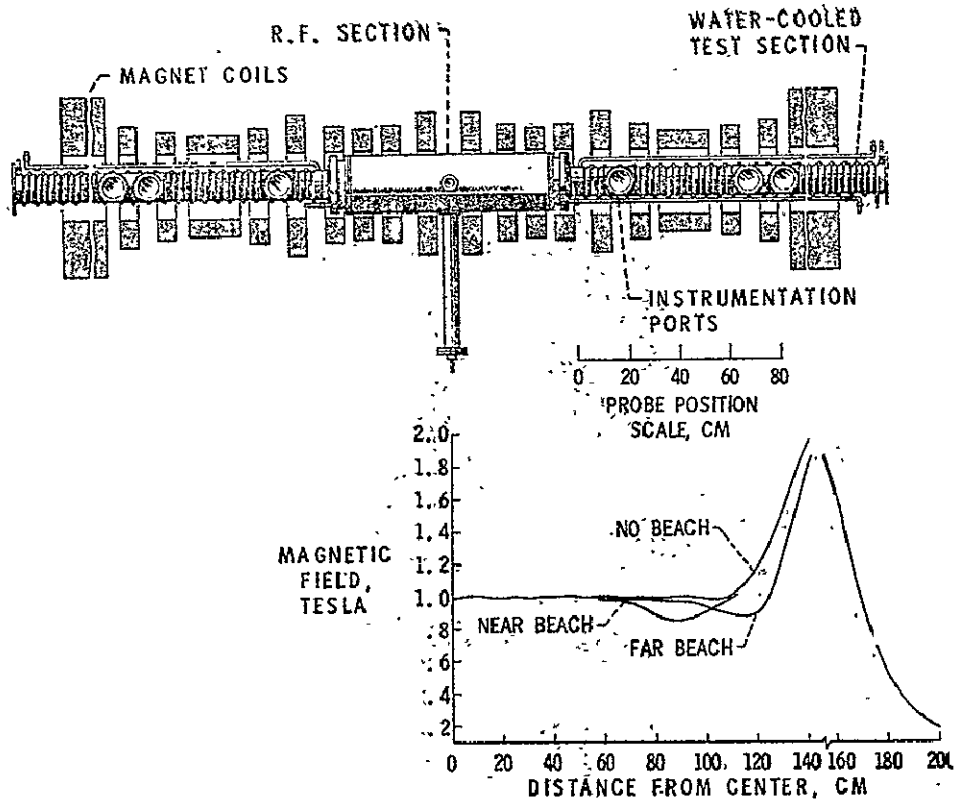

Figure 1. - Magnetic field and vacuum-chamber configuration.

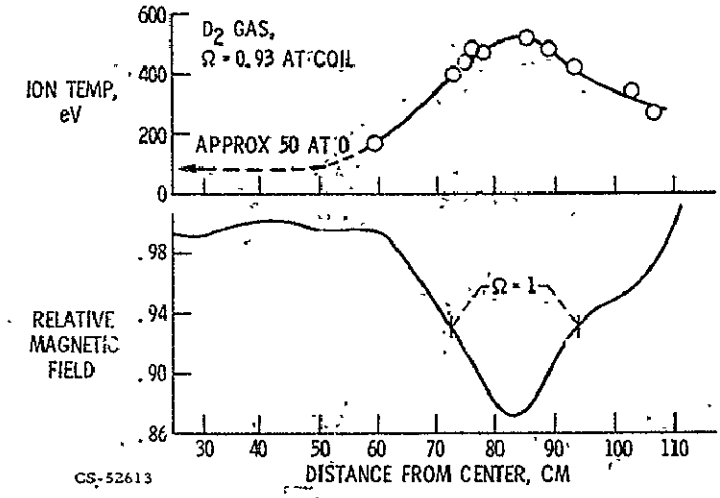

Figure 2. - Ion temperature at magnetic beach.

OBSERVATION OF ION HEATING IN A PLASMA SUBJECT TO THE CONTINUITY EQUATION OSCILLATION

by J. Reece Roth, NASA Lewis Research Center

A photograph of the modified Penning discharge used in this experiment is shown in Fig. 1. The plasma is confined in a superconducting magnetic mirror apparatus with a mirror ratio of 2.5:1, and a maximum field on the axis that can be varied up to two Tesla. The plasma is 15 cm in diameter at the midplane, and can be operated in the steady state for several hours.[1] When a high DC potential is applied to the anode ring, thermalized ions of high kinetic temperature are observed coming out through the magnetic mirrors.[1,2] These ions have a quite accurately Maxwellian energy distribution along a radius in velocity space.[1,2]

These high ion temperatures were investigated further, with the results shown in Figure 2. The ion kinetic temperature is shown plotted as a function of direct-current anode voltage for four background pressures of deuterium gas. The kinetic temperature is approximately linearly proportional to the anode voltage up to the limit of the power supply used. This suggests that ions of any desired energy can be produced by going to a sufficiently high anode voltage. The only other steady-state heating system to produce such high ion temperatures is the Burnout-V device at Oak Ridge National Laboratory.

A retarding potential energy analyzer was used to measure the efflux of ions as a function of time. Results are shown in Figure 3. The zero level is the baseline between pulses. The charged-particle efflux displays pulsar-like sharp, narrow peaks between broad, flat minima. For different plasma conditions, these pulses display fine structure, periodic interpulses and other interesting detailed features. The particle efflux, the light output, and the electrostatic fluctuations were in phase at the same frequency. The light output was monitored at two axial and azimuthal stations with a pair of photomultipliers, and showed that the plasma was oscillating in unison with a single phase and frequency. Parametric variation of the plasma properties showed that the frequency of this oscillation depended on both the electron and neutral number densities, but not on the magnetic field.

These characteristics suggested that the oscillation in question is a new phenomenon, and this subsequently proved to be the case. This oscillation was labeled the continuity-equation oscillation, because it arises as a consequence of periodic solutions to the coupled pair of continuity equations for neutrals and charged particles in a slightly ionized gas.[3,4] The frequency is proportional to the square root of the product of electron and neutral number densities, and is independent of magnetic field.[3,4]

The oscillation frequency was systematically studied as a function of the electron and neutral number densities. Figure 4 shows the results.

The observed frequency is plotted as a function of the product of relative electron and neutral number density. The square root dependence predicted theoretically holds over a range of 5 orders of magnitude in the density product.[5]

The following table summarizes the best temperatures, densities, and confinement times simultaneously observed in this experiment thus far:

Ion Kinetic Temperature, T_i, kev	5
Electron Kinetic Temperature, T_e, eV	200
Plasma Number Density, n_e, particle/m^3	2×10^{16}
Ion Confinement Time, sec	27

The ion temperatures listed are gratifying, but the densities and confinement times are quite low. These are now limited by the rapid loss of ions out the mirrors. Confinement time and density can be improved with a closed configuration such as the bumpy torus. This consists of 12 magnetic mirrors end-to-end in a toroidal array. Such a superconducting magnet facility is presently under consideration for future use in this experiment. The modified Penning discharge scheme will be applied to this configuration. It is one of the few steady-state plasma injection and heating schemes capable of being applied to a toroidal geometry. A reasonable goal for the bumpy torus would be an increase of a factor of 10 in confinement time and number density.

REFERENCES

1 J. R. Roth, "Modification of Penning Discharge Useful in Plasma Physics Experiments," Rev. Sci. Instr., vol. 37, pp. 1100-1101, (1966).

2 J. R. Roth and M. Clark, "Analysis of Integrated Charged Particle Energy Spectra from Gridded Electrostatic Analyzers," Plasma Physics, vol. 11, pp. 131-143, (1969). See also NASA TN D-4718.

3 J. R. Roth, "New Mechanism for Low-Frequency Oscillations in Partially Ionized Gases," Phys. Fluids, vol. 10, pp. 2712-2714, (1967).

4 J. R. Roth, "Periodic, Small-Amplitude Solutions to Volterra's Problem of Two Conflicting Populations, and Their Application to the Plasma Continuity Equations," Journal of Math. Physics, vol. 10, pp. 1412-1414, (1969). See also NASA TN D-4472.

5 J. R. Roth, "Experimental Observation of Continuity-Equation Oscillations in Slightly Ionized Deuterium, Neon, and Helium Gas," Plasma Physics, vol. 11, pp. 763-777, (1969). See also NASA TN D-4950.

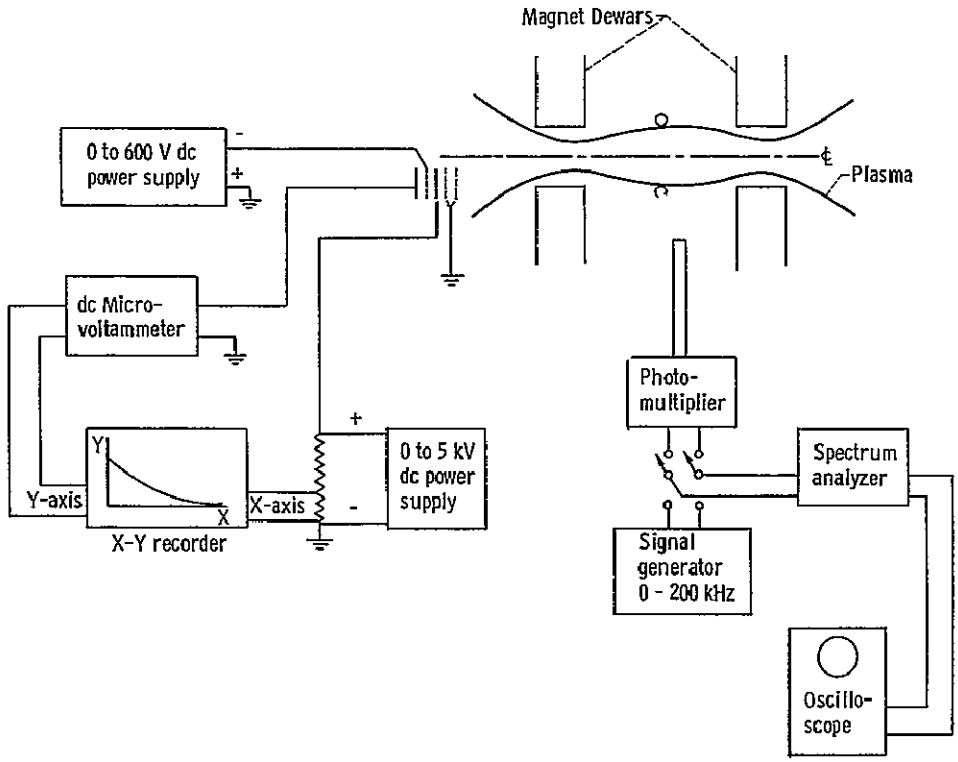
Magnet Dewars
0 to 600 V dc
power supply
-
+
℄
Plasma
dc Micro-
voltammeter
Photo-
multiplier
+
Y
Y-axis
X
X-axis
-
0 to 5 kV
dc power
supply
Spectrum
analyzer
X-Y recorder
Signal
generator
0 - 200 kHz
Oscillo-
scope

FIGURE 1

RELATION OF ANODE VOLTAGE TO DEUTERIUM KINETIC TEMPERATURE FOR VARIOUS BACKGROUND GAS PRESSURES

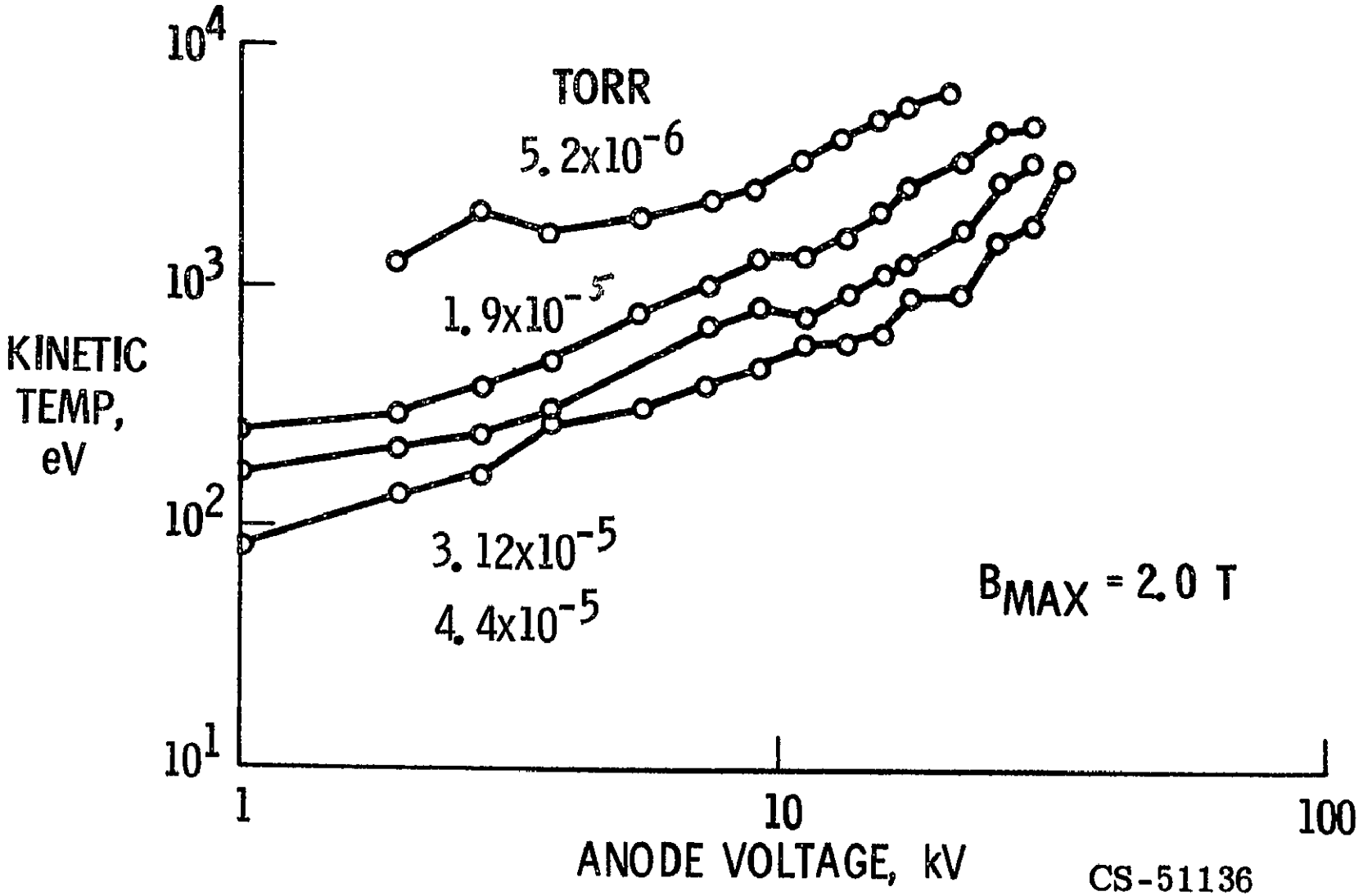

FIG. 2

CHARGED PARTICLE EFFLUX VS TIME

← t

GJ-8

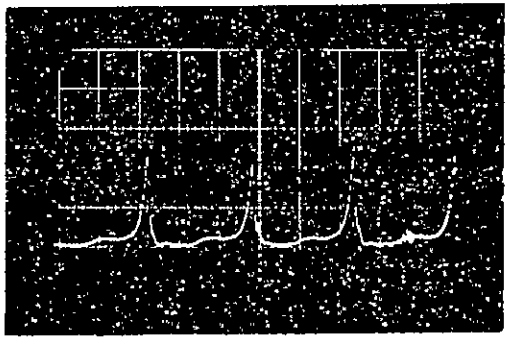

20 μSEC/CM, $p_T = 8.1 \times 10^{-6}$ TORR

GJ-13

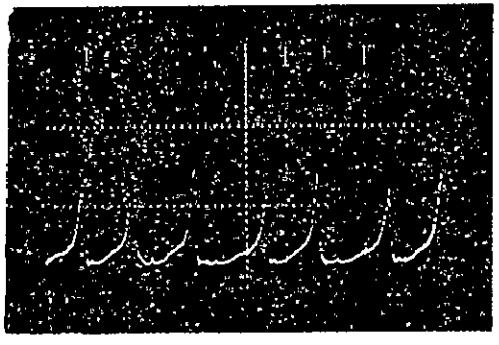

20 μSEC/CM, $p_T = 1.2 \times 10^{-5}$ TORR

GJ-19

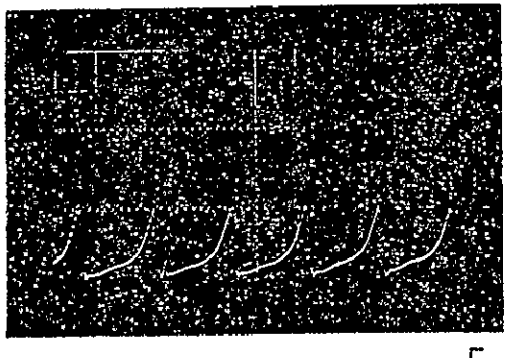

10 μSEC/CM, $p_T = 1.7 \times 10^{-5}$ TORR

GJ-21

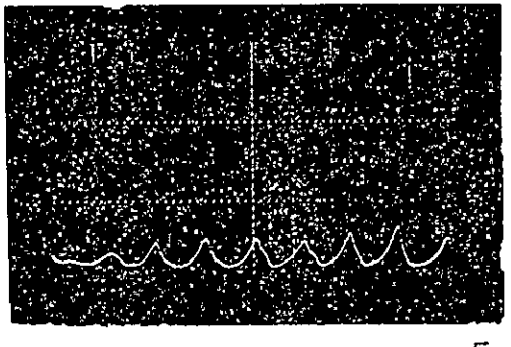

10 μSEC/CM, $p_T = 2.6 \times 10^{-5}$ TORR

FIGURE 3

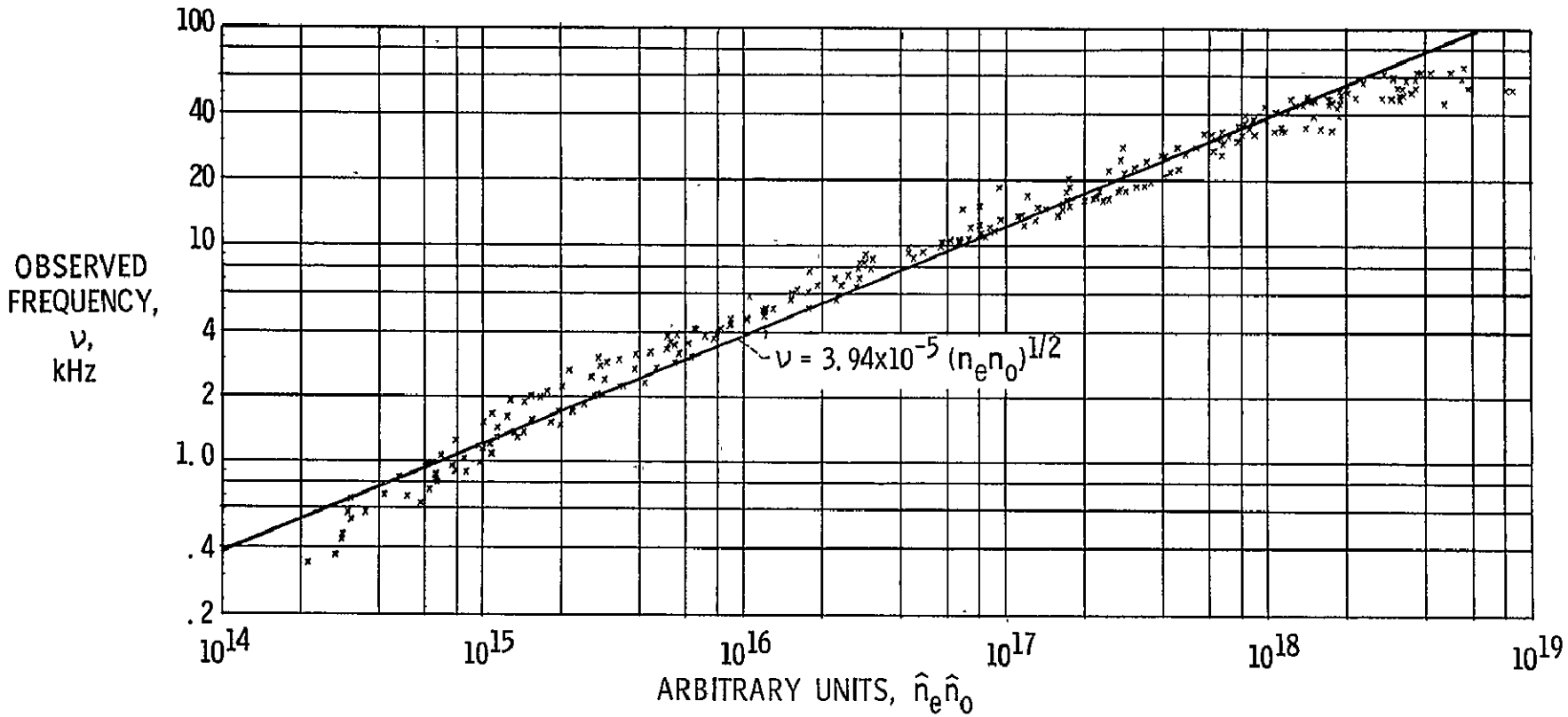
OBSERVED FREQUENCY, ν, kHz
100
40
20
10
4
2
1.0
.4
.2
$\nu = 3.94 \times 10^{-5} (n_e n_0)^{1/2}$
10^{14}
10^{15}
10^{16}
10^{17}
10^{18}
10^{19}
ARBITRARY UNITS, $\hat{n}_e \hat{n}_0$

FIGURE 4

FINITE BETA INSTABILITIES PROPAGATING PERPENDICULAR TO A MAGNETIC FIELD

by Lewis C. Himmell, NASA Lewis Research Center

A theoretical analysis was performed to determine the effect of finite beta on electromagnetic modes propagating perpendicular to a uniform magnetic field in a fully ionized plasma described by a loss-cone distribution. The theory includes the effects of all components of the four vector potential. It was found that finite beta creates new resonant mode instabilities which propagate at frequencies that are very close to the ion cyclotron frequency and its harmonics. The theory was applied to the Dory-Guest distribution functions which are of the form

$$f_c^{(j)} = \frac{1}{\sqrt{\pi}\,\alpha_\perp^2 \alpha_{||}^2\, j!} \left(\frac{v_\perp}{\alpha_\perp}\right)^{2j} \exp\left[-\frac{v_\perp^2}{\alpha_\perp^2} - \frac{v_{||}^2}{\alpha_{||}^2}\right] \quad (j=1,2,\ldots) \tag{1}$$

and predicted unstable waves with growth rates as large as a few percent of the ion cyclotron frequency for a value of beta of one-half.

The dispersion relation describing resonant modes near the ion cyclotron frequency for example is of the following form:

$$\frac{\alpha_\perp^2}{c^2} = \frac{\beta}{2\lambda}\left[\frac{\alpha_{oo}(1)}{X-1} + \frac{H(X)}{(X-1)D(X)}\right] \tag{2}$$

where

$$\beta = \frac{\omega_{pi}^2}{\omega_{ci}^2}\,\frac{\alpha_\perp^2}{c^2}\,, \quad \lambda = \frac{k^2\alpha_\perp^2}{2\omega_{ci}^2} \quad \text{and} \quad X = \left(\omega/\omega_{ci}\right)^2$$

The propagation vector is denoted by $\vec{k}$ while $\omega_{pi}, \omega_{ci}, \omega$ and C refer to the ion plasma frequency, the ion cyclotron frequency, the complex frequency of the wave and the speed of light respectively. The term involving $\alpha_{oo}(1)$ is the usual electrostatic contribution to the dispersion relation while the second term on the right side of the equation gives the finite beta effect. Since the functions $D(x)$ and $H(x)$ are second and third degree polynomials in x respectively, Eqn. (2) can be solved analytically for x.

An analysis was made of the distributions corresponding to the first four values of j for $\beta \leq 0.5$. When $\lambda = 0.5$ for example, the $j = 1$ and $j = 4$ distributions are stable while the $j = 2$ distribution is unstable. Growth rates of the order of a few percent were found for $\beta = 0.5$. The $j = 3$ distribution was found to be unstable for $\beta < 1.0 \times 10^{-3}$. Larger values of β make this distribution stable.

Table I lists growth rates in units of ω_{ci} as a function of β for the $j = 2$ distribution. The "resonant" approximation is seen to be a good one since ω_R/ω_{ci} is so close to unity.

TABLE I

GROWTH RATES FOR j = 2 DISTRIBUTION IN UNITS OF ION CYCLOTRON FREQUENCY

β	$1 - \omega_R/\omega_{ci}$	ω_I/ω_{ci}
0.5	-5.2×10^{-2}	3.12×10^{-2}
0.1	-6.2×10^{-3}	1.84×10^{-2}
0.01	-1.53×10^{-4}	2.04×10^{-3}
0.001	-9.85×10^{-6}	2.05×10^{-4}
0.0001	-9.35×10^{-7}	2.05 X 10-5
0.00001	-9.30×10^{-8}	2.05 X 10-6
0.000001	-9.30×10^{-9}	2.99 X 10-7

INSTABILITIES AND PLASMA TURBULENCE STUDIED USING CORRELATION TECHNIQUES.

Jack H. Noon, Rensselaer Polytechnic Institute, Troy, N. Y.

A hollow cathode gas-fed arc facility has been used at Rensselaer to carry out correlation measurements on low frequency instabilities in a highly ionized argon plasma. Study of the higher frequency oscillations which are not of a coherent nature is planned.

A schematic of the arc and associated instrumentation is shown in Fig. 1. The actual construction is easily varied for different experiments. The discharge vessel is fabricated of 6 inch inner diameter pyrex pipe sections. The cathode is a hollow bariated tungsten cylinder. Gas can be introduced through cathode or anode. The electrode separation can be adjusted over a range of one meter. Axial and radially movable Langmuir probes measure steady state plasma parameters and perturbations in charged particle density and plasma potential. An axial magnetic field of up to 2000 gauss is supplied using 12" inner diameter solenoid coils. By powering the coil in the neighborhood of the cathode independently, the magnetic field in this region B_c can be varied with respect to the main magnetic field B_H.

Fig. 2 shows how the amplitude (V) and frequency (f) of the dominant coherent instability (an ion acoustic wave) are affected by B and p. This wave can be suppressed entirely by increasing p or by increasing B_c relative to B_H. A similar effect has been reported in the MPD arc by workers at Langley. Fig. 3 shows changes in floating potential V_f and in plasma potential V_p (calculated knowing the electron temperature) which occur when the wave is suppressed. The plasma potential must be positive with respect to the cathode for onset of the instability. The enhanced loss of electrons from the core could be due to either increased axial losses or radial losses, but all our data is consistent with an increased rate of radial plasma transport.

Another coherent instability (a drift wave) close in frequency to the ion acoustic wave appears to have little effect on plasma losses. This can be explained in terms of the phase difference ϕ between the perturbed charged particle density and the fluctuations in plasma potential. A difference of $\pi/2$ is found between the two cases. A theoretical dispersion relation has been developed to predict the growth rate and frequency dependence of these oscillations as a function of B and p and to explain the effect of gas pressure on ϕ.

Bohm or anomalous diffusion is usually attributed to fluctuating electric fields which are not of a coherent nature. To establish the effect of general plasma turbulence requires a wider range of pressure and magnetic field than those studied up to the present, and the use of both auto-correlation and cross-correlation measurements of axially separated probes. It is hoped to establish by these measurements, correlating the spectra of density fluctuations and electrostatic field fluctuations, whether a cascade in wave number space leads to a universal turbulent spectrum, irrespective of the means used to excite turbulence in the plasma medium. A technique for measuring the form of the energy distribution of the charged particles is also under investigation.

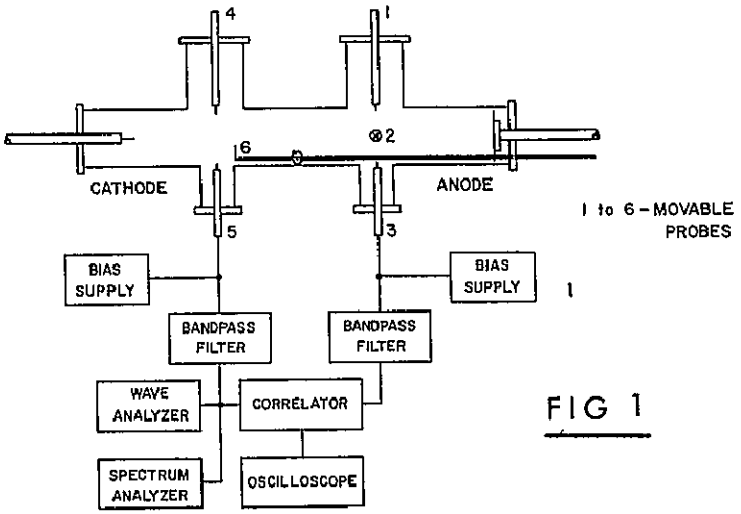

FIG 1

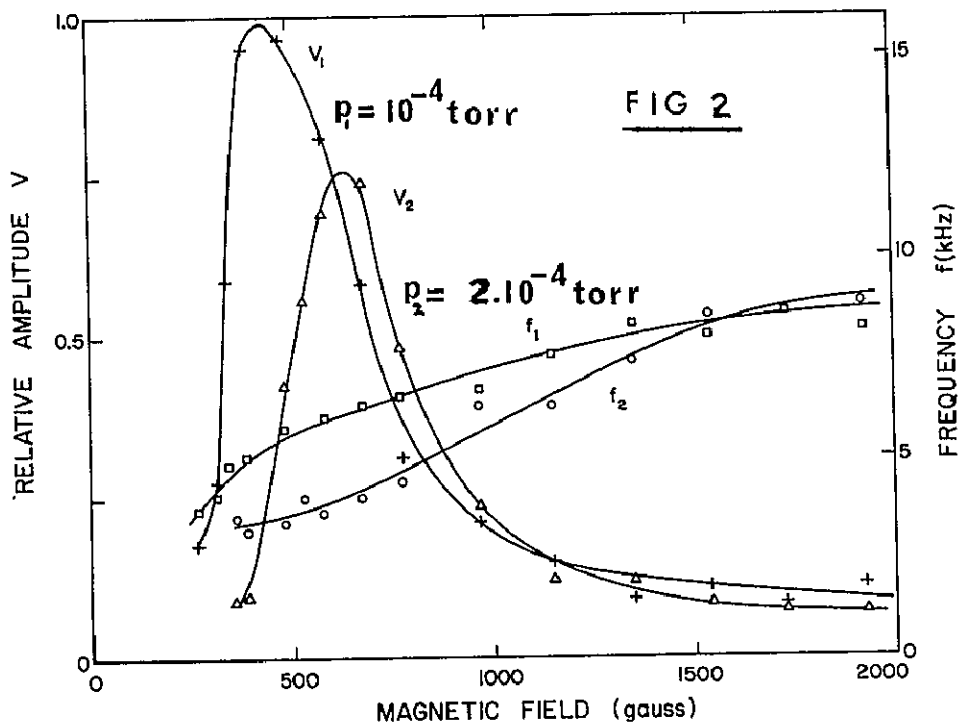

FIG 2

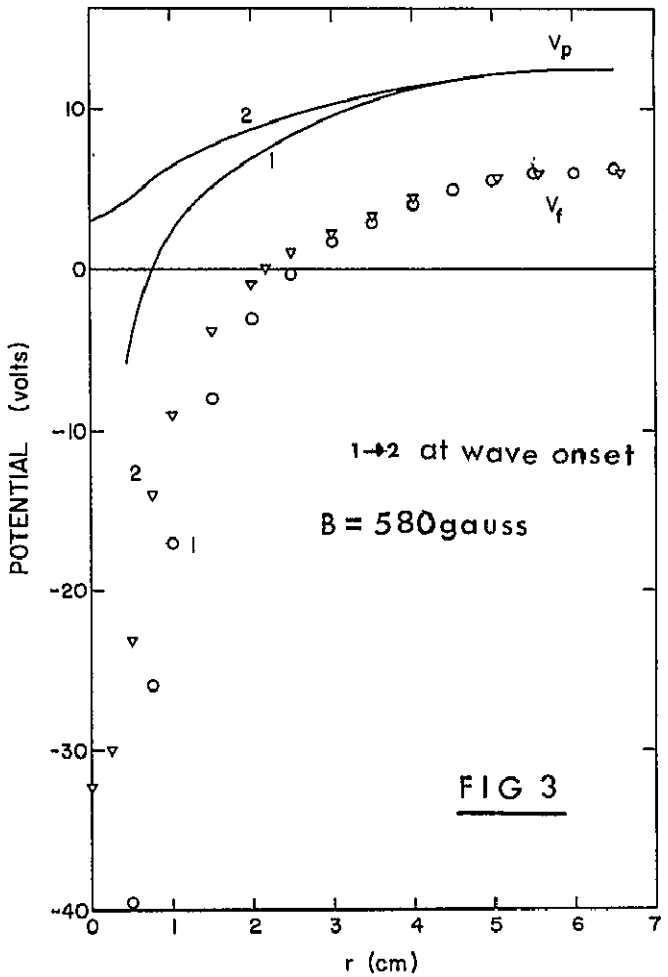

FIG 3

THEORY FOR PLASMA INSTABILITIES IN MPD ACCELERATORS AND BARIUM CLOUDS

John J. Kim*
NASA, Langley Research Center
Hampton, Va.

MPD Accelerators.- This study is concerned with a theoretical evaluation of the experiments for onset at a critical magnetic field of rotating disturbances in the Linear Hall Current Accelerator[1] (LHA) and the MPD Arc.[2,3] The evaluation mainly concerns the theories for the E x B instability[4,5] and the electrothermal instability.[6] The applicability of other mechanisms[7,8] and acoustic wave instabilities have not yet been explored. The E x B instability is attractive since in the LHA where measurements inside the electrode region could be performed the onset of the instability occurs in a region of large density gradient (near the cathode). It is also important that the necessary condition, $E \cdot dn_o/dx > 0$, for the onset of the E x B instability,[4,5] seems to be satisfied, although further measurements are required to obtain full assurance of the electric field E near the cathode. On the other hand the frequency characteristics of the rotating disturbance as a function of the applied magnetic field seems to be in better agreement with the electrothermal instability.[6] The variation of onset with mass flow (or pressure) and molecular weight is approximately satisfied for both types of instabilities.[4,5,6] Another criterion for the distinction between the two instabilities is the observation of a helical type of disturbance in the LHA. Sufficiently detailed measurements inside the electrode region of the MPD arc would have to be performed to identify a comparable helical shape. The theories for the E x B instability[4,5] do not explicitly predict a helix, although an intuitive nonlinear generalization of the analysis appears to be consistent with this result. The electrothermal instability theory as applied to the MPD arc,[6] however, does predict a helical instability in the following manner. The theory[6] deduces two disturbance modes, one purely rotating and the other a mixed mode which combines a rotational and a radial wave in the direction of the electric field. The analysis of the mixed mode is not pursued in the analysis[6] to its fullest extent since the experiment for the interelectrode region of the MPD arc only shows the rotational disturbance. (Note: The helical disturbance observed in the exhaust of the MPD arc has its axis in the flow direction but not in the radial direction.) The helical disturbance observed in the LHA can be interpreted as a mixed mode consisting of a rotational wave and axial wave in the electric field direction. It is also of importance that only the mixed mode[6] analysis predicts the onset of an instability, whereas the single rotational mode analysis does not yield an onset. The experimental results from the LHA[1] thus permit a more detailed check of the theory for electrothermal instability.[6] The theory[6] gives the correct pitch of the helix. Experiments and electrothermal instability theories for striations observed in rectangular geometries[9] (related to MHD generators) need to be further analyzed to evaluate their relevance to the experiments in the LHA and the MPD arc.

*NRC-NASA Resident Research Associate

Another means for comparison between the two instabilities is under investigation which concerns their growth rates and motion as predicted by linear analysis. The growth rates and motion of disturbances will be compared with the results of pulsed experiments. The nonlinear post onset conditions, involving arc columns or spokes, of the E x B and electrothermal and other instabilities must be evaluated in detail to permit a better comparison with experiments.

Barium Clouds.- Attempts have been made to explain the striation phenomenon in barium clouds released in the upper atmosphere[1] on the basis of the dissipative E x B instability as developed by Simon[2] which involves collisions with neutrals. An application of the E x B instability to the barium cloud has recently been reported.[3] Striations have, however, also been observed at very high altitudes (12 to 13 earth radii) in a recent experiment.[4] It is suggested that a possible origin of these high altitude striations could be the drift wave instabilities[5] which do not depend on collisions with neutrals. These instabilities have been thoroughly studied experimentally and theoretically in the fusion program. The flute-like disturbances due to these drift wave instabilities could be used for interpretation of the striations in the barium clouds. It is then of special interest that the wave fronts of drift wave instabilities may be alined with the magnetic field or have an angle to it. The experimental observations need to be refined to evaluate their angle with respect to the magnetic field. The extension of the E x B instability to the collisionless case (including inertial effects) will also be explored.

The drift motion of the barium cloud is primarily used to study strength and direction of electric fields in the magnetosphere. In the cases where striations are found the cloud drift motion (and the electric fields) would most likely be judged by the motion of the striations. The angle of the striations with respect to the magnetic field is then of considerable importance for the interpretation of electric fields. The possible relation of drift wave instabilities to auroral striation phenomena will also be discussed.[6]

Acknowledgment is made of discussions with F. Allario, R. V. Hess, O. Jarrett and B. D. Sidney.

REFERENCES

MPD Accelerators:

1. Sidney, B. D.; Allario, F.; Hess, R. V.: Onset of Rotating Disturbance in Linear Hall Current Accelerator. AIAA Paper N. 69-381. AIAA Seventh Electric Propulsion Conference, Williamsburg, Va., Mar. 3-5, 1969.

2. Allario, F.; Jarrett, O., Jr.; and Hess, R. V.: Onset of Rotating Disturbance in the Interelectrode Region and Exhaust Jet of an MPD Arc. AIAA Paper 69-232. AIAA Seventh Electric Propulsion Conference, Williamsburg, Va., Mar. 3-5, 1969.

3. Jarrett, O.; Allario, F.; Sidney, B. D. and Hess, R. V.: Experiments for Onset of Rotating Disturbance in Linear Hall Current Accelerator and MPD Arc. 6th Intercenter and Contractor's Conference on Plasma Physics, NASA Langley Research Center, Dec. 8-10, 1969.

4. Simon, A.: Instability of a Partially Ionized Plasma in Crossed Electric and Magnetic Fields, Phys. of Fluids, vol. 6, no. 3, March 1963, pp. 382-388.

5. Hassan, H. A. and Thompson, C. C.: Onset of Instabilities in Coaxial Hall Current Accelerators. AIAA Seventh Electric Propulsion Conference, Williamsburg, Va., Mar. 3-5, 1969.

6. Smith, J. M.: Electrothermal Instability - An Explanation of the MPD Arc-Thrustor Rotating-Spoke Phenomenon. NASA TM X-52535, Technical paper proposed for presentation at Seventh Electric Propulsion Conference, Williamsburg, Va., Mar. 3-5, 1969.

7. Fay, J. A. and Cochran, R. A.: An Actuator Disc Model for Azimuthally Nonuniform MPD Arcs. AIAA J., vol. 7, no. 9, September 1969.

8. Roth, R.: Private communication through F. Allario.

9. Nedospasov, A. V.: Striations. Vol. 11, no. 2, Soviet Phys. USPEK HI (1968), pp. 174-187

Velikhov, E. P.; Degtyarev, L. M.; Samarskii, A. A.; and Favarsokii, A. P.: Calculating the Ionization Instability in Low-Temperature Magnetized Plasma. Sov. Phys. DOKLADY, vol. 14, no. 1, (1969), pp. 68-71.

Lengyel, L. L.: On the Numerical Simulation of Ionization Instability. Preprint, Institut fur Plasmaphysik, Garching bei Munchen, F. R. of Germany.

Barium Clouds:

1. Haerendel, G.; Lüst, R.; Rieger, E.; Volk, H.: Highly Irregular Artificial Plasma Clouds in the Auroral Zone. Max Planck Institut für Physik und Astrophysik. Muenchen. MPI-PAE/Extraterr 21, January 1969.

2. Simon, A.: Instability of a Partially Ionized Plasma in Crossed Electric and Magnetic Fields. Phys. of Fluids, vol. 6, no. 1, pp. 382-388 (1963).

3. Linson, L. M. and Workman, J. B.: Formation of Striations in Ionospheric Plasma Clouds. Bull. Am. Phys. Soc. Abstract 7B7, vol. 14, no. 11, Nov. 1969.

4. Private information to the author by David Adamson and Leo D. Staton of the Interplanetary and Magnetospheric Physics Section at NASA Langley Research Center.

5. Krall, N. A.: Drift Waves. Advances in Plasma Physics, vol. 1, pp. 153-199.

6. McCormac, B. M., Edit.: Aurora and Airglow, Rheinhold Publ. Co., 1966.

Walt, M. Edit.: Auroral Phenomena. Stanford Univ. Press, Stanford, California 1965.

Chamberlain, Joseph W.: Physics of the Aurora and Airglow. Academic Press, 1961.

GRAVITOHYDROMAGNETIC INSTABILITY IN CONTRASTREAMING FLUIDS

S. P. Talwar*
NASA, Langley Research Center
Hampton, Va.

The hydromagnetic stability of a multicomponent system composed of infinitely conducting gravitating fluids is investigated by the normal mode analysis. The effects of hydromagnetic and gravitational coupling between the components are studied in an initially static and a contrastreaming configuration. It is found that an N-component static nongravitating system allows, in general, (N+1) mixed magnetosound modes in addition to a purely Alfven mode. The gravitational coupling results in an instability leading to an incipient fragmentation, whose size depends profoundly on nonthermalization in the composite medium. Finally, the conditions of contrastreaming instability in plasma-plasma and neutral gas-plasma gravitating streams are derived in view of their likely importance to star formation from primordial matter.

*NRC-NASA Resident Research Associate

TRANSVERSE INSTABILITIES IN SELF-FOCUSING STREAMS

by

Willard H. Bennett
North Carolina State University

Broadly stated, the objective in this program has been to investigate the instabilities in magnetically self-focusing streams in which the mean free paths of the stream electrons are more than several orders of magnitude longer than the stream diameter and magneto-hydrodynamic methods of analysis cannot be applied. Electron beams have been produced which are electrically pinched in order to insure complete neutralization of the beam electron space charge, and the current and voltage were then to be increased until the conditions for the magnetic pinch were satisfied, whereupon the instabilities could be studied. A directional probe which has been developed recently a this Laboratory has been used for measuring the radial potential distribution in and around these pinches.

Using the value of energy of transverse motion, B, as measured in high voltage beams, the current required for the magnetic pinch to become dominant appears to be about the same as the maximum current which has been obtainable in these experiments with our present equipment. There have been several instances when it appeared that the beam pinched to a smaller radius than could be expected with an electric pinch alone. However, in order to make an adequate study of these beams and their instabilities, it will be necessary to make measurements at current values up to much more than the minimum critical pinch current.

CASCADE MECHANISM OF NONLINEAR INTERACTIONS BETWEEN MODES IN A TURBULENT PLASMA

C. M. Tchen

The City College of the City University of New York

By means of a hydrodynamic model, valid for a plasma of hot electrons and cold ions, we have established the development of spectra of kinetic and electrostatic energies. The nonlinear interactions have been described by two transfer functions valid for the nonlinear transfer of modes across each spectrum, and by a production function serving the coupling between the two spectra. The closure problem, as characteristic to any nonlinear system, has of course to be solved, and in the present theory, the approximation is resorted to the cascade concept. The concept helped in the derivation of the equations for the energy spectra, and in the formulation of a "turbulent relaxation frequency". The latter frequency is very important in determining the structure of turbulent transport coefficients entering in all the above nonlinear transport phenomena. Finally the equations of energy spectra are solved for the collisional and collisionless cases. Some of the theoretical results have been confirmed by experiments in gas plasmas. The spectra of kinetic and electrostatic energies are investigated for both the collisional and collisionless cases. In the former case, the spectrum of potential energy from the electrostatic potential fluctuations, as a function of the wave number k, and denoted by G(k) follows the laws $G \sim k^{-3/2}$ and $k^{-9/2}$ in the inertial and dissipative subranges respectively. In the latter case, the dissipative law $G \sim k^{-5}$ is derived. The solutions of the kinetic energy spectrum are also found. The anomalous diffusion, called the Bohm diffusion, is derived in the present theory, and is found to play a role of a sink of energy flux across a potential spectrum.

MEASUREMENTS OF THE COHERENT OSCILLATIONS AND TURBULENCE IN PLASMA USING RESISTIVELY- AND CAPACITIVELY-COUPLED PROBES

by John S. Serafini, NASA Lewis Research Center

The knowledge of the diffusive and other transport properties of a plasma depends upon the experimental study of plasma turbulence and oscillations. Fluctuating plasma parameters which need to be measured include the particle densities, the potentials and/or fields. The writer's previous work (Refs. 1 and 2) used resistively-coupled electrostatic (Langmuir) probes to sense the plasma fluctuations. These fluctuations exhibited both coherent-like and random-like properties. The writer's present work is a continuation of these studies which additionally employs an electrostatic probe capacitively coupled to the plasma (such as one described by J. A. Schmidt in Ref. 3). The fluctuations sensed by this type of probe are considered to be fluctuations in potential.

The measurements have been obtained in a crossed-field plasma source (axial electric and radial magnetic fields) with a slightly ionized, low current, low-pressure argon discharge employing a hot cathode. The plasma had an average electron temperature of about 10 ev and an average electron number density of about 5.0×10^{10} cm^{-3}.

Amplitude spectra from .1 kilohertz to 6 megahertz as well as the autocorrelations which have been obtained allow comparison of the density and potential fluctuations. The spectra obtained with both types of probes contain a peak indicative of the coherent oscillation and are otherwise generally similar. At the higher frequencies the spectra obtained with the two types of probes do not agree in slope. Possible reasons for the observed similarities and dissimilarities in the spectra are discussed.

Previous work on the space-time correlations found that the coherent part of the current-density fluctuations were well-correlated over the measured range. The present work on correlations provides a like result for the potential fluctuations sensed by capacitively-coupled probes. In addition correlations of the potential fluctuations sensed by capacitively-coupled probes with the current-density fluctuations sensed with a resistively-coupled probe indicate strong correlations near the frequency of the coherent oscillation. The effect of the turbulent-like part of the fluctuations is also observed to be present in all of the correlation results. It appears as minor peak in the curves of the correlation coefficient versus time-delay at values of time-delay near zero.

Also presented are spectra of measurements of the fluctuations from two capacitively-coupled probes being sensed differentially. These differential-mode spectra are compared to the spectra of the fluctuations from the individual probes. From these results is deduced that the differential-mode spectra depend (1) on whether the fluctuation is due to a coherent oscillation or is turbulent-like in nature at the portion of

the spectrum of interest and (2) on the temporal and spatial scales of the fluctuations. Such information prescribes necessary conditions if fluctuating electric fields are to be directly measured by use of such probe systems.

REFERENCES

1 J. S. Serafini, Bull. Am. Phys. Soc. 13, 278 (1968), see also NASA TM X-52366 (1967).
2 J. S. Serafini, Bull. Am. Phys. Soc. 13, 1567 (1968), see also NASA TM X-52501 (1968).
3 J. A. Schmidt, Rev. of Scientific Instruments 39, 1297 (1968).

CROSSED-FIELD DEVICE

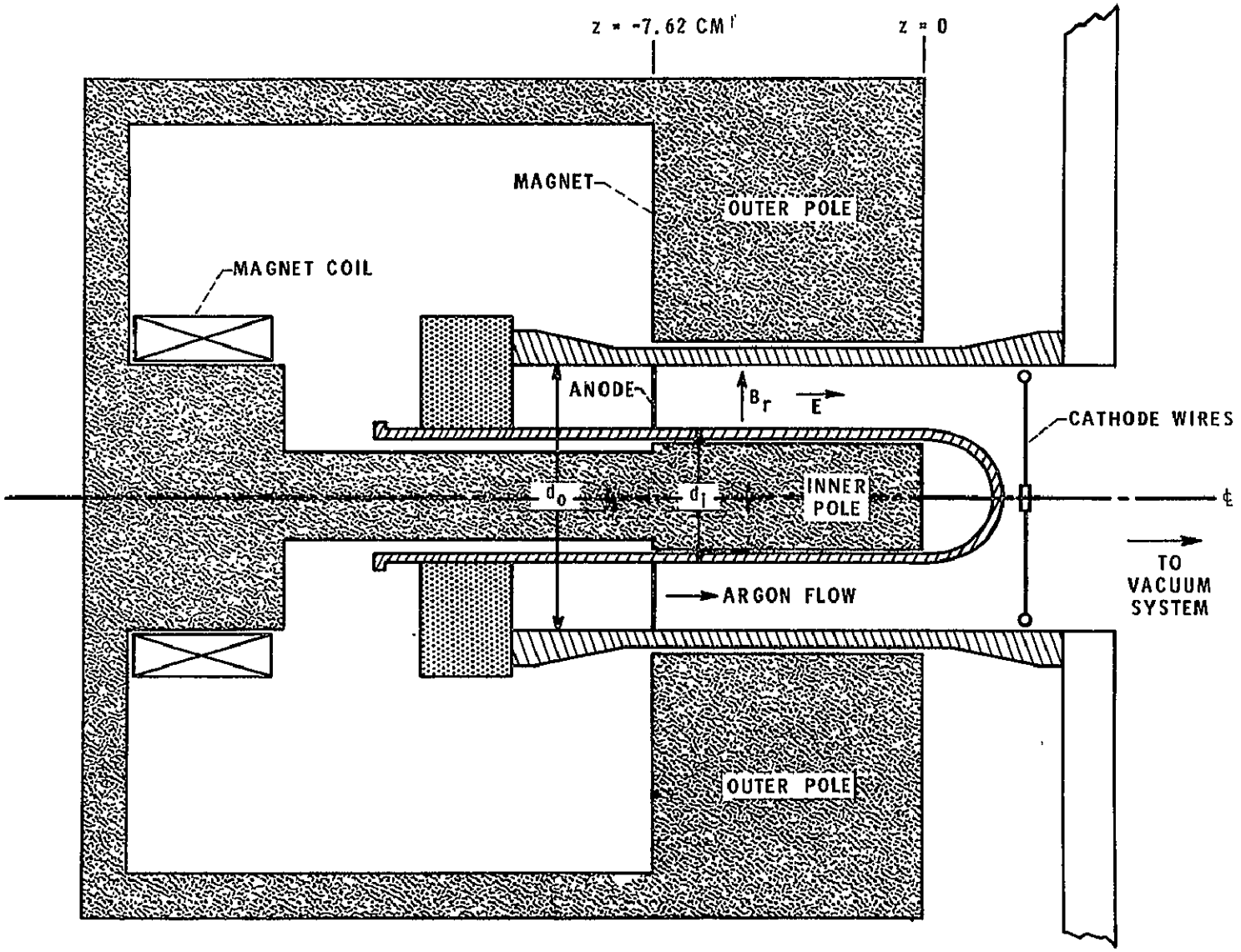

DENSITY–POTENTIAL CORRELATIONS

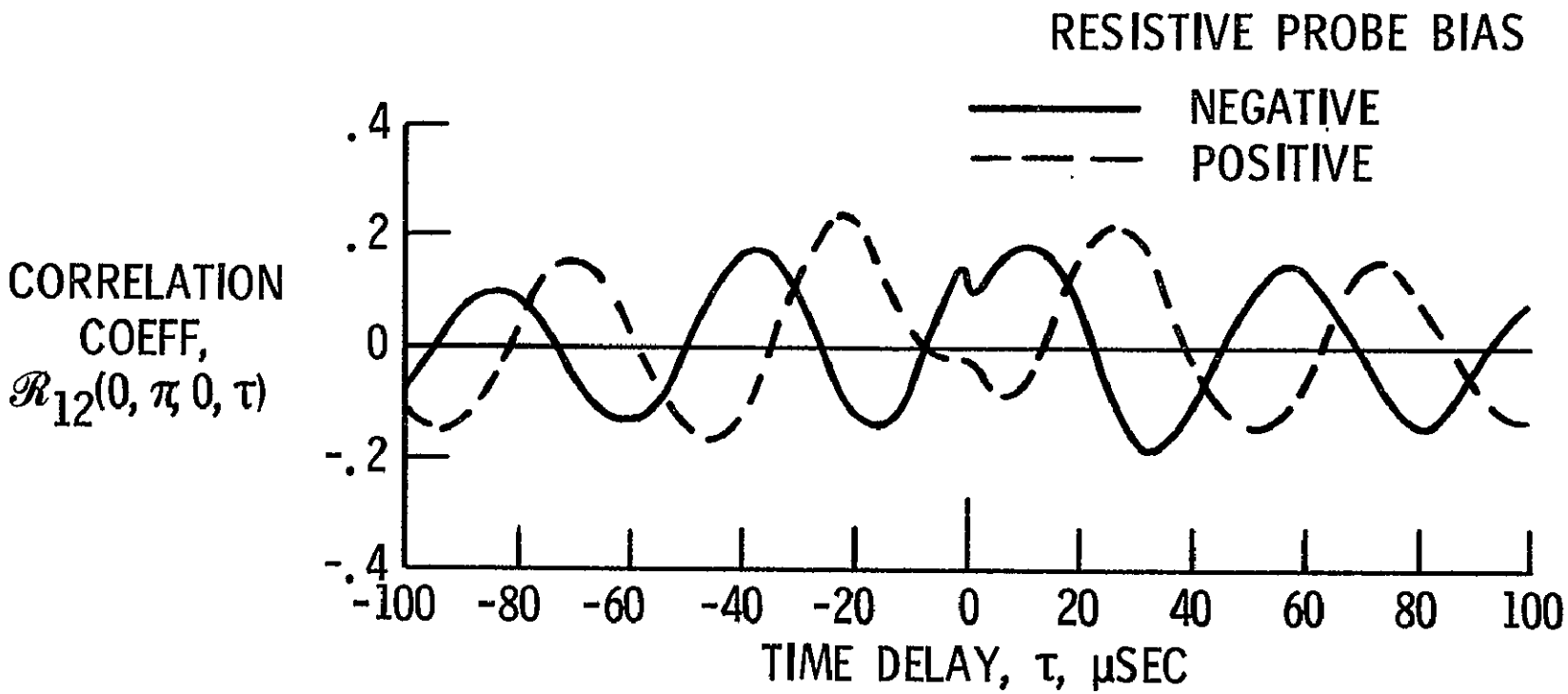

POTENTIAL AND DIFFERENTIAL-MODE SPECTRA

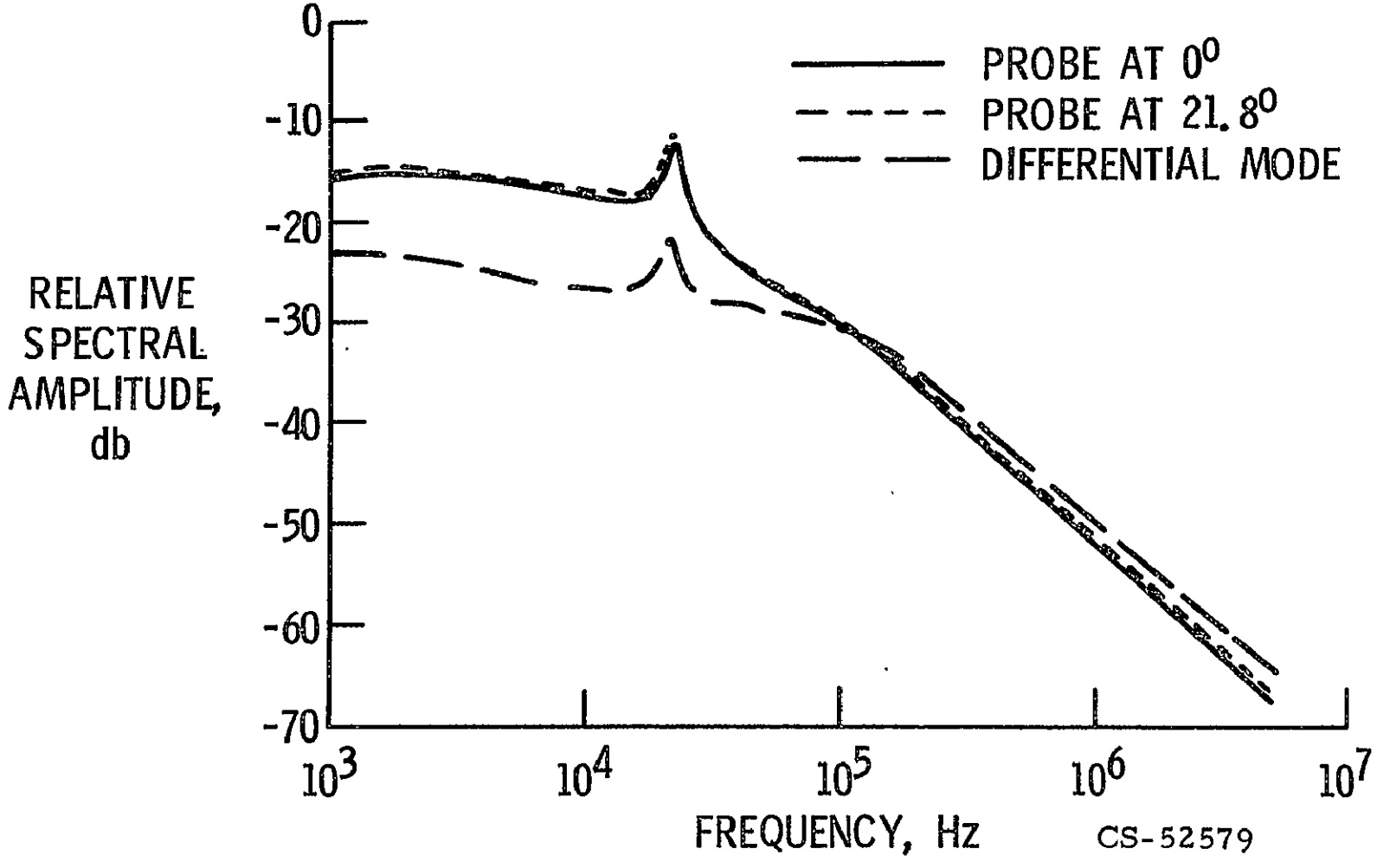

INVESTIGATION OF MICRO-ELECTRIC FIELDS IN PLASMA

Ward Halverson
NASA Electronics Research Center
Cambridge, Massachusetts

The interaction of the small scale electric fields with the charged particles of a plasma determines the basic physical properties which distinguish a plasma from an un-ionized gas. The micro-electric fields arise from Coulomb potentials around the plasma particles, density fluctuations (both thermodynamic and turbulent), and electromagnetic radiation. This interaction can be studied by injecting charged particles into a plasma and observing the dynamics of these "test" particles. The behavior of the test particles is representative of that of the "field" particles of the plasma and can be used for the computation of plasma transport properties, spectroscopic data, as well as the trajectories of energetic particles in geophysical or astrophysical plasmas. Measurements of test particle interactions with a plasma essentially provide a direct experimental test of plasma kinetic theory which has been formulated for many years and has been generally accepted without direct proof.

An earlier experiment[1] indicated that the energy loss of 5 to 10 KeV proton test particles losing energy to a fully ionized lithium plasma is less than predicted by 40 to 50%. Unfortunately, the experimental error was of the same order as the energy discrepancy, and a more precise measurement is necessary for a good comparison.

An experimental program is now underway at ERC which will measure the energy loss of fast protons injected into a lithium plasma of known properties. The plasma is formed by a magnetically confined reflex arc with electron density of 5×10^{12} cm^{-3} and electron temperature of about 1.5 eV. The test protons, with energies from 1 to 20 KeV, interact mainly with the plasma electrons and lose energy at the rate of a few eV per cm of plasma traversed. The main experimental problem is the very small energy loss of the test particles in the plasma.

A method has been devised to increase the effective path length of the test particles in the plasma. (See Figure 1.) Fast neutral hydrogen atoms are passed through the magnetically confined lithium arc and a fraction of the neutrals are ionized by charge exchange collisions in the plasma. The resultant protons are captured by the magnetic field and lose energy in the part of the gyro-orbits which is in the plasma column. The proton orbits drift tangentially around the arc column because of the radial gradient of the confining magnetic field, and the average proton energy will be related to the angular position of the orbit gyrocenters. The captured protons are lost mainly by charge exchange in the plasma, and an energy analysis of the particles lost from a narrow angular region of the arc column will show a series of peaks. (See Figure 2.) The energy difference between two consecutive peaks of the energy spectrum will represent the energy loss during a complete precession of the captured proton gyrocenters around the arc axis. The peak widths are related to the energy dispersion of the test particles in the plasma.

At present, all of the major experimental components have been constructed and are undergoing tests in the laboratory. A first test with the lithium arc, neutral particle accelerator, and neutral particle energy analyzer operating simultaneously was successfully conducted recently. Measurements of test particle energy loss will begin as soon as the microwave interferometer bridge for plasma density measurement and a system for measuring the captured proton precession rate are put into operation.

1. W. Halverson, Energy Loss of Fast Test Ions in a Plasma. Bull. Am. Phys. Soc. 13, 318 (1968) and Association Euratom - C.E.A. EUR-CEA-FC-472 (1968).

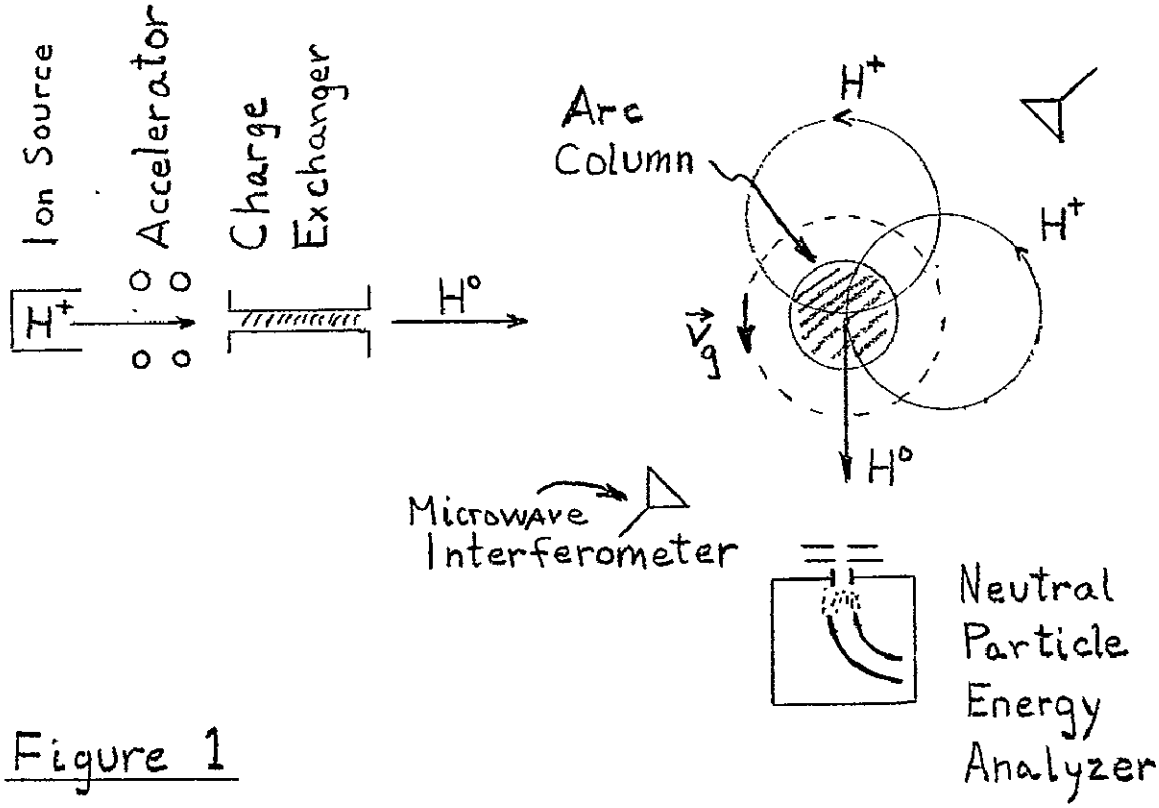

Figure 1

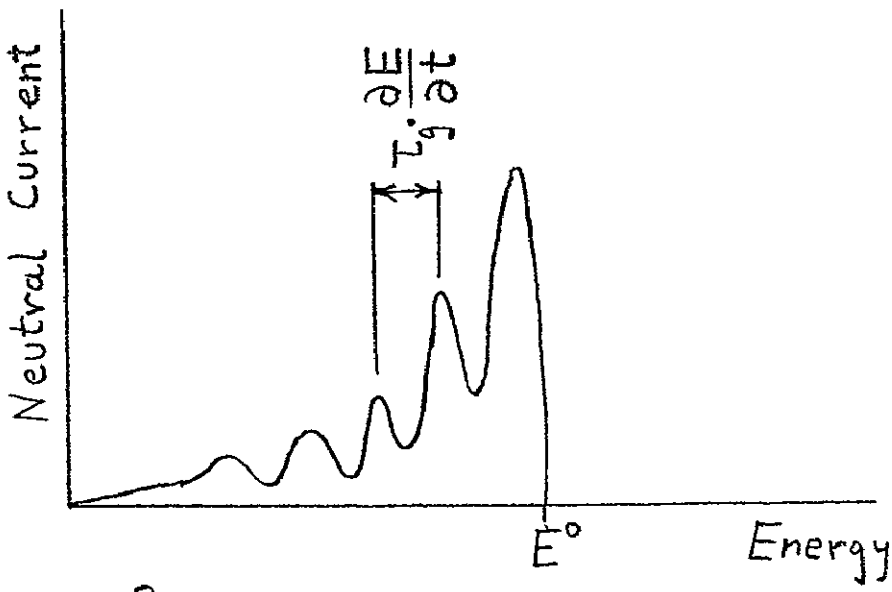

Figure 2

INFLUENCE OF CONTROLLED TURBULENCE ON GASEOUS DISCHARGES

by

S. T. Demetriades, G. S. Argyropoulos, and G. Fonda-Bonardi
STD Research Corporation, Pasadena, California

ABSTRACT

The properties and behavior of an electrical discharge perpendicular to a plasma stream can be influenced by introducing gasdynamic turbulence of controlled properties in the flow. This study has shown analytically (Ref. 1) that fine-grained, intense turbulence can prevent the formation of arc filaments, and has verified experimentally that such turbulence can increase the conductance of the discharge channel. Four areas are currently under investigation:

1. Measurement of the increase of cross-arc conductance Σ as a function of turbulence parameters under different operating conditions. The scale and intensity of introduced turbulence are being controlled by means of different wire screens placed in the plasma stream. Preliminary results shown on Fig. 1 illustrate the substantial increase of conductance that is obtained when turbulence is introduced.

2. Measurement of the relative erosion rate of the electrodes. This investigation was started very recently and only incomplete results are available. It appears that turbulence promotes a much more uniform erosion of the electrode (cathode) surface, and that the arc is not attached to a small area, but is either diffuse or moves very rapidly and evenly over the entire surface of the electrode. Anode erosion is negligible with or without turbulence in the stream. The net amount of material removed from the electrodes appears larger in the presence of turbulence. This may be due to higher surface temperatures because of enhanced heat transfer to the electrodes through the turbulent boundary layer, since in the few tests made the flow of coolant water was maintained constant. Also, this effect depends on the operating conditions, in particular the chamber pressure and the plasma enthalpy and velocity.

3. Measurement of turbulence properties (in particular, turbulent cell dimensions and density fluctuations) and correlation to the observed conductance enhancement. Turbulence properties are determined by means of a laser interferometer which measures the average (integrated) refractive index along a thin cylinder transverse to the plasma flow. A special arrangement permits simultaneous duplication of the measurement along two parallel paths which can be displaced with respect to each other along the axis of the plasma jet, from zero to 3 cm; this is equivalent to two identical, parallel interferometers each having an independent detector. Analysis of the detected signals permits computation of the decorrelation intervals of the turbulence parameters both as functions of time interval at a fixed distance, or as functions of distance at a fixed time interval. Figure 2 shows a schematic diagram of the double interferometer.

4. Analytical and theoretical studies relating to the interpretation of the experimental results and the prediction of model performance. The theory of the phenomenon and a general dispersion criterion have been developed (Ref. 1): Prevention and/or dispersion of arc filaments by turbulence is accomplished when the sufficient condition $D_2 > 1$ is satisfied, where D_2 depends on the plasma properties, the operating conditions, and the turbulence scale and intensity. Computation of D_2 under the operating conditions of the experiments is obtained by utilizing computer programs that have been developed at STD Research Corporation in the past for the detailed analysis and prediction of plasma properties in MHD flows (Refs. 2 and 3). Results of these computations are shown on Figs. 3 and 4 for two different levels of turbulence intensity. These results indicate that turbulence is more effective in dispersing arc filaments at lower arc pressures and electron temperatures and are in excellent agreement with the experimental measurements.

REFERENCES

1. Paper "Dispersion of Arc Filaments by Turbulence," presenting theoretical results developed under this project, and submitted for publication to the Physics of Fluids on 17 July 1969.

2. Demetriades, S. T. and Argyropoulos, G. S., "Ohm's Law in Multicomponent Nonisothermal Plasmas with Temperature and Pressure Gradients," Phys. Fluids 9, 2136-2149 (1966).

3. Argyropoulos, G. S. and Demetriades, S. T., "Influence of Relaxation Effects in Nonequilibrium J × B Devices," J. Appl. Phys. 40, 4500-4509 (1969).

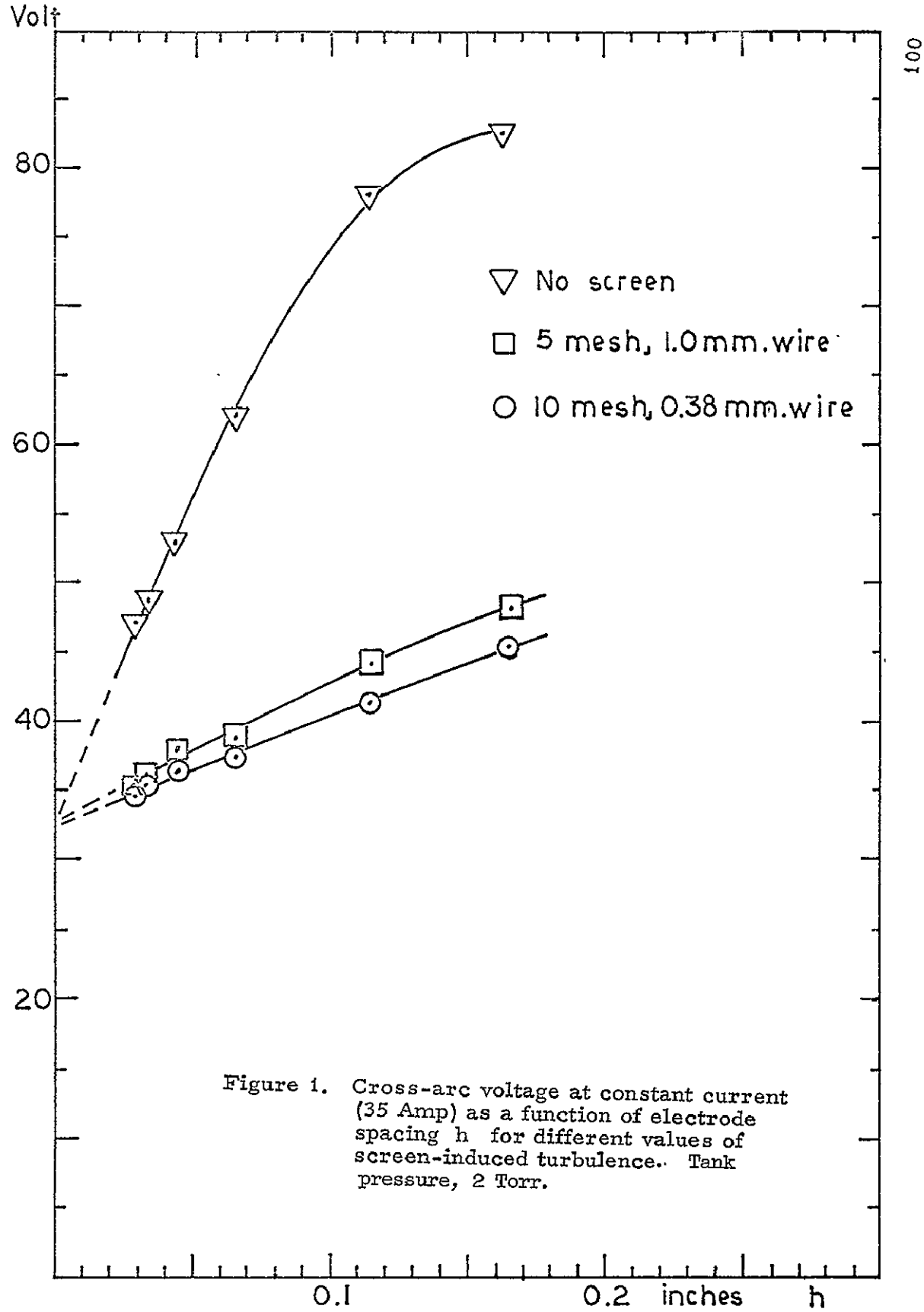

Figure 1. Cross-arc voltage at constant current (35 Amp) as a function of electrode spacing h for different values of screen-induced turbulence. Tank pressure, 2 Torr.

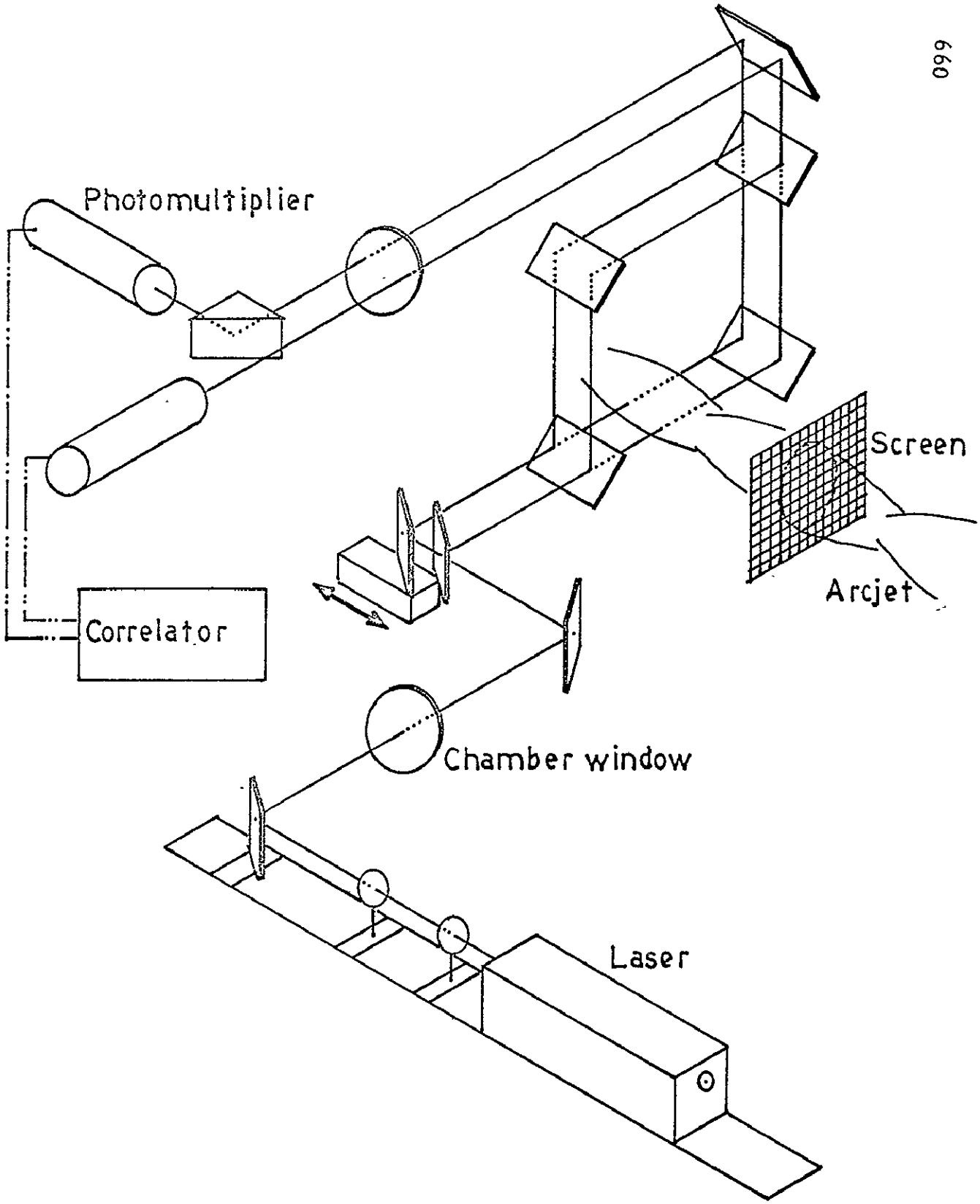

Figure 2. Layout schematic diagram of laser interferometer with two parallel paths

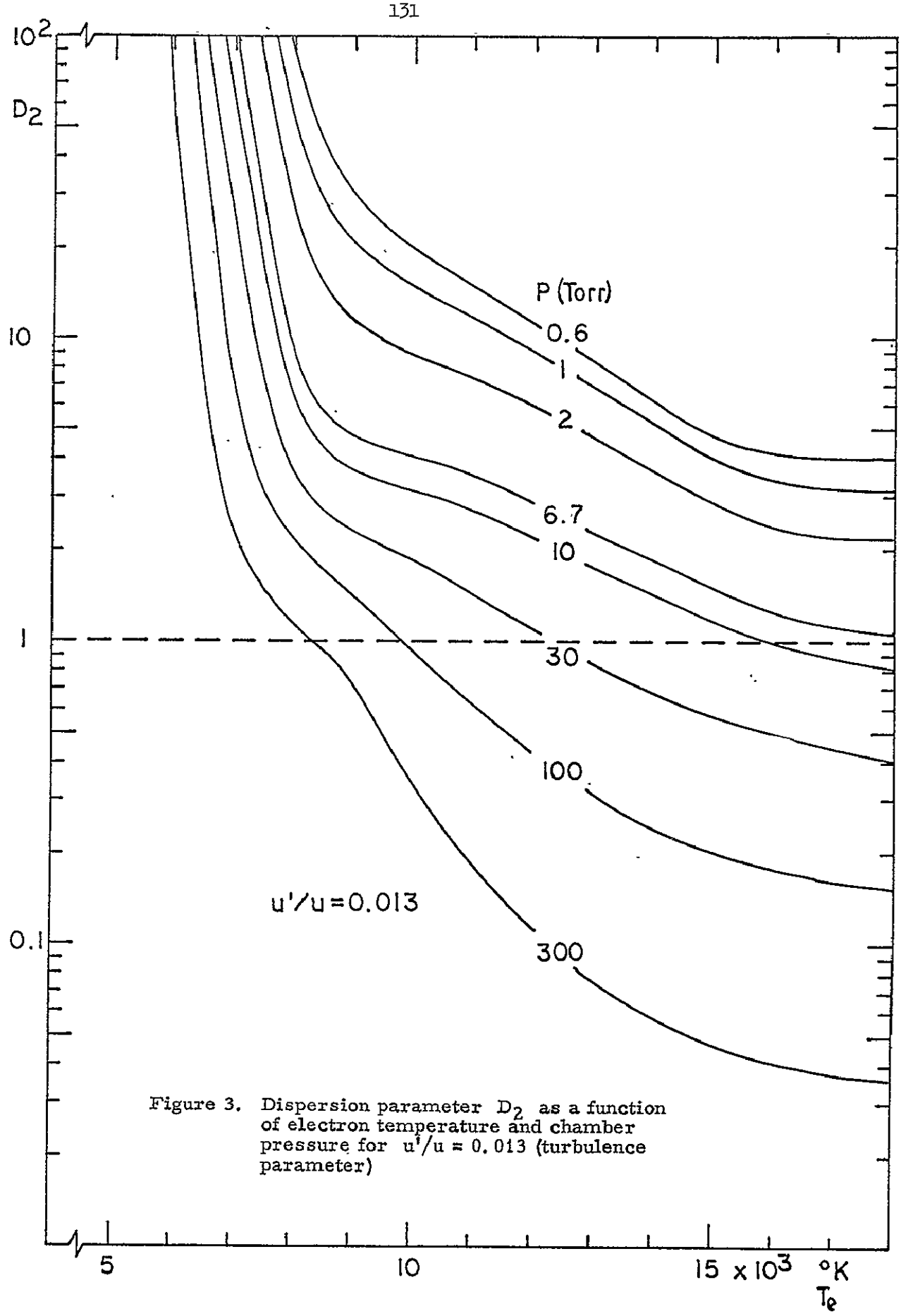

Figure 3. Dispersion parameter D_2 as a function of electron temperature and chamber pressure for $u'/u = 0.013$ (turbulence parameter)

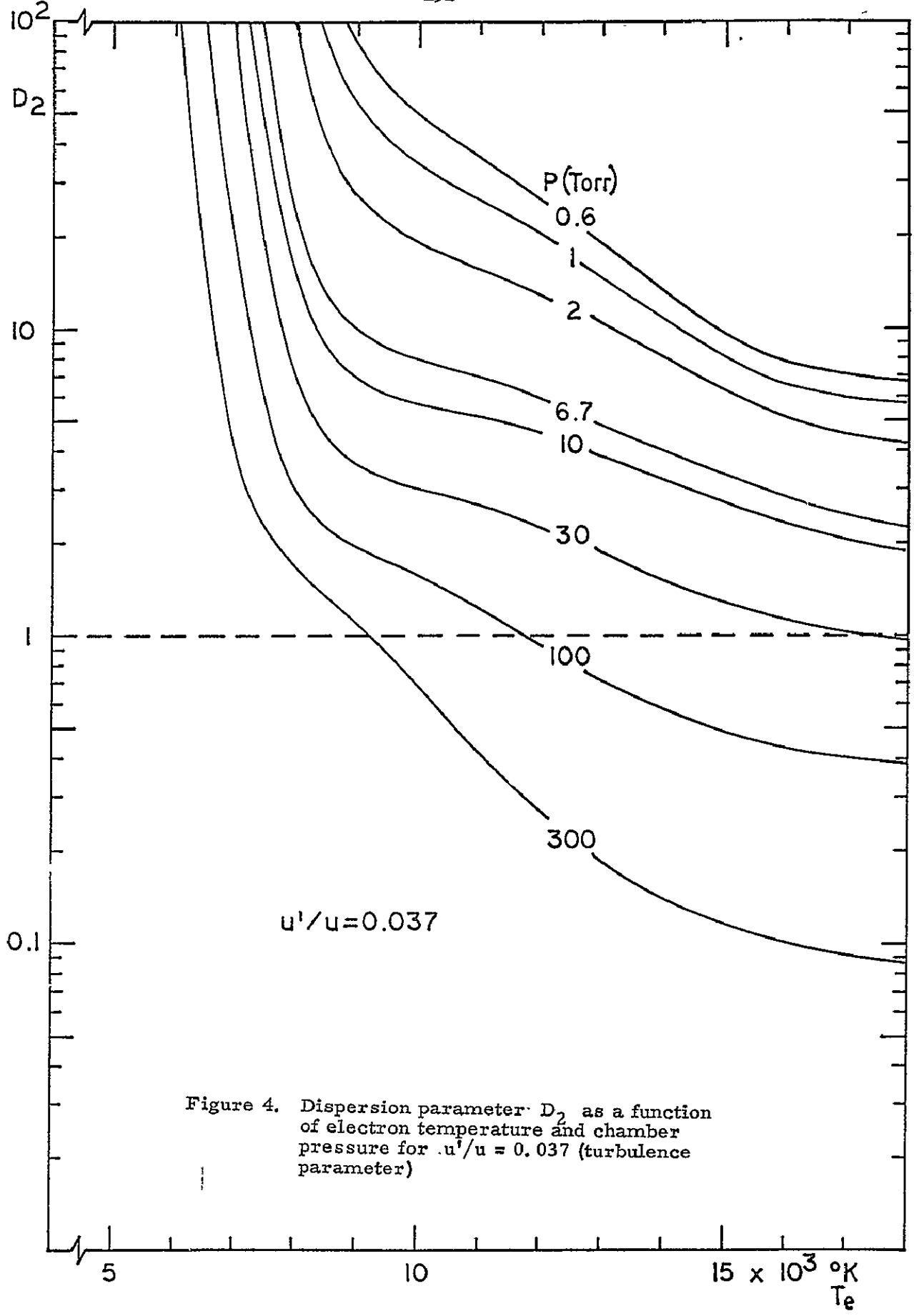

Figure 4. Dispersion parameter D_2 as a function of electron temperature and chamber pressure for $u'/u = 0.037$ (turbulence parameter)

ATTACHMENT OF ARTIFICIAL PLASMA CLOUDS TO THE MAGNETIC FIELD LINES OF THE EARTH

Leo D. Staton
NASA, Langley Research Center
Hampton, Va.

The release of an artificially produced, ionized barium, plasma cloud into the earth's magnetosphere initiates several transitory physical processes of both theoretical and practical interest. The initial phases include the ionization of the initially deposited neutral barium atoms and the expansion of the resulting plasma blob in a spherically symmetrical fashion until a size is reached at which there occurs a rough balance between the gas pressure within the plasma and the effective pressure of the magnetic field. During this period and for some time subsequent to it the plasma cloud as a whole is moving with respect to both the magnetic field and the ambient magnetospheric plasma, because of the initial velocity imparted to the cloud by the space vehicle which released it. It is only after the cloud has come to rest with respect to the magnetospheric plasma that optical tracking methods can be used to measure the cloud velocity and from this velocity to allow the deduction of the ambient, steady, electric-field component perpendicular to the magnetic field.

The time required for the synchronization of the transverse cloud velocity with that of the ambient plasma (i.e. the time required for "attachment" of the cloud to the field lines) is of practical interest because of its importance in designing such an experiment. The physical processes responsible for this synchronization are of theoretical interest for both fundamental plasma physics and magnetospheric physics. Theoretical effort to date in describing these processes has taken three approaches. Common to all three is the idea that the relative motions among the magnetic field lines, the plasma cloud, and the ambient magnetospheric plasma are capable of launching disturbances which may be propagated along and guided by the magnetic field lines.

The first approach recognizes that the polarization electric field which is induced in the cloud by its relative motion with respect to the B field is capable of driving electric currents through that electric circuit composed of the magnetic lines passing through the opposite (charged) faces of the cloud and of a highly conducting path connecting these same lines within the ionosphere. These currents are carried down one of these lines and up the other by electrons of the ambient magnetospheric plasma, which have very high mobility along the lines. In this way the kinetic energy of the relative cloud motion is dissipated in ionospheric heating. A central feature of the model is that the "transmission line" for these currents is filled with the magnetospheric plasma, which has an effective dielectric constant high enough to reduce the electromagnetic propagation velocity to the level of the Alfven velocity.

A second, more rigorous approach is to seek solutions of the MHD equation for a related, mathematically tractable, problem in an attempt to gage the validity of the model described above. It is possible to obtain a rigorous, one-dimensional formulation of an MHD problem in which an infinitely long strip-like current source in the x-y plane (with the current flow across the strip) excites a pure MHD wave propagating along the z-axis. Unfortunately, the one-dimensional character of the solutions is destroyed if the source strip is truncated to finite size. This fact implies that a correction must be added to the first model above to account for the inevitable divergence of some energy away from the direction of the transmission line.

The third approach, one which was originally proposed by workers at the Max Planck Institute, ignores the polarization electric field and instead regards the magnetic field lines as frozen into both the magnetospheric and cloud plasmas. As the cloud moves the lines are then distorted, resulting in a magnetic disturbance which propagates down the field lines with Alfven velocity. The magnetospheric plasma is then disturbed with the result that the cloud relative momentum becomes shared with the particles of the magnetospheric plasma.

Continued work is required since, at present, theoretical values of the synchronization, or attachment, time for the computing models are very nearly equal, allowing no certain description of the physical processes involved.

COMPUTER SIMULATION OF EXPANSION OF IONIZED BARIUM CLOUD PERPENDICULAR TO THE EARTH'S MAGNETIC FIELD LINES

F. C. Grant
NASA, Langley Research Center
Hampton, Va.

The elongated form of the ionized barium cloud suggests that the motion transverse to the Earth's magnetic field be modelled by the two-dimensional motion of a large number of infinitely long rods of charge with appropriate masses. A computer program based on the work of Hohl and Hockney has been prepared to simulate the cloud's transverse motion. A more precise treatment of the dynamics has been introduced so that the treatment of the electronic rods exactly parallels that of the ionic rods.

Large amounts of computing time are required for the simulation, so a prime concern is to use the smallest number of rods consistent with good simulation. Another primary concern is to use the proper initial conditions. These two matters are subjects of parametric study.

When the cloud is subdivided into a sufficiently large number of small charged masses and they are properly started, the subsequent transverse motion provides a measure (when compared to observed cloud motion) of the exciting magnetic field fluctuations, or turbulence, of the Earth's magnetic field. The effect of magnetic field fluctuations on the transverse diffusion may be estimated theoretically.

References

1. Hohl, F.: One- and Two-Dimensional Models to Study the Evaluation of Stellar Systems. Symposium on Computer Simulation of Plasma and Many-Body Problems. NASA SP-153, 1967, pp. 323-336.

2. Hockney, R. W.: Gravitational Experiments with a Cylindrical Galaxy. Astrophys. J., vol. 150, no. 3, Dec. 1967, pp. 797-806.

RADIATION FROM AN ELECTRIC DIPOLE SOURCE IN ANISOTROPIC COMPRESSIBLE MEDIA

A. K. Sundaram*
NASA, Langley Research Center
Hampton, Va.

A detailed discussion on the radiation characteristics of an electric dipole embedded in an infinite homogeneous, anisotropic, compressible plasma is made. The cases treated include the effects of Hall and electron inertia terms in the generalized Ohm's law and finite pressure in the momentum equation. The investigation bridges the gap between the MHD and the conventional magnetoionic theories on radiation from electromagnetic sources. Mathematically, the far fields are obtained using a simple procedure outlined in the analysis which deviates from the existing theory,[1] and it is shown that the method has some advantage in obtaining the radiation resistance. From physical point of view, the directional distribution of waves excited from the dipole source is discussed when Hall and electron inertia effects are included and the results thus derived hold good for all frequencies, particularly for frequencies comparable to ion cyclotron frequency. The validity of the theory is also examined in detail for a special case when $\vec{E}+\vec{V}\times\vec{B}=0$, as usually treated in the literature.

Reference

1. Lighthill, M. J.: Phil. Trans. Roy. Soc. (London) 252, 397 (1960).

*NRC-NASA Postdoctoral Research Associate

SIMULATION OF SOLAR WIND-EARTH MAGNETOSPHERE INTERACTION

by D. L. Chubb, NASA Lewis Research Center

A laboratory simulation experiment of the interaction of the solar wind and the earth's magnetic field is being conducted at NASA-Lewis. The plasma flow is produced by an MPD arc and a magnetic dipole is used to simulate the earth's magnetic field.

Preliminary results were encouraging. Regions of intense light were observed in locations similar to those of the earth's radiation belts. A short movie will be presented of these preliminary results. Although these results are encouraging significant improvements are necessary to obtain a proper simulation of the solar wind-earth magnetosphere interaction. Density and velocity requirements necessary to obtain a proper simulation will be discussed. These requirements result from the following simulation criteria: (1) bow shock thickness less than shock standoff distance; (2) stagnation magnetic field twice field for undisturbed dipole; (3) collisional mean free paths greater than dimensions of experiment; and (4) hypersonic flow.

In addition to the simulation criteria, diagnostic results of a collisionless stagnation flow will be presented. These diagnostics consist of plasma potential and magnetic field measurements. Finally, modifications that are being made to produce a proper simulation of the whole solar wind-earth interaction will be discussed.

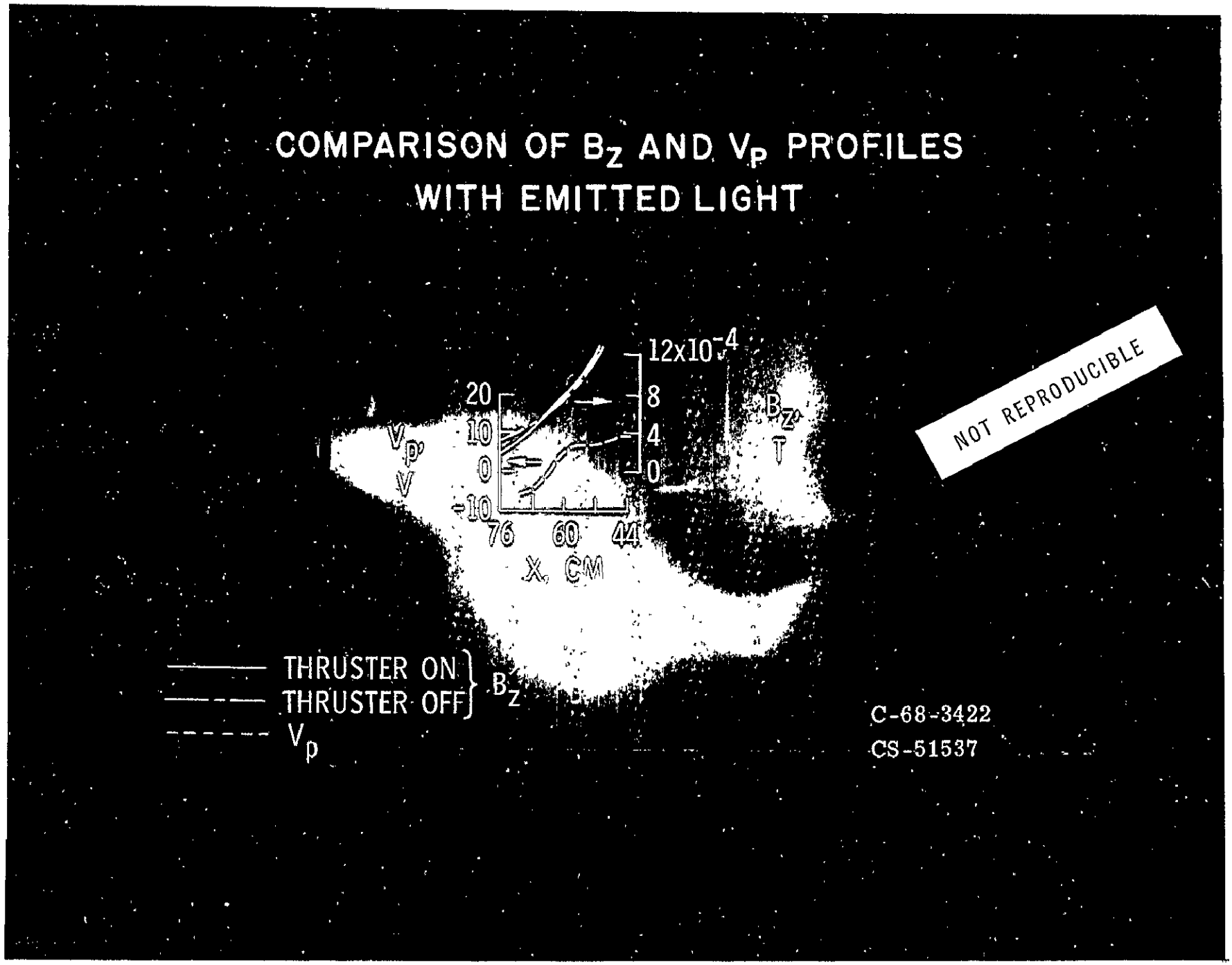
COMPARISON OF B_Z AND V_P PROFILES
WITH EMITTED LIGHT
12x10⁻⁴
8
4
0
B_Z, T
20
10
0
-10
V_P, V
76
60
44
X, CM
THRUSTER ON
THRUSTER OFF
B_Z
V_p
NOT REPRODUCIBLE
C-68-3422
CS-51537

Figure 1

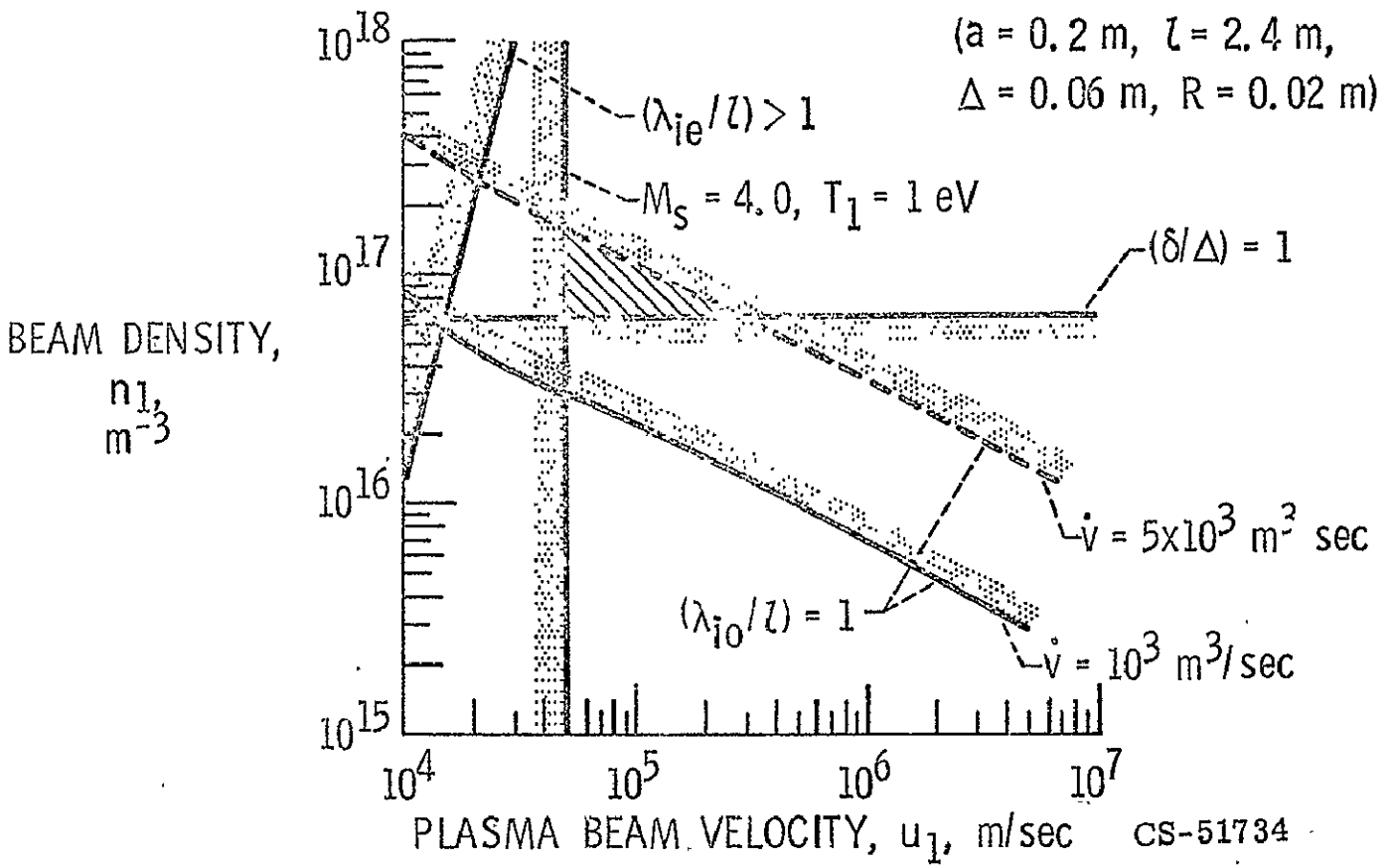

Figure 2.- - Simulation criteria for stagnation point at 0.2 meter from magnet. (a = 0.2 m; ℓ = 2.4 m; Δ = 0.06 m; R = 0.02 m.)

PLASMA IN THE EARTH ENVIRONMENT AND INTERPLANETARY SPACE

Albert G. Opp
NASA Headquarters

(No Abstract)

CURRENT AND PLANNED RESEARCH IN ARGON ION LASERS IN THE PLASMA PHYSICS AND GAS LASER BRANCH

P. Brockman
NASA, Langley Research Center
Hampton, Va.

The argon ion laser offers the possibility of continuous single mode operation at high power in the visible and medium power in the UV. There are a wide range of applications including underwater communications, materials testing, and deep-space communications. Continuous argon ion lasers have been operated at output powers over 100 watts and at efficiencies up to $\simeq$ 0.2 percent. Tube diameters are typically a few millimeters but an increase in laser power with tube diameters up to 15 mm has been shown.[1]

The interest in argon ion lasers at Langley evolved from plasma accelerator experiments involving various high-power nonequilibrium gas discharges at low pressures. To date the program has consisted of equipping a laboratory, designing and building several experiments, and beginning cooperative research with Old Dominion University.

One experiment has consisted of looking for gain in the plume of the continuous MPD arc. At about the time these measurements were begun gain in a pulsed MPD arc was reported.[2] To date, both double pass balanced gain measurements (Fig. 1-A) and internal cavity measurements (Fig. 1-B) using a pulsed TRW laser have indicated less than measurable gains ($\leq$ 1%), across the plume. It is still possible that inversion does exist in the rotating spoke which is evident in the MPD arc for many operating conditions. Future experiments will consist of looking for gain in the spoke using a d.c. laser as a probe and of operating spoke free at much higher powers using the millisecond pulse power supply described at this meeting.[3]

Additional experiments have consisted of constructing and operating 2.7 and 7 millimeter internal diameter quartz lasers. These are static filled lasers in which the fill pressure can be varied. The 7 mm i.d. laser has been operated at a range of pressures and currents from 15 to 30 amperes. For these conditions performance is similar to that reported in reference 1.

Quasi-steady operation at power inputs up to 1 MW will be studied using flat pulses of 1 millisec. or longer, and the limitations due to radiation trapping will be investigated. In this manner the problems for high-power steady lasers will be studied without involving materials problems. Efforts will be made to obtain proper quasi-steady conditions through simulation of steady-state conditions of the lasing plasma and of the tube walls. For example, preheating the quasi-steady pulsed laser with a steady d.c. discharge will be used to investigate the effect of gas temperature on radiation trapping.

An additional laser is under construction. This is a hollow-cathode, hollow-anode design with metal constricting apertures,[4] (Fig. 2). In this design studies of high-power operation will be made and investigation of potential drop along the axis as well as a study of applying varying potential to the apertures. For operation at high input powers large-diameter hollow cathodes which have been operated for steady operation of the MPD arc at currents up to 900 amps will be used.

The work under the Old Dominion University grant will be discussed in another talk.

REFERENCES

1. Herziger, G., and Seelig, W.: High-Efficiency Ion Lasers. "Ionenlaser hoher Leistung" Zeitschrift fur Physik, Vol. 219, No. 1, pp. 5-31, 1969.

2. Leonard, R. Leon; Ahlstrom, Harlow G., and Hertzberg, Abraham: Stimulated Emission in the MPD Arc. Bull. of The Amer. Phys. Soc., Series II, Vol. 13, No. 11, November 1968.

3. Hoell, J. M.; Burlock, J., and Jarrett, O.: Design of a Quasi-Steady MPD Thruster and Spectroscopic Velocity Measurements. Paper presented at this conference.

4. Noon, J. H.; Holt, E. H., and Jennings, W. C.: Argon Ion Laser Utilizing a Hollow Cathode Gas-Fed Arc. Rensselaer Polytechnic Inst. report, ECOM-3032, October 1968.

MPD ARC GAIN MEASUREMENTS

A. BALANCED

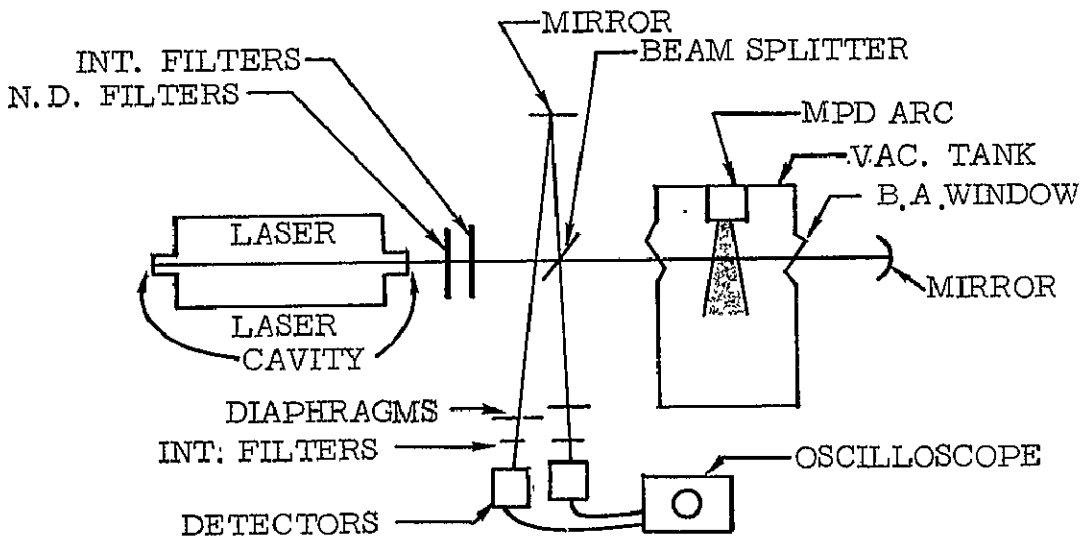

B. INTERNAL CAVITY

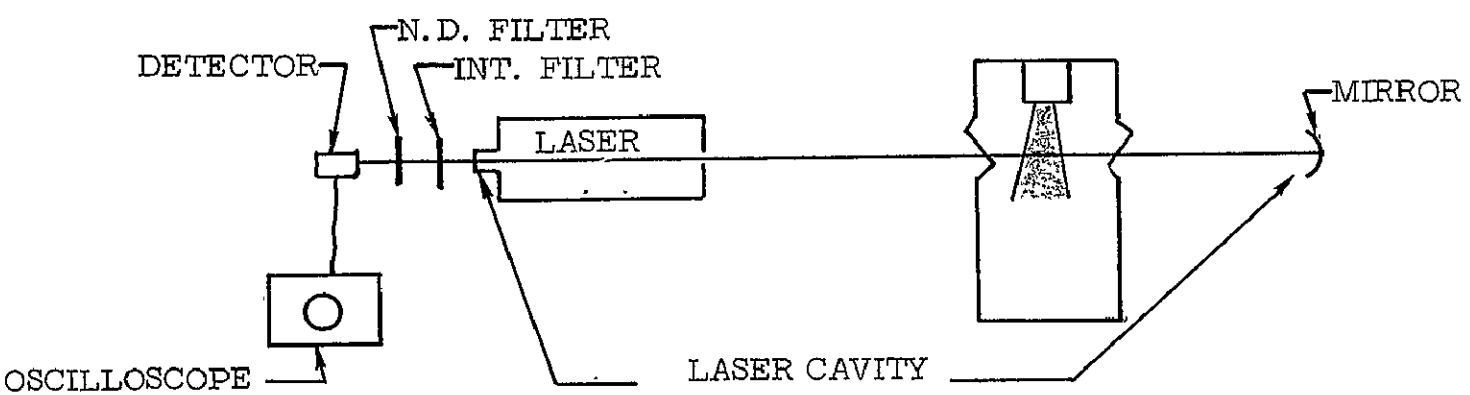

FIGURE 1.

HOLLOW CATHODE DISCHARGE LASERS

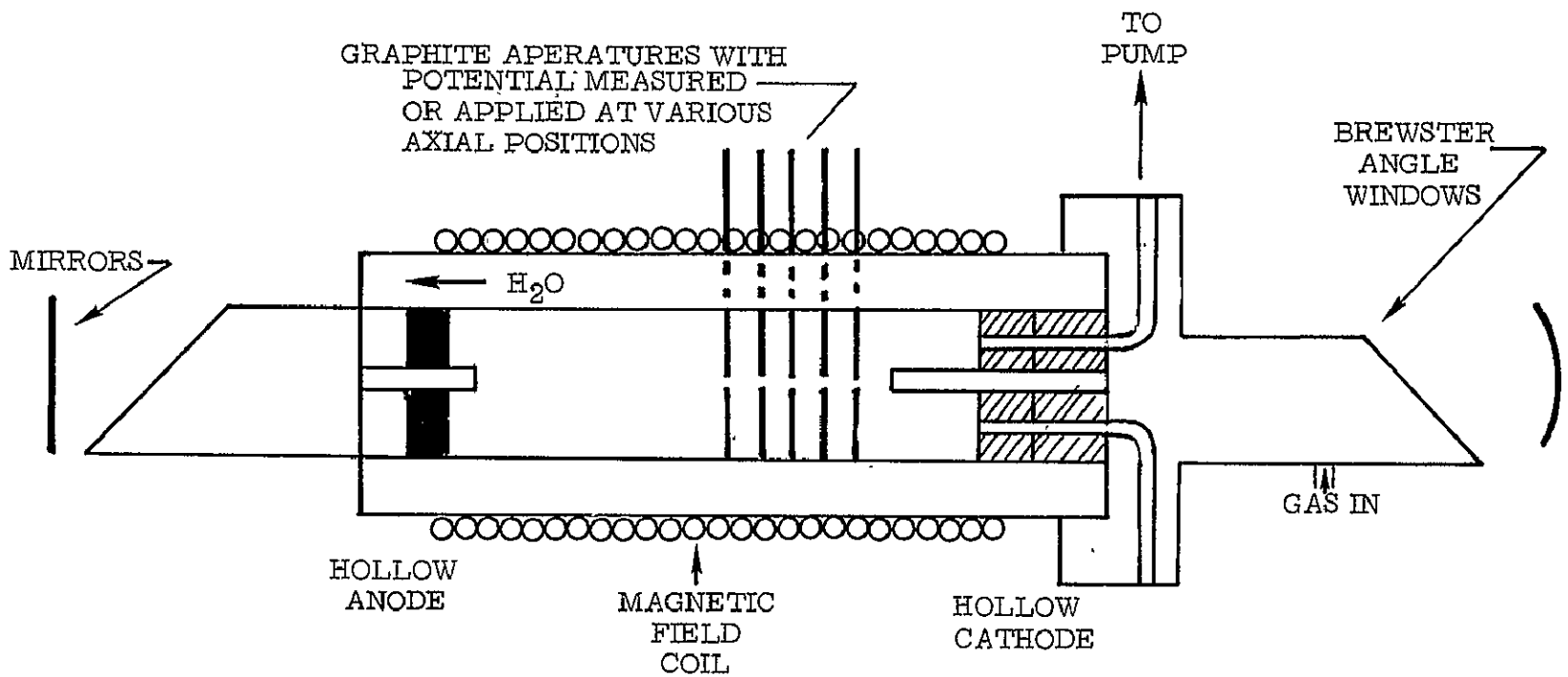

FIGURE 2.

SPECTROSCOPIC MEASUREMENT IN AN MPD ARC*

N. M. Nerheim+

Jet Propulsion Laboratory
Pasadena, California

ABSTRACT

Spectroscopic studies of the emission spectra of the plasma produced by an MPD arc have revealed a highly non-equilibrium distribution of the argon ion excited states. For some operating conditions, the spectra suggested the possibility that population inversions may occur for some of the excited levels. Furthermore, the spontaneous emission of an argon ion laser[1] was noted to be very similar to the spectra of the MPD arc. Because of the similarities, an investigation of the conditions necessary to produce population inversions in the MPD exhaust was started. The beam of a static argon ion laser was directed through the flowing plasma and monitored to detect any changes in the beam intensity. An enhancement of the beam would indicate stimulated emission and therefore an inversion of the upper and lower states of the laser line. The instrumentation was sufficiently sensitive to detect a 1% change in the beam intensity. The probing laser beam was directed through the MPD exhaust at right angles to the flow direction, and a multiple-pass mirror system was used to increase the path length in the plasma to about 500 cm. The exhaust plume was probed as a function of position over a wide range of arc operating conditions, exhaust pressure, and beam strength.

No evidence of stimulated emission was found. The method used was limited to the investigation of the normal A^+ lasing lines that constitute the output of the probing beam, the strongest of which is the 4880 Å line. Because the lower levels of these lines are the resonant levels, direct spectroscopic measurements of the ratio of the upper and lower levels of the transition could not be made. This ratio can be measured for transitions originating from the higher energy levels and the study revealed the possibility of population inversions for some of these lines. However, this speculation is strongly influenced by the accuracy of the transition probabilities used to calculate the population densities from the measured line intensities. Because of the lack of experimental values for the lines originating from the higher energy level, the transition probabilities of a number of lines with 4d upper levels were determined. The measurements were made by H. N. Olsen using techniques that were very similar to those used previously by Olsen[2] to determine argon A-values. The radiation source for these studies was the

---

*This work represents the results of one phase of research carried out in the Propulsion Research and Advanced Concepts Section of the Jet Propulsion Laboratory, California Institute of Technology, under Contract NAS7-100, sponsored by the National Aeronautics and Space Administration.

+Member Technical Staff

plasma produced by a free-burning 400 ampere DC arc in argon at 1.1 atm. A plane-grating monochromator was used to isolate the individual line and fused silca optical components were used to allow observation of lines with wavelengths in the near uv region. Side-on observations were corrected for the background continuum and the measured integrated intensities were inverted using a standard Abel inversion technique. The A-values obtained were lower than the theoretical values by nearly a factor of two, but agreed well with one set of experimental values. A comparison of the published sets of ArII transition probabilities show that there are significant differences in the available values. The comparison is given in terms of the temperature differences that will result from the use of different sets of A-values when they are used to determine plasma temperatures. Additional measurements of transition probabilities are planned. These measurements will include argon atom lines and possibly some xenon lines.

(1) R. I. Rudko, C. L. Tang, J. Appl. Phys., 38, 4731 (1967).

(2) H. N. Olsen, JQSRT, 3, 305 (1963).

ULTRAVIOLET SPECTRUM OF LOW PRESSURE ARGON ION DISCHARGES

G. Ofelt, J. Becher and E. Young
Old Dominion University, Norfolk, Va.

The objective of the study is to understand the basic excitation mechanisms of the argon ion laser in order to be able to increase the power output and efficiency. This study is being conducted in close cooperation with the Plasma Physica and Gas Laser Branch of the Aero-Physics Division at the Langley Research Center and is intended to be a joint effort utilizing the plasma technique experience of that group together with the spectroscopic experience of the Optics and Spectroscopic Group at Old Dominion University.

Previous investigations have been concerned with visible and near UV spectroscopic observations. However, we intend to examine resonance transitions for singly ionized argon which lie in the vacuum UV region at approximately 1000 Å. Since radiation trapping is believed to be a major limitation of argon ion lasers, it seems important to examine spectral line intensities in this region which will lead to a determination of populations of the various states of the ion. This study was undertaken to improve the technology of gas lasers and diagnostics and to examine the lasing system with the aid of spectroscopic techniques in the UV region. It is hoped that information will also be obtained for establishing population inversions for multiply-ionized argon which may cause lasing action for wave lengths as low as 1850 Å. Parametric dependence of the operating conditions will be investigated for creating population inversion among the various lasing levels.

Laser configurations to be investigated are both continuous and pulsed time durations from microseconds to milliseconds. Variation of pressure, current density, and capillary diameter are to be made in the course of this investigation.

We have conducted a preliminary investigation on a small diameter discharge (approximately 4 mm) for the purpose of calibrating our spectroscopic equipment for the argon discharge application. Initial studies were conducted at relatively high pressures of approximately 1 Torr, as compared to the approximately 0.1 Torr laser working pressures at this capillary diameter. The intent was to obtain as strong as possible line intensities during the initial investigation to facilitate the initial orientation. The experimental configuration used for this preliminary study of the argon ion discharge consist of an approximately 5 cm long capillary discharge tube, 4 mm in diameter, which was mounted to a 1/2 meter Seya Monochromator. Observations were made from the visible region of the spectrum to approximately 300 Å with the aid of a dosium salicitate scintilator in front of the photomultiplier tube. The output signal was analyzed by a PAR box car integrator which enables improved signal-to-noise ratio when the electronics is operated in the pulsed mode operation. The discharge power supply is capable of

supplying up to 1000 amps at 1000 V, for a period of 50 secs. Examinations of argon ion discharges made at this laboratory show a production of a continuum from approximately 1000 Å to the near UV. This is the molecular transition which is caused by the close proximity of argon atoms while undergoing a pulsed excitation. Descrete lines are superimposed on this continuum. At present, we are attempting to establish the experimental parameters that influence the production of the continuum and their relation to the lasing lines. In addition, hydrogen is present as an impurity which should aid in the determination of the gas temperature.

FEASIBILITY OF A MAGNETOGASDYNAMIC CROSS-FIELD LASER*

G. R. Russell+

Jet Propulsion Laboratory
Pasadena, California

ABSTRACT

An analytic study has been carried out to determine if population inversions of atomic excited states can be attained in the entrance and exit regions of a cross-field accelerator using argon as a working fluid. A computer program is used in the analysis which includes the simultaneous effects of electron heating, ionization and recombination rates, and the rates of population of atomic excited states. The generalized equations for a three component fluid with different specie temperatures are formulated using the theory of Zhdanov (Ref. 1), and include a generalized Ohm's law and electron energy equation. Electron thermal conductivity, thermal diffusion, and radiative transport are included. Optically thin free-free and free-bound radiation losses are calculated using the theory of Biberman, et al (Ref. 2); also included is the nonequilibrium thin line radiation resulting from transitions between excited states. The resonance transitions result in a leakage loss from the thin line wings plus the effect of diffusion of photons in the thick line core.

A ten level hydrogen-like model is used to calculate the collisional-radiative recombination and ionization rates, and the populations of the first ten transition arrays of atomic argon. It is not assumed either for the case of ionization or recombination that the rates of change of excited state populations tend to zero as is done by Bates and Kingston (Ref. 3). Radiative transition probabilities are calculated using the theory of Bates and Damgaard (Ref. 4). Collisional excitation and deexcitation cross sections are evaluated using the theory of Gryzinski (Ref. 5) for transitions permitted by the selection rules for dipole radiation.

Solutions have been obtained for constant pressure accelerator flows and for flows accelerated in divergent ducts. Depending on the initial conditions of the flow prior to acceleration, population inversions are predicted for both the entrance and exit regions for atomic transitions in the infrared. At the accelerator entrance the sudden increase in electron temperature leads to an inversion of the 5p-3d transition array. The predicted gain for this transition is relatively small and would not allow oscillation in a cavity less than about one meter in length. In the exit region of the accelerator

---

*This work represents the results of one phase of research carried out in the Propulsion Research and Advanced Concepts Section of the Jet Propulsion Laboratory, California Institute of Technology, under Contract NAS7-100, sponsored by the National Aeronautics and Space Administration.

+Group Supervisor

where the electron temperature is rapidly decaying, electron capture associated with collisional-radiative recombination causes inversions of the 4d-5p transition array. Depending on the final values of the electron temperature and density, the gain for this transition array is large enough to make it possible to attain oscillation in a cavity of the order of 10 cm in length.

On the basis of these predictions, a cross field laser has been constructed at JPL to attempt to produce lasing in a cavity placed downstream of the accelerator exit. In this device argon is pre-heated in four MPD arcs, exhausted into a water-cooled plenum chamber, and then expanded through an uncooled graphite Mach 3 nozzle. The gas then passes through a constant pressure cross-field accelerator containing twenty-one uncooled thoriated tungsten electrode pairs. Provision is made to vary the current density and potential along the accelerator axis to minimize the flow of Hall currents. The laser cavity is located at a fixed point in a large vacuum tank that houses the entire experiment. The cavity is positioned relative to the accelerator exhaust by moving the accelerator and associated equipment, including the electromagnet, on a track within the vacuum tank during a test. Design of the complete system including the laser cavity and associated optics has recently been completed. Preliminary diagnostic studies of the gas properties in the accelerator have begun prior to attempting to provide the correct threshold excited state populations required to achieve oscillation in the laser cavity.

(1) Zhdanov, V. M. (PMM Vol. 26, No. 2, 1962, pp 280-288), pp 401-413, Applied Mathematics and Mechanics (Translation).

(2) Biberman, L. M., Norman, G. E., and Ulyonov, K. N., Opt. and Spect. 10, pp 297-299, 1961.

(3) Bates, D. R. and Kingston, A. E., Plant Space Sci., 1963, Vol. 11, pp 1-22.

(4) Bates, D. R. and Damgaard, A., Phil. Trans. Roy. Soc. (London) 242A, 14 (1949).

(5) Gryzinski, M., Phys. Rev., Vol. 138, No. 2A, pp 336-358, 19 April 1965.

MOLECULAR LASERS USING ELECTRICAL DISCHARGES AND HIGH FLOW RATES. CURRENT AND PLANNED RESEARCH IN THE PLASMA PHYSICS AND GAS LASER BRANCH

F. Allario, R. Lucht and R. V. Hess
NASA, Langley Research Center
Hampton, Va.

Within the past few years, considerable research on gasdynamic molecular lasers using mixtures of CO_2 with various gases has been performed with the aim of obtaining high laser power. This system although attractive because of its large input capability, has proven to have extremely low efficiency. Recently, interest in other systems capable of producing high laser power has arisen because of their relatively high efficiency, although limited power inputs. Among these systems are electrical discharge lasers[1,2,3] operating in relatively high flow rates and chemical laser systems.[4,5] In both systems, rapid progress is being made in increasing laser power per unit length and there is promise of even higher power input and higher efficiencies than presently available.

In the last six months, members of this Branch in collaboration with Prof. Hassan of North Carolina State University, have developed plans for research in molecular lasers using electrical discharges and high flow rates of CO_2, H_e and N_2 mixtures. Some preliminary studies have already been performed.

Professor Hassan will discuss aspects of the theoretical program at this conference[6] and in this paper some preliminary experimental results and plans for future work will be discussed. In figure 1, a schematic of the apparatus used to study electrical discharge lasers with high flow rates is shown. As is indicated, a simple electrode configuration and gas injection scheme were used, but results obtained indicated that an improved version would probably be more desirable for applying greater power to the electrical discharge. Furthermore, a convenient optical cavity was chosen but again calculations show that the choice of an improved optical cavity could lead to a substantial increase in efficiency of the system. Volume flow rates in the one-inch-diameter tube were varied between 5 and 150 liters/min, the upper limit being set by available flow meters. Electrical power was supplied by a 100 kw (10 kv, 10 A) d.c. power supply. The laser beam showed a multimode structure and power was recorded with a conventional power meter. A gain-measuring system has also been assembled with an auxiliary laser to measure laser gain parallel and perpendicular to the flow axis.

A parametric study has been performed of the variation of laser output power with flow rates of the constituents (CO_2, N_2, H_e) and has been related to the voltage-current characteristics of the discharge. These preliminary results show that almost an order of magnitude increase in power output can be expected by varying the flow rate considerably less than 2 orders of

magnitude. For example, laser power was increased from less than 10 watts (efficiency ∿ 5%) to approximately 60 watts (efficiency ∿ 10%) for a tube length of less than half a meter (18") by increasing the flow rate from 5 to 130 liters 1/min. These results by far exceed the maximum power outputs per meter for no-flow lasers and are consistent with recently published results in references 1 and 2, showing that convective cooling of the gas mixture by the high flow rate helps to maintain a low gas temperature leading to enhanced laser power. The comparatively low efficiencies obtained (∿ 5% and 10%) suggests that improvement in the optical cavity and flow uniformity are needed; at the lower flow rates cooling of the laser tube walls is desirable. However, the more pertinent result for the present high flow rate experiment is that it was possible to increase input power to the discharge by increasing the flow rate, which for a given efficiency of course corresponds to an increase in laser power. The inability in the present experiment to obtain further increase in laser power arises from the fact that the input power was limited by the flow rates and the difficulties in obtaining higher current densities due to the transition from glow discharge to arc-discharge operation which prevents the attainment of further useful power for lasing.

It was further observed in our experiment that the discharge appeared to strike in an annulus between the electrodes rather than distributed over the cross section. Thus, optimum use is not made of convective cooling and the current density is not uniformly spread over the cross section. An improved electrode configuration and injection system should permit higher power inputs in the present experimental setup and should also permit operation at higher pressures without transition from glow- to arc-discharge yielding higher laser powers.

A research program is planned to investigate the operation of molecular lasers with electrical discharges and high flow rates, at comparatively high pressures (> 50 torr) and large tube diameters. Problems associated with cross-flow lasers[2,3] will be investigated using various techniques including magnetic fields to prevent bowing of the discharge with the flow. Operation of glow discharges with flow rates at high pressures involves new research problems concerning the transition of the (abnormal) glow to arc discharge. Diagnostics of the distribution of electric field, particle density and electron temperature are planned, together with transverse gain measurements to relate the distribution of lasing action to the distribution of plasma properties in the discharge. Transverse gain measurements along the tube length should yield information on the efficiency of multiple excitation of N_2 along the discharge (and cavity) length, and should allow a comparison of long tube lasers and short transverse flow lasers. Fluid mixing schemes will also be studied.

High power pulsed operation of electrical discharges at high pressures and high flow rates will be investigated to determine the limits of current density and power to which the discharge laser can be extended since in

pulsed operation, heating of the gas and filling of the lower laser level can be kept small through the use of short pulses.[7] Diagnostics on pulsed discharges are also planned utilizing the powerful techniques of time sampling and signal averaging.

A program is also in progress to study the feasibility of excitation mechanisms other than the glow discharge for molecular and chemical lasers in cooperation with Prof. Richard Schneider from the University of Florida. As a preliminary experiment, the effect on a conventional CO_2 laser of the high energy products released in the reaction of He^3 with thermal neutrons will be investigated. Experiments at higher particle densities than in conventional tube lasers are ultimately planned for investigation. The effect of neutrons on HF chemical lasers using UF_6 as fluoride source will also be studied.

REFERENCES

1. Deutsch, T. F. et al.: CW Operation of High-Pressure Flowing CO_2 Lasers. Appl. Phys. Letters, 15, 3, p. 88 (August 1969).

2. Tiffany, W. B. et al.: Kilowatt CO_2 Gas-Transport Laser. Appl. Phys. Letters, 15, 3, p. 91 (August 1969).

3. Private communication from Wayne Burwell on the work of Clyde Brown and others at United Aircraft Research Laboratories.

4. Saunders, A.: Experimental and Theoretical Study of Chemical Inversion in Gas Lasers. Paper to be presented at this conference.

5. Cool, T. A.: Chemical Laser by Fluid Mixing. Bull. Am. Phys. Soc., 14, 11, p. 1107 (Nov. 1969).

6. Hassan, H. A.: The Role of Electrical Discharges in Population Inversion in CO_2 Flow Lasers. Paper to be presented at this conference.

7. Hill, A. E.: Multijoule Pulses from CO_2 Lasers. Appl. Phys. Letters 12, 324 (1968).

SCHEMATIC OF HIGH FLOW, N_2: He: CO_2, ELECTRICAL DISCHARGE LASER SYSTEM

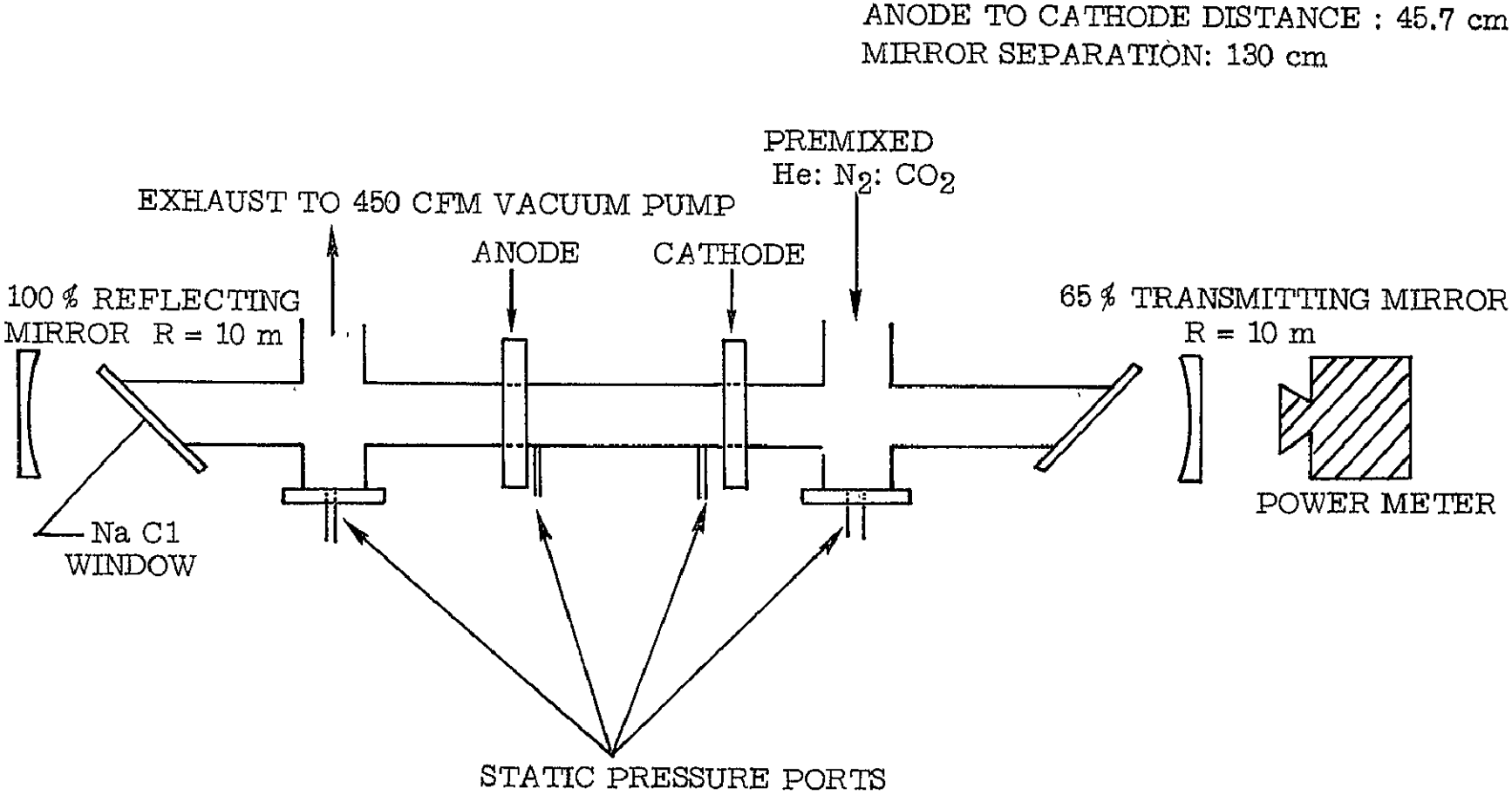

FIGURE 1.

THE ROLE OF ELECTRICAL DISCHARGES IN POPULATION INVERSION IN CO_2 FLOW LASERS*

H. A. Hassan

North Carolina State University, Raleigh, North Carolina 27607

The objective of this research is to analyze CO_2 laser systems in which the population inversion is obtained by electrical discharges. This entails solving the governing equations for various laser parameters, such as mass flow rate, length and diameter of the tube laser, pressure and composition. In such discharges excitation of CO_2 molecules to the upper laser level results mainly from energy transfer from vibrationally excited N_2 while the lower laser lever is depopulated mainly by collisions with He.

If one assumes that molecules in different quantum states are different species, then the governing equations are the conservation of species equations, the overall momentum and energy equations, and an electron energy equation. These equations, together with the reactions given in Eq. (5) below, will serve as the basis of our model. The considerations presented here are based on these equations.

Examination of the conservation of species equation, which can be written as

$$\rho \frac{\rho Y_i}{\rho t} + \rho \vec{u} \cdot \nabla Y_i + \nabla \cdot (\rho Y_i \vec{V}_i) = W_i \ , \ Y_i = \rho_i / \rho \qquad (1)$$

where ρ is the density, $\vec{u}$ the mean velocity, V_i and W_i are the diffusion velocity and mass rate of production of species i, shows that there are three characteristics times in a steady laser system. These are

$$t_o = \frac{L}{U_o} \ , \ t_d = \frac{d^2}{D_o} \ , \ t_r = \frac{T_o}{W_o} \qquad (2)$$

where L and d are the length and diameter of the tube, respectively, and U_o, ρ_o, D_o and W_o are characteristic velocity, density, diffusion coefficient and production rate, respectively For a successful laser operation

$$t_r < t_o \qquad (3)$$

For a given temperature, t_r is inversely proportional to the pressure; thus, for an increase in pressure an N_2 molecule can be excited and de-excited many times for a given tube length. When $t_d > t_o$ the laser is of the gas-transport type; in this case the cooling is mainly due to the convective cooling $\dot{m} C_p \Delta T$. This can be seen from

$$\frac{t_d}{t_o} = \frac{d^2 U_o}{D_o L} = \frac{4}{\pi} L_e^{-1} \frac{\dot{m} C_p}{K L} \qquad (4)$$

---

* Supported, in part, by Grant NGR 34-002-115

where L_e is the Lewis number (of order unity), m is the mass flow rate, C_p is the specific heat at constant pressure and K is the thermal conductivity. The parameter $\frac{\dot{m} C_p}{K L}$ can be thought of as the ratio of convective cooling to cooling by conduction and diffusion through the wall. Thus to improve the laser power one needs to operate with high $\frac{\dot{m} C_p}{K L}$.

For a given laser system t_r is obtained from consideration of the rates of vibrational energy transfer in the system. Based on the recent survey of Taylor and Bitterman[2], the important relaxation precesses in a CO_2 laser system are

$$N_2 \ (V = 0) + e \rightleftarrows N_2 \ (V = 1) + e \qquad \text{(i)}$$

$$CO_2 \ (0,1^1,0) + M \rightleftarrows CO_2 \ (0,0^0,0) + M + 667 \ C_m^{-1} \qquad \text{(ii)}$$

$$CO_2 \ (0,0^0,1) + N_2 \ (V = 0) \rightleftarrows CO_2 \ (0,0^0,0) + N_2 \ (V = 1) + 18 \ C_m^{-1} \qquad \text{(iii)}$$

$$CO_2 \ (0,0^0,0) + M \rightleftarrows CO_2 \ (0,m^{\ell},0) + M + E_{trans.} \qquad \text{(iv)} \qquad (5)$$

where M stands for any species in the system: CO_2, N_2, H_e, H_2O, CO, etc. Reaction (ii) describes the exchange of energy between translational and vibrational modes while reactions (iii) and (iv) describe the vibration - vibration energy exchange. Examination of the rates indicates that H_e is active in depopulating the lower laser level and has little effect on the upper laser level. On the other hand H_2O is active in depopulating all laser levels. This indicates that there is an optimum H_2O concentration beyond which a loss in laser power will take place.

The role of H_e in a CO_2 laser system is discussed next. It has been suggested that, in addition to depopulating the lower laser level, it has a high thermal conductivity; this results in a decrease in the gas temperature and this, in turn, increases the population inversion. However, increased conductivity results in an increase in the wall losses and this results in a decreased efficiency. Thus, the explanation for the improved efficiency, especially in the gas-transport lasers, must lie somewhere else. It is proposed here that the improved efficiency is a result of the high electron temperature in the discharge. This can be seen from the electron energy equation

$$\vec{J}_e \cdot \vec{E} = 3 \ k \ N_e \ m_e \ (T_e - T) \ \Sigma \ \frac{\delta_s \nu_{es}}{m_s} \qquad (6)$$

where $\vec{J}_e$ is the electron current, $\vec{E}$ the electric field, T_e the electron temperature, T the gas temperature N_e the electron number density, and m_s the particle mass, δ_s the energy-loss factor and ν_{es} is the collision frequency of species s. The quantity δ_s is unity for monatomic gases and large for heavy particles (about 18 for N_2)[3], thus to maintain a high electron temperature one needs to employ an inert monatomic carrier gas.

References

1. Tiffany, W. B., et. al: App. Phys. Letters, Vol. 15, No. 3, p. 91, 1969.
2. Taylor, R. L., and Bitterman, S., Rev. Mod. Phys. Vol. 41, No. 1, pp. 26-47, 1969.
3. Demetriades, S. T., Phys. Rev., Vol. 158, p. 215, 1967.

PUMPING MECHANISM OF CO_2 LASER AND FORMATION RATE OF CO_2 FROM CO AND O*

C. J. Chen+

Jet Propulsion Laboratory
Pasadena, California

ABSTRACT

The pumping mechanism of a high-current pulsed pure CO_2 laser has been investigated. It was found that there is a time delay of the laser pulse behind the current pulse. For a fixed gas pressure, there is an upper bound discharge current and pulse width below which the time delay decreases as the discharge current is increased. Above the upper bound current, the time delay is independent of the discharge current and the pulse width. The delay time decreases very rapidly as the gas pressure is increased. The gas pressure p and the delay time t exhibit the inversed cubic relation as $t \propto 1/p^3$. The intensities of the atomic oxygen line 7771 Å and the band head of the 0-1 band of CO 4835 Å increase as the magnitude and/or pulse width of the discharge current is increased. These intensities reach a plateau for certain upper bound values of the discharge current and current pulse width. After the current pulse is over, the line intensities decay gradually to zero. The electron density measured typically is about 10^{10} cm^{-3} and decreases to about 1% of this initial value when the laser pulse appears. The electron temperature drops from about 2ev to the gas temperature within 50μs. The gas temperature, which varies from room temperature to 400°K by heating the gas with a temperature tape, was measured with a thermocouple in the center of the tube.

These experimental results indicate that the pumping mechanism of the upper level of the CO_2 laser is due to the reaction $CO + O \rightarrow CO_2^*$. During the pulse discharge, the CO_2 is decomposed into CO and O. The saturation phenomena as shown in delay time as a function of discharge current and pulse width, and the plateau phenomena, as shown in line and band head radiation indicate the percentage of CO_2, which decomposed into CO and O depends upon the discharge power input which is proportional to the magnitude of the current and the pulse width. For a sufficiently high power input, the CO_2 is totally decomposed into CO and O. The saturation and plateau phenomena appear when CO_2 is totally decomposed. After the current pulse is over, CO and O start to recombine to form excited CO_2^* molecules. Each recombination contributes one excited CO_2^* molecule. Thus, the recombination rate of CO and O is equal

---

*This work represents the results of one phase of research carried out in the Propulsion Research and Advanced Concepts Section of the Jet Propulsion Laboratory, California Institute of Technology, under Contract NAS7-100, sponsored by the National Aeronautics and Space Administration.

+Member Technical Staff

to the rate of pumping of the upper laser level. The delay time of the laser pulse behind the current pulse is the time required to build up the laser upper state population to meet the threshold condition for oscillation. By equating the threshold population density of the upper laser level to the number of CO_2^* molecules formed, the rate constant K can be determined:

$$K = \frac{2.88 \times 10^{13} (kT)^3}{pt} \text{ cm}^6 \text{ sec}^{-1}$$

The value of K can be obtained by measuring T, p.and t. The result for a pressure range from 4 to 10 mm Hg at a temperature of 300°K is

$$K = 8.5 \times 10^{-35} \text{ cm}^6 \text{ s}^{-1}$$

The temperature dependence of the value of K is obtained by measuring the time delay at different gas temperatures which is accomplished by using a heating tape wrapped around the discharge tube and the tubing upstream of the flowing gas system. The temperature dependence is assumed to be in the following form:

$$K = A\, e^{-\frac{B}{T}}$$

Evaluation of the constants A and B yields the complete expression for the reaction constant:

$$K = 2.19 \times 10^{-32}\, e^{-\frac{1670}{T}} \text{ cm}^6 \text{ s}^{-1}$$

It should also be noted that the water vapor impurity in the tube, which is very difficult to entirely remove even with elaborate precautions, does not affect the measured reaction rate in the present case. Since the recombination energy in the reaction with OH is carried away by the product H, the CO_2 molecule formed by this process is in the ground state (both electronic and vibrational). Therefore, there is no contribution to the population of the upper energy level of the laser.

CONTINUOUS-WAVE CHEMICAL LASER OPERATION WITHOUT SUSTAINING EXTERNAL ENERGY SOURCES*

Terrill A. Cool
Laboratory of Plasma Studies,
Cornell University, Ithaca, N. Y. 14850

Continuous-wave laser operation at 10.6μ has been achieved in the DF-CO_2 and HF-CO_2 molecular systems by purely chemical means. Both lasers operated solely by the simple mixing of bottled gases; no external sources of energy were required.

A chain reaction mechanism has been found which provides continuous pumping of the upper CO_2 laser state by vibrational energy released from chemical reaction. The reactions can be sustained continuously without an external source of energy. The chemical reactions are:

$$F_2 + NO \longrightarrow ONF + F$$
$$F + D_2 \longrightarrow (DF)^* + D$$
$$D + F_2 \longrightarrow (DF)^* + F \qquad (1)$$

The analogous set of reactions obtained by substituting hydrogen in place of deuterium has also been employed successfully. The vibrational-rotational energy of the vibrationally excited $(DF)^*$ or $(HF)^*$ product molecules of the above reactions is coupled to the upper CO_2 laser level by means of intermolecular vibrational energy transfer processes.

Experimental results concerning the performance capabilities of these first purely chemical lasers will be presented. These measurements show that the DF-CO_2 system is capable of high optical gain and high power output. More significantly, this laser offers a remarkably efficient means for the continuous direct conversion of chemical energy into laser output.

The DF-CO_2 purely chemical laser offers unique possibilities for efficient self-contained energy storage and utilization.

---

*Supported by NASA under contract NGL 33-010-064 and by ONR under contract N 00014-67-A-0077-0006.

EXPERIMENTAL AND THEORETICAL STUDY OF CHEMICAL INVERSION IN GAS LASERS

Andrew R. Saunders
NASA, Langley Research Center
Hampton, Va.

Production of critical inversion densities by chemical reactions in gas lasers has assumed increasing importance in recent years. Pulsed and c.w. gas lasers using chemical inversion were operated successfully quite recently utilizing vibrationally excited hydrogen halides formed in chemical reactions.[1,2] Highest power levels were obtained in a continuous flow reactor where the vibrational energy of the hydrogen halide was used to excite the $00^\circ1$ level in CO_2 to obtain laser emission on the $00^\circ1 \rightarrow 10^\circ0 \rightarrow$ and $00^\circ1 \rightarrow 02^20$ transitions.[3]

In our recent studies[4] we have investigated chemical inversion in CO_2^* formed in low pressure $CO - O_2$ flames at 50 - 80 torr. The radiative transitions for CO_2 are shown in figure 1. It was known from earlier work[5] that electronically or vibrationally excited CO_2 can form in the reactions

$$CO + O \rightarrow CO_2\ (^3B_2)$$

$$CO_2\ (^3B_2) \rightarrow CO_2\ (^1B_2)$$

$$CO_2\ (^1B_2) \rightarrow CO_2\ \left(^1\Sigma_g^+\right)(v_1, v_2, v_3)$$

Radiative transitions from the excited electronic level $^1B_2$ take place into vibrational levels of the $^1\Sigma_g^+$ ground state of CO_2. By comparison of experimental measurements of radiative emissions corresponding to the $11^10 \rightarrow 02^20$, $10^\circ0 \rightarrow 01^10$ and $00^\circ1 \rightarrow 00^\circ0$ transitions with the theoretical values for equilibrium vibrational distribution as shown in figure 2 for the latter two, it was shown that for nearly equilibrium population of the $10^\circ0$ symmetric stretching and 020 bending modes the population of the $00^\circ1$ assymmetric stretching mode is substantially less than the equilibrium value. In addition the data show a definite correlation between the electronic transitions populating the vibrational levels and the infrared emission intensities for these levels. Thie preferential filling of the bending and symmetric stretching vibrational energy levels of CO_2 may be explained by the transition from the bent $^1B_2$ state to the linear $^1\Sigma_g^+$ configuration. In this transition the bending mode vibration would be preferentially excited and energy readily transferred into the symmetric stretching mode by Fermi resonance coupling whereas the uncoupled assymmetric stretching mode would be populated largely by collisional transfer.

Comparing these results obtained by chemical excitation on CO_2 with the results of electron impact excitation in a CO_2 electric discharge laser

cavity the role of electron impact excitation as the primary process in producing 00°1 inversion becomes quite apparent. In the recent studies of Clough and Thrush[6] on the formation of vibrationally excited N_2O in the reaction $N + NO_2 \rightarrow N_2O\ (v_1, v_2, v_3) + O$ at about 0.1 torr preferential excitation of the v_1 and v_2 modes was observed similarly to our results with CO_2. Since N_2O is isoelectronic with CO_2 and the distribution of the vibrational energy levels is very similar, these results strongly support our observations on the $CO - O - CO_2$ system.

At this point a substantial experimental and theoretical effort is required to evaluate the electronic, vibrational and rotational energy transfer processes controlling chemical inversion. Quantum mechanical calculations are required to predict the probabilities of electronic and vibrational excitation in a given reaction and the initial energy distribution of the species formed in the reaction. Using the rate parameters available for given systems we shall attempt to relate the internal electronic, vibrational and rotational energy transfer processes in the presence of chemical reactions to the inversion densities obtained in a laser cavity for the same system. Complexity of the chemical rate processes is indicated by the rate processes on CO_2 inversion as shown in figure 3.

The initial effort will be concentrated on measurements of the rotational and vibrational distributions of the laser emission radiation in halogen-halide and other chemical lasers in pulsed and c.w. operation using high flow rates as a function of the reaction kinetics. The theoretical studies will be concentrated on solution of the radiation coupled chemical kinetic rate equations with detailed description of the fluid dynamic and chemical rate processes. Mechanisms leading to higher inversion densities and total radiated power will be examined both experimentally and theoretically.

References

1. Corneil, Paul H.; and Pimentel, George C.: Hydrogen-Chlorine Explosion Laser. II. DCl. J. Chem. Phys., vol. 49, no. 3, Aug. 1968, pp. 1379-1386.

2. Gross, R. W. F.: Chemically Pumpsed CO_2 Laser. J. Chem. Phys. vol. 50, 1969, pp. 1889-1890.

3. Cool, Terrill A., Falk, Theodore J., and Stephens, Ronald R.: DF-CO_2 and HF-CO_2 Continuous-Wave Chemical Laser, Applied Physics Letters 1970.

4. Koopmann, R. K.; and Saunders, A. R.: Non-Equilibrium Vibrational Energy Distribution of CO_2 in CO-O_2 Flames at Reduced Pressure. Jour. Quant. Spectr. and Radiative Transfer. 1970.

5. Callomon, J. H.; and Gilby, A. C.: The Carbon Monoxide Flame Spectrum Under High Resolution. Chem. Soc. Journ. (Brit.), 1963, pp. 1471-1475.

6. Clough, P. N.; and Thrush, B. A.: Formation of Vibrationally Excited N_2O in the Reaction of Nitrogen Atoms with NO_2. Proc. Roy. Soc. vol. A309, 1969, pp. 419-431.

RADIATIVE TRANSITIONS IN CO_2

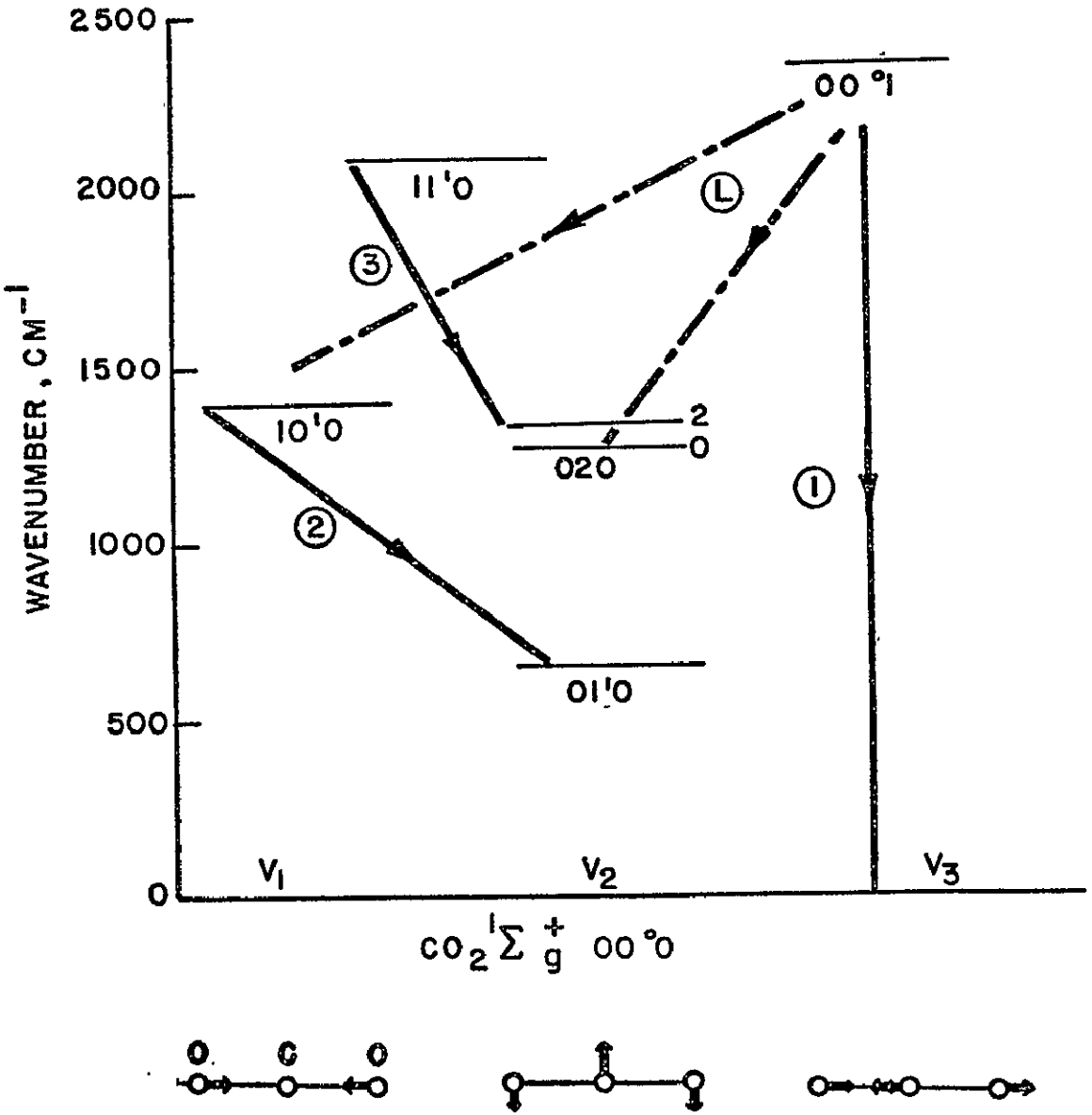

FIGURE 1.

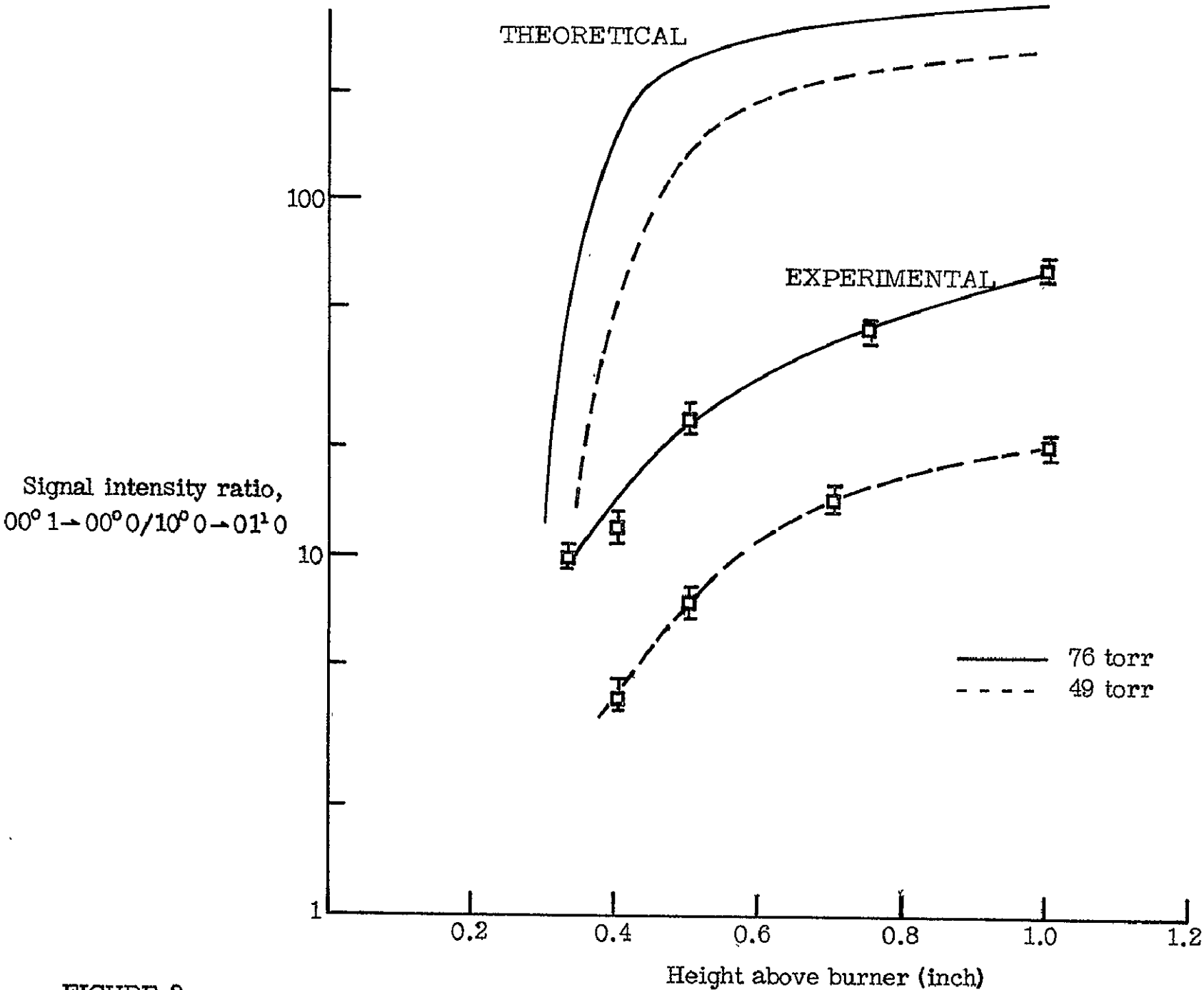
THEORETICAL
EXPERIMENTAL
100
10
1
Signal intensity ratio,
$00^0 1 \rightarrow 00^0 0 / 10^0 0 \rightarrow 01^1 0$
76 torr
49 torr
0.2
0.4
0.6
0.8
1.0
1.2
Height above burner (inch)

FIGURE 2.

CO_2 INTERNAL ENERGY TRANSFER KINETICS

INTERMOLECULAR

$$CO_2(v_1,v_2,v_3) \rightleftharpoons CO_2(v_1) + CO_2(v_2) + CO_2(v_3) \quad (1)$$

$$CO_2(^1B_2) \rightleftharpoons CO_2(v_1) + CO_2(v_2) + CO_2(v_3) \quad (2)$$

$$CO_2(v_1) \rightleftharpoons CO_2(v_2) \quad (3)$$

$$+ CO_2(v_2) \rightleftharpoons CO_2(v_1,v_2) \quad (4)$$

TRANSLATIONAL - VIBRATIONAL AND V - V

$$CO_2(v_3) + M \rightleftharpoons CO_2 + M \quad (5)$$

$$\rightleftharpoons CO_2(v_2) + M \quad (6)$$

$$CO(v_2) + M \rightleftharpoons CO_2 + M \quad (7)$$

$$\rightleftharpoons CO_2(v_1) + M \quad (8)$$

Where $M = N_2, H_2O, CO, O_2, H_e, M$

RADIATIVE

$$CO_2(v_3) \rightleftharpoons CO_2 + h\nu \quad \text{EXP} \quad (9)$$

$$\rightleftharpoons CO_2(v_2) + h\nu \quad \text{LASER} \quad (10)$$

$$\rightleftharpoons CO_2(v_1) + h\nu \quad \text{LASER} \quad (11)$$

$$CO_2(v_1v_2) \rightleftharpoons CO_2(v_2) + h\nu \quad \text{EXP} \quad (12)$$

$$CO_2(v_1) \rightleftharpoons CO_2(v_2) + h\nu \quad \text{EXP} \quad (13)$$

FIGURE 3.

Thermal Laser Excitation by Mixing in a Highly Convective Flow

Wayne G. Burwell
United Aircraft Research Laboratories

CW infrared laser emission has been achieved from the mixed flow region formed by injection of CO_2 or N_2O into a vibrationally excited N_2 stream, formed via the rapid adiabatic expansion of thermally excited (1000-3000°K) N_2 through a supersonic nozzle. Population inversion and laser emission have been achieved on the 001 100 transition in CO_2, brought about by near-resonant vibrational energy transfer during collisions with excited N_2. Results are presented showing the influence of flow properties downstream of the expansion nozzle on optical gain and laser power characteristics. An analysis of nonequilibrium flow/optical field interactions is presented. Effects of penetration and mixing are represented as instantaneous changes in free-stream composition, specific enthalpy and Mach number. Subsequent vibrational and radiative energy transfer processes are coupled with fluid flow conservation equations. Qualitative agreement between the thermal mixing laser analysis and the experimental results has been found.

INVESTIGATIONS ON A PLASMA-FOCUS APPARATUS

N. W. Jalufka and J. H. Lee*
NASA, Langley Research Center
Hampton, Va.

Investigations are under way to learn more about the plasma in a plasma-focus apparatus. This is a relatively newly-discovered method of producing extremely hot and very dense plasmas, of the order of 50 million degrees Kelvin, 10^{19} particles per cubic centimeter, and a million atmospheres pressure. The method is of much interest in the scientific community and of considerable potential in several fields of both research and practical application.

Some of the results obtained to date are as follows:

1. Neutron time-of-flight measurements have been successfully used to obtain the neutron energy distribution - with, however, lower resolution than is desired but much better than that obtained by others. The statistics is currently being improved by using large (15") scintillators.

2. Some of the distributions had a rounded peak (like a Gaussian), indicating thermalization, but some had a sharp-pointed peak, indicating a beam model, or pure radial collapse.

3. The width of the neutron spectrum was measured and compared with predictions of theoretical models of the plasma focus. It was found that the half width of neutron spectra is much greater than expected from thermalized ions at temperature of 5 keV. Therefore either the ions are not thermalized or $T \geq 10$ keV.

4. The electron temperature was also measured with soft x-rays (bremsstrahlung) by using differential absorbers made of aluminum and copper. The temperature was found to be in excess of 5 keV.

5. Other investigators had found soft x-rays, of order 10 keV. Some had found up to 300 keV. We were the first to report 500 keV and greater.

6. The x-rays are from a point source rather than a rod-shaped or moving lines, giving sharp pictures of x-rays penetrating more than 1 inch thick aluminum sheet, or equivalent.

7. We have pinhole-camera x-ray pictures that show the shape of the plasma near the central electrode.

The big unsolved problem at the time we started this experiment and still at the present time is whether or not the plasma is thermalized. We have recently exposed nuclear-emulsion stacks to measure the x-ray energies or spectrum in various directions. These have been sent to Vanderbilt and Brookhaven for analysis and will be used to derive the electron velocity distribution.

*Vanderbilt University

With nuclear emulsion, refined measurements are planned for (1) angular distribution of hard x-rays, (2) calibration of emulsions with radio isotopes and an electron accelerator, and (3) electron and proton spectra with a magnetic spectrometer.

A preliminary spectroscopic investigation in the region between 500 Å and 1400 Å has been carried out. A one meter, normal incidence, vacuum spectrograph was used to record the spectra photographically.

The (time integrated) spectra in the region above 1000 Å was dominated by copper line radiation (CuII, CuIII) while the spectra below 1000 Å was dominated by line radiation from ionized oxygen (OIII, OIV, OV, OVI).

Spectra were also recorded with a center electrode cap of aluminum and carbon. These spectra were predominated by line radiation from highly ionized stages of the electrode material. Some copper lines were still observed but were very weak indicating that some electrode material is carried by the current sheet. The use of the different electrode materials had no apparent effect on the production of hard x-rays.

An investigation of the radiation in the soft x-ray region is planned. Spectra of the radiation in this region will be obtained with a bent crystal spectrograph. Line radiation in this region is due to transitions in highly ionized atoms and it will be possible therefore to identify and classify these lines. An attempt will be made to determine the shape and peak of the bremsstrahlung continuum. The peak of this continuum radiation is a strong function of temperature (electron) and these measurements should give some indication of the temperature obtained in the plasma focus.

An investigation of the effects of different gases will be made and spectra of the highly ionized atoms of these gases will be recorded and classified. Also the effects of different electrode materials will be investigated further.

ATTENUATION OF X-RAYS FROM PLASMA FOCUS

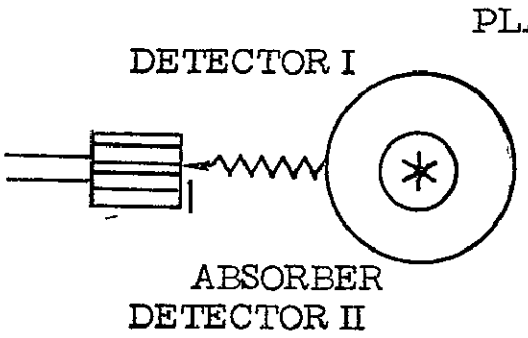

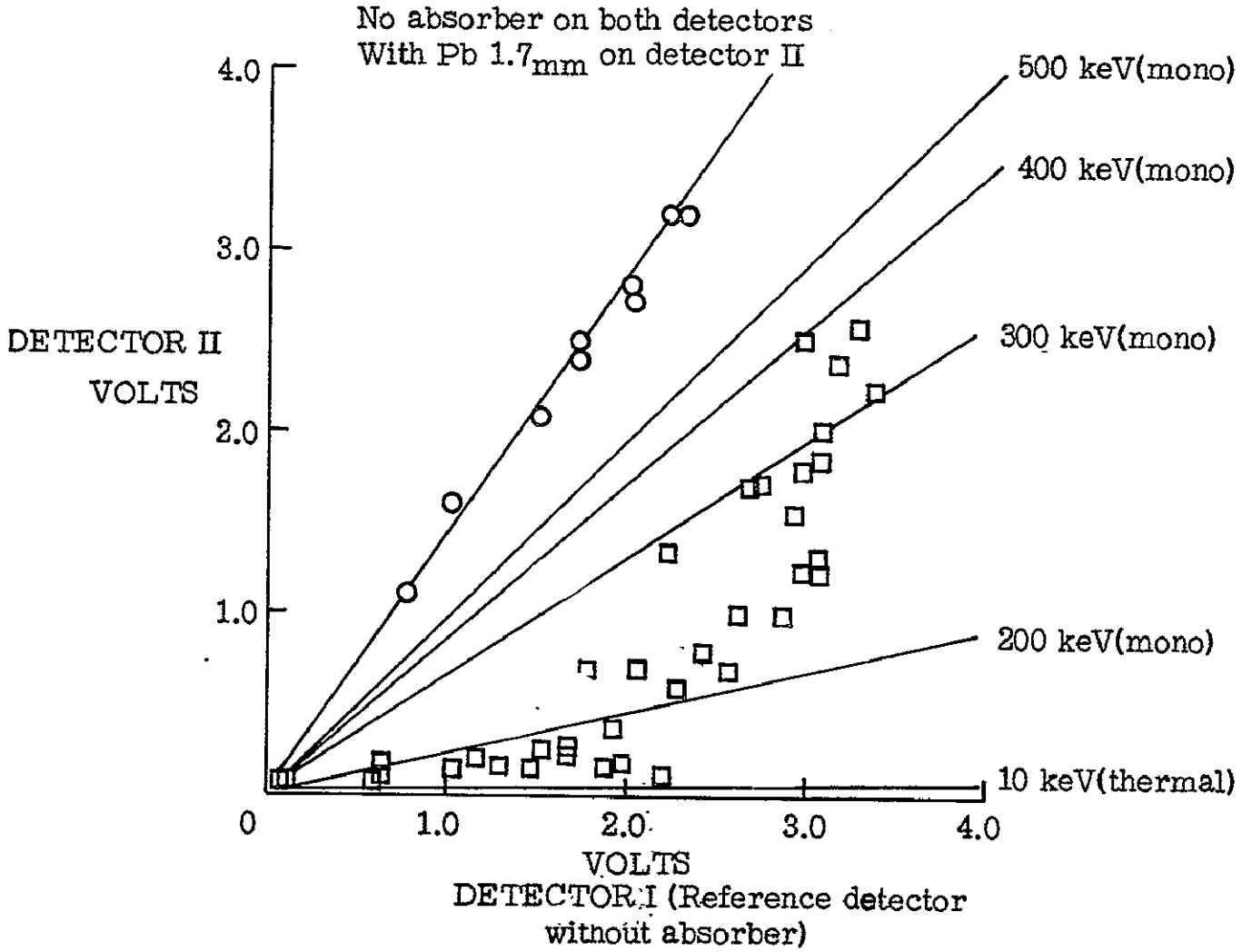

AN INVESTIGATION OF HARD X-RAYS FROM A PLASMA FOCUS

J. H. Lee, D. S. Loebbaka, and C. E. Roos
Vanderbilt University, Nashville, Tennessee

Presented at the Sixth NASA Intercenter and Contractor Conference
on Plasma Physics at Langley Research Center,
December 8, 9, and 10, 1969

INTRODUCTION

A dense plasma focus produced by fast collapse of current sheets at the end of a coaxial electrode is a copious source of neutrons (from d-d or d-t reaction) and x-rays. Despite extensive studies of this device by many workers, the mechanism of neutron and x-ray productions is not well understood. A few models have been proposed but none of which is universally accepted.. The boiler model is based on the assumption that ions and electrons are thermalized in the plasma focus at a kT of a few keV and anisotropy of the neutron yield and spectra are results of plasma CM motion. The beam-target model considers a high current of charged particles accelerated in an electric or magnetic field giving the production mechanism as well as the anisotropy. Accurate spectral distributions of neutrons and x-rays would distinguish between these models. With the plasma focus apparatus at the Langley Research Center a maximum photon energy of greater than 500 keV has been observed by means of differential absorber method.[1] However, the determination of the spectral distribution of x-rays was difficult since the absorption coefficients for most elements are near a minimum for the energy range in consideration. This investigation is an effort to obtain the spectrum of hard x-rays from the plasma focus using electron sensitive nuclear emulsions to clarify corresponding electron distribution in the plasma supplementing other diagnostics currently used to determine the nature of a plasma focus at the Center. This report covers the first phase of the work initiated in February, 1969.

EXPERIMENT

The plasma focus apparatus used in this experiment is described in a separate presentation of this conference. Hard x-rays are emitted simultaneously with neutrons at the maximum compression of the plasma. However, it is found that no correlation exists between the intensities of neutrons and x-rays, excluding the possibility of significant neutron induced gamma-ray emission. To determine the adequate dose of exposures a trial set of 13 emulsion (400 micron thick Ilford K-5) stacks were placed around the source at varying distances from 15 to 90 cm. and exposed to 100 runs of plasma focus formation. The second series of experiments were carried out to determine the spectral distribution of electron tracks produced in the emulsion by either photoelectric or Compton effect of x-rays from the plasma focus. For this run 600 micron thick Ilford emulsions obtained by a new order were used. The emulsions, stacked behind a 1.5 mm thick lead absorber, were placed at a distance of 90 cm from the source on the axis of the electrode. Discharges in helium were also used for comparison with the deuterium plasma. The electron ranges were measured under a Leitz scanning microscope equipped with an 18 micron field of view reticle grid.

RESULTS AND DISCUSSION

The histogram in Figure 1. is a result of electron range measurements in 3 plates with 3807 tracks (longer than 18 microns) observed over background. The ranges were converted to electron energies using the relation given by Barkas.[2] A few tracks extended more than 600 microns indicating electron energies of greater than 500 keV. In the figure the dotted curves represent the expected electron track distributions, arbitrarily normalized, for three different models of the source. The curves were obtained by taking account of the attenuation through the lead absorber and the efficiency of nuclear emulsion. A kT = 10 keV is chosen for the curve for Maxwellian electron distribution since it is maximum temperature one could reasonably assign for the plasma focus. It is clear that a Maxwellian distribution alone cannot account for the high energy spectrum observed. The curve for thick target bremsstrahlung is drawn for an electron beam with kinetic energy of 500 keV. This model, by itself, cannot fit the observed spectrum. The power law curve is derived from the electron distribution, $f(E) \propto E^{-\gamma}$ and the best fit value of $\gamma = 4 \pm 1$. (The spectrum of thick target bremsstrahlung corresponds roughly to $\gamma = 0.5$.) The present results are in agreement with the power law distribution reported for the energy range up to 40 keV by Meskan, et al. although the accelerating mechanism (turbulent heating) is yet questionable.[3] It is interesting to note that such distribution of electrons is proposed for astrophysical x-ray sources, such as SCO-X-1.[4] After determination of response function of emulsion to monoenergetic gamma-rays the experimental results will be analyzed in detail and comparison experiment with a theta pinch will be carried out. Beside the scanning of the electron tracks, the recoil protons produced by neutrons were also studied. The results show that the maximum neutron energy reaches 3 MeV, confirming the measurement made by the time-of-flight method, and anisotropy of neutron yields in axial and radial direction is 1.6 ± 0.4, which is higher than the expected value (1.25) for the boiler model.

CONCLUSIONS

There is a strong indication that the hard x-ray spectrum observed with nuclear emulsions are produced by a power law distribution of electrons in the plasma focus. The detailed study of this dependence should give decisive information on the proposed heating mechanisms in the plasma. The authors are grateful for the support and encouragement on this investigation by G. P. Wood (NASA), J. P. Barach (VU), and colleagues associated with the plasma focus apparatus at the Langley Research Center. We also wish to express our thanks to Mrs. T. Davis, Mr. S. Thatphithakkul and Mrs. U. Ahuja for their excellent scanning efforts.

---

1. J. H. Lee, H. Conrads, M. D. Williams, L. P. Shomo, H. Hermansdorfer, and K. H. Kim, Bull. APS II 13, 1543 (1968).
2. W. H. Barkas, Nuclear Research Emulsions, p. 443, Academic Press (1963).
3. D. A. Meskan, H. L. L. Van Paassen, and G. G. Comisar, Aerospace Report TR-0158 (3220-50)-1 (1967).
4. M. Oda, Proc. Conf. Cosmic Rays, Vol. 1, p. 68 (1965).

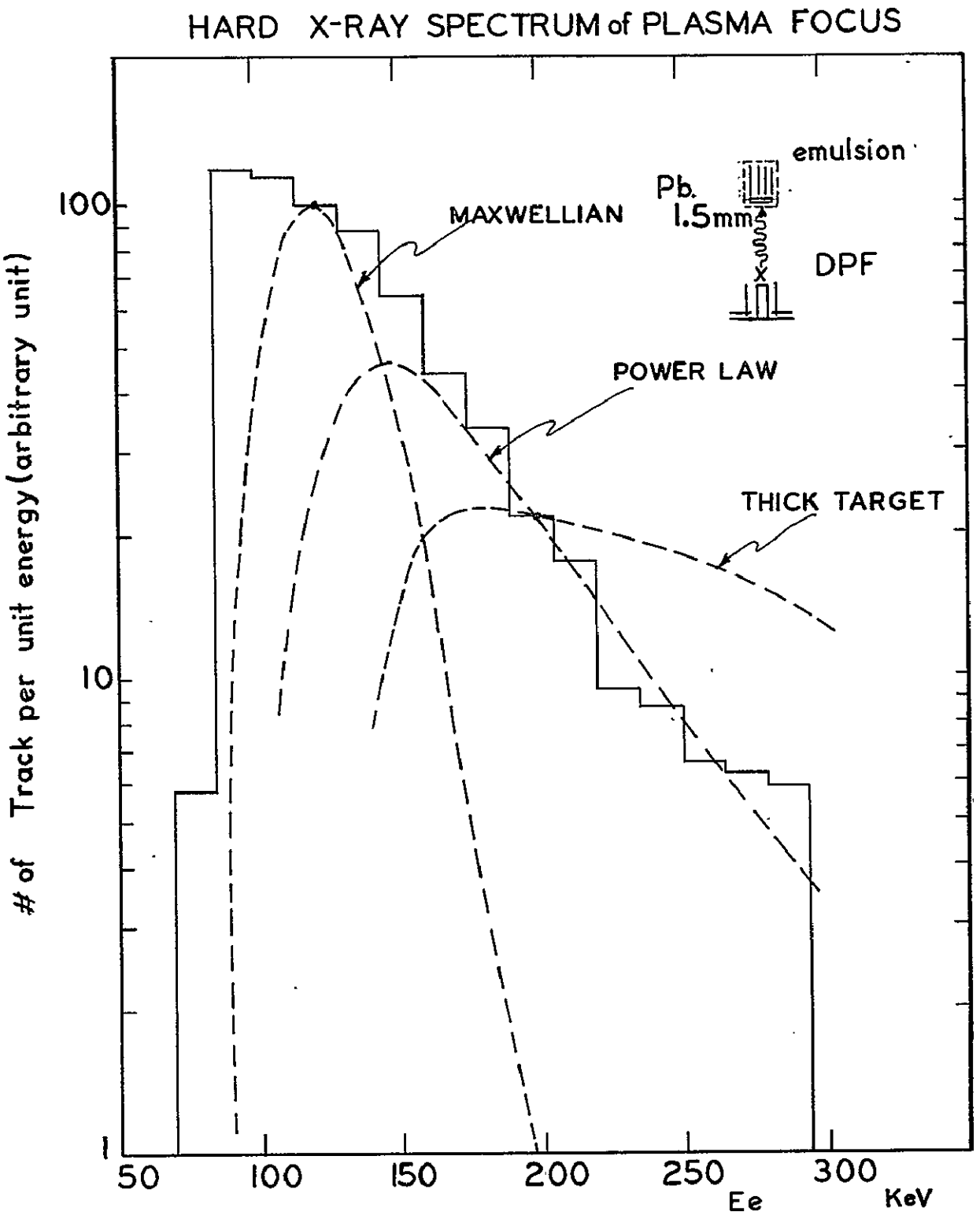
HARD X-RAY SPECTRUM of PLASMA FOCUS
emulsion
Pb.
1.5mm
DPF
MAXWELLIAN
POWER LAW
THICK TARGET
# of Track per unit energy (arbitrary unit)
100
10
1
50
100
150
200
250
300
Ee
KeV

Fig. 1

TIME-INTEGRATED NEUTRON FLUX MEASUREMENTS ON A PLASMA FOCUS BY GAMMA SPECTROMETRY

L. P. Shomo and K. H. Kim*
NASA, Langley Research Center
Hampton, Va.

The plasma focus is produced by the discharge of a 20 kilovolt - 25 kilojoule capacitor bank between the electrodes of a coaxial plasma gun filled with deuterium under pressures of a few Torr. The 1 mega-ampere discharge yields up to 10^{10} neutrons in a burst of approximately 100 nanoseconds half-width. The extremely short duration of the neutron production time prevents direct measurement of the neutron flux. Instead, the decay products of a silver target activated by the neutron burst from the plasma focus are counted. Figure 1 shows the experimental apparatus. A brief summary of the sequence of operation is: (1) A burst of 2.45 MeV neutrons is produced; (2) some of the neutrons enter the polyethylene moderator and are thermalized; (3) the silver becomes activated by the thermalized neutrons through the two processes Ag^{107} (n, γ) Ag^{108} and Ag^{109} (n, γ) Ag^{110}; (4) the activated silver decays by beta and gamma emission; (5) the gammas are detected by a three by three inch NaI (Tℓ) detector; (6) the multichannel pulse-height analyzer provides the energy resolved gamma intensity spectrum, and (7) the intensity of the 656 keV gamma peak of Ag^{110} with 24 second half-life is measured.

The use of a discrete gamma peak eliminates some of the corrections and uncertainties inherent in the beta counting method. The dead-time correction due to the 125 microsecond characteristic dead-time of a four-geiger-tube beta counting system can be neglected due to the 1 microsecond dead-time characteristic of NaI (Tℓ) detectors. The beta counting method nondiscriminately counts betas from decaying Ag^{110} and Ag^{108} having half-lives of 24 seconds and 2.3 minutes, respectively. This introduces errors due to the uncertainties of two neutron capture cross sections, and complicates the calibration procedure due to the two different half-lives. The greater penetrating power of the 656 keV gammas allows the use of a thick silver target thereby eliminating any disadvantage suffered by the gamma counting method due to the relative weakness of the 656 keV gamma peak. Thus the use of the 656 keV gamma peak of Ag^{110} provides a significant increase in accuracy over the normally used beta counting technique. Yields of 10^9 to 10^{10} neutrons per burst from the plasma focus device have been measured by this method with an estimated uncertainty of ± 16 percent, which includes the ± 5 percent error contributed by the calibration source.

This improved method is presently being applied to neutron flux anisotropy measurements on the plasma focus device. It is hoped that these improved measurements will shed some light on the validity of either the boiler or target models of the plasma focus mechanism.

*North Carolina College, Durham, N. C.

NEUTRON YIELD MEASUREMENT SYSTEM

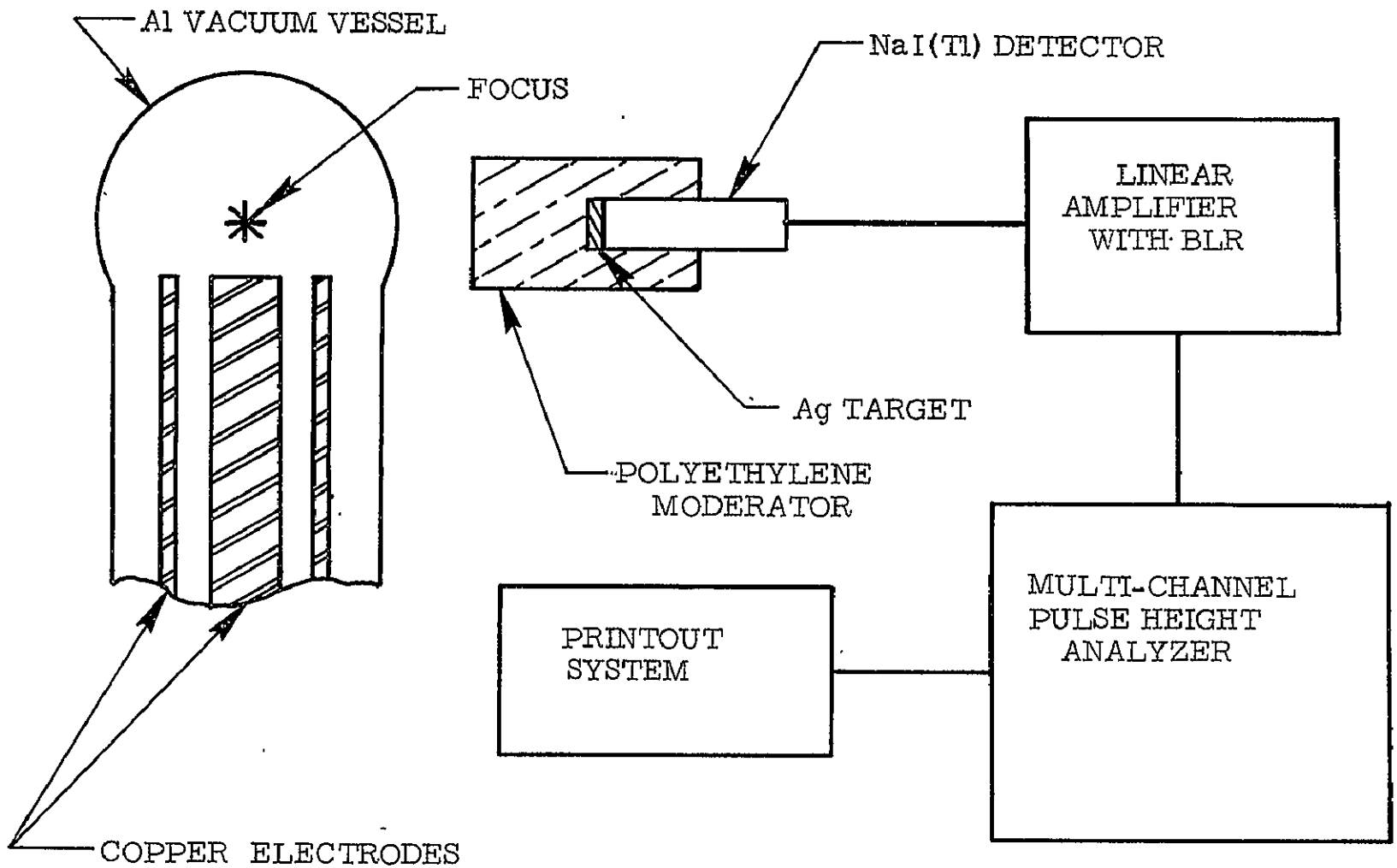

FIGURE 1.

COMPUTER SIMULATION OF PLASMAS

Velvin R. Watson

NASA Ames Research Center, Moffett Field, California

Recent advances in computers and cathode ray tube displays have made the computer an attractive tool for solving some problems in plasma dynamics. A recent investigation at Ames Research Center has shown that the computer is particularly useful for studying the dynamics of a collisionless plasma using a computer simulation technique. An application of this technique is described in this paper, and several problems that can be investigated using this technique are listed. The further application of the computer to provide insight into the dynamics of a collisional plasma is currently being investigated.

The computer simulation technique was used to study the plasma dynamics within a very high specific impulse accelerator. This simulation was accomplished by representing the many ions and electrons in the plasma by several thousand representative particles. These several thousand representative particles were assumed to constitute a good statistical sample of the actual ions and electrons in the plasmas. Starting with an initial distribution, the simultaneous motion of the representative particles was calculated as a function of time. First the electric and magnetic fields were calculated from the distribution of particles; next the motion of the individual particles during a small increment in time was calculated using these fields with the equations of motion; and then the change in the distribution of particles caused by the motion of the particles during the small increment of time was calculated. This procedure was repeated for each new time increment and the field and particle positions were recorded for each time increment to provide a time history of the self-consistent fields and particle motion.

The motions of the particles, the electric potential, and the magnetic field were displayed simultaneously on a cathode ray tube. These displays, which were recorded on motion picture film, illustrated the coupling between the particle motions and the fields. In particular, the displays illustrated how the plasma motion modified the applied electric potential, how the currents induced large magnetic fields, how the ions received their energy directly from the electric field, and how the ions were deflected toward the accelerator exhaust by the induced magnetic field.

This computer simulation technique should be useful for solving a number of problems involving collisionless plasmas, including the

following: (1) the flow of a collisionless plasma around bodies, (2) the flow of plasma within the "Mather Focus" at the end of the cathode of a coaxial plasma gun, (3) propagation of waves in collisionless plasmas--particularly in inhomogeneous plasmas.

An investigation of the techniques for applying the computer to solve problems in collisionless plasma dynamics indicated that one should not always proceed as far as possible with analytical mathematics prior to formulating the problem for the computer. The computer simulation technique described above employs the equation of motion for each of the several thousand particles. Instead of solving these several thousand equations one could have solved the Vlasov equation (which has been obtained from the particle equations of motion by further use of analytical mathematics) by a finite difference technique. Both techniques were used to solve for the voltage-current characteristics of a one-dimensional diode and the solutions were compared with experimental measurements of voltage and current. The computer simulation technique produced a much more accurate representation of the experimental measurements than the solution of the Vlasov equation by a finite-difference technique.

The results of the computer simulation are the visual displays of the plasma motion rather than a closed form mathematical expression for some continuous function, such as a distribution function. The changes in the dynamics due to changes in parameters are therefore observed visually rather than interpreted from an analytical expression for the distribution function. In a sense, the computer simulation is similar to a laboratory experiment where one changes the parameters and observes the results. Several major advantages of the "computer experiment" over the laboratory experiments are (1) measurements of the plasma properties can be made without perturbing the plasma with probes, (2) a microscopic as well as a macroscopic picture of the plasma is obtained, and (3) the plasma temperatures are not limited by availability of power supplies or by the technology of cooling at the plasma boundaries.

The author believes there is a great potential for the "computer experiment" as a tool for solving problems in plasma dynamics and recommends that the computer facilities for performing these "computer experiments" be expanded to be commensurate with this potential.

REPORTS

1. Watson, Velvin R.: "A Collisionless Model for High Specific Impulse Accelerators," AIAA 7th Electric Propulsion Conference, Williamsburg, Virginia, March 3-5, 1969.
2. Watson, Velvin R.: "Computer Simulation of a Plasma Accelerator," Stanford University Institute for Plasma Research Report No. 313, May 1969.

PULSED COAXIAL PLASMA GUN

William C. A. Carlson

NASA Ames Research Center, Moffett Field, California

Experiments have been conducted on a pulsed coaxial plasma gun powered with electrical energy from a 20 KV capacitor bank. Experiments to date have been conducted with between 3 and 20 KJ of electrical energy. The discharge is initiated by introducing gas into the evacuated, electrically energized gun. This mode of operation results in a distributed region of current flow which remains relatively fixed in space, rather than in a localized traveling current sheet which is typical for most similar guns. This later mode of operation has been described as a "snow plow model."

Several techniques have been used to determine the plasma velocity. These include streak photography, doppler shifting of radiation from the H_α line, and impact pressure on a target. These experiments indicate that the velocity produced by the gun operating in the distributed or deflagration mode is approximately an order of magnitude greater than that obtained when operation is in the traveling current sheet or detonation mode.

NEW SPECTRAL LINES OF HIGHLY-IONIZED NEON FROM THE LANGLEY THETA PINCH

Hans Hermansdorfer, Langley Research Center

To help meet the "widespread and urgent demand for basic spectroscopic data (wavelengths, energy levels, transition probabilities, ionization potentials, and electronic binding energies) from a wide variety of fields of science and technology -- plasma physics, solid-state physics, astrophysics, thermodynamics, spectrochemistry, laser research," the theta-pinch facility has been engaged in a program to produce and interpret new spectroscopic data. The method and the results to date, including identification of a score of new neon lines, are described.

In addition, the theta-pinch personnel have achieved the following, which are listed here but are not discussed in the paper:

Put the new grazing-incidence UV spectrometer ($10 \leq \lambda \leq 1000$ Å) into proper operation

Experimented with the ratio of working gas to carrier gas, e.g., NE: D_2, and with various fractions of the capacitor bank, to produce the correct temperature of the plasma and sufficient intensity of the spectral lines

Received and further developed shutter from Dr. Schneider for controlling duration of exposure

Attempted to produce O_KIII Line @ 23.3 Å - "satellite" line due to inner-shell transition

Diagnosed and eliminated cause of prefires and capacitor failures

Published "laboratory observation of a visible emission line of highly ionized argon at 4412 Å" in Astrophysical Journal

Published "Tables for the Calculation of Radial Multipole Matrix Elements by the Coulomb Approximation" in Astrophysical Journal

Began effort to produce new spectra in isoelectronic sequence of B I to Ar XIV

Collaborated on development of zone-plate camera with NRL for EUV photography of the Sun

Designed and obtained apparatus for Thompson-scattering measurement of T_e

Designed and procured sliding-spark light source (currently used for U spectra at University of Florida).

A METHOD FOR THE CALCULATION OF LARGE NUMBERS OF DIPOLE AND QUADRUPOLE TRANSITION PROBABILITIES

L. P. Shomo and G. K. Oertel*
NASA, Langley Research Center
Hampton, Va.

The present status of our knowledge of transition probabilities or of f-values is poor compared to that of the wavelengths of atomic spectral lines. F-values are known only for a small number of the lines for which wavelengths are known, and the accuracy of the available values is usually poor. Although f-values as well as wavelengths are atomic constants obtainable in terms of integrals over wave functions, only the former involve the overlap between two different atomic states, so that cancellations often lead to radial matrix elements which are small compared to the uncertainties of the individual atomic wave functions.

The calculation of f-values requires a knowledge of the wave functions of the two states involved in the transition. It is necessary to employ approximations to determine the wave functions for nonhydrogenic atoms or ions since Schrödinger's equation can be solved analytically only in the simple one-electron atom case. Several techniques that provide approximate wave functions have been developed. The most sophisticated of these techniques is the self-consistent-field method. The Coulomb approximation method is applicable to many lines of interest, and for those transitions where its assumptions are met, it gives f-values which are in close agreement with the self-consistent-field results. Even for relatively simple systems where the time required for self-consistent-field calculations is still relatively short, the Coulomb approximation method will result in a reduction of computing time by about three orders of magnitude.

The Coulomb approximation formalism was generalized to the multipole case[1] to meet the need for knowledge of forbidden electric-multipole transition probabilities in astrophysics, and because large numbers of matrix elements, both dipole and quadrupole, are required for computations of the Stark broadening of isolated ion lines.[2] Tables for computing Coulomb approximation radial matrix elements were calculated[1] for dipole transitions s-p, p-d, d-f, f-g, g-h, and h-i, and for quadrupole transitions p-p, d-d, f-f, g-g, h-h, i-i, s-d, p-f, d-g, f-h, g-i, and h-j. A FORTRAN IV computer program was developed[3] which takes the energy levels of a given element and stage of ionization and applies the appropriate selection rules and calculates dipole and quadrupole line strengths, transition probabilities, wavelengths, and

*NASA Headquarters, Washington, D. C.

dipole f-values for all allowed transitions. The input is restricted to levels with no equivalent electrons and LS-coupling. Absorption oscillator strengths for Helium I calculated by this computer program are compared with f-values calculated by other methods in Figure 1.

References

1. Oertel, G. K.; and Shomo, L. P.: Tables for the Calculation of Radial Multipole Matrix Elements by the Coulomb Approximation. Astrophys. J. Suppl., vol. XVI, no. 145, 1968.

2. Cooper, J.; and Oertel, G. K.: Electron-Impact Broadening of Isolated Lines of Neutral Atoms in a Plasma. Phys. Rev., vol. 180, no. 1, 1969.

3. Shomo, L. P.; Oertel, G. K.; and Freer, C. S.: A Method for the Calculation of Large Numbers of Dipole and Quadrupole Transition Probabilities. Proposed NASA TN, 1969.

TABLE I. - ABSORPTION OSCILLATOR STRENGTHS FOR NEUTRAL HELIUM

Transition	Self-consistent field	Scaled Thomas - Fermi	Coulomb approximation +	Coulomb approximation ++	Variational calculations Goldberg	Variational calculations Hylleraas	Sum rule modified	Effective charge	Wiese et. al. "best values"	
$1^1S - 2^1P$	0.2719		0.2531			0.3555			0.2762	SP
3^1P	0.07203		0.06825			0.0722			0.0734	SP
4^1P	0.02738		0.02795			0.0282			0.0302	W
5^1P			0.01414						0.0153	LS
6^1P	0.00793		0.008134			0.0082			0.00848	LS
$2^1S - 2^1P$	0.3578	[0.342	0.3723	0.3719	0.389	0.392	0.370	0.3861	0.3764	SP
3^1P	0.1646	0.242	0.1492	0.1431	0.157	0.150	0.156	0.2948	0.1514	SP
4^1P	0.0508	0.0684	0.04865	0.04970	0.0570	0.062	0.0503	0.08728	0.0507	W
5^1P		0.0296	0.02218	0.01936	0.0252	0.025	0.0221*	0.03818	0.0221	
6^1P	0.01257*	0.0157]	0.01209		0.0136	0.012	0.0124		0.01257	
$2^1P - 3^1S$	0.04640	[0.0278	0.04806	0.04859		0.04797		0.02304	0.0480	W
4^1S	0.00824*	0.00549	0.008579	0.008308		0.00686		0.004150	0.00824	
5^1S		0.00211	0.003213	0.003041				0.001519	0.00308	CA
6^1S	0.00151*	0.00105]	0.001593	0.001491				0.0007502	0.00151	
$2^1P - 3^1D$	0.7253	[0.575	0.7104	0.7006	0.755	0.7357		0.6947	0.711	W
4^1D	0.1205*	0.114	0.1207	0.1168	0.118	0.132		0.1199	0.1205	
5^1D	0.04308*	0.0436	0.04346	0.04106	0.0416	0.04313		0.04355	0.04308	
6^1D		0.0218]	0.02105	0.02054	0.0199			0.02115	0.0213	CA
$2^3S - 2^3P$	0.60021	0.538	0.5457	0.5319	0.542	0.559	0.535	0.6686	0.53908	SP
3^3P	0.05705	0.0638	0.05982	0.06478	0.0826	0.052	0.0768	0.1876	0.06446	SP
4^3P	0.02083	0.0256	0.02370	0.02581	0.0270	0.031	0.0232	0.06502	0.0231	W
5^3P		0.0124	0.01143	0.01022	0.0123	0.013	0.0114*	0.02999	0.0114	
6^3P		0.00694	0.006372		0.00665	0.007	0.0061*		0.0061	
$2^3P - 3^3S$	0.07639	0.0692	0.06813	0.07204		0.07662		0.02700	0.693	W
4^3S	0.01159*	0.0105	0.01014	0.008939		0.00520		0.004288	0.01159	
5^3S		0.00376	0.003581	0.003159				0.001488	0.00365	CA
6^3S		0.00182	0.001720	0.001527				0.0007089	0.00176	CA
$2^3P - 3^3D$	0.6234	0.611	0.6168	0.6089	0.553	0.6530		0.6969	0.609	W
4^3D	0.1229*	0.123	0.1244	0.1192	0.129	0.0792		0.1325	0.1229	
5^3D	0.04668*	0.0472	0.04759	0.04550	0.0512	0.04951		0.04958	0.04668	
6^3D		0.0236	0.02374		0.0260			0.02446	0.0215	CA

\+ Calculated by computer program in appendix A
++ Calculated by linear interpolation in the original tables of Bates and Damgaard (ref. 6)
* Selected as "best value" by Wiese et. al. (ref. 9)
SP Results of variational calculations of Schiff and Perkeris (ref. 17)
W Results of variational calculations of Weiss, A. W. presented by Wiese et. al. (ref. 9)
LS Results of Low and Stewart quoted by Dalgarno and Stewart (ref. 19)
CA Coulomb approximation results presented by Wiese et. al. (ref. 9)
[ ] Results enclosed may be considered less accurate than the Coulomb approximation results (see appendix E)
—— Coefficient of fractional parentage used

HARTREE-FOCK CALCULATIONS OF ENERGY LEVELS AND TRANSITION PROBABILITIES OF ARGON I AND OF HIGHLY-IONIZED ATOMS IN THE BORON I ISOELECTRONIC SEQUENCE

Louis J. Shamey*
NASA, Langley Research Center
Hampton. Va.

Numerical Hartree-Fock calculations are being performed to obtain accurate nonrelativistic atomic wavefunctions. As an initial approximation, the Hartree-Fock-Slater (HFS) self-consistent calculations are performed, using the well-known programs of Herman and Skillman. This procedure does not distinguish between different terms within a configuration, thus resulting in only one set of energies and orbitals for a given configuration. These orbital energies, screening constants, and wavefunction slopes are invaluable as input estimates for the more accurate (and sensitive) Hartree-Fock (HF) calculations, using the well-known programs of Charlotte Froese-Fischer. Because this Hartree-Fock calculation does distinguish between the different LS terms within a configuration, each term will be associated with its own set of orbital wave functions and energies; for this reason, the so-called average energy is no longer the same constant for the different term energies and thus should not be subtracted from the diagonal electrostatic matrix elements, as is commonly done.

These Hartree-Fock calculations are currently being applied to two theoretical spectroscopic problems, the work still being in progress. The HF results are used as the best available theoretical wavefunctions, from which all appropriate atomic parameters can be calculated. The first application is a calculation of forbidden transitions in Argon I $3p^5 4p - 3p^6$. Electric quadrupole transitions take place between $3p^6\ {}^1S_0$ and $3p^5 4p\ {}^1D_2$. Spin-orbit interactions couple the $3p^5 4p\ {}^3D_2$, ${}^1D_2$, and ${}^3P_2$ terms. Intermediate coupling calculations were performed to obtain the transition probabilities $A(J\text{-}J')$ of order 10^3, which are relatively strong for forbidden transitions. Calculations are still in progress for obtaining magnetic dipole transition probabilities within this same transition array.

The second application of these HF calculations is a systematic investigation of the spectrum, both energy levels and transition probabilities, of highly ionized atoms in the Boron I iso-electronic sequence, with particular emphasis on two atoms currently being studied in the laboratory: Ne VI, for which much is known observationally, and Argon XIV, for which little is known. Also of interest will be the appropriate stages of ionization for Mg, Al, Si, S, Ca, and Fe. The effects of configuration interaction and spin-orbit interaction are to be included in these calculations. This work is still in its early stages; preliminary results are encouraging.

*NRC-NASA Resident Research Associate

LASER ENERGY ABSORPTION IN NON-UNIFORM PLASMAS

Loren C. Steinhauer and Harlow G. Ahlstrom

University of Washington - Department of Aeronautics and Astronautics

The advent of high power pulsed lasers, now makes it possible to heat a dense plasma to extremely high temperatures. Short, powerful laser pulses may heat the plasma to very high temperatures before dispersive mechanisms act to cool the plasma. One of the first questions that must be answered is how does the plasma react during the actual heating process, i.e. during the laser pulse.

Under certain conditions of interest, some effects can be neglected: thermal conductivity, electron-ion equilibration, and plasma motion. This case for a general, non-uniform overdense plasma has been solved using the method of matched asymptotic expansions to obtain an analytic solution.

Solutions have been calculated for all ranges of the absorptivity. These solutions show that the heating is either "simultaneous" when the absorptivity is small or due to a "heating wave" when the absorptivity is large. In the "simultaneous" case, the entire underdense region is heated simultaneously. A hot spot is produced near the critical density where the laser frequency equals the plasma frequency, and much of the laser radiation is reflected and lost. In the "heating wave" case, a heating wave propagates into the underdense region but never reaches the critical density. No hot spot is produced, and none of the laser energy is lost to reflection.

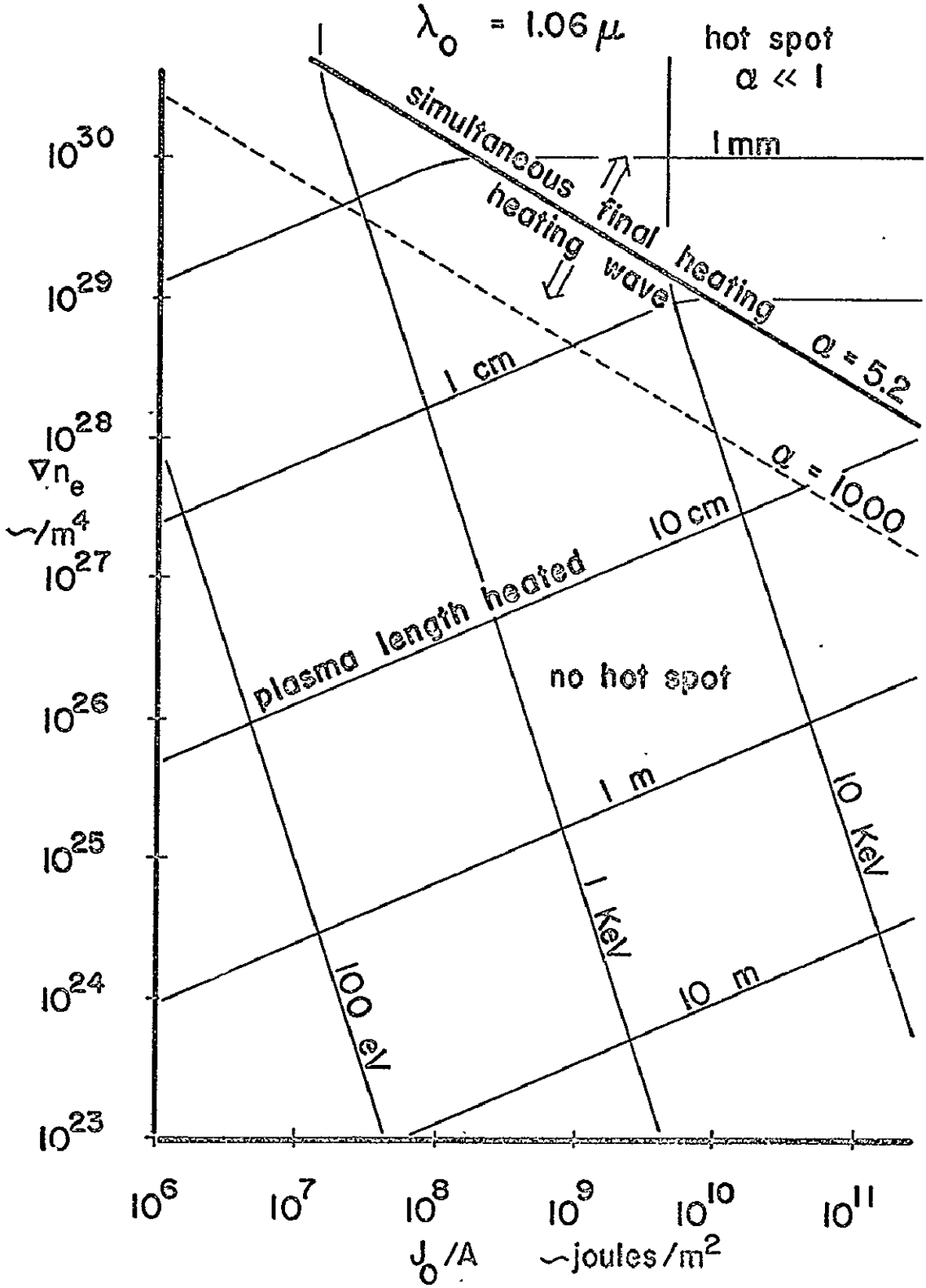

SUMMARY OF PLASMA CONDITIONS WHICH CAN BE ACHIEVED FOR A LINEAR DENSITY GRADIENT WITH A Nd^+ GLASS LASER

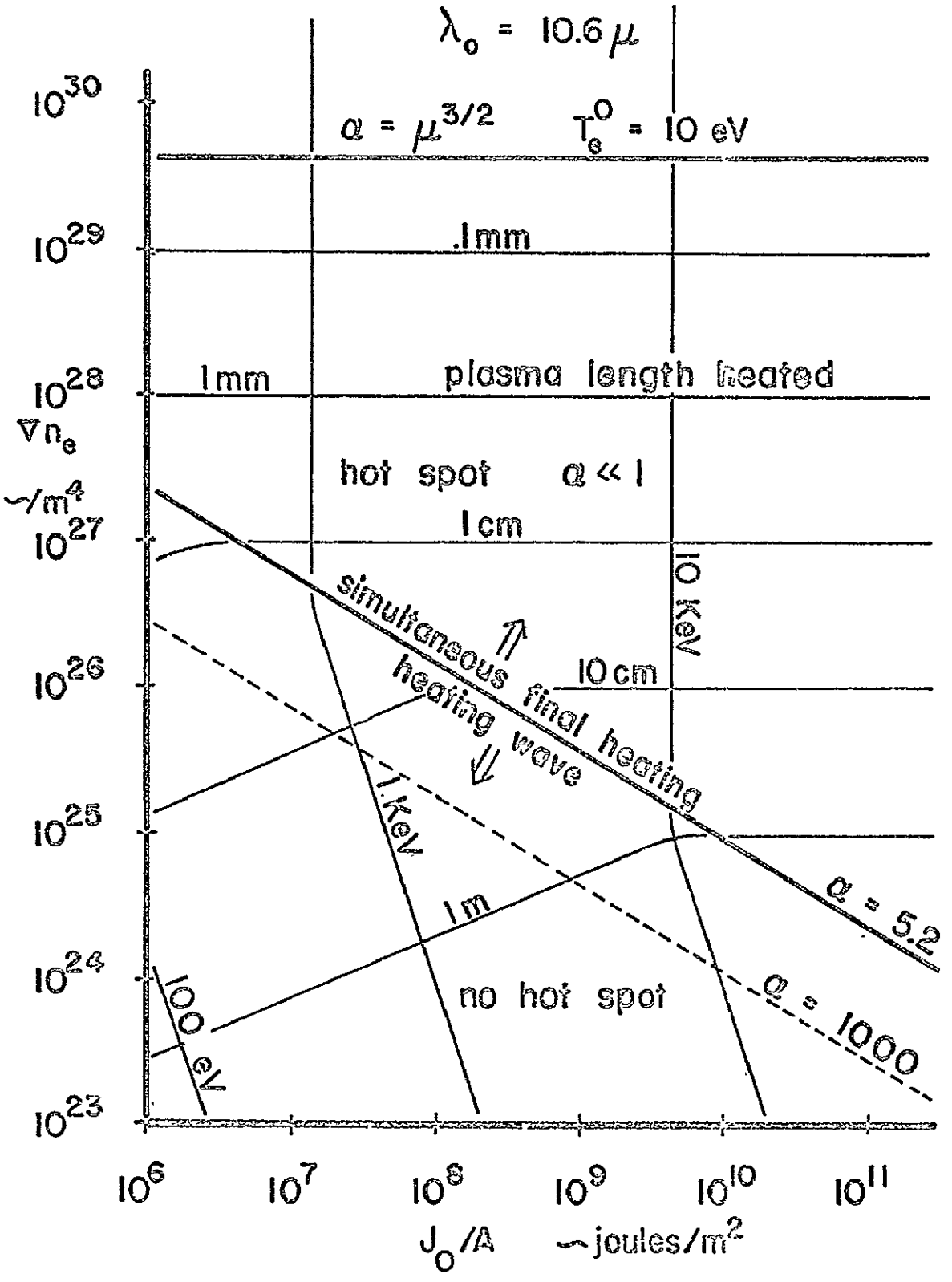

SUMMARY OF PLASMA CONDITIONS WHICH CAN BE ACHIEVED FOR A LINEAR DENSITY GRADIENT WITH A CO_2 GAS LASER

METHODS FOR ESTIMATING DYNAMIC MOVEMENT AND STRESS OF METAL PLATES WHICH CONDUCT CURRENT FROM AN UNDERDAMPED CAPACITOR BANK DISCHARGE

M. D. Williams and J. A. Moore
NASA. Langley Research Center
Hampton, Va.

Collector plates (metal plates with clamping through bolts) are used with many high current low inductance experiments. They are subjected to large pulse forces which must be structurally supported. The estimation of the movement and stress caused by these forces is a problem which occurs continually in the design of plasma devices. One solution to the problem has been to design the collector plates to support the peak undamped force under static conditions (the maximum conceivable load, neglecting resonances). The analysis and results presented here are for dynamic conditions.

The analysis treats two theoretical models: (1) the mass-spring oscillator, and (2) the traveling wave model.

The mass-spring oscillator model is valid for force pulse wavelengths much larger than the collector plate dimensions in the direction of the force. The mass of this model is driven by the force developed by a damped ringing capacitor bank discharge. Mechanical damping and damping due to collector plate movement are neglected. The equation of motion is solved and the peak movement, normalized with respect to static displacement, is plotted for various electrical to mechanical frequency ratios, n, and bank damping ratios, δ, (fig. 1). In practice, this model describes collector plate movements when driven by capacitor banks with frequencies not greater than several kHz.

For bank frequencies much larger than several kHz the force pulse wavelengths are much smaller than the usual collector plate dimensions in the direction of the force and the traveling wave model is applicable. The equation of motion for the traveling wave model is presented. The peak collector plate stress is localized in the first force pulse wavelength and is found to be a function of the bank damping ratio only. Peak stress normalized with respect to static stress is plotted as a function of damping ratio, δ, (fig. 2).

The results of this analysis exhibit several physically understandable phenomena and can be used to design and/or estimate the strength of collector plate systems.

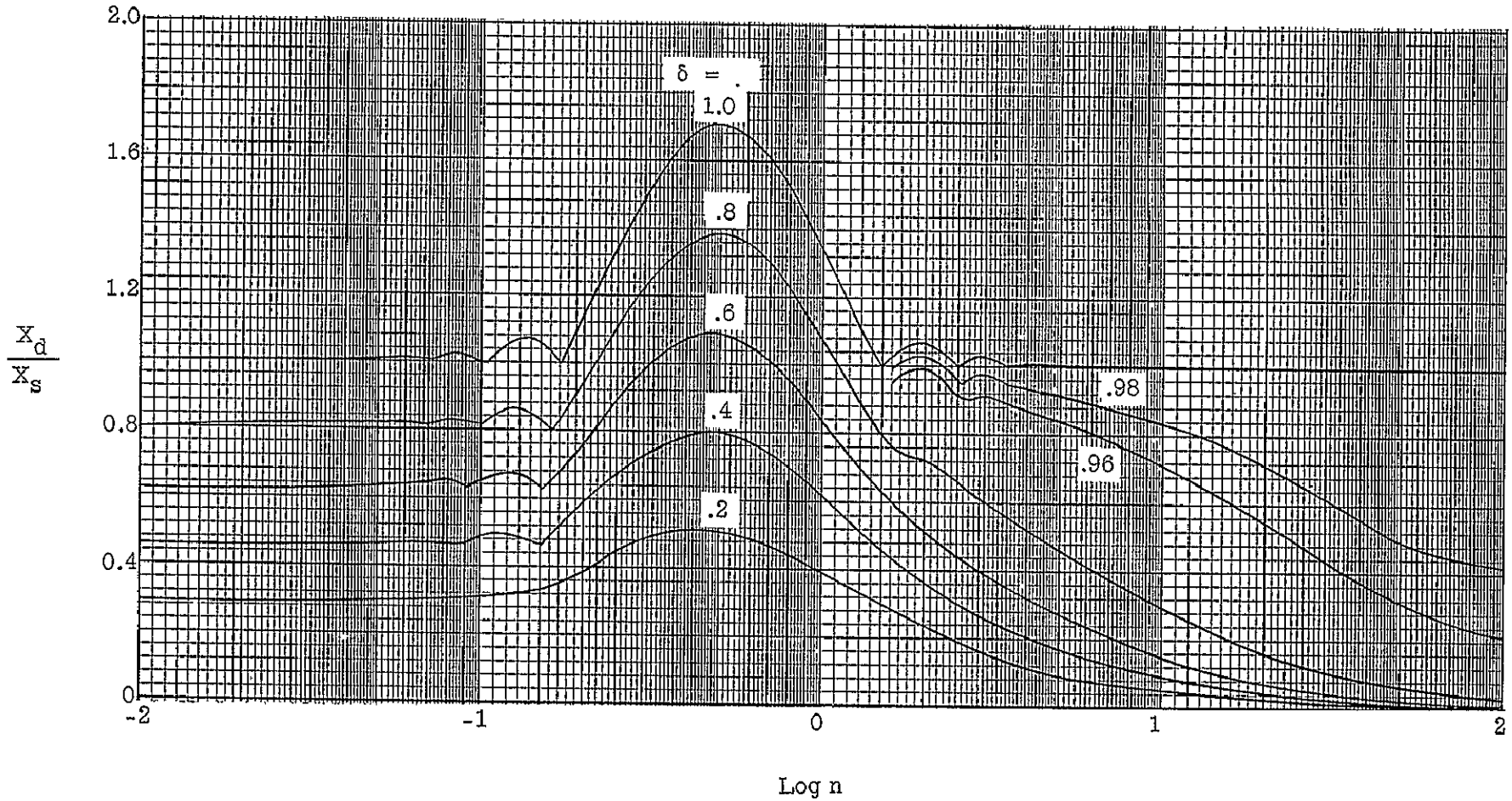

Figure 1. - Normalized maximum movement of mass-spring model

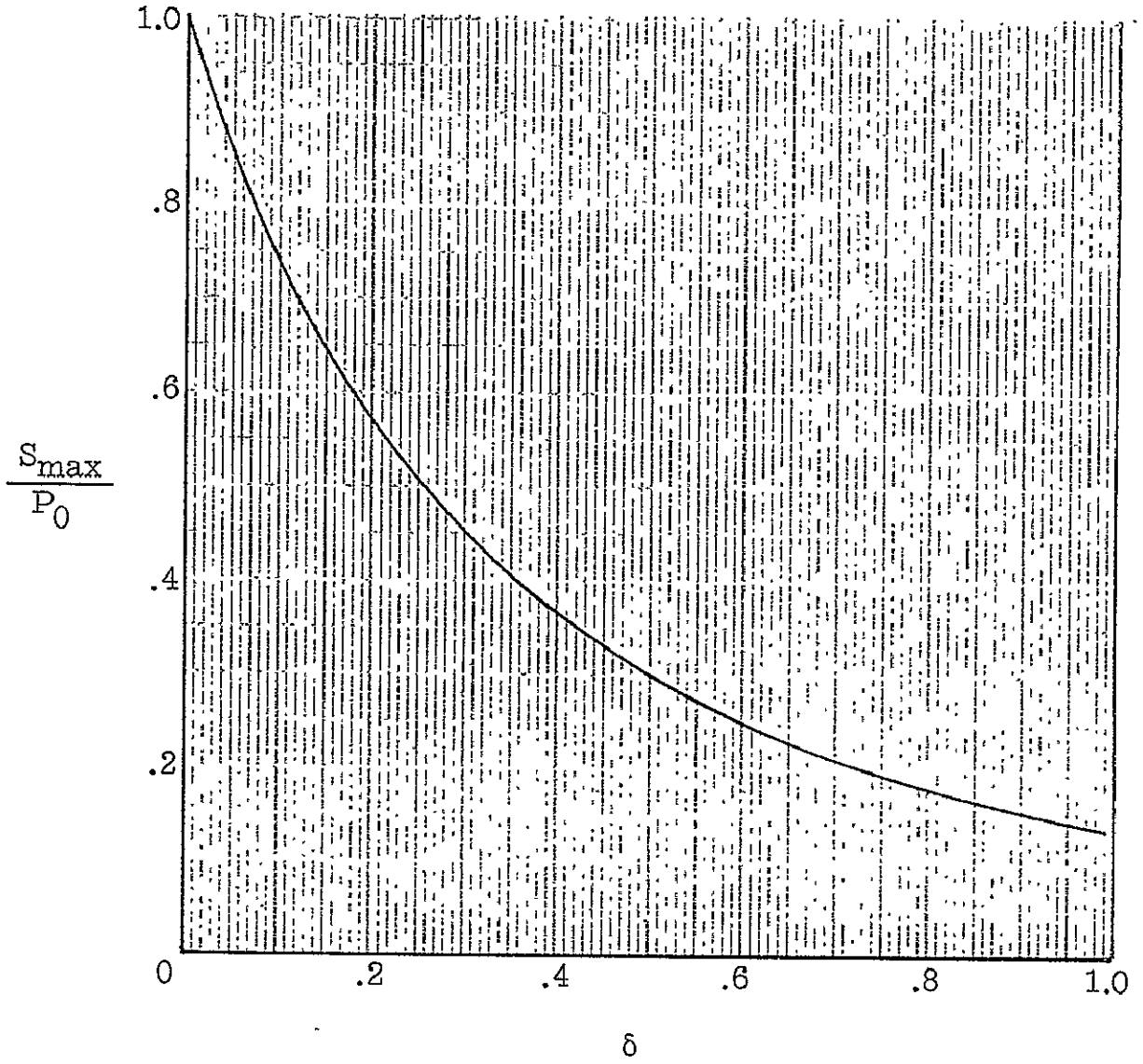

Figure 2. - Normalized maximum stress of wave model

ON THE MOTION OF VORTICITY IN MAGNETOHYDRODYNAMICS

Robert C. Costen
NASA, Langley Research Center
Hampton, Va.

A new equation has recently been derived for the motion of vorticity in a general MHD fluid, including the effects of viscosity, compressibility, nonhomogeneity, and nonconservative forces. The derivation of this equation was made possible by introducing a kinematic modification in the derivation of Kelvin's circulation theorem. In Kelvin's derivation, one obtains a formula for $\frac{d}{dt} \iint \vec{\omega} \cdot \hat{n} \, d\sigma$, which is the time rate of change of the flux of vorticity $\vec{\omega}$ through a surface σ of finite area, where σ is taken to move with the fluid. If the fluid is inviscid, subject to conservative forces only, and if the density ρ is a constant or is a single valued function of the pressure p, one finds that $\frac{d}{dt} \iint \vec{\omega} \cdot \hat{n} \, d\sigma = 0$ and concludes that under these conditions vorticity moves with the fluid. In our modified derivation, one also finds an expression for $\frac{d}{dt} \iint \vec{\omega} \cdot \hat{n} \, d\sigma$, but in this case the surface of integration σ is taken to move - not with the fluid velocity $\vec{v}$ - but with an arbitrary abstract velocity field $\vec{U}(x,y,z,t)$. The abstract velocity field $\vec{U}$ is then chosen so that $\frac{d}{dt} \iint \vec{\omega} \cdot \hat{n} \, d\sigma \equiv 0$ without imposing any restrictions on the fluid medium or the force fields. The velocity field $\vec{U}$ so chosen may then be regarded as defining the motion of the vorticity $\vec{\omega}$, and $\vec{U}$ is found to satisfy the equation

$$(\vec{U} - \vec{v}) \times \vec{\omega} - \frac{1}{\rho} \operatorname{div} \overleftrightarrow{P} + \frac{q}{\rho} (\vec{v} - \vec{v}_s) - \frac{1}{\rho} (\rho_e \vec{E} + \vec{J} \times \vec{B}) = \nabla \phi$$

where ρ is the fluid density, $\overleftrightarrow{P}$ is the pressure tensor including viscous terms, q is the source density of distributed fluid sources, $\vec{v}_s$ is the velocity of the source fluid, $\rho_e \vec{E} + \vec{J} \times \vec{B}$ is the Lorentz force density, and $\phi(x,y,z,t)$ is an arbitrary scaler field. Note that $\vec{U}$ is not, in general, determined uniquely because of the arbitrary function ϕ. Physically, this means that for general distributions of vorticity there are arbitrarily many flux-preserving motions. But in cases where a vortex tube is isolated, the displacement velocity $\vec{U}$ of the tube should be uniquely determined. The fluid source density q is included in this equation since the axis of a vortex is frequently a convenient place for injecting or withdrawing fluid. The pressure tensor $\overleftrightarrow{P}$ has been retained in full form to illustrate that a displacement velocity $\vec{U}$ may be assigned to the vorticity even in the presence of viscous diffusion.

Little progress has been made to date in solving this nonlinear equation. But one may neglect viscosity and linearize the equation for the case of weak vorticity, weak fluid source density, and weak electromagnetic forces. This gives typically

$$\rho_o(\vec{U} - \vec{v}_o) \times \vec{\omega}_1 + q_1 (\vec{v}_o - \vec{v}_s) - \frac{\rho_1}{\rho_o} \nabla P_o - \vec{J}_1 \times \vec{B}_o = 0$$

where $\vec{\omega}_1$, q_1, ρ_1, and $\vec{J}_1$ are first-order perturbation fields. Here ρ_o = cont. and the other zero order fluid fields satisfy the equation $\frac{\partial \vec{v}_o}{\partial t} + \nabla \left(\frac{v_o^2}{2} + \Phi_o\right) = -\nabla\phi_o$ where Φ_o is the gravitational potential and ϕ_o is an arbitrary function. The terms of the vortex motion equation all have the dimensions of force per unit volume. The first term $\rho_o(\vec{U}-\vec{v}_o) \times \vec{\omega}_1$ is represents the Magnus force density on vortex filaments which do not move with the unperturbed flow velocity $\vec{v}_o$. The second term $q_1(\vec{v}^o - \vec{v}^s)$ represents the force density required to accelerate the source fluid from the source velocity $\vec{v}^s$ to the flow velocity $\vec{v}_o$. The third term $-\frac{\rho_1}{\rho_o} \nabla P_o$ a "bouyancy" force which acts upon density variations in the presence of the unperturbed pressure gradient. The equation states that the vorticity moves in such a manner that the Magnus force, source force, bouyant force, and electromagnetic force densities balance.

For application of this equation to an isolated vortex tube, it is convenient to integrate it over the cross-sectional area of the tube. This gives

$$\rho_o \langle \vec{U} - \vec{v}_o \rangle \times \vec{\Gamma}_1 + \langle \vec{v}_o - \vec{v}_s \rangle Q_1 - \frac{\langle \nabla P_o \rangle}{\rho_o} M_1 - \vec{I}_1 \times \langle \vec{B}_o \rangle = 0$$

where Γ_1 is the circulation of the vortex tube, Q_1 is the mass of source fluid being added to the vortex tube per unit length, M_1 is the excess mass present in the tube per unit length, and $\vec{I}_1$ is the total axial electric current in the tube. Brackets $\langle\rangle$ denote mean values over the cross section of the tube. The source term, the bouyancy term, and the electromagnetic term each make the motion of the vortex tube deviate in some manner from the zero order fluid velocity $\vec{v}_o$. The effect of the $\vec{I}_1 \times \langle \vec{B}_o \rangle$ term on vortex motion is well known, and our comments will be restricted to the other terms.

One application of the source term is to the effect of the fluid boundary layer at a wall on the motion of a vortex whose axis intersects the wall. If fluid is sucked up from the boundary layer into the vortex as it moves (which will occur if the vortex is sufficiently strong to have a low pressure core) the boundary layer constitutes a fluid source with velocity $\vec{v}_s = 0$. The effect, as seen from solving the equation for this case, is to cause the vortex to move to the right of the direction of the unperturbed flow $\vec{v}_o$.

The bouyancy term applies to vortices which have a low density core. All vortices in a compressible fluid which have flow velocities approaching the speed of sound are naturally bouyant. Weaker vortices as well as vortices in an incompressible fluid may be made bouyant by injecting a lower density fluid into the core. The less dense fluid remains in the core of the vortex provided the radial pressure gradient in the vortex exceeds the other pressure gradients in the flow. One effect of bouyancy on a vortex whose axis lies in a horizontal plane is to cause the vortex to move laterally in the plane under the action of the downward pressure gradient due to gravity. This should cause the trailing vortices from the wing of an airplane, if made bouyant, to approach each other. Another effect of bouyancy is to cause two parallel vortices in near proximity to exert an attractive force on each other. This attractive force arises because each low density core is in the radial pressure gradient field of the other vortex. This effect on vortices of like sense, which are revolving about each other, is to reduce their revolution rate. The effect on vortices of opposite sense and equal strength, which are drifting at constant separation, is to increase their drift velocity. The maximum changes in drift speed and revolution rate of vortex pairs due to bouyant attraction is on the order of 10%. Larger effects result from the downward pressure gradient caused by gravity.

LOW-ENERGY ION ATOM EXCITATION*

R. Novick
Columbia Astrophysics Laboratory
Columbia University
New York, New York 10027

ABSTRACT

Experimental and theoretical studies have been made of the excitation cross sections of various neutral excited states of He in low-energy He^+ - He collisions.[1] Two striking results of the experimental observations are the large value of the cross section at low energies with thresholds slightly above the final state energies, and the strong oscillatory dependence of the cross sections on projectile energy. These phenomena can be interpreted in terms of the molecular-potential energy curves of the He_2^+ system. To understand the low-energy excitation it is noted that, in the diabatic approximation, the gerade ground term is repulsive and pseudocrosses all of the excited state terms.[2] These pseudocrossings occur at a value of internuclear separation, R_I, of about 1 a.u. In the course of collisions with small enough impact parameters, the internuclear separation decreases and passes through R_I. As the system passes through the pseudocrossing, excitation occurs by the mechanism discussed by Landau, Zener, and Stuckelberg.[3] This accounts for the large cross section at low energies. Since the thresholds occur slightly above the final state energies, they provide a direct measure of the energy location of the pseudocrossing.[4] Previously it was proposed that the oscillations were produced by an interference effect which arose from the double passage of the system through the crossing at R_I. However, it has now been shown[5] that any phase difference thus developed is strongly dependent on the impact parameter b; consequently, the integration over impact parameters required to obtain total cross sections averages out this interference effect. Such a phase difference might contribute to the oscillations reported in differential inelastic cross sections[6] but cannot explain the structure observed in the total cross-section data.

In a recent paper, Rosenthal and Foley show that in addition to the crossing between the ground state and excited state curves at R_I, other crossings between two or more excited states exist at relatively large values of internuclear separation, $R_o \approx 20$a.u. In this model the excitation mechanism is essentially identical with that previously considered and hence the large cross sections at low energies, and the threshold energies, are explained as before. However, the oscillations are now considered to arise when two excited states populated at R_I develop a phase difference between R_I and R_o before mixing again at R_o. Since the resulting phase difference is weakly "b"-dependent, it manifests itself in the form of oscillatory structure in the total cross section. Rosenthal and Foley show that their model correctly predicts the oscillatory structure in the excitation functions of the 3^3S and 3^1S states, and, moreover, they predict that these oscillations should be in antiphase as is in fact observed.[1]

---

*This work was supported by the National Aeronautics and Space Administration under Grant NGR 33-008-009.

New experimental studies have been made of the 2P excitation functions and of the velocity dependence of the cross sections. The latter studies were accomplished by using He^3 and He^4 in various combinations. These new data provide strong additional support for the theory of Rosenthal and Foley.

The results presented here have stimulated considerable efforts to understand the detailed interactions occurring in low-energy ion-atom collisions. The theory recently developed by Rosenthal and Foley has been remarkably successful in leading to an understanding of those results. Some unanswered questions remain, however, and further theoretical efforts will be needed to answer them. It is clear that the full elucidation of the detailed structure of the excitation functions will provide a powerful test of our understanding of the dynamics of the unbound molecular state formed during these inelastic conditions.

1. S. Dworetsky, R. Novick, N. Tolk, and W. W. Smith, Phys. Rev. Letters 18, 939 (1967).
2. W. Lichten, Phys. Rev. 131, 229 (1963).
3. L. Landau, Physik. Z. Sowjet. 2, 46 (1932); C. Zener, Proc. Roy. Soc. (London) A137, 696 (1932); E. C. G. Stuckelberg, Helv. Phys. Acts 5, 370 (1932).
4. S. H. Dworetsky and R. Novick, "Experimental Tests of the Post-Collision-Interaction Model for the He^+ - He Excitation Functions," to be published.
5. H. Rosenthal and H. M. Foley, "Phase Interference Effects in Inelastic He^+ - He Collisions," to be published.
6. D. C. Lorents, W. Aberth, and V. W. Hesterman, Phys. Rev. Letters 17, 849 (1967).

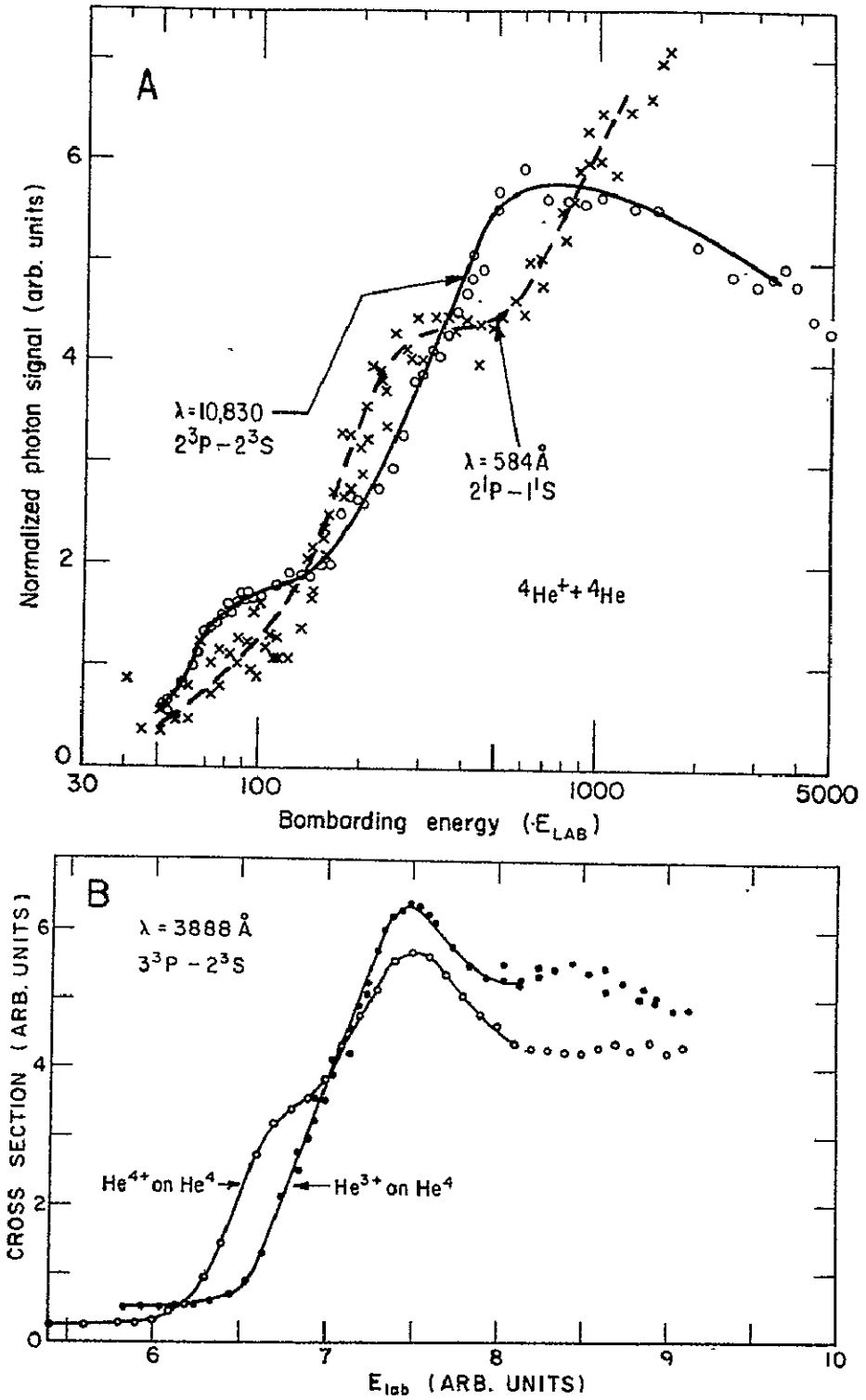

Fig. 1. (A) Cross sections for the excitation of the 2P states of He in He^+ - He collisions. (B) Detailed threshold behavior of the 3888-Å excitation function for $^4He^+$ - ^4He and $^3He^+$ - ^4He collisions.

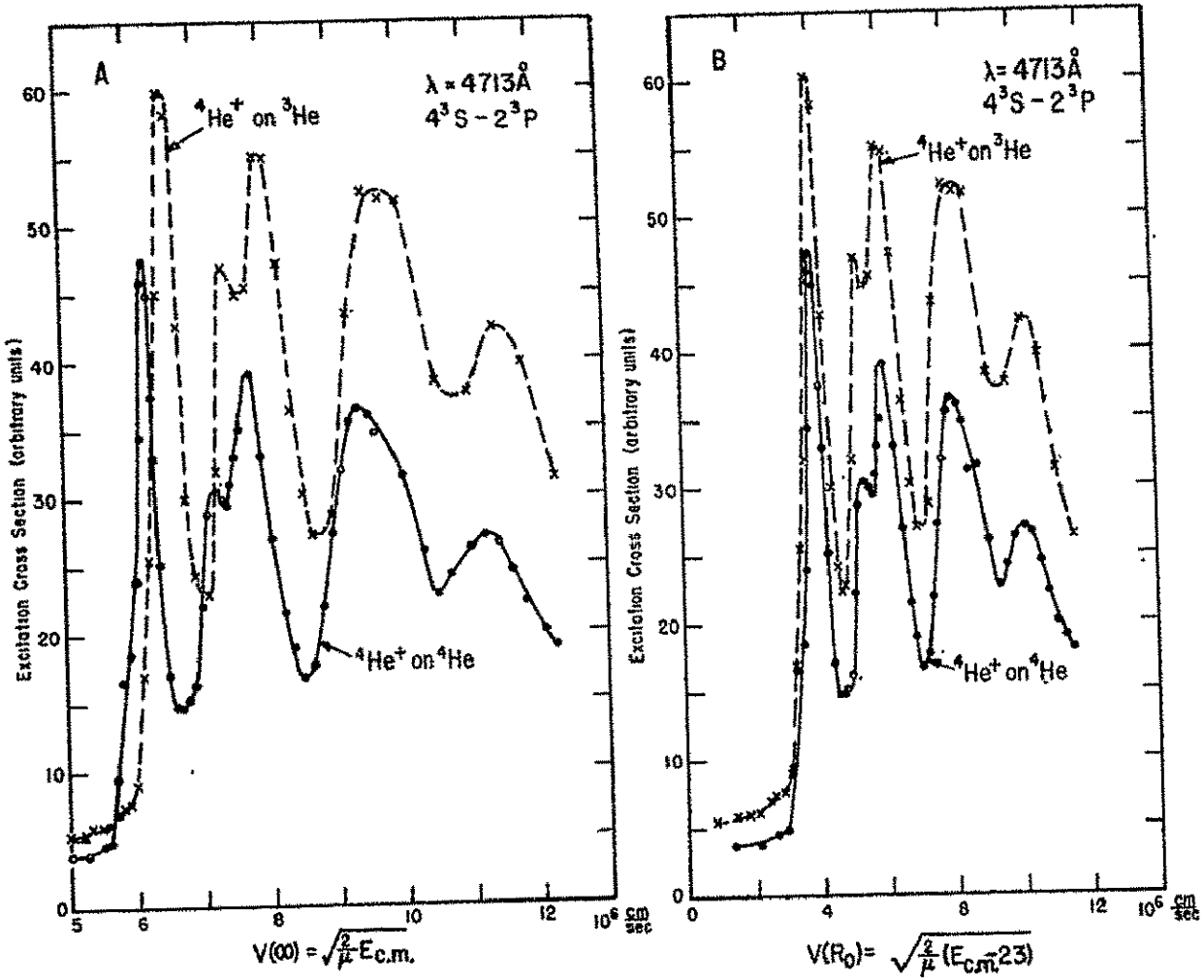

Fig. 2. (A) Excitation cross section for the 4713-Å He I line in $^4He^+ - ^4He$ and $^4He^+ - ^3He$ collisions plotted versus relative velocity at infinite internuclear separation, v(∞). (B) Excitation cross section for the 4713-Å He I line in $^4He^+ - ^4He$ and $^4He^+ - ^3He$ collisions plotted versus relative velocity in the final state.

PLASMA CHEMISTRY AND ION-MOLECULE INTERACTIONS

by John V. Dugan, Jr., NASA Lewis Research Center

Calculations of non-equilibrium number densities N_e have been extended to argon plasmas for electron temperatures from 8,000 to 15,000 K.[1] The N_e values are far below Saha at intermediate values of neutral density for optically thick plasmas. The results are non-hydrogenic for T_e = 8,000 K; however, N_e values are sensitive to the choice of model atom.

Studies of an expanding hypersonic air stream have begun. The conditions consist of temperatures from 5,000 to 50,000 K and pressure ratios P/P_o from 10^{-4} to 10 where P_o is atmospheric pressure. Preliminary calculations are for a nitrogen model with species N_2, N, N_2^+, N^+, N^{++} and e^-. The relaxation times for electron energy equilibration with heavy species are calculated from (elastic and inelastic) semi-classical collision coefficients.

Numerical calculations of ion-molecule collision trajectories have been extended to including vibrational degrees of freedom on lifetimes of ion-molecule collision complexes. The nature and formation of such complexes has been studied via computer plots and computer-made motion pictures.[2] The nature of hindered dipole motion has been studied also. This behavior has chemical implications.

REFERENCES

1 J. R. Rose and J. V. Dugan, Jr., (unpublished).
2 J. V. Dugan, Jr., R. B. Canright, Jr., R. W. Palmer and J. L. Magee, presented at VI International Conference on Electronic and Atomic Collisions, MIT Press, pp. 333-340.

TURBULENCE IN PLASMAS WITH COLLISIONS

G. Sandri

Aeronautical Research Associates of Princeton, Inc.
50 Washington Road, Princeton, New Jersey 08540

1. Plasma turbulence and gasdynamic turbulence are analogous but differ in many respects. The major interaction among plasma particles is the electrostatic Coulomb force which is analogous to the intermolecular force in a neutral gas but has an infinite range. As a consequence, plasmas behave, under some conditions, like neutral gases but are much more unstable.

2. It has been possible to develop a satisfactory theoretical description for dilute neutral gases which starts with the equations of motion of each of the particles in the presence of the forces exerted by all the others (Liouville equation) and leads through systematic expansions, first to a microscopic description (kinetic equation) and then to a macroscopic description (fluid equations). Fluid-dynamic turbulence is described by macroscopic equations. A parallel theory is available for plasmas in weak magnetic fields if they are microstable. This class of plasmas can be described by a well established kinetic equation which simplifies, for most practical instances of stable plasmas, (ϵ = dielectric function $\sim$ 1) to the Landau-Fokker-Planck equation. On the basis of this equation, Spitzer and co-workers have calculated the transport properties of stable plasmas, in satisfactory agreement with the available observations. Furthermore, from the kinetic equation for stable plasmas, one can deduce the magnetohydrodynamic equations and, in principle, describe MHD macroturbulence.

3. A complication in the description of plasmas arises from the fact that strong magnetic fields are often encountered in plasmas of interest. For "collisionless" plasmas subject

to strong magnetic fields, a theory has been developed (the Chew-Low-Goldberger theory) which is based on an expansion in powers of a parameter proportional to the Larmour radius. This theory shows a remarkable feature in contrast to the description that applies to neutral gases; namely, the kinetic and fluid descriptions cannot be sharply separated. A further complication in describing plasmas is due to the fact that the condition of stability ($\epsilon \neq 0$) is seldom met in plasma work. For a collisionless system, linear microinstabilities have been investigated extensively and what is believed to be a fairly complete classification is now available (in fact, a beginning of nonlinear instability theory exists). The theory of MHD macroturbulence has not been developed to a great extent, largely because of the belief that microinstabilities are so damaging as to require the most immediate attention. A standard approach to the problem of microturbulence is the "quasilinear" theory, which is designed for collisionless plasmas. We outline, below, a program for investigating microturbulence in plasmas when collisions cannot be neglected.

4. The first part of our program consists in investigating the behavior of turbulent magnetized plasmas by a method which is quite different from the quasilinear theory. Our approach consists in determining first the velocity distribution of charged particles in the presence of random electric and magnetic fields, and making then the velocity distribution function consistent with Maxwell's equations. To present, our work has been mainly concerned with the first phase of this approach. We find that it is possible to derive a kinetic description for particles subject to random magnetic fields from the Liouville equation for the entire system. The kinetic equation is satisfied by the ensemble average of the velocity distribution function of the particles. This equation can be shown to reduce to a Fokker-Planck equation if the magnetic field fluctuations are not very strong and the kinetic energy of the particles is large. This implies that the Fokker-Planck equation for magnetic Brownian motion is limited to situations that correspond to

average fields which are not very strong. When the mean field is very strong, or, alternatively, the kinetic energy of the particles is small, a considerably more complex description of the system than that afforded by the Fokker-Planck equation is needed. We have not completed a derivation of a suitable equation in this case. We find, however, that it is possible to describe a number of situations in terms of equations representing both the precession of the velocity vectors about the mean field and the "decay" of the distribution due to the interaction with the turbulent magnetic field. The precession frequency and the decay coefficient are somewhat complicated functions of the autocorrelation of the magnetic field fluctuation. In general, the decay coefficient is negative, thus making the system unstable. Furthermore, the presence of turbulence makes the system of charged particles exhibit paramagnetic or diamagnetic behavior, depending on the structure of the autocorrelation function. The effect is exhibited by the shift in the precession frequency induced by the turbulence.

5. The second part of our program aims at developing a kinetic theory for unstable, spatially homogeneous plasmas. For example, a plasma with the "loss cone" instability is envisaged. The techniques that we use stem from our analysis of stable plasmas. In this case, the two-particle velocity distribution function, as obtained by standard methods (adiabatic theory), has an infinite spatial range when the relative velocity vector is nearly parallel to the relative separation vector. We can show, however, that the two-particle correlation function has a finite spatial range if the effect of the decay of the velocity distribution is properly taken into account. The method that has allowed us to develop a satisfactory two-particle correlation for stable plasmas is a local study of the phase space in the region where the adiabatic theory yields an infinite range.

The loss cone instability is analyzed with the same method, i.e., in the vicinity of $\epsilon = 0$ where the two-particle correlation function diverges. The resulting two-particle distribution function will then be utilized to determine the evolution in time of the velocity distribution function which is initially unstable.

6. We discuss the results available on the unstable homogeneous plasmas, as well as the work in progress on understanding the behavior of plasmas in the presence of fluctuating magnetic fields. We also outline methods for extending our approach to electrostatic fluctuations and for making the velocity distribution function consistent with Maxwell's equations.

HIGHER APPROXIMATIONS TO PLASMA TRANSPORT PROPERTIES

W. E. Meador
NASA, Langley Research Center
Hampton, Va.

The purpose of this study is to investigate the accuracies of the standard Chapman-Enskog and Grad 13-moment approximations in predicting transport phenomena in plasmas under a variety of conditions. Both methods are questionable when first-order perturbation limits are exceeded - e.g., when electron diffusion velocities are sufficiently large to invalidate linear flux-force relations. In addition, since the Grad approximation is specifically an expansion in the eigenfunctions of Boltzmann's binary elastic collision operator for Maxwellian molecules, the reliability of that method must be checked for more extreme potentials even to first order. Hence an investigation of the limitations of these techniques is imperative for a critical evaluation of much of the current literature.

The method employed in the present research for determining these limitations involves the use of an approximate kinetic equation which is solved exactly and to which the Chapman-Enskog and Grad approximations can also be applied. Comparisons between the calculated results for various transport and other plasma properties thus provide valuable insight into the desired accuracies. The essential features are summarized in the following paragraphs.

First-order (i.e., nearly equilibrium) plasmas are found to be described quite accurately by the corresponding Chapman-Enskog theory, but not as reliably in some aspects by the 13-moment approximation. While the latter method predicts the diagonal transport coefficients of electrical and thermal conductivity to within one or two percent, errors on the order of 30 percent exist for such off-diagonal coefficients as thermal diffusion when the interaction potentials are very soft or very hard. Similar errors occur in the entropy density, the collisional production rate of entropy, and second-order contributions to the electron pressure tensor, all of which are corrected to nearly the exact results by the addition of a few higher moments. Third-order contributions to the electron current density and the phase angles by which the current density and the heat flux lag an applied oscillating electric field are poorly predicted by the 13-moment approximation, the errors in these cases corresponding to factors up to four in the limits of hard and soft particles.

All of the aforementioned errors are explained by the inadequate description of certain collision integrals when the 13-moment approximation is used to close out the macroscopic equations of change. However, a new phenomenon appears when a steady-state plasma becomes spatially inhomogeneous through second order by means of an applied electric field inducing transverse pressure and temperature gradients. The prediction of such gradients by the 13-moment approximations is extremely poor (even for Maxwellian molecules) because of the neglect of a new and important driving force for heat transfer which appears with the addition of the next nine moments. A similar phenomenon occurs in the viscous flow of neutral gases through circular pipes and presents a somewhat different description of heat transfer from the picture of Navier and Stokes and the perturbation expansion of Chapman and Enskog.

The following publications have been generated by this research:

(1) A Semiempirical Collision Model for Plasmas. NASA TR R-310, 1969.

(2) A Critical Analysis of the Grad Approximation for Closing Out the Magnetohydrodynamic Equations for Plasmas. NASA TR R-325, 1969.

(3) Third-Order Contributions to Electrical Conduction in Plasmas. NASA TN D-5477, 1969.

(4) Induced Pressure and Temperature Gradients in a Plasma as a Result of Weak Electric Fields. NASA TN L-6877, 1969.

(5) Fourth Approximation to Heat Transfer in Viscous Gases Flowing Through Circular Pipes with Constant Temperature Gradients. NASA TR L-7018, 1970.

NONLINEAR TRANSITION LAYER SOLUTIONS FOR PLASMAS USING GENERALIZED FUNCTIONS

Robert C. Costen
NASA, Langley Research Center
Hampton, Va.

Progress has been made in the application of generalized functions to obtain transition layer solutions of the Vlasov equations (Maxwell's equations and the collisionless Boltzmann equation with electromagnetic forces). The objective is to find analytic solutions for the fine structure of layers of rapid transition in a two-component plasma with an applied magnetic field for possible application to the magnetopause. It is hoped that this may also lead to solutions for the structure of collisionless shocks.

Layers of rapid transition are well suited for mathematical description by the use of generalized functions. For example, consider the representation $F(\vec{r},\vec{w},t)\, H_n(x)$ for a distribution function, where F is an analytic function of position $\vec{r}$, velocity $\vec{w}$, and time t, and $H_n(x)$ is the Heaviside unit step function defined, for example, by the sequence

$$H_n(x) = \frac{1}{2}\,(1 + \tanh nx)$$

where n is the sequence index. This representation $F(\vec{r},\vec{w},t)H_n(x)$ engenders a rapid variation in the distribution function near the plane $x = 0$ (plasma-vacuum interface) and slow variations elsewhere. The sequence index n governs the thickness of the transition layer; as $n \to \infty$ the thickness of the transition layer goes to zero.

A formal method has been developed for finding solutions of the Vlasov equations where the distribution functions and electromagnetic fields are all generalized functions. The hyperbolic tangent representation of the step function (given above) is adhered to throughout because its derivatives have the convenient form

$$\delta_n(x) = 2n\,(H_n(x) - H_n^{\,2}(x))$$

$$\delta_n'(x) = 4n^2\,(H_n(x) - 3H_n^{\,2}(x) + 2H_n^{\,3}(x))$$

where $\delta_n(x)$ is the Dirac delta function sequence. The acceleration term in the Boltzmann equation

$$\left(\frac{\partial}{\partial t} + \vec{w}\cdot\frac{\partial}{\partial \vec{r}}\right)F + \frac{Ze}{m}\,(\vec{E} + \vec{w}\times\vec{B})\cdot\frac{\partial}{\partial \vec{w}}F = 0$$

is nonlinear. Therefore the generalized function formalism used must embrace products. This is a departure from the usual generalized function theory, where products are not defined except in a convolution sense. The extension

to products is a simple one for the family of generalized functions treated above, for any product takes the form of a power of n multipolied by some polynomial in $H_n(x)$. (The consideration of whether such products are integrable in the limit $n \to \infty$ is not relevant in the physics of transition layers, because n, which governs the width of the transition layer, always remains finite.) Thus a class of generalized functions is defined which includes products of the members of the class. The basic element of the class is $n^{\alpha} H_n^{\beta}(x)$, where the power α is an integer and the power β is a non-negative integer.

We seek solutions of the Vlasov equations from this class of generalized functions; that is, each field in the Vlasov equations is taken to have either the form

$$\vec{B}_n(\vec{r},t) = \sum_{\alpha=-A}^{A} \sum_{\beta=0}^{\infty} \vec{B}_{\alpha\beta}(\vec{r},t)\, n^{\alpha} H_n^{\beta}(x)$$

or the form

$$F_n(\vec{r},\vec{w},t) = \sum_{\alpha=-A}^{A} \sum_{\beta=0}^{\infty} F_{\alpha\beta}(\vec{r},\vec{w},t)\, n^{\alpha} H_n^{\beta}(x)$$

where the coefficients $\vec{B}_{\alpha\beta}$ and $F_{\alpha\beta}$ are analytic functions. The infinite summation over β is assumed to be uniformly convergent and allows the shape of the field in the transition layer to vary as any analytic function of $H_n(x)$. Negative powers of n are included because they can become significant when multiplied by positive powers of n in the nonlinear term of the Boltzmann equation. By substituting series of this type for each of the fields in the Vlasov equations and applying an identity theorem for generalized functions, one obtains a set of equations for the series coefficients. Any analytic solution of this derived set of equations constitutes a transition layer solution of the original Vlasov equations.

A method which has proven to be successful in obtaining solutions of the derived set of equations is as follows: Pick a priori the highest allowable order (power of n) for each of the fields. The equation corresponding thereto, which is the highest order equation, will normally have the applied magnetic field (which is known) as one of the factors in the acceleration term of the Boltzmann equation. Thus the highest order equation is linear and can easily be solved for simple cases. One then proceeds to the equation corresponding to the next lower power of n. In the nonlinear term of this equation one of the factors is already known from solution of the previous higher order equation; hence this equation is linear also and amenable to solution in simple cases. By continuing to work downward in this fashion through equations of decreasing order one obtains asymtotic solutions in the expansion parameter n^{-1} for each of the fields. The accuracy of these solutions increases as the transition layer becomes thinner (n increases).

RESEARCH ON THE LOW DENSITY HOLLOW CATHODE

Guiseppe Palumbo, Paul J. Wilbur, and William R. Mickelsen

Colorado State University, Ft. Collins, Colo.

A mercury vapor hollow cathode discharge is being investigated for application to electron bombardment thrusters. The hollow cathode is located at one end on the axis of an annular pole piece which carries magnetic flux to the main discharge of the thrusters. In conventional designs there is no magnetic field inside the pole piece. Preliminary experiments reported here indicate that substantial reduction in discharge power consumption can be attained by addition of a magnetic field internal to the cathode pole piece. Possible reasons for these results are discussed.

CONSTRICTED ARC PLASMA JETS

Charles E. Shepard

NASA Ames Research Center, Moffett Field, California

Existing constricted-arc supersonic plasma jets produce streams of very high enthalpy at relatively low density in a variety of gases. Performance data for air and nitrogen[1,2] show that enthalpies corresponding to superorbital velocity can be produced at densities corresponding to flight at altitudes down to about 60 km. Although existing constricted-arc jet facilities have proved very useful at Ames, there is a clear need for higher operating pressure in order to produce higher Reynolds numbers and to simulate flight at lower altitudes.

When the pressure is increased beyond the normal operating level, two related problems become apparent. The constrictor disks that make up the arc tube can fail either due to inadequate water cooling or to electrical breakdown (arc-over) between adjacent constrictor disks. For the same total constrictor length, thinner disks reduce arc-over tendencies but are more difficult to cool. The performance of thinner, better cooled constrictor disks similar to those developed by Maecker has been studied both by means of computer calculations and by experiment. The results of the studies indicate that the maximum constrictor wall heat transfer rate can be increased from the present value of 3 kW/cm^2 to about 10 kW/cm^2.

Although water cooling is necessary for steady-state operation, heat capacity cooling offers some important advantages for short time operation. Not only are the parts cheaper and easier to make and modify, but also higher heat transfer rates can be maintained for pulsed operation than for steady-state water cooling, as shown in Figure 1. Two schemes for short time runs are being investigated. Millisecond operation from a LC lumped parameter discharge line has already been shown to be feasible in a contract study by General Dynamics/Convair for Ames. Power levels of hundreds of megawatts for several milliseconds appear practical with about 10^6 joule energy storage. Alternately, lower resistance inductors now being sought should permit test times of tens of milliseconds at many tens of megawatts power.

Short time operation of a heat capacity cooled arc jet from a conventional DC power supply may also be advantageous. Economy in construction and power supply costs for heat capacity cooling were important factors for a new 6 cm internal diameter constricted-arc jet. This device is a prototype of a steady-state constricted arc jet that will provide high radiative heat transfer rates to blunt

test bodies. The device consists of a 6 cm I.D. x 2.4 meter long constrictor tube followed by a divergent nozzle having an exit diameter of 10 cm. Thirty-six ½ inch diameter tungsten rods form a heat capacity cooled multiple cathode at the upstream end of the constrictor tube. Ninety ¼ inch diameter rods make up the multiple anode that is located along the nozzle surface. The design goals are a total enthalpy of 116 MJ/kg and an impact pressure of 1.0 atm.

Preliminary tests of the 6 cm diameter, heat capacity cooled constricted-arc jet at power levels up to 14 megawatts have produced total enthalpies in excess of 120 megajoules/kg and a test body impact pressure of about 0.4 atm. These tests indicate that useful heat transfer data can be obtained in the .2 to .5 second test intervals. As shown in Figure 2, calorimeter rake measurements indicate a nearly uniform radial heat transfer profile over about half of the exit diameter.

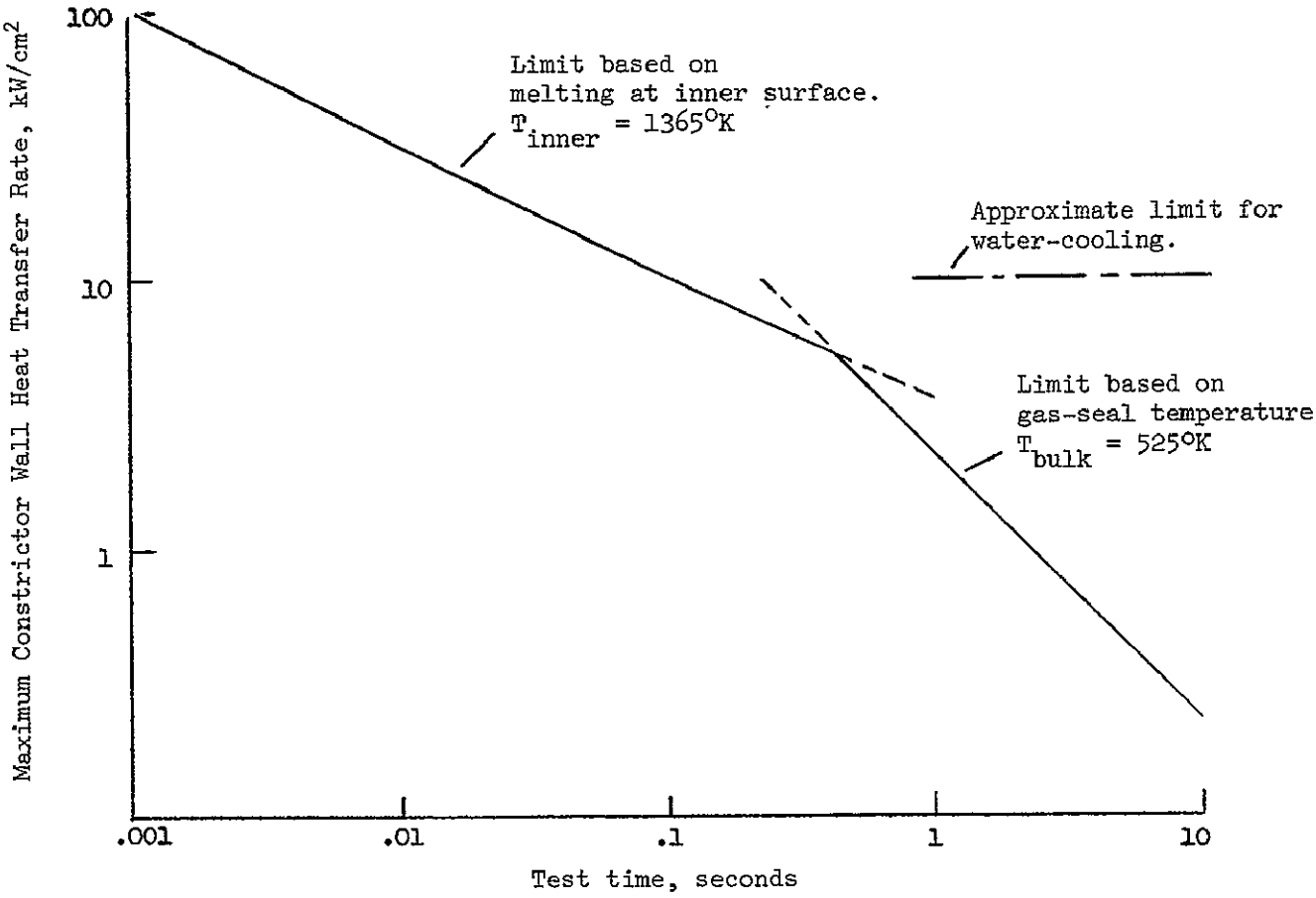

Figure 1. Maximum constrictor heat transfer rate at inner wall as a function of test time.

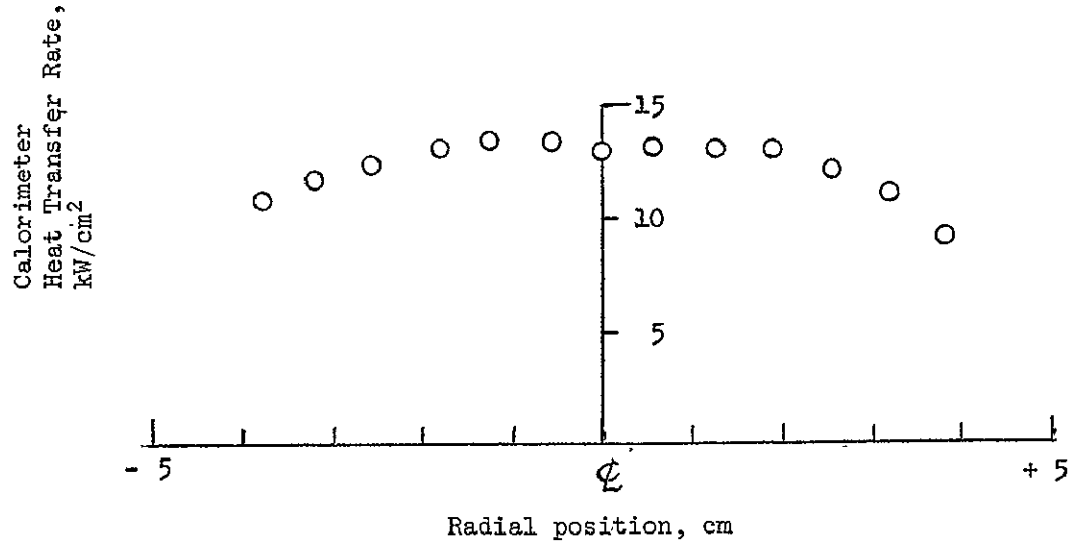

Figure 2. Approximate radial distribution of heat transfer rate based on time to melt 1/8 inch diameter copper calorimeter rods.

DEVELOPMENT PROGRESS ON A CROSSED FIELD ROTARY-ARC IN A CONFINED VORTEX CONFIGURATION FOR ACCELERATING HYPERVELOCITY NOZZLE FLOWS

Roger B. Stewart, NASA Langley Research Center

During the past several years we have carried out experimental and theoretical studies of the flow behavior in an arc heater employing an electromagnetically driven confined vortex. These efforts have been directed toward the development of a device that will produce high Reynolds number nozzle flows with gas velocities that approach reentry flight speeds. Several small (500 kw) arc driven devices have been operated extensively to determine the variation of performance and the ability to predict performance for different operating conditions and heater configurations. Early experiments are reported in reference 1 and a more recent range of performance is shown in figure 1 along with a schematic diagram of the device. At the high mass flow rate (10 gms/sec) nearly 60 percent of the arc input power appears as net energy addition to the gas (thermal plus directed kinetic energy). At the low mass flow rates the efficiency is 48 percent. Test results indicate that the overall performance rises significantly as the Hall parameter increases. This implies that substantial gains in performance can be obtained by operating at high magnetic field strengths. This is a unique advantage of these devices.

The theoretical studies have been reported in reference 2. Closed form solutions for the azimuthal velocity, induced magnetic field and pressure distribution within the vortex have been obtained from the coupled set of electromagnetic and fluid dynamic equations within the MHD approximation. Numerical solutions to the non-linear energy equation have been obtained using a fifth degree polynomial for the variation of electrical conductivity with temperature. Solutions to the energy equation provide the temperature distribution, Mach number distribution, and power required to heat and accelerate the vortex. Experimental measurements of pressure, velocity distributions inside the vortex chamber, and the power required confirmed the theoretical predictions. The experimental and theoretical studies have been applied to design and build a larger device with twice the arc gap and magnetic field strength, (B_z = 4 webers/meter^2). This device will soon be tested. In addition, the Structures Research Division, at Langley Research Center, is constructing a third and larger device and the Australian National University at Canberra is also contemplating the construction of similar type of arc heater with an accelerating vortex. The ultimate performance of these devices is not known at present, however, experimental studies with these new devices will define new performance levels and furnish scaling data. Figure 2 lists typical performance.

In addition to the vortex studies we have carried out experiments with a device that incorporates a mechanically and electrically coupled linear accelerator section downstream of the circular channel, figure 3. Higher pressures and larger plasma interaction lengths are an advantage of this two-stage device over a single accelerating cycle. Steady state operation

of the vortex-linear device has shown a 58 percent efficiency for energy input to the gas.[2] Considering the relatively low magnetic field strength (1.1 webers/meter^2) this represents a considerable increase in performance over the single stage vortex device operating at the same field strength.

Basic research studies applicable to both accelerators concerns the fundamental behavior of high current arcs that are driven over cold metal surfaces by electromagnetic means. We have carried out an extensive series of experiments on arc behavior which are reported in references 3 and 4. Of particular interest is the large increase in current sheet (or diffused arc) rotational velocities in the spiral cathode devices compared with concentric circular electrode geometries. An attempt to link this behavior with the radial displacement effect of the highly ionized region of the arc at the cathode has been made in reference 5. An order of magnitude argument indicates that significant additional "local" Lorentz forces may be present on the cathode sheath in spiral vortex geometries as compared with circular geometries. Figure 4 indicates the basic geometries studied and shows the results with velocity as a function of driving force for these different configurations. The cathode current sheet velocities for the spiral cathode are more than four times higher than the velocities for the circular cathode. The velocities in excess of 8000 meters/second are believed to be higher than any yet reported at the pressure levels shown.

The behavior of several particular rotary arc devices has been studied both theoretically and experimentally. The confined vortex flow that is heated and driven electromagnetically appears to offer higher simultaneous velocity and Reynolds number performance than is presently available with conventional arc heaters. Upcoming experiments with larger devices will define the hypervelocity nozzle flow conditions that can be achieved.

REFERENCES

1. Stewart, R. B. and Wallio, M. A.: "The Experimental Performance of an Arc Driven Vortex Type Heater Accelerator," Fourth Hypervelocity Techniques Symposium, Tullahoma, Tenn. 1965

2. Stewart, R. B.: "An Analysis of an Electromagnetically Driven Confined Vortex with High Positive Radial Reynolds Numbers." AIAA Joint Electric Propulsion and Plasmadynamics Conference, Colorado Springs, Colorado, 1967, Paper No. 67-730

3. Sabol, A. P., Stewart, R. B., and Duckett, R. J.: "An Experimental Study of the Behavior of High Current Arcs Driven by Strong External Magnetic Fields," Proc. of Eighth Symposium on Engineering Aspects of MHD, March 1967

4. Sabol, A. P., Stewart, R. B. and Duckett, R. J.: "Experimental Results of High Current Arcs Driven Supersonically in Straight and Circular Channels," NASA TN (proposed)

5. Stewart, R. B., Sabol, A. P.: "Arc Motion in High Pressure Crossed Field Devices," to be published as AIAA Technical Note

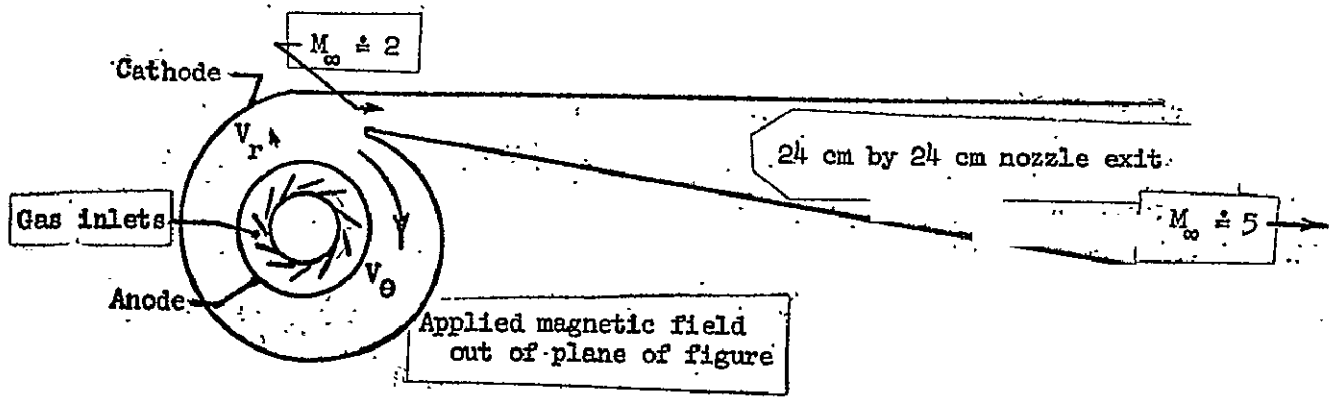

(a) Schematic of experimental vortex accelerator and nozzle system.

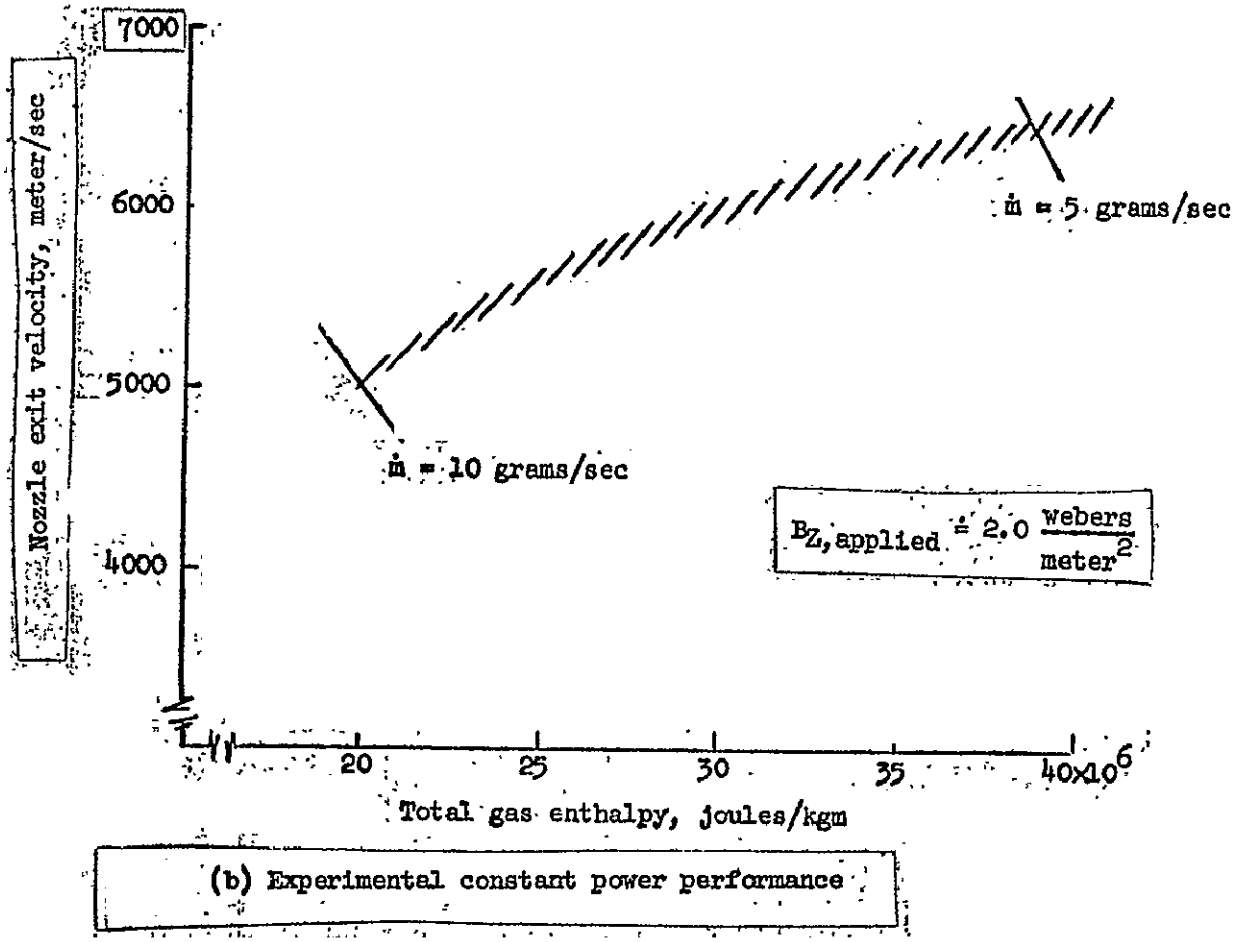

(b) Experimental constant power performance

Figure 1. - Pilot model vortex accelerator.

Conditions at 2.0 by 3.8 cm accelerator exit

Accelerator exit velocity	3800 meters/second = 12,400 ft/sec
Exit Mach number	2.0
Static temperature	6500° K
Static pressure	0.14 atmosphere

Conditions at 24 cm by 24 cm nozzle exit

Total enthalpy	41.1×10^6 Joules/kgm = 17,700 Btu/lb_m
Stream velocity	6400 meters/second = 21,100 ft/sec
Mach number	5.0
Static pressure	0.006 atm
Pressure altitude	58 Km
Static temperature	4700° K
Running time (with uncooled nozzle)	30 seconds

Figure 2. - Experimental conditions achieved in 500 kw vortex heater accelerator.

ARC DEVELOPMENT TUNNEL

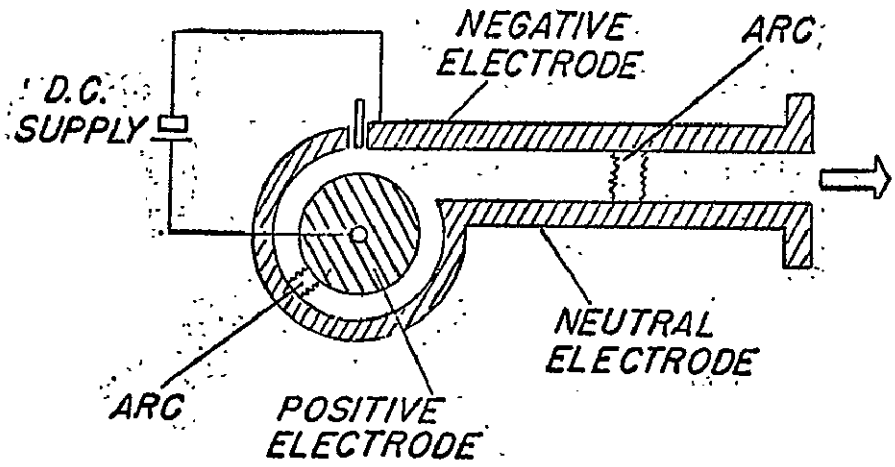

ROTARY ARC LINEAR JXB ACCELERATOR

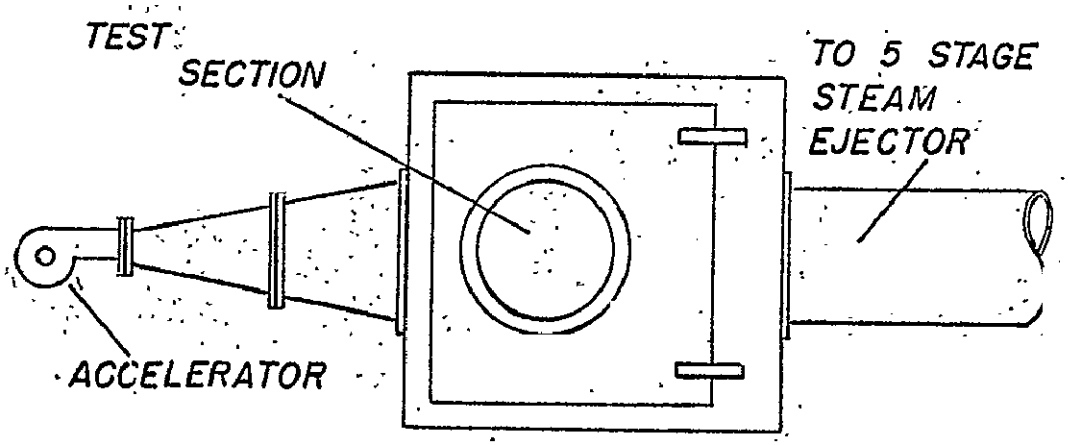

The rotary arc linear J × B accelerator is an experimental high current device which makes use of arc entrainment to induce a fluid motion. The device is being tested for its ability to produce a high velocity flow comparable to reentry conditions. Gas introduced in the rotary section experiences the combined effect of two accelerators placed in tandem and it exits through a 1 x 1 inch channel with a nozzle blow-down system.

Stream static pressure, psia	3.1
Total enthalpy, Btu/lb	11,400
Weight flow, lb/sec	0.017
Efficiency by heat balance, percent	58.0
Applied magnetic field, weber/meter^2	1.14
Arc current, amperes	805
Arc voltage, volts	440

Figure 3. - Vortex linear plasma device.

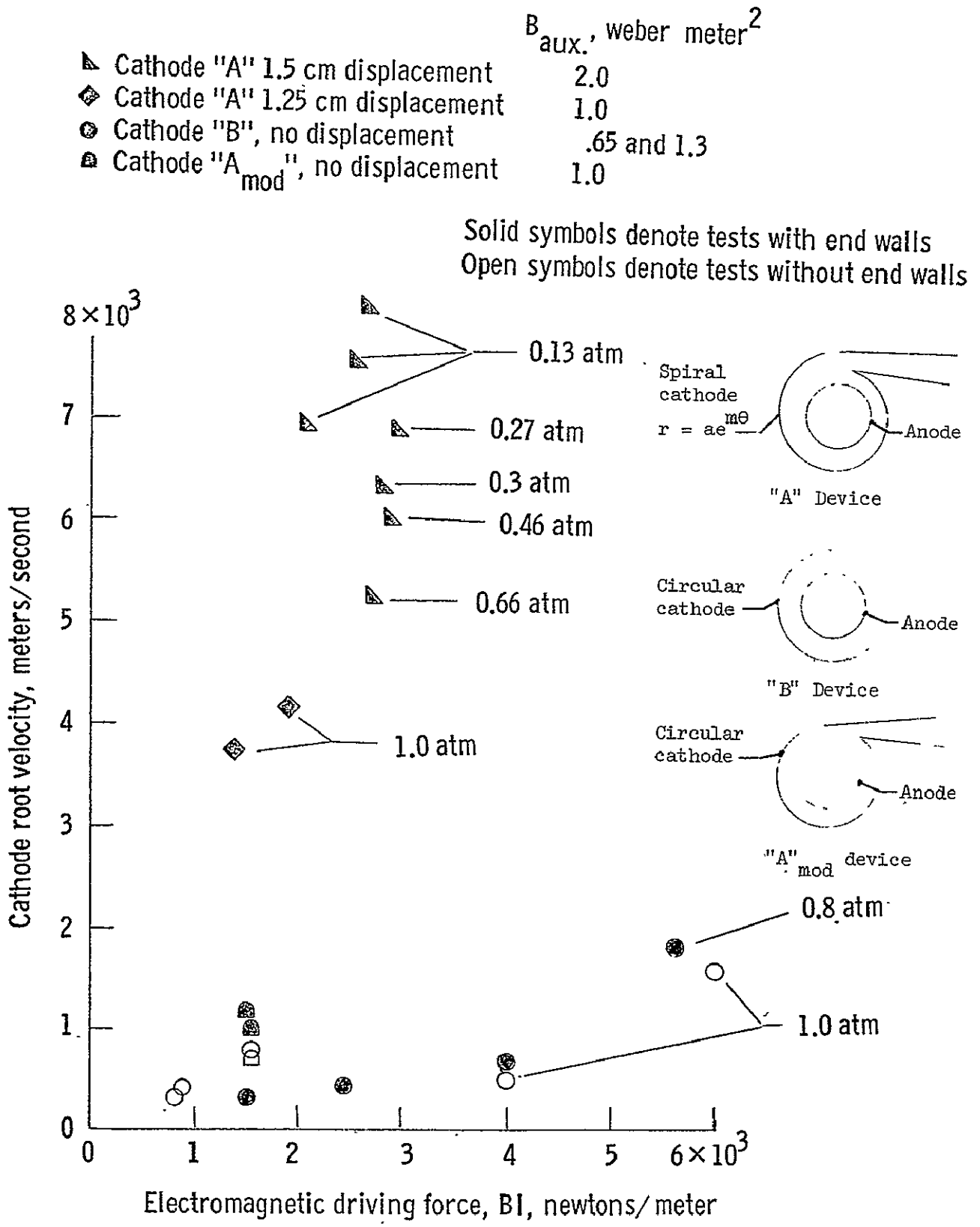

Figure 4. - Spiral and circular cathode experimental results.

COMPARISON OF THEORETICAL AND FLIGHT-MEASURED IONIZATION IN A BLUNT BODY REENTRY FLOW FIELD

P. W. Huber, J. S. Evans, and C. J. Schexnayder
NASA, Langley Research Center
Hampton, Va.

In order to define, circumvent, or alleviate the radio attenuation which occurs during spacecraft atmospheric entry one must first be able to describe the magnitude and distribution of electron concentration in the plasma flow near the antenna, and then to determine the interaction of the em field with this plasma. In the real-life situation, many factors such as reaction rates, ablation, separated flow, angle of attach, antenna configuration, etc., combine to make the complete problem too complex to assess on a purely theoretical basis. As an alternative, one lays the groundwork using idealized theoretical models for various facets of the problem and then assesses the applicability of these models by comparison with data from the laboratory, or with flight measurements when the problem cannot be properly simulated on the ground. One purpose of the Langley Research Center project RAM program is to obtain reentry flight data which can be interpreted in terms of models for the plasma flow, for em propagation, and for alleviation of signal attenuation. Towards this end, RAM vehicles of hemisphere-9° cone configuration have reentered the earth's atmosphere, at near-orbital velocity, at near-zero attitude, and with both ablating and nonablating heat shields. They were equipped with various onboard plasma diagnostic sensors, various communication systems, and a material injection scheme to modify the plasma and reduce attenuation. The vehicle's nose radius is 0.5 feet.

The purpose of this paper is to draw conclusions relative to the reentry plasma ionization by comparison of results from theoretical models with the onboard diagnostic data and with the passive data obtained from interpretation of the signal attenuation.

The theoretical models which are employed in the comparison include the following: (1) Pure air inviscid and merged boundary-layer-inviscid blunt-body flow-field models in which the various air species chemical kinetics reaction rates can be treated as independent parameters, (Ref. 1); (2) pure air boundary-layer correlations in which the influence of ambipolar electron-ion diffusion and wall recombination are exhibited; (3) boundary-layer program in which the effects of alkali ablation contaminants on the ionization profiles are exhibited, and (4) a nonhomogeneous slab plane wave em plasma propagation model for determining signal attenuation due to the plasma (Ref. 2).

The flight data used in the comparison includes onboard measurements of collected current from a rake of eight Langmuir probes extending 7 cm into the flow field at the aft part of the vehicle, onboard reflected power measurements from 15 reflectomers located at four station along the body (four different frequencies), and onboard measurements of VSWR for three

of the communications antennas. Ground-based received signal strength measurements for different polarizations were made for the four communications antennas (four different frequencies) from a number of different range stations in radio contact with the spin stabilized reentry vehicle. The vehicle reentered at 25,100 ft/sec and its attitude was maintained at less than three degrees during the reentry data period. RAM C-1 had a NARMCO ablating heat shield which contained more than 10^3 ppm of sodium and potassium, while RAM C-2 had a beryllium and teflon heat shield which was free of alkali contaminants.

Some of the conclusions which have resulted from the comparison of the theoretical with the experimental data are briefly summarized below, along with the basis upon which they are reached:

1. NO^+ air reaction rate.- Computer experiments show that the peak profile ionization, and the C and X-band signal attenuation for pure air are quite sensitive to the NO^+ rate in the altitude range above about 120 Kft. C-band signal attenuation data in this altitude range for the flight with a beryllium heat shield followed by a teflon body coating shows good agreement with that computed using the NO^+ rate recently measured in a shock tunnel, reference 3, while the X-band data agreement is not as good, but closer to this rate than the older rate of reference 4 which is slower by a factor of three. These results are shown in Fig. 1.

2. Ablation ionization.- Theoretical ionization profiles and signal attenuations were computed for cases where alkali material is contained in the boundary layer due to the NARMCO heat-shield ablation. Comparison of the signal attenuation data for the NARMCO flight, RAM C-1, with that of the beryllium-teflon flight, RAM C-2, and comparison of the theoretical model for pure air with the ablation impurity model both show a large effect of the ablation impurities. Furthermore, the air model using the fast NO^+ rate is in reasonably good agreement with the RAM C-2 attenuation data, while the ablation model, although not agreeing quantitatively, shows the same qualitative trends as the RAM C-1 data below altitudes of about 180 Kft. Comparison with the low altitude signal recovery data, where ablation rates are highest, is shown in figure 2. In figure 3, attenuation data from RAM C-1 at higher altitudes is compared with the ablation model to suggest the very interesting probability that the impurity ionization disappears at about 200 Kft due to lack of ionization time. This is seen in the sudden drop of attenuation as compared with local equilibrium theory.

3. Electron-ion diffusion.- Theoretical correlations are made for the RAM high altitude regime which show that the effects on peak profile ionization due to ambipolar electron-ion diffusion and wall recombination are very large at altitudes much above 230 Kft. Reflectometer measurements and VSWR indications of the peak electron concentration confirm this result, while the Langmuir probe profile measurements show, in addition to this large reduction, a pronounced distortion of the profile away from the wall as compared with a theoretical model with no electron-ion diffusion.

REFERENCES

1. Evans, J. S.; Schexnayder, C. J.; and Huber, P. W.: Computation of Ionization in Reentry Flow Fields. Accepted for publication, AIAA J.

2. Swift, C. T., and Evans, John S.: Generalized Treatment of Plane Electromagnetic Waves Passing Through an Isotropic Inhomogeneous Plasma Slab at Arbitrary Angles of Incidence. NASA TR R-172, December 1963.

3. Dunn, M. G., and Lordi, J. A.: Measurement of $NO^+ + e^-$ Dissociative Recombination in Expanding Air Flows. Report A1-2187-A-10, Sept. 1968, Cornell Aero. Lab., Buffalo, N. Y.

4. Lin, S. C., and Teare, J. D.: Rate of Ionization Behind Shock Waves in Air. II. Theoretical Interpretations. The Physics of Fluids, Vol. 6, No. 3, March 1963, pp. 355-375.

COMPARISON OF RAM C-2 ATTENUATION DATA WITH AIR THEORY

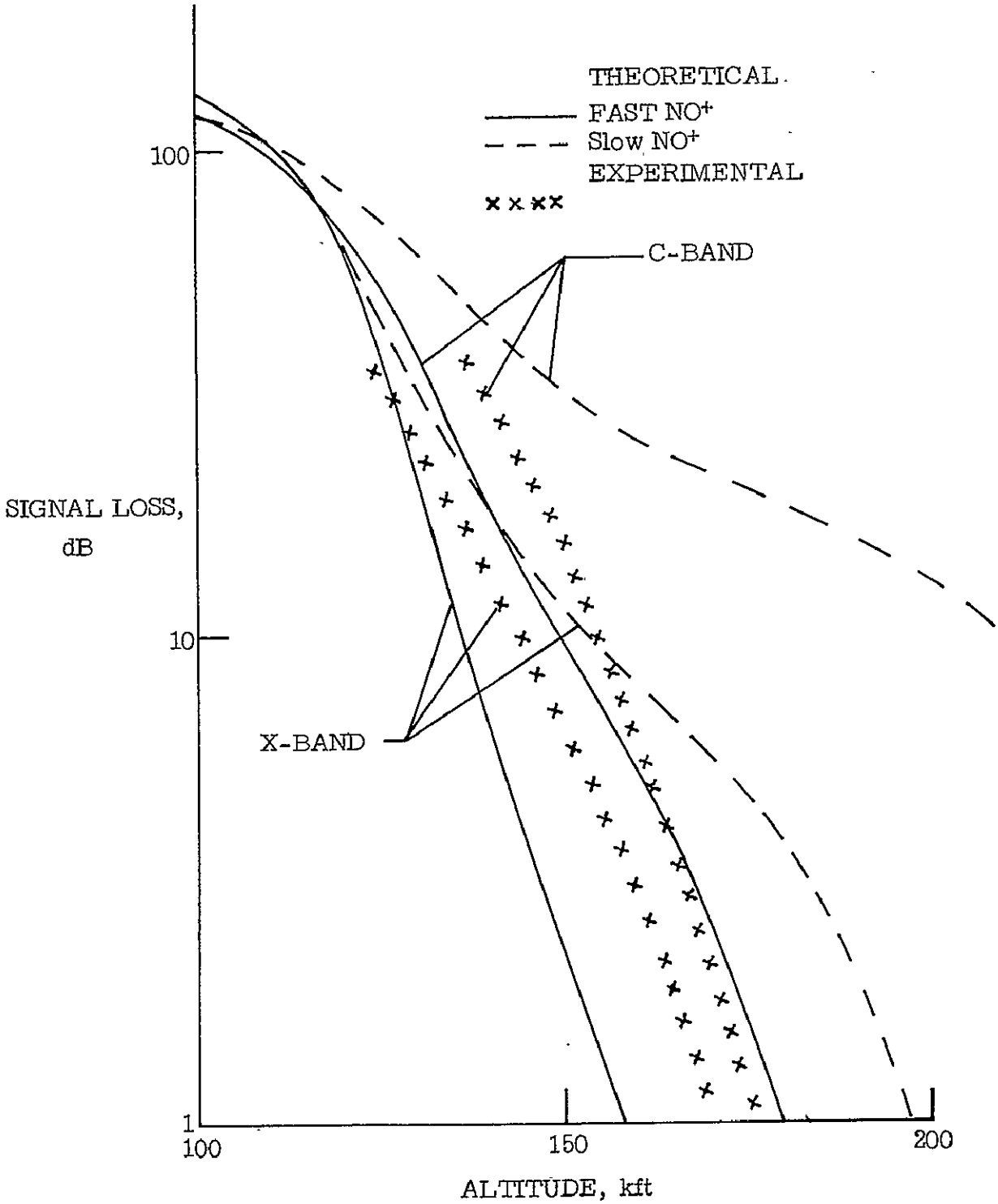

FIGURE 1.

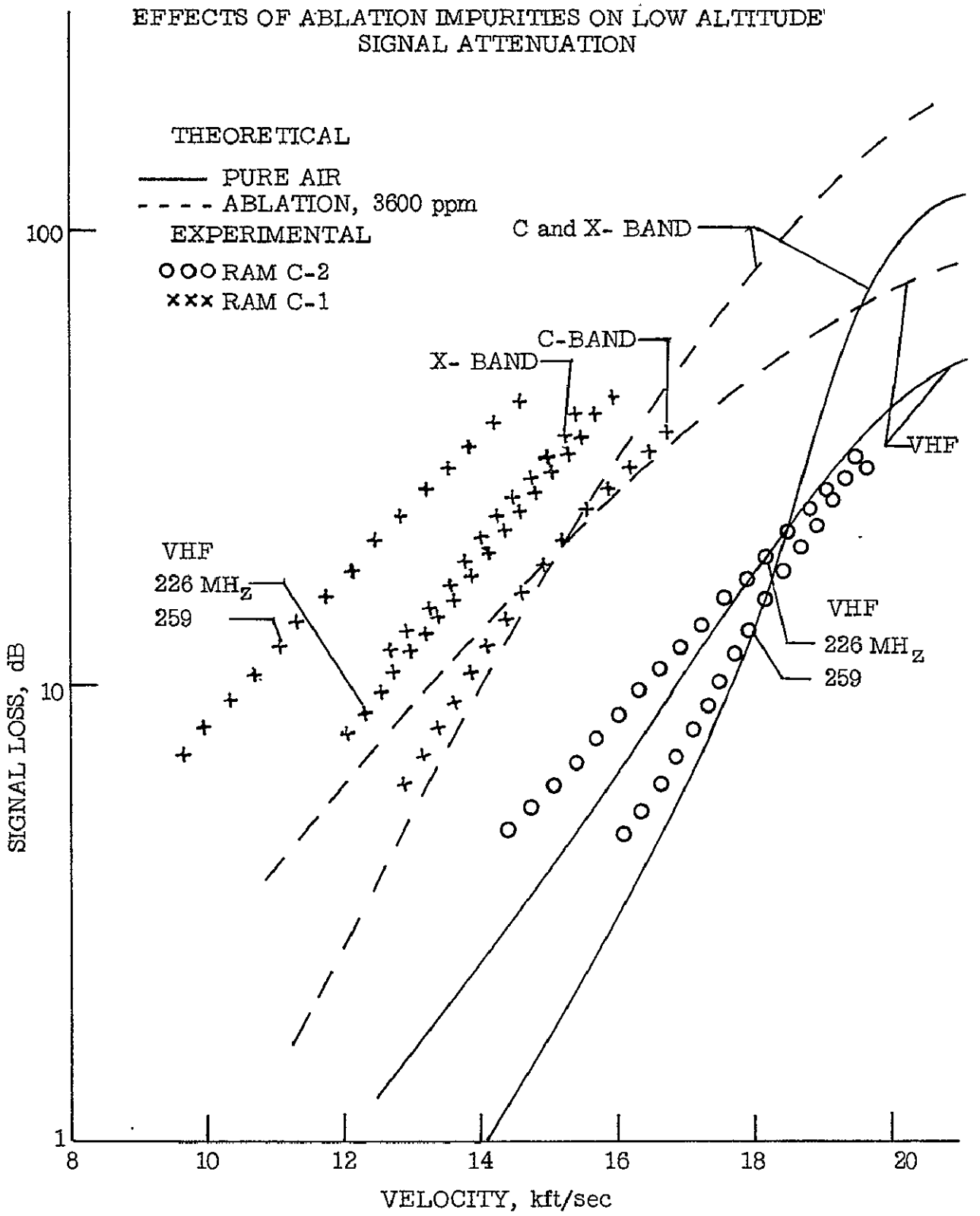
EFFECTS OF ABLATION IMPURITIES ON LOW ALTITUDE SIGNAL ATTENUATION
THEORETICAL
PURE AIR
ABLATION, 3600 ppm
EXPERIMENTAL
RAM C-2
RAM C-1
C and X- BAND
C-BAND
X- BAND
VHF
VHF
226 MHz
259
VHF
226 MHz
259
SIGNAL LOSS, dB
100
10
1
8
10
12
14
16
18
20
VELOCITY, kft/sec

FIGURE 2.

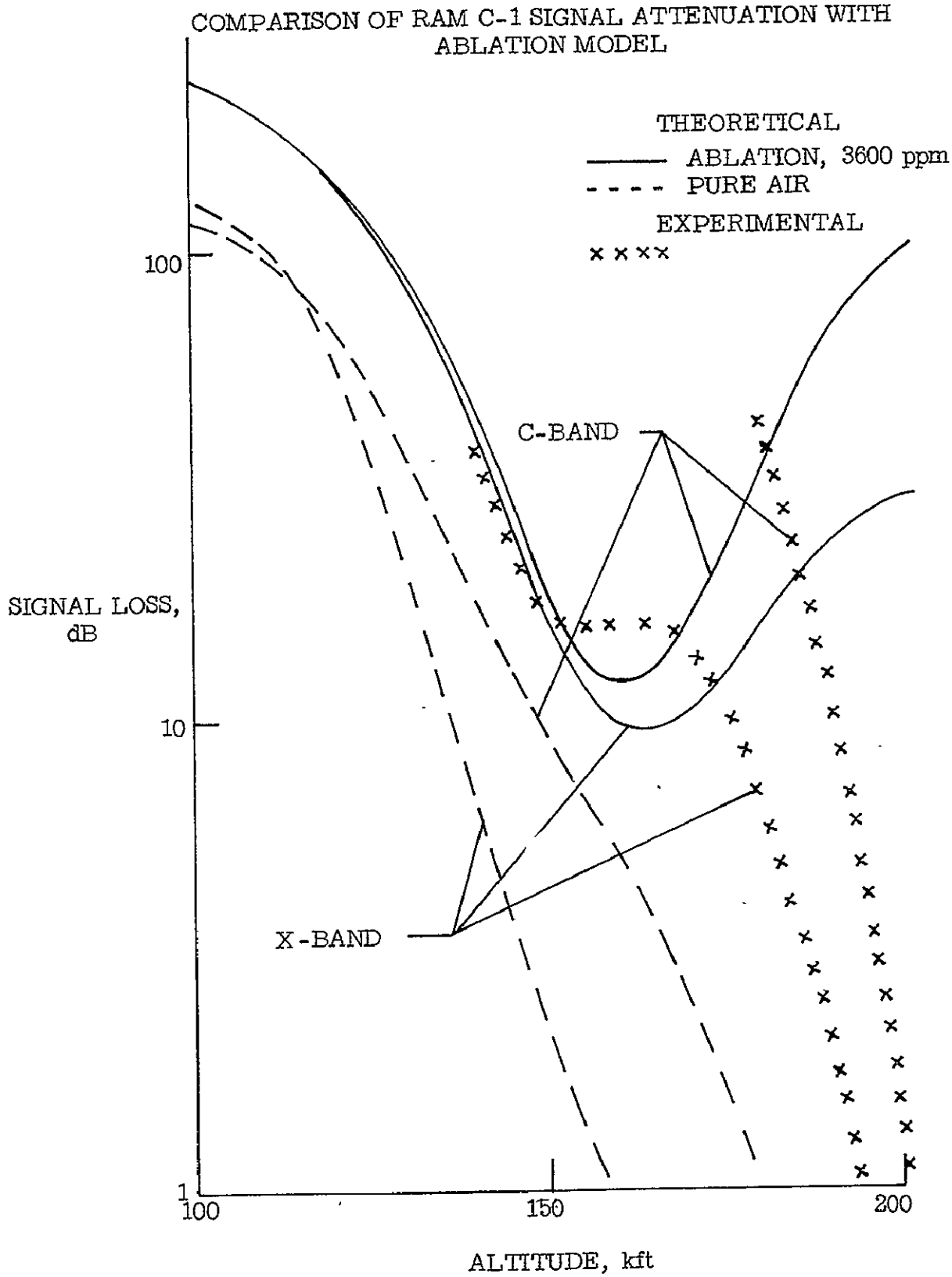
COMPARISON OF RAM C-1 SIGNAL ATTENUATION WITH ABLATION MODEL
THEORETICAL
ABLATION, 3600 ppm
PURE AIR
EXPERIMENTAL
C-BAND
X-BAND
SIGNAL LOSS, dB
100
10
1
100
150
200
ALTITUDE, kft

FIGURE 3.

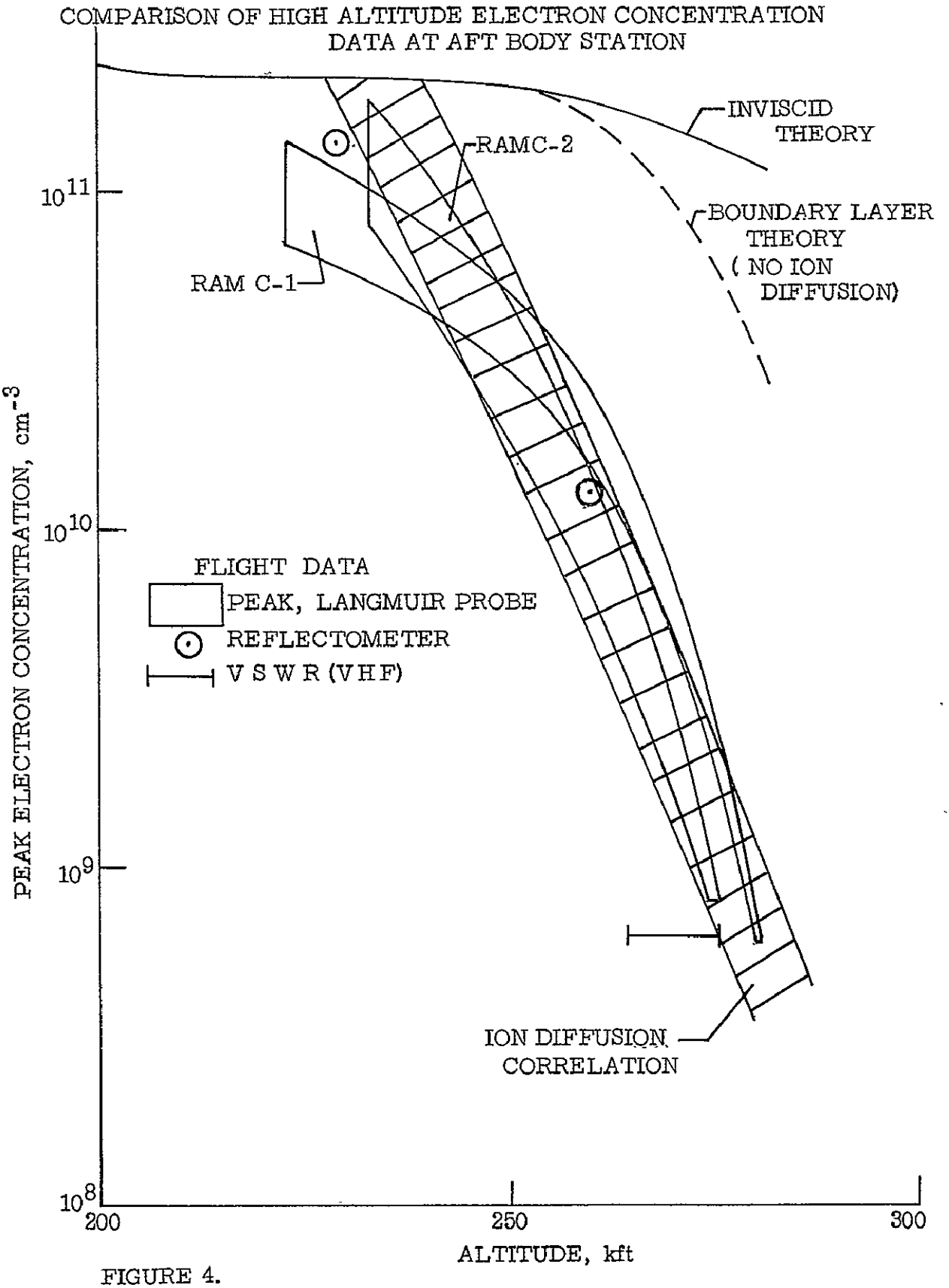
COMPARISON OF HIGH ALTITUDE ELECTRON CONCENTRATION DATA AT AFT BODY STATION
INVISCID THEORY
RAMC-2
BOUNDARY LAYER THEORY (NO ION DIFFUSION)
RAM C-1
FLIGHT DATA
PEAK, LANGMUIR PROBE
REFLECTOMETER
V S W R (VHF)
ION DIFFUSION CORRELATION
PEAK ELECTRON CONCENTRATION, cm-3
10^11
10^10
10^9
10^8
200
250
300
ALTITUDE, kft

FIGURE 4.

THEORETICAL IONIZATION PROFILES IN BLUNT BODY ATMOSPHERIC ENTRY FLOW FIELDS

J. S. Evans, C. J. Schexnayder, and P. W. Huber
NASA, Langley Research Center
Hampton, Va.

Techniques are described for the computation of electron concentration profiles in the shock layer surrounding a blunt-nosed vehicle during entry into Earth's atmosphere at near-orbital speed and at altitudes where ion diffusion effects can be neglected. Emphasis is on careful treatment of finite rate chemistry and boundary-layer effects. A streamtube approach is used to calculate gas composition and flow properties in both the inviscid and viscous parts of the shock layer. Each streamtube (see fig. 1) begins immediately behind the shock front with free-stream composition and fully excited internal energy. Simultaneous integration of flow equations and chemical kinetic equations is carried out for streamlines defined by specified pressure distributions. The equations and their solution are modeled after reference 1. For the body shown (sphere-cone; d_N = 1 ft., cone half angle = 9°) the boundary layer is too thin to have an appreciable effect on N_e profiles below about 175,000 feet and nearly fills the shock layer at 230,000 feet. Thus, increasing numbers of streamlines are swallowed by the boundary layer as altitude increases. Streamlines are followed into the boundary layer on the basis of a mass flow criterion, but only gas composition is computed, since the flow properties are found from boundary-layer calculations.

The species and the reactions are shown in figure 2. The atmosphere is assumed to consist of O_2 (21%) and N_2 (79%). All possible atoms, diatomic molecules, and their singly charged positive ions are included, and, in addition, the negative ions O^- and O_2^- are also. The reactions are divided into three groups: neutral, charge production, and charge exchange. Since the charged species make up only a tiny fraction of the total gas, the thermodynamic properties of the mixture is for all practical purposes controlled by the neutral reactions. Creation and destruction of charges takes place only through the charge production reactions. The charge exchange group is important because it provides paths for rapid buildup and/or destruction of species which would otherwise be slow to change. For example, the rate of recombination of O^+ by reaction 11 (3-body recombination) is negligible at 175,000 feet but the rate of exchange with NO to produce NO^+ is rapid. Then NO^+ combines with e^-.

The importance of adequate provision for charge transfer is illustrated in figure 3, where, with no charge transfer reactions, O^+ and N^+ build up to smaller initial values than they should and then decrease not at all during the expansion. A limited system of two charge transfer reactions, which connect O^+ to O_2^+ and N^+ to N_2^+, gives higher initial values but they are still essentially frozen during the expansion. In the latter case e^- remains quite high because of the failure of the atomic ions to disappear. The effect of calculations like the above on N_e profiles at 156,000 ft, x/d_N = 4, is shown in figure 4.

In figure 5 the body streamline values of γ_e are plotted against altitude at several body stations and are compared with local ionic equilibrium values. (For local ionic equilibrium all ion concentrations are in equilibrium with local concentrations of the neutral species at the local temperature.) Since local ionic equilibrium represents a lower bound, electrons cannot recombine as completely at 100,000 feet as they can at 175,000 feet. If the lower bound can be removed then further recombination can take place. One way to lower the bound is by injecting water into the flow as shown on the figure. It was calculated at altitude = 131,000 feet, $W^* = 1$ (W^* = mass flow of water/mass flow of air) by means of another streamtube program (ref. 2) which has been developed to study the effects of water injection on N_e profiles during atmospheric entry. This analysis accounts for the presence of accelerating and evaporating water droplets in the flow, as well as chemical reactions introduced by adding hydrogen.

REFERENCES

1. Lomax, Harvard, and Bailey, Harry E.: A Critical Analysis of Various Numerical Integration Methods for Computing the Flow of a Gas in Chemical Nonequilibrium. NASA TN D-4109, August 1967.

2. Schexnayder, Charles J.; Evans, John S.; Bushnell, Dennis M., and Weigel, Barbara I.: Streamtube Analysis to Calculate Electron Concentration in the Presence of Accelerating and Evaporating Liquid Droplets, Proposed NASA TN.

FLOW FIELD AND TYPICAL STREAMLINE PATHS

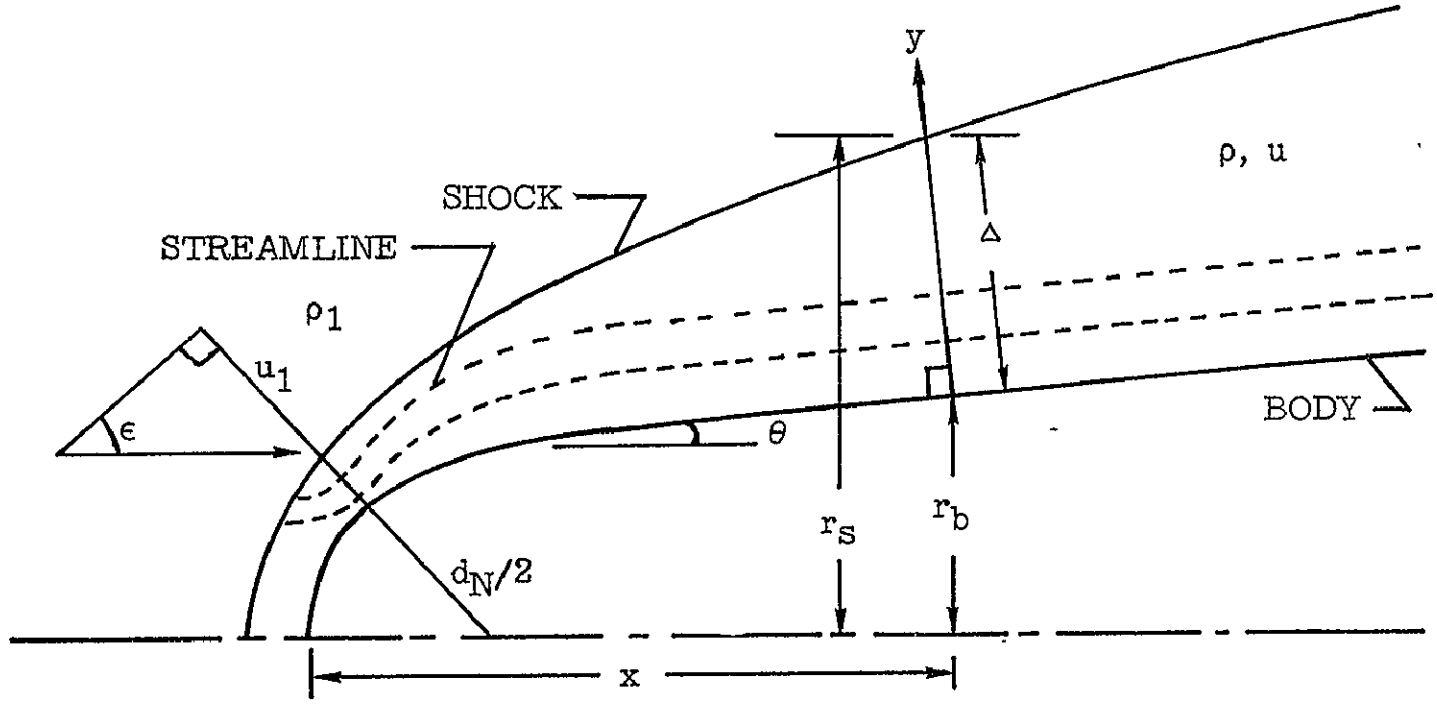

FIGURE 1.

SPECIES AND REACTIONS FOR EARTH ENTRY

SPECIES

O_2, N_2, O, N, NO, NO^+, O_2^+, N_2^+, O^+, N^+, e^-, O^-, O_2^-

REACTIONS

NEUTRAL:

1. $O_2 + M \rightarrow O + O + M$
2. $N_2 + M \rightarrow N + N + M$
3. $NO + M \rightarrow N + O + M$
4. $O + N_2 \rightarrow NO + N$
5. $O + NO \rightarrow O_2 + N$

CHARGE PRODUCTION:

6. $O + O \rightarrow O_2^+ + e^-$
7. $N + N \rightarrow N_2^+ + e^-$
8. $N + O \rightarrow NO^+ + e^-$
9. $N_2 + e^- \rightarrow N_2^+ + e^- + e^-$
10. $N + e^- \rightarrow N^+ + e^- + e^-$
11. $O + e^- \rightarrow O^+ + e^- + e^-$
12. $O_2 + e^- \rightarrow O_2^+ e^- + e^-$
13. $NO + e^- \rightarrow NO^+ + e^- + e^-$
14. $O + O \rightarrow O^+ + O^-$
15. $O + N \rightarrow N^+ + O^-$
16. $O + NO \rightarrow NO^+ + O^-$

CHARGE EXCHANGE:

17. $N_2 + NO^+ \rightarrow N_2^+ + NO$
18. $N + NO^+ \rightarrow N^+ + NO$
19. $O + NO^+ \rightarrow O^+ + NO$
20. $O_2 + NO^+ \rightarrow O_2^+ + NO$
21. $N_2 + O_2^+ \rightarrow N_2^+ + O_2$
22. $N + O_2^+ \rightarrow N^+ + O_2$
23. $O + O_2^+ \rightarrow O^+ + O_2$
24. $N_2 + O^+ \rightarrow N_2^+ + O$
25. $N + O^+ \rightarrow N^+ + O$
26. $N_2 + N^+ \rightarrow N_2^+ + N$
27. $O^- + M \rightarrow O + e^- + M$
28. $O_2^- + M \rightarrow O_2 + e^- + M$
29. $O_2 + e^- \rightarrow O^- + O$
30. $O + NO^+ \rightarrow N^+ + O_2$
31. $NO + NO^+ \rightarrow N_2^+ + O_2$
32. $O + NO^+ \rightarrow O_2^+ + N$
33. $N + NO^+ \rightarrow N_2^+ + O$
34. $N + NO^+ \rightarrow O^+ + N_2$
35. $NO + NO^+ \rightarrow O_2^+ + N_2$
36. $N_2 + O^+ \rightarrow N^+ + NO$
37. $NO + O^+ \rightarrow N^+ + O_2$
38. $N + O_2^+ \rightarrow O^+ + NO$
39. $O + N_2^+ \rightarrow N^+ + NO$
40. $O_2 + O^- \rightarrow O_2^- + O$

FIGURE 2.

STREAMLINE VARIATION OF CHARGED SPECIES

(ALTITUDE = 156,000 ft)

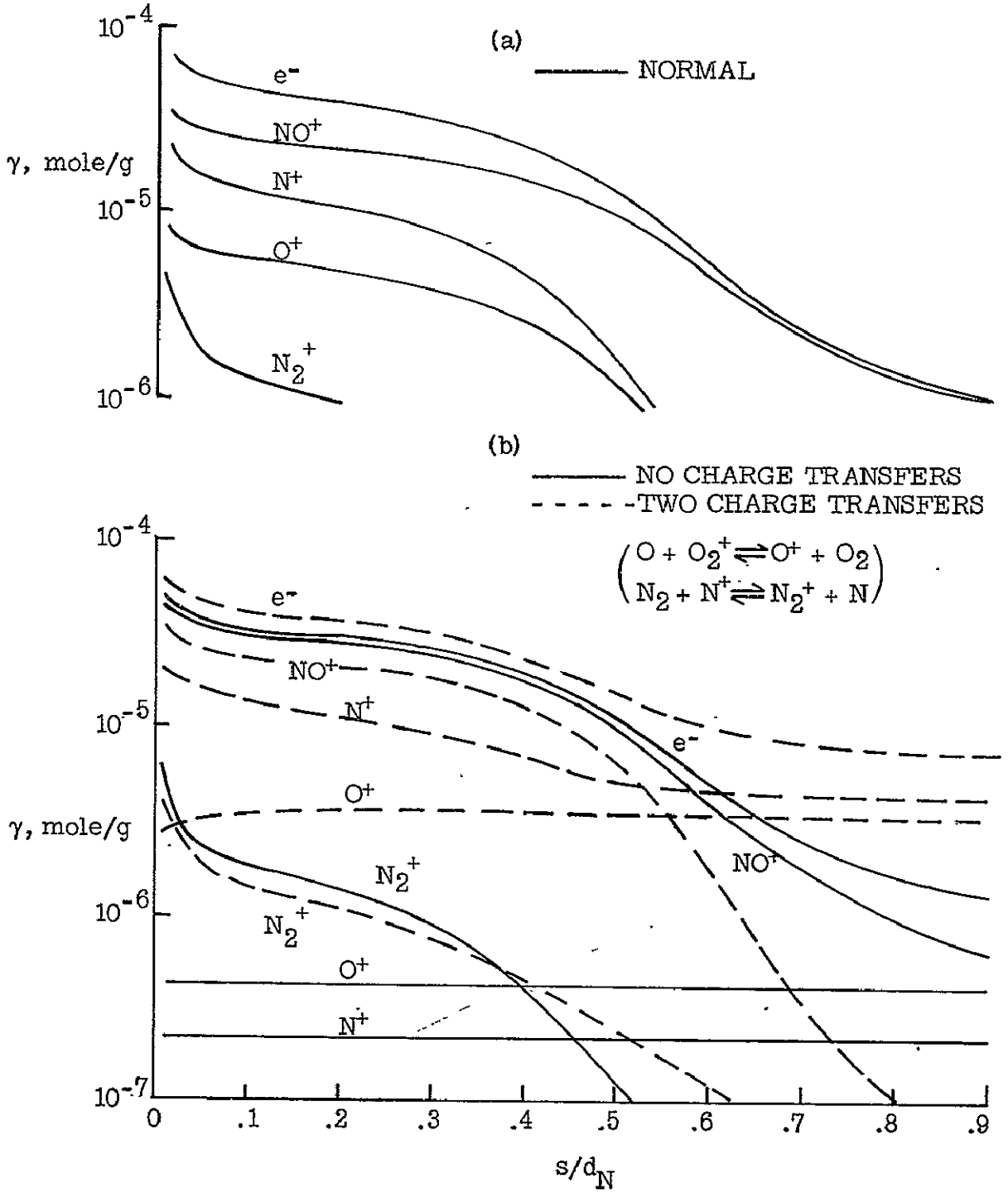

FIGURE 3.

EFFECT OF CHARGE TRANSFER REACTIONS ON N_e PROFILES
(ALTITUDE = 156,000 ft; $x/d_N = 4.$)

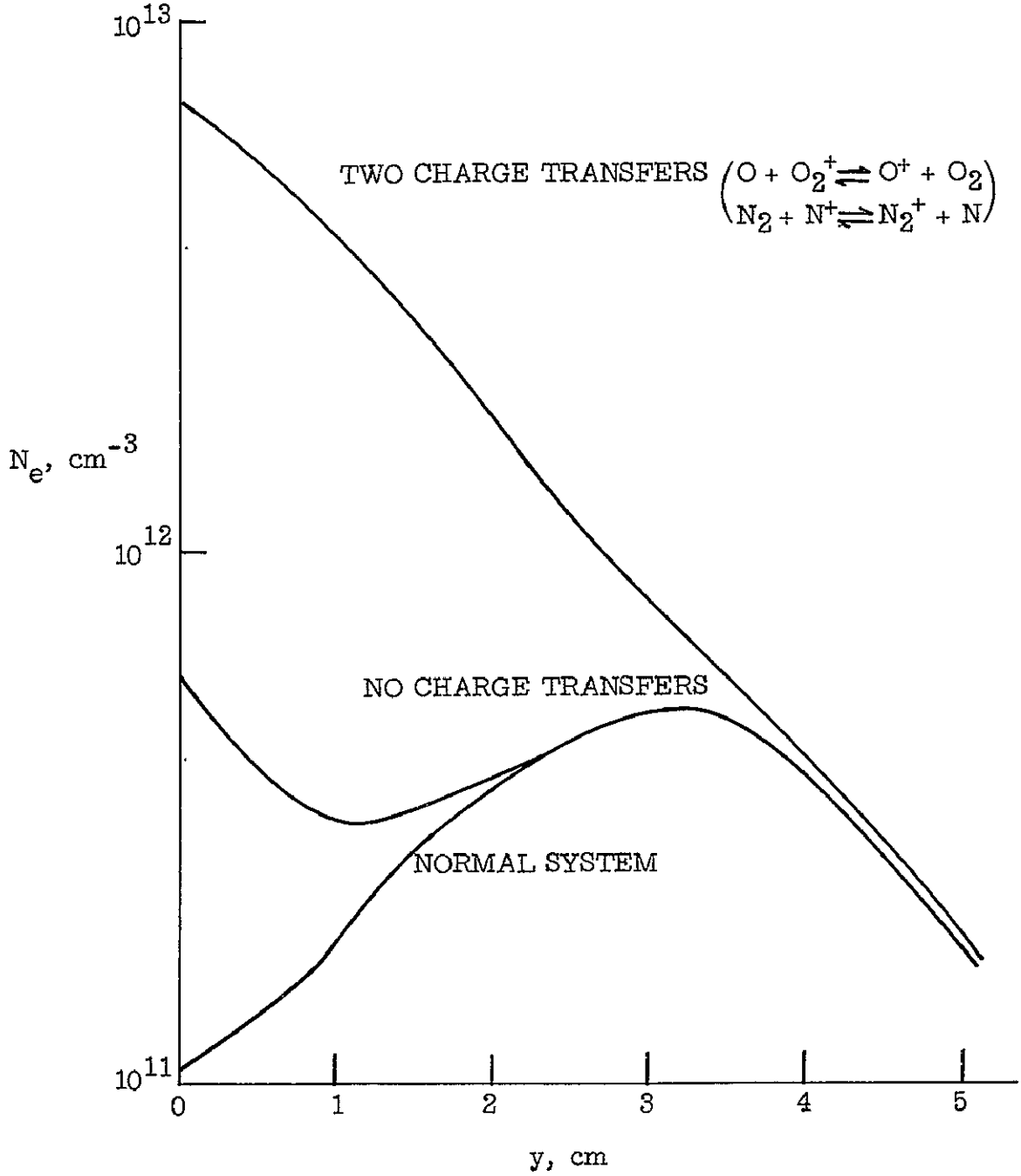

FIGURE 4.

IONIZATION LEVEL AS A FUNCTION OF ALTITUDE FOR BODY STREAMLINE

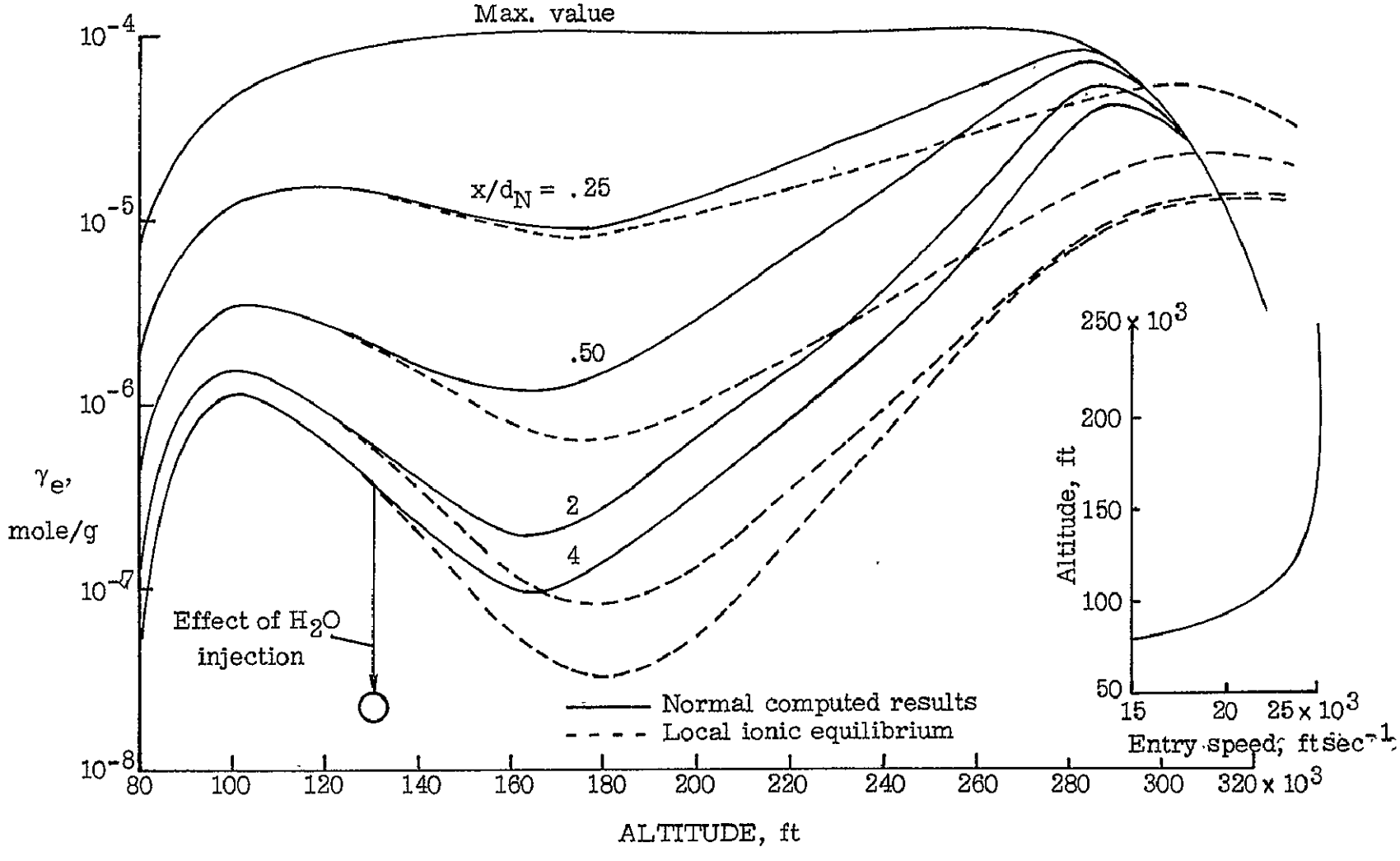

FIGURE 5.